

Springer Transactions in Civil  
and Environmental Engineering

Harvinder Singh

---

# Steel Fiber Reinforced Concrete

Behavior, Modelling and Design

 Springer

**Springer Transactions in Civil  
and Environmental Engineering**

More information about this series at <http://www.springer.com/series/13593>

Harvinder Singh

# Steel Fiber Reinforced Concrete

Behavior, Modelling and Design

 Springer

المنارة للاستشارات

Harvinder Singh  
Department of Civil Engineering  
Guru Nanak Dev Engineering College  
Ludhiana, Punjab  
India

ISSN 2363-7633                      ISSN 2363-7641 (electronic)  
Springer Transactions in Civil and Environmental Engineering  
ISBN 978-981-10-2506-8              ISBN 978-981-10-2507-5 (eBook)  
DOI 10.1007/978-981-10-2507-5

Library of Congress Control Number: 2016951650

© Springer Science+Business Media Singapore 2017

This work is subject to copyright. All rights are reserved by the Publisher, whether the whole or part of the material is concerned, specifically the rights of translation, reprinting, reuse of illustrations, recitation, broadcasting, reproduction on microfilms or in any other physical way, and transmission or information storage and retrieval, electronic adaptation, computer software, or by similar or dissimilar methodology now known or hereafter developed.

The use of general descriptive names, registered names, trademarks, service marks, etc. in this publication does not imply, even in the absence of a specific statement, that such names are exempt from the relevant protective laws and regulations and therefore free for general use.

The publisher, the authors and the editors are safe to assume that the advice and information in this book are believed to be true and accurate at the date of publication. Neither the publisher nor the authors or the editors give a warranty, express or implied, with respect to the material contained herein or for any errors or omissions that may have been made.

Printed on acid-free paper

This Springer imprint is published by Springer Nature

The registered company is Springer Nature Singapore Pte Ltd.

The registered company address is: 152 Beach Road, #22-06/08 Gateway East, Singapore 189721, Singapore

المنارة للاستشارات

# Preface

The last three or four decades saw a systematic growth of organized research efforts in understanding the behavior of concrete produced by dispersing short steel fibers at the time of mixing. These efforts led to the development of numerous material models and analysis methods to capture the response of the steel fiber reinforced concrete (SFRC). Concrete is a quasi-brittle material and it possesses a low tensile strain capacity. However, the inclusion of the steel fibers in the mix at the time of the concrete production significantly improves the brittle characteristics of the concrete; it starts exhibiting a better performance not only under static and quasi-statically applied loads, but also under fatigue, shock, and impulsive loadings. Nevertheless, this improvement depends heavily on the pouring methods and the procedure used in the SFRC placement and its compaction in the molds.

The recent developments in the control methods and techniques to assess the amount and orientation of the steel fibers in the hardened concrete have given a big boost to the use of the SFRC, confidently, in various engineering applications, such as the elevated slabs, the ground supported slabs, the beams, etc. The improved post-cracking characteristic of the concrete caused by the steel fibers enables the designers to rely on the tension capacity of the SFRC alone. If properly designed, one of the greatest benefits to be gained by using SFRC is improved long-term serviceability of the structure. Serviceability is the ability of the structure or part thereof to maintain its strength and integrity and to provide its designed function over its intended service life. This monograph presents a forward analysis method to proportion the concrete sections reinforced by means of the steel fibers as well as the conventional longitudinal reinforcing bars in the section tension zone, unlike the previous models that seek input from the standard experimental investigations or some empirical expressions as a prerequisite to formulate the material constitutive model. The fiber parameters, such as fiber volume fraction and its aspect ratio along with the concrete compressive strength can be determined easily to attain a desired material response and the strength in its hardened state.

This monograph is a modest attempt to explore the world of concrete, especially SFRC as it applies to the analysis and design of structural members. It attempts to

summarize the vast amount of the research information related to the SFRC becoming available these days at one place. I hope it will prove useful to the consulting engineers who want to use the SFRC in routine design assignments as the generic model and the design charts presented here would help them to quickly proportion the members, decongest the regions of the maximum moments by making use of the steel reinforcing bars and the steel fibers to resist the load in unison. It will also be helpful to the academician and the researchers who want to understand the SFRC better and explore it further. For the convenience of the readers, the notation/symbols are given and explained at the point of their use in the text.

Before concluding the preface, I would like to express my sincere appreciation and thanks to all those who are working continuously across the globe to explore this material for the betterment of the humanity. The author also acknowledges his debt to various agencies, particularly the RELIM, CNR-DT and different sources on the Internet, for their published material and various images/photos, respectively to which references are made in the monograph for the benefit of the readers. The author also expresses his gratitude to University Grants Commission, New Delhi, who contributed in making this monograph possible. The support and help provided by Nina Concrete Systems and MRH Associates are greatly appreciated and acknowledged. At the end, the author would like to express his heartiest appreciation for all those at Guru Nanak Dev Engineering College, Ludhiana, who rendered help and support in this work.

Ludhiana, India

Harvinder Singh

# Contents

<b>1 Introduction</b> . . . . .	1
1.1 Historical Developments . . . . .	1
1.2 Concrete Microstructure . . . . .	9
1.3 Mechanical Properties . . . . .	13
1.4 Uniaxial Stress-Strain Response of Concrete . . . . .	15
1.5 Fiber Reinforced Concrete . . . . .	20
1.6 Conventional Reinforced Concrete . . . . .	24
References . . . . .	28
<b>2 Material Models</b> . . . . .	29
2.1 SFRC Constitutive Models . . . . .	30
2.1.1 Compressive Model . . . . .	30
2.1.2 Tension Model . . . . .	32
2.2 Analytical Tensile-Constitutive Model Based upon Drop-Constant Relationship . . . . .	40
2.3 Experimental Characterization of the Tensile Response . . . . .	45
2.3.1 RILEM TC162-TDF (2002) Procedure . . . . .	47
2.3.2 CNR-DT 204 (2006) Guidelines . . . . .	50
2.3.3 <i>fib</i> Model Code (2010) . . . . .	53
References . . . . .	55
<b>3 Design of SFRC Flexural Members</b> . . . . .	59
3.1 Structural Design—Concept . . . . .	60
3.2 Flexural Responses of SFRC Members . . . . .	61
3.2.1 Uncracked Phase . . . . .	62
3.2.2 Linear-Elastic Cracked Phase . . . . .	63
3.2.3 Non-linear Cracked Phase . . . . .	64
3.2.4 Fiber Pullout/Fracturing Phase . . . . .	66
3.3 Analysis at Ultimate Limit State . . . . .	66
3.4 Design of RC Sections . . . . .	75
3.5 Design of SFRC Sections . . . . .	78



3.6	Variation of $M_u$ with the Fiber-Parameters ( $V_f$ and $l/d$ ) and Reinforcement-Index . . . . .	85
3.7	Influence of the Fiber-Index and Reinforcement-Index on the Rebar-Straining . . . . .	88
3.8	Influence of the Fiber-Parameters ( $V_f$ and $l/d$ ) on the Fiber-Index ( $\beta$ ) . . . . .	90
3.9	Moment-Curvature Response of SFRC Members . . . . .	91
3.10	Design Method Assisted by Experimental Investigations . . . . .	94
3.11	Design of SFRC Doubly-Reinforced Members . . . . .	99
	References. . . . .	107
<b>4</b>	<b>Design of SFRC Members for Shear . . . . .</b>	<b>109</b>
4.1	Introduction . . . . .	109
4.2	Shear Behavior of Beams . . . . .	110
4.3	Shear-Transfer Mechanism . . . . .	112
4.3.1	Uncracked Concrete in the Flexural Compression Zone . . . . .	113
4.3.2	Interface-Shear Transfer . . . . .	114
4.3.3	The Dowel Action of Longitudinal Reinforcement . . . . .	114
4.3.4	Arch Action . . . . .	115
4.3.5	Residual-Tensile Stresses Across Cracks . . . . .	115
4.4	Factors Influencing Shear Capacity . . . . .	115
4.4.1	Depth of Member (D) . . . . .	116
4.4.2	Shear Span-to-Depth Ratio ( $a/d$ ) . . . . .	116
4.4.3	Longitudinal Reinforcement ( $p_t$ ) . . . . .	117
4.4.4	Axial Force (A) . . . . .	117
4.5	Design Shear Strength of SFRC Beams . . . . .	118
	References. . . . .	122
<b>5</b>	<b>Analysis and Design of SFRC Slabs . . . . .</b>	<b>123</b>
5.1	General . . . . .	123
5.2	Limit Analysis . . . . .	124
5.2.1	Mechanism Conditions . . . . .	125
5.2.2	Equilibrium Conditions . . . . .	125
5.2.3	Yield Conditions . . . . .	125
5.3	Solution Using Energy Principle . . . . .	128
5.4	Flexural Modeling of Reinforced Concrete Rectangular Slabs . . . . .	131
5.5	Assumptions . . . . .	132
5.6	Development of the Model . . . . .	134
5.6.1	Collapse Mechanism . . . . .	135
5.6.2	Equilibrium and Yield Criterion . . . . .	136
5.6.3	Solution . . . . .	136
5.7	Strength Requirement of the Supporting-Beams . . . . .	144
5.8	Critical Beam-Strength Parameter . . . . .	146
5.9	Some Important Observations . . . . .	150

5.10 Slab-System with Discontinuous Edges at Outer Boundary . . . . .	151
5.11 Design of SFRC Slabs . . . . .	153
References. . . . .	157
<b>6 Construction Practice . . . . .</b>	<b>159</b>
6.1 Introduction . . . . .	159
6.2 Effect of the Fiber Addition on Concrete Properties . . . . .	160
6.2.1 Consistency. . . . .	160
6.2.2 Pumpability. . . . .	161
6.3 Mix Proportioning of SFRC . . . . .	162
6.4 Specifications . . . . .	162
6.4.1 Specification by Type and Fiber Content . . . . .	163
6.4.2 Specification by SFRC Performance . . . . .	163
6.5 Storage of Fibers . . . . .	163
6.6 Addition of Steel Fibers to Concrete . . . . .	164
6.7 Mixing and Placement Operations . . . . .	164
References. . . . .	165
<b>Index . . . . .</b>	<b>167</b>

## About the Author

**Dr. Harvinder Singh** is currently Professor at Guru Nanak Dev Engineering College, Ludhiana. He is engaged in teaching, research, and consultancy in structural engineering. He has authored numerous technical publications, one laboratory manual, and has edited three books. He was granted a research award by the University Grants Commission, New Delhi. He is a state technical auditor and structural consultant involved in various infrastructure projects and is a member of several professional bodies. He is an editorial board member and reviewer for several international journals published by ACI, ICE, and ASCE. His current research interests are mathematical modeling and limit analysis of engineering structures, largely directed towards solving practical problems and improving the related design practices.

# Chapter 1

## Introduction

### 1.1 Historical Developments

Cement is thought to be older than humanity itself, having formed naturally around twelve million years ago, when a naturally occurring limestone reacted with the oil shale. The oil shale is an organic-rich fine-grained sedimentary rock. Amazingly, humans have been using oil shale as a fuel since prehistoric times, since it burns easily without any processing. It is believed that a cementitious material in the form of Calcium oxide/quicklime may have been formed during the thermal decomposition of the limestone caused by burning oil shale. As the quicklime is not a stable product and, when cooled over a period of time, it might have reacted, spontaneously, with  $\text{CO}_2$  from the air to convert back to a hardened product existing in the form of calcium carbonate. This process is still in use, albeit with a more advanced technology to manufacture the cement these days. Nevertheless, cement is not a concrete. But similar to the cements, the concrete has been in existence in varying forms for thousands of years.

Concrete is a composite building material; whereas, the cement is a basic binding medium that helps various ingredients to bind together and take a final shape of the mould after its hardening. When the naturally occurring sand and the water come in contact with the quicklime/burnt limestone, it started behaving like a plastic-like material which adhere various materials together after its hardening, over a period of time. Over thousands of years, these materials were improved upon, combined with other materials and, ultimately, morphed into modern concrete. The time period during which the concrete was first invented depends on how one understands the term *concrete*. The word concrete comes from the Latin word 'concretus', meaning compact or condensed or grown together, and it is generally used for a material that has been produced by combining two or more types of other materials, e.g. a composite material formed from the naturally occurring stone particles and the lime. The oldest concrete discovered was on the floor of a hut found in Israel. Historically, it dated back to about 7000 BC. The concrete found in

the floor of the hut is believed to be made by burning a limestone to produce the quicklime, which was somehow mixed with the water and the stone particles, and that finally took the shape of a solid mass after its hardening. Since then, this material has been used for many amazing things throughout its history, including architecture, infrastructure, and many more.

Some ancient concrete-like structures dating back to 6500 BC were also found in the *Nabataea* of what we know these days as Syria and Jordan. These concrete look like structures were constructed by the Nabataea traders or *Bedouins*, who occupied and controlled a series of oases and developed a small empire in the neighbourhoods of southern Syria and northern Jordan. Figure 1.1 shows one such piece of the concrete-like material extracted from the site.

The *Nabataea* are thought to have devised an early variety of the hydraulic concrete—which hardens when exposed to the water—produced using the lime and by 700 BC, they were building kilns to supply mortar for the construction of the rubble-wall houses, the concrete floors, and the underground waterproof cisterns, etc. These cisterns were kept secret from the outside world and were probably one of the reasons the *Nabataea* were able to thrive in the desert. Figure 1.2 depicts one such cistern found in Israel.

In making concrete, the *Nabataea* understood the importance of maintaining the mix as dry (or low-slump) as possible, as the use of the excess water introduces voids and weaknesses into the concrete. With time, they also developed building practices, included tamping, etc. to set a freshly laid concrete using special instruments to produce the desired surface finish and other surface textures, etc. into the solid mass formed after hardening of the material.

German archaeologist Heinrich Schliemann discovered the concrete floors in the royal palace of Tiryns, Greece. The floors are found to be made up of a mixture of the lime and pebbles; constructed around 1400–1200 BC. Figure 1.3 shows the remains of the flooring. The Assyrian Jerwan Aqueduct dating back to 688 BC was built using the waterproof concrete. It was a 80 km long aqueduct, which included a 10 m high section to span a 300 m wide valley and it was constructed to carry the



**Fig. 1.1** Ancient concrete sample extracted at an ancient city Nabataea (Syria) (Source Internet)



**Fig. 1.2** Remains of a Nabataean cistern found north of southern Israel. Investigations discovered that it consists of hydraulic concrete made using lime as a cementitious material and were impervious enough to prevent the leakage of stored water into the soil (*Source* Internet)



**Fig. 1.3** Flooring made up of concrete-like material found in royal palace of Tiryns, Greece (*Source* Internet)

water to the then capital city of Nineveh—an ancient Mesopotamian city on the easterly bank of the Tigris River, which was the capital of the Neo-Assyrian Empire. Its ruins are found across the river from the modern-day major city of Mosul in the Ninawa Governorate of Iraq.

Knowledge of this lime-based material possessing binding properties spread through the Egypt and the Ancient Greece and it finally reached the Romans around 300 BC. During the Roman Empire, the concrete (then, known as *opus caementicium*) was used extensively in the construction of various ancient Roman buildings. It was found to be made up of a mixture of the quicklime, the pozzolana—a grounded volcanic rock—and the aggregates of the pumice. This material was later on termed as ‘pozzolanic’ cement in the history books. It is believed that this name was chosen after the name of the village ‘Pozzuoli’ near Vesuvius where it was used in ancient times.

The widespread use of this material in many of the Roman structures, a central issue in the history of the Roman architecture, freed the Roman construction from the restrictions of the conventional use of pit-and-brick materials and permitted them to construct revolutionary new inventions both in terms of the structural complexities and the dimensions. Arches and aesthetically ambitious architecture became a lot easier to make. Figures 1.4 and 1.5 shows a typical structural form that became reality after the invention and the revolutionary use of this construction material. The Roman Pantheon was the largest (43.4 m diameter) unreinforced solid concrete dome constructed at that time in the world. It was constructed by the emperor Hadrian almost 2,000 years ago.

Amazingly, the ancient Roman buildings and structures, some of the most spectacular in the world, have withstood chemical and physical onslaught for these 2,000 years and are still standing. However, after the fall of the Roman Empire in 476 AD, the techniques for constructing buildings using the lime-based cementitious materials were lost until the discovery of old manuscripts, in 1414 AD, describing those techniques that again rekindled interest in constructing buildings with concrete.



**Fig. 1.4** *Colosseum*—Arches and aesthetically ambitious architecture became reality after the invention of concrete in the Roman period and these have withstood chemical and physical onslaught for long 2,000 years and are still standing (*Source* Internet)



**Fig. 1.5 Roman Pantheon**—The first concrete building believed to be built in the world. The building has a largest unreinforced solid concrete dome (43.3 m diameter) built at that times. The building has sections large enough to keep the stress level in its different components sufficiently small to withstand the loads (*Source* Internet)

In the year 1678, Joseph Moxon reported about a hidden fire in the lime that appeared when water was added to it. To his surprise, the lime again transformed to a stone-like material after the cooling. However, it was not until 1756 that the technology took a big leap forward when British John Smeaton discovered a technique to produce cements from the hydraulic lime. He used the limestone containing clay to produce clinkers. The mixture of the limestone and the clay in certain ratio was burnt till they turned into clinkers. The clinkers were then grounded into the powder form to produce cement. He utilized this material in the construction of historic Eddystone Lighthouse (also, known as Smeaton's lighthouse) in Cornwall, England. The lighthouse was built about 18 m high at that time; it had a diameter of 8 m at the base, which was reduced to 5 m at its top. The lighthouse was constructed with a slightly curved profile (see, Fig. 1.6) with a massive base made up of concrete, which strengthened along its height. It was an engineering strategy to counter the natural forces caused by the wind and the waves, etc. by keeping the centre of gravity of the building nearer to its base. Figure 1.6 shows the lighthouse in its present form along with the profile of the original lighthouse constructed at that time.

Maybe this was the greatest driver behind the advanced usage of the concrete. This building encouraged many others across the world to explore the material in constructing many other similar structures/buildings. As a results of these efforts, a number of patents were issued to different inventors: Bry Higgins (1789) issued a patent for using hydraulic cement (*stucco*) for the exterior plastering; James Parker (1796) from England patented natural hydraulic cement by calcining nodules of impure limestone containing clay, called Parkers Cement or Roman Cement; Louis





**Fig. 1.6** *Eddystone Lighthouse*—The 18 m high lighthouse built by British John Smeaton (1759) on the Eddystone Rocks, about 14 km south of Rome Head, England (UK). The original lighthouse was built using the granite blocks joined together using ‘hydraulic lime’—a concrete that sets under the water, and the marble dowels. However, this structure was pulled down, except for its base and moved to Plymouth and then rebuilt it on a new base adjacent to the original location (*Inset* the original Eddystone Lighthouse) (*Source* Internet)

Vicat of France (1812) prepared artificial hydraulic lime by calcinating synthetic mixtures of the limestone and the clay.

The birth of the modern concrete as we know it today can be attributed to a stonemason Joseph Aspdin from Leeds. He produced the cementitious material by heating chalk and clay together, then grinding it down to a fine powder and got out a patent for the process to produce the cement in year 1824. He named it Portland Cement due to the resemblance of the hardened product formed over a period of time to the stones found in the Portland. A few years later, in 1845, Isaac Johnson modified the process used by Joseph to produce cement. He used very high temperature to fire a mixture of the chalk and the clay in the kiln, similar to the technique used these days for manufacturing cements. At high temperatures (1400–1500 °C) used in the process, clinking occurs and it leads to the production of a minerals which was found to be very reactive and stronger than the cementitious material developed by the Joseph.

With an increasing structural use of the concrete, mostly in the second half of the 1800s, the interest shifted from the crafting to the scientific use of the material, with a focus more on devising and developing testing methods to estimate the material load carrying capacity. In 1836, the first test for finding the tensile strength and the compressive strength of concrete took place in Germany. The tensile strength refers to the concrete’s ability to resist tension when it is pulled apart by applying forces;

whereas, the compressive strength refers to the concrete's ability to resist a compression. It was established by that time that the concrete is very weak in the tension; it failed abruptly when pulled apart, but it is capable of supporting a huge magnitude of the load when subjected to the compressive loads. Understanding of these characteristic of the concrete give a big boost to the construction of massive concrete structures in the form of domes, vaults, etc. in the subsequent years; the concrete was used mainly to carry the compressive load and the stress level in the members was kept sufficiently small by providing massive sections that the concrete could withstand on its own.

Pettenkofer and Fuches (1849) performed the first chemical analysis of Portland cement and later on, Henri Le Chatelier of France (1887) established oxide ratios to calculate the right quantity of the lime required to produce Portland cement. He identified the three basic constituents of the cement and named these: (a) *Alite* (tricalcium silicate), (b) *Belite* (dicalcium silicate), and (c) *Celite* (tetracalcium aluminoferrite) and proposed that the hardening of the mix is mainly caused by the formation of crystalline products in the material from a reaction that occurs when water was added to the cement. And by the year 1890, it was established that the addition of the gypsum to the mixture during the clinking process significantly alters the setting characteristics of the cement. In the later years, the gypsum was used successfully to delay the setting of the cement paste.

The second half of 1800s also saw a systematic growth of organized research efforts in the field of the concrete as a building material, especially in the UK and USA. These efforts led to the establishment of Institution of Civil Engineers (ICE), in the year 1818, in the United Kingdom (UK). An association of the cement users at Louisiana Purchase Exhibition, St. Louis (1904); which, later on, morphed to an organization, known as the National Association of Cement Users (NACU) in the history books (1905), was established in the USA.

These two institutions plays a pivotal role in shaping the future research efforts in the concrete technology, the knowledge transfer and establishing best practices within the civil engineering and the construction since their inception. The archives of the ICE contain a number of research publications as old as 1836. The NACU made annual conventions as their regular activity to disseminate the latest developments in the concrete technology among different stack holders; the first one held at Indianapolis and released the first Proceedings volume related to the research work done on concrete so far. Later years saw a huge growth of the activities of the organization and its membership. The Association's influence was increased manifold overseas by the year 1912 and many standards were being employed outside the USA in the construction using concrete as a building material. The name of the organisation was changed to American Concrete Institute (ACI) in the year 1913 to reflect its true scope. It introduced various medals and prizes to encourage further quality concrete research. The proceedings publication, which was stopped in 1912 due to the paucity of the funds, was revived in the form of a journal to promote and disseminate the research among the concrete users.

The ACI Journal was finally approved as a monthly periodical in the year 1929 after the formation of the first publications committee. By that time, it was felt that

the annual Institute conventions and annual volume of the proceedings were not adequate to present the vast amount of the research data and the field information becoming available. The efforts of the ACI finally consolidated in the form of the first design handbook 'SP-3' (1939) and the first Building Code 'ACI 318' (1941). In the year 1967, ACI released the first Manual of Concrete Practice that comprised a set of 17 standards and 23 reports related to the concrete design and practice. It subsequently issued a design handbook for the concrete structures based upon the concept of the ultimate strength (1967).

It was an established fact by that time that the microstructure of the material plays an important role in controlling the strength properties of the concrete. The strength of the material resides in its solid part; therefore, the voids existing in the microstructure of a material are detrimental to its strength. The quantity of water used in the concrete mix—expressed as a ratio of the quantity of water ( $w$ ) to the cement content ( $c$ ) i.e.  $w/c$ -ratio—was observed to be a single most factor influencing the ease with which concrete can be handled and placed during the construction and the strength it would develop after its hardening. A. Abrams Duff in 1918 reported that *“When the compressive strength is plotted against the water ratio.... a smooth curve is obtained....It is seen at once that the size and grading of the aggregate and the quantity of cement are no longer of any importance, except in so far as these factors influence the quantity of water required to produce a workable mix....The strength was found to depend only on one factor....The ratio of the water to the cement ( $w/c$ ) in the concrete”* and postulated a law that the strength of the concrete develops in inverse proportion to the  $w/c$ -ratio used in the concrete mix. This law earned a wide attention from the global concrete community. He, later on, recognized the effect of particle size and the particle size distribution of the concrete mix (1918) and also put in the concept of the fineness modulus (1919) along with the test methods to determine the workability of the concrete and its flexural strength (1922). This test now-a-day is known as the slump test and is used widely in practice to determine the fresh state characteristics of the concrete.

Today's concrete is made using the Portland cement, coarse and fine aggregates of stone and sand, and the water. Proportioning methods are developed to achieve a desired value of the concrete compressive strength and other concrete performance parameters required in the final product. Over a period of time, admixtures and other techniques were developed to control setting properties of the concrete mix. This invention played a key role in escalating the concrete use during environmental extremes conditions, such as underwater conditions, high or low temperatures, hauling concrete over long distances, and so on. The use of admixtures in the concrete also led to use in a variety of other special purposes, like resistance to freezing and thaw (1930); achieving higher compressive strength (1980) by means of the silica fume and super plasticizer, etc. In 1984, ACI expanded its role in concrete research by establishing the Concrete Materials Research Council. The name of the Council was changed to the Concrete Research Council in 1991, and the mission was expanded to include research related to concrete construction and structures, in addition to concrete materials.

The second half of 1900s saw an exponential increase in research activities connected to the concrete microstructure, its influence on the strength properties, such as compressive strength, flexural strength, tensile strength, etc. And it is now well documented in the form of the scientific publications, the design guidelines and the codes of practice formulated on the basis of the experimental results and the performance studies carried out globally in the yesteryears. The following section provides birds overview related to the established microstructure of the concrete and its other mechanical attributes.

## 1.2 Concrete Microstructure

It is now an established fact that the properties of any material originate from its internal microstructure. There exists a coupling between the mechanical properties of the material and the microstructure it possesses. Whatever modification in the one parameter has a significant effect on the other. This phenomenon enables the material technologist to modify the material mechanical properties by making suitable alterations in its microstructure, which indicates the type, extent, size, form, and distribution of different phases present in the material matrix. As the strength of the material resides in its solid part, the voids therefore left in the material because of any reasons are detrimental to its strength. It is therefore utmost important to fill in these voids by adding material particles at the time of concrete production that are finer than the cement particles or by adding something that fills the empty spaces in the matrix by combining with the products of the hydration reaction.

The concrete usually consists of three different materials mixed together in the presence of water. The cement acts as a binding media that forms a solid mass by adhering the fine content, usually sand, and coarse content in the form of crushed stones together. Figure 1.7 shows a typical polished section of a concrete sample that shows that how different constituents of concrete are packed together to form a solid mass. The process initiates when water is added to the mix of these three basic constituent materials which triggers the hydration reactions in the cement. In the hardened concrete at the macroscopic scale, it consists of two phases: (a) aggregates of varying sizes, and (b) the binding fabric, which consists of an incoherent mass of the hydrated cement paste. Tests have shown that in the hydrated cement paste, incoherent mass always exists there due to the non-homogeneous distribution of the solids and the voids (as shown in Fig. 1.7). It did not influence the behavior of the hardened cement paste when considered in isolation and consequently, it is generally ignored while modelling the compression behavior of the paste. But the scenario changes, entirely, when the fine and the coarse aggregates are added to the cement at the time of the mixing. It leads to the formation of a very thin layer of separation around coarse particles in the concrete. This layer is called as interfacial transition zone. Figure 1.8 depicts a typical microscopic view of the interfacial transition zone. This layer typically extends to a distance of 10–50  $\mu\text{m}$  around coarse particles in the concrete [Maso (1996), Bentur and Alexander (1995)]. The



**Fig. 1.7 Concrete**—A concrete in its hardened state consists of hydrated cement paste, Fine aggregates (usually, sand) and coarse aggregates (crushed stone particles). It formed when the cement hydrates in the presence of water and leads to the formation of different products of hydration that, later on, fill in the empty spaces left between different constituents of the concrete and finally, giving it a capacity to support the load

interfacial transition zone is generally weaker than either of the two main constituent materials of the concrete, namely, the aggregates and the hydrated cement paste; therefore, it exercises a far greater influence on the mechanical behavior of concrete than is reflected by its size.

The different physical properties of the constituent materials in the concrete mix lead to the formation of this region of discontinuity, especially, at the interface of the coarse particles and the hydrated cement paste. The release of the heat in the concrete mass because of the hydration process causes differential expansion of the aggregates embedded in the hydrated cement paste and with the passage of time, it leads to the formation of a zone of separation around coarse particles when they return to the normal ambient temperature with the passage of time. Figure 1.8 depicts typical zones of separation developed around coarse particles in the concrete. These are indicated by the black lines around coarse particles in the Fig. 1.8a; while Fig. 1.8b shows an enlarged microscopic view of the zone of the separation existing around coarse aggregates in the concrete mix.

The coarse aggregates being stronger than both of the fine aggregates and the hydrated cement paste in concrete usually have no direct influence on the concrete strength, except in the case where the concrete is made by using highly porous and weak aggregates, such as pumice, etc. Nevertheless, the size and the shape of coarse aggregates do exercise a considerable influence on the strength of concrete. The large size coarse aggregates, particularly elongated and flaky ones, have a higher tendency to accumulate water films on its surface. This phenomenon, known as

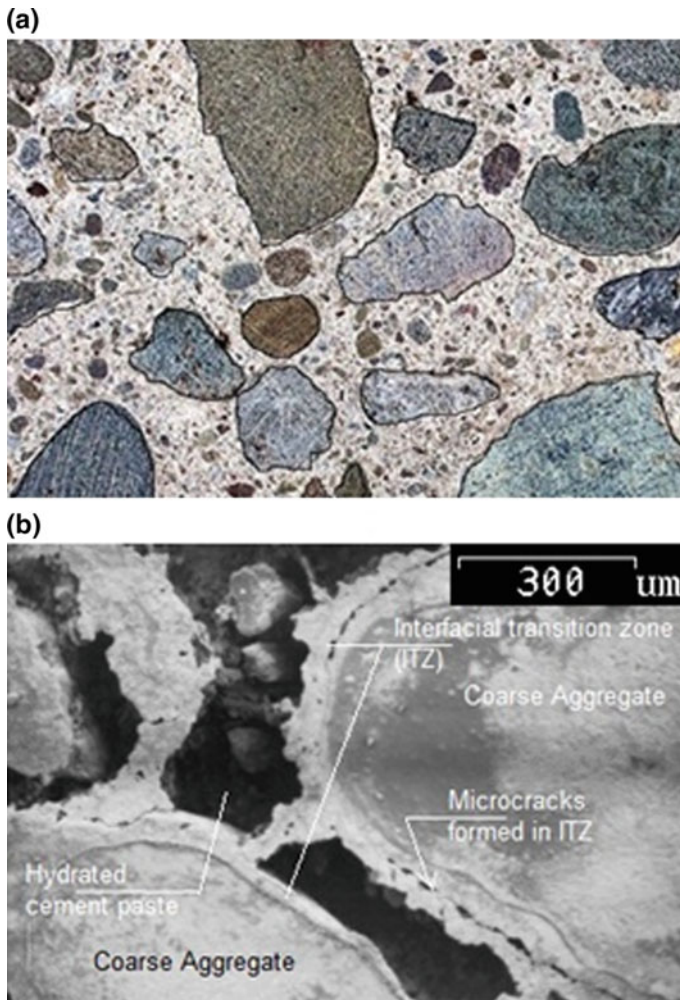


**Fig. 1.8** *Interfacial transition zone*—A line of separation or discontinuity formed mostly around coarse particles in the concrete (shown by *dark lines* in **a**). This zone dictates the strength properties exhibited by concrete. Generally, the volume and size of the voids in this zone are larger than found elsewhere in the bulk of the cement paste. Because of a relatively higher water-cement ratio near the surface of the coarse particles, especially, the flaky and large round sized particles, the size and concentration of crystalline compounds, such as calcium hydroxide and ettringite are larger in this zone that leads to formation of the surface of discontinuity around their surface—a strength-limiting phase in concrete. It is also seen as a zone of weakness, both in terms of strength and in terms of the permeation of fluids. The high porosity prevailing in this zone affects the transport properties of concrete: **a**) a polished surface of the concrete specimen; **b**) Microscopic magnified image of a concrete

bleeding, generally leads to the further weakening of the interfacial transition zone in the concrete and it becomes comparatively more prone to the microcracking than other regions in the hardened concrete mass. This happens because of a relatively

higher water-cement ratio developed closer to the larger aggregate than away from it in the bulk of the cement paste. This phenomenon is found to be a major factor responsible for the shear-bond failure generally observed at the surface of coarse aggregates in the concrete when crushed in the compression.

At the microscopic scale, the chemistry of the concrete plays a greater role in controlling the behavior exhibited by the interfacial transition zone developed around coarse aggregates. The Portland cement in its anhydrous state consists mainly of angular particles typically in the size range from 1 to 50  $\mu\text{m}$ . It is produced by pulverizing a clinker, which is a heterogeneous mix of several compounds formed by the high-temperature reactions between the calcium oxide and silica, aluminium oxide, and iron oxide during the clinkering process. The chemical composition of a typical clinker compound corresponds approximately to C3S (45–60 %), C2S (15–30 %), C3A (5–15 %), and C4AF (5–10 %).

When Portland cement is dispersed in the water, the calcium sulphates (C3S and C2S), and the other high-temperature compounds of calcium, such as C3A and C4AF, begin to pass into solution. It contributes to the dissipation of these compounds into various ions and consequential saturation of the liquid phase of the concrete mix. The Tricalcium silicate (C3S) rapidly reacts to release the calcium ions and the hydroxide ions into the solution. It is accompanied by the release of a great amount of heat during the hydration process and promptly produces the solution pH to over 12. The pH of the solution increases due to the formation of alkaline hydroxide ( $\text{OH}^-$ ) ions during the chemical reactions taking place in the concrete mix. Equation 1.1 represents the hydration process that takes place in the solution. It leads to the decomposition of the Tricalcium silicate (C3S) and the Dicalcium silicate (C2S) into the Calcium Silicates Hydrates (C–S–H) along with the formation of hydroxide ions ( $\text{OH}^-$ ) and release of an enormous amount of energy.

Tricalcium silicate + Water  $\Rightarrow$  Calcium silicate hydrate + Calcium hydroxide + heat



Dicalcium silicate + Water  $\Rightarrow$  Calcium silicate hydrate + Calcium hydroxide + heat



(1.1)

Within a few minutes of the cement hydration, the needle-shaped crystals of the calcium trisulfoaluminate hydrate (C–S–H), called as *ettringite*, starts forming in the cement paste because of the chemical reaction between the calcium, the sulphate, the aluminates, and the hydroxyl ions. With the passage of the time, the large size prismatic crystals of the calcium hydroxide and very small fibrous calcium silicate hydrates begin to fill the empty space in the matrix, formerly occupied by the water and dissolving cement particles. Afterwards, depending on the alumina-to-sulphate ratio of the Portland cement, the ettringite may become unstable and breaks up to form the monosulfoaluminate hydrate. This ratio plays an important role in

controlling the quantity of monosulfoaluminate hydrate in the concrete mass. A French engineer Henri Le Chatelier had established this fact, way back in 1887. Now-a-days, putting a cap on the chemical composition at the time of clinkering during the cement manufacturing is a standard practice across the world. Out of various compounds released during the hydration process, only the calcium silicates contribute to strength of the concrete. Nevertheless, the Tricalcium silicate (C3S) is responsible for most of the early-age strength of the concrete and the Dicalcium silicate (C2S) is responsible for the strength exhibited by it at longer period of times.

The van-der Waals forces of attraction existing between various solid products formed during the hydration process contribute to strength exhibited by the concrete. The products of the hydration generated in the cement paste tend to adhere strongly not only to each other, but likewise to the solids having a low surface-area, such as calcium hydroxide, anhydrous clinker grains, and aggregates and it finally build a microstructure of the concrete.

It is important to note that the high water-cement ratio prevailing near the surface of the coarse aggregates leads to the formation of products of hydration that primarily consists of relatively large sized crystals. This phenomenon contributes to the establishment of a more porous framework of crystals near the surface of coarse aggregates than those made in the cement paste (Fig. 1.8b). The relatively less adhesion capacity of the large sized calcium hydroxide crystals in the interfacial transition zone formed around coarse aggregates in the concrete lowers the strength as these possess smaller surface area and the correspondingly weak van-der Waals forces of attraction. They also act as a preferred cleavage sites for the failure owing to their inclination to form an oriented structure. These factors ultimately lead to further weakening of the interfacial zone at early ages in the concrete. However, as the hydration process progress over a period of time, the poorly crystalline C-S-H and the second generation of smaller size crystals of the ettringite and the calcium hydroxide generated by the slow chemical reactions in the cement start filling the empty space existing between the frameworks created by the larger ettringite and the calcium hydroxide crystals; thereby improving the microstructure of the concrete with the passage of the time. Such interactions are the prime source of the strength gain by the concrete with time.

### 1.3 Mechanical Properties

The presence of the interfacial transition zone around the surface of coarse aggregates in the concrete mass is the primary source of limiting strength and other characteristics exhibited by the concrete. It also influences the elastic modulus of concrete. The experimental investigations in the past have revealed that the components of concrete *viz*: coarse aggregates and the hydrated cement paste if tested alone, and separately, under the compressive load usually undergoes an elastic load-displacement response until the failure and these possess a high stiffness. The concrete, whereas if tested under identical test conditions exhibits an inelastic



behavior with a reduced stiffness in comparison to the cement paste and the coarse aggregates.

Figure 1.9 demonstrates one such typical response exhibited by the concrete, the hydrated cement paste and the aggregates tested alone under an identical set of test conditions. This happens because of the presence of the interfacial transition zone in the concrete, which the aggregates and the cement paste did not have. This zone acts as a bridge between the hydrated cement paste and the coarse aggregate and is an only medium to transfer stresses across different phases of the concrete. The presence of the voids and other microcracks in the interfacial transition zone do not allow an effective stress-transfer across its thickness. It therefore leads to the diminution in the load carrying capacity of the concrete, irrespective of the load type. It is important to note that the concrete fails abruptly under the tensile loading; whereas, it holds about ten times higher compressive load than its tensile strength, although the principal cause of the failure in both cases is the limited tensile strength of the concrete. The tensile stresses do develop in the material owing to the Poisson's effect even if the primary load is compressive in nature.

The lower tensile strength of the concrete can be attributed to the presence of a weaker zone of separation—interfacial transition zone—mainly around coarse aggregates. Considerable energy is needed for the formation of new microcracks and extension of those already existing in the interfacial transition zone of the concrete mass under a compressive load than the tensile loading; wherein, these cracks propagate rapidly and that happens at a much lower stress level. The size of coarse aggregates and its grading; cement-content and water-cement ratio; humidity

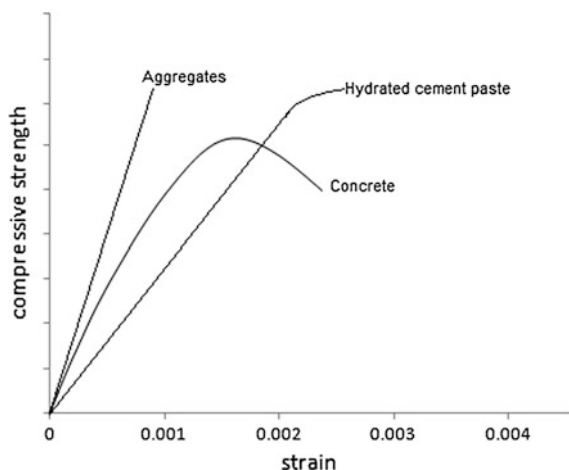


**Fig. 1.9** *Material strength*—The aggregates and the hydrated cement paste exhibit a linear elastic response upon stressing, whereas the concrete does not. The presence of the interfacial transition zone around the surfaces of coarse particles in the concrete can be attributed to the nonlinearity exhibited by concrete, when it is strained beyond the elastic range. The interfacial transition zone did not exist in case of the naturally occurring aggregates and the hydrated cement paste

and curing conditions of concrete have a considerable influence on the extent of microcracking developed in the concrete. A concrete mix containing poorly graded aggregates is more prone to the segregation and thereby leads to the formation of a relatively thick water film at the surface of the coarse aggregates. Usually, the concrete containing a larger fraction of flaky and large sized coarse aggregates tends to have a thicker water film around them, especially beneath the particle, under an identical set of casting conditions. The interfacial transition zone developed under this set of conditions is relatively more porous and weak in nature and it acts as a cleavage plain for the microcracks in the interfacial transition zone to develop into cracks more easily under the tensile stresses than the compressive stresses.

The water-cement ratio used in the mix also found to play a crucial part in controlling the microstructure that the concrete would develop into with the passage of time. An increase in the water-cement ratio during the concrete production leads to the formation of coarser crystals in the matrix and the transition zone, thereby increasing the porosity of the matrix which ultimately leads to a reduction in the concrete strength. The concrete with a low water-cement ratio possesses smaller size crystals of the hydration products; thereby giving an enhanced concrete strength owing to relatively higher Van-der Waals forces acting in the matrix. Normally, at a stress level higher than approximately 70 % of the ultimate concrete compressive strength, the stress concentrations developed at the large voids in the cement matrix become large enough to initiate cracking and with the increasing stress level, the matrix gradually cracks; the cracking spread into other regions of the matrix until they join other cracks originating from the interfacial transition zone. This process leads to an abrupt failure of the concrete. This normally takes place when the crack system existing in the matrix becomes continuous throughout the concrete member (see, Fig. 1.11f).

Unlike the normal strength concrete, high-strength concrete generally behaves more like a homogeneous material. This presumably happens because of the existence of a stronger interfacial transition zone in the concrete matrix, caused by the reduction of excess bleeding and filling of the empty spaces and other microcracks by mineral admixtures, such as silicafume, rice husk ash, etc. added at the time of the concrete production. Because of an improved microstructure, the high strength concrete show a steeper stress-strain response, comparatively less volumetric dilation and most importantly, reduced permeability than the normal concretes.

## 1.4 Uniaxial Stress-Strain Response of Concrete

It is given in the previous section that the interfacial transition zone in the concrete relatively possesses more capillary voids, the microcracks, and the coarser calcium hydroxide crystals than the bulk of the concrete matrix. This unique feature of the interfacial transition zone plays a crucial role in dictating the constitutive relationship of the concrete. Nevertheless, the improvement in the density of the interfacial transition zone over a longer duration, especially after 1 year or so, helps

to improve the strength of the concrete in general and its elastic modulus in particular. The slow chemical interactions going on within the concrete microstructure contribute considerably towards the strength gain over the longer times.

Figure 1.10 depicts a typical stress-strain response of the concrete, under uniaxial compression and tension, tested under the standard loading conditions [Hsu et al. (1963); Hsu and Slate (1963)]. It is important to note that the concrete cracks when it is strained under a tensile stress beyond its limited tensile strain, generally ranging from 0.00012 to 0.00016. However, the failure is more gradual when the concrete specimen is subjected to a compressive loading. Normally, the concrete specimen fails to carry any additional load when it is strained beyond a strain value of 0.0035. This occurs irrespective of the concrete grade. It is observed that the peak of the strength occurs generally near a strain of 0.0020, irrespective of the concrete grades and thereafter, the concrete exhibits a strain-softening response. Normally, the internal cracks in the specimen became continuous when it is strained beyond a strain of 0.0035 and fails to support any additional load.

It is important to note that strength exhibited by the concrete unlike other structural materials, such as steel, etc. depends upon a number of factors, including type of the stress (compression or tension); type of the loading (static or cyclic); the

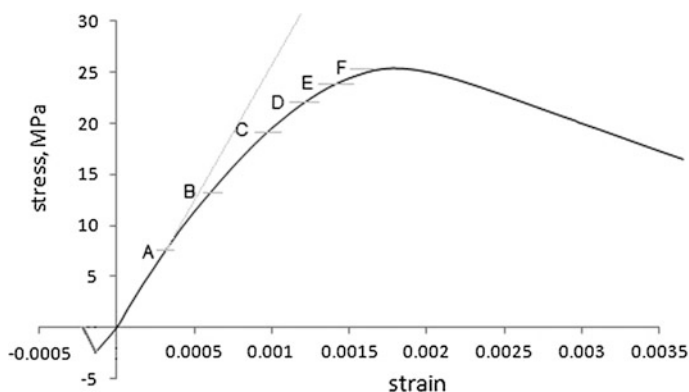


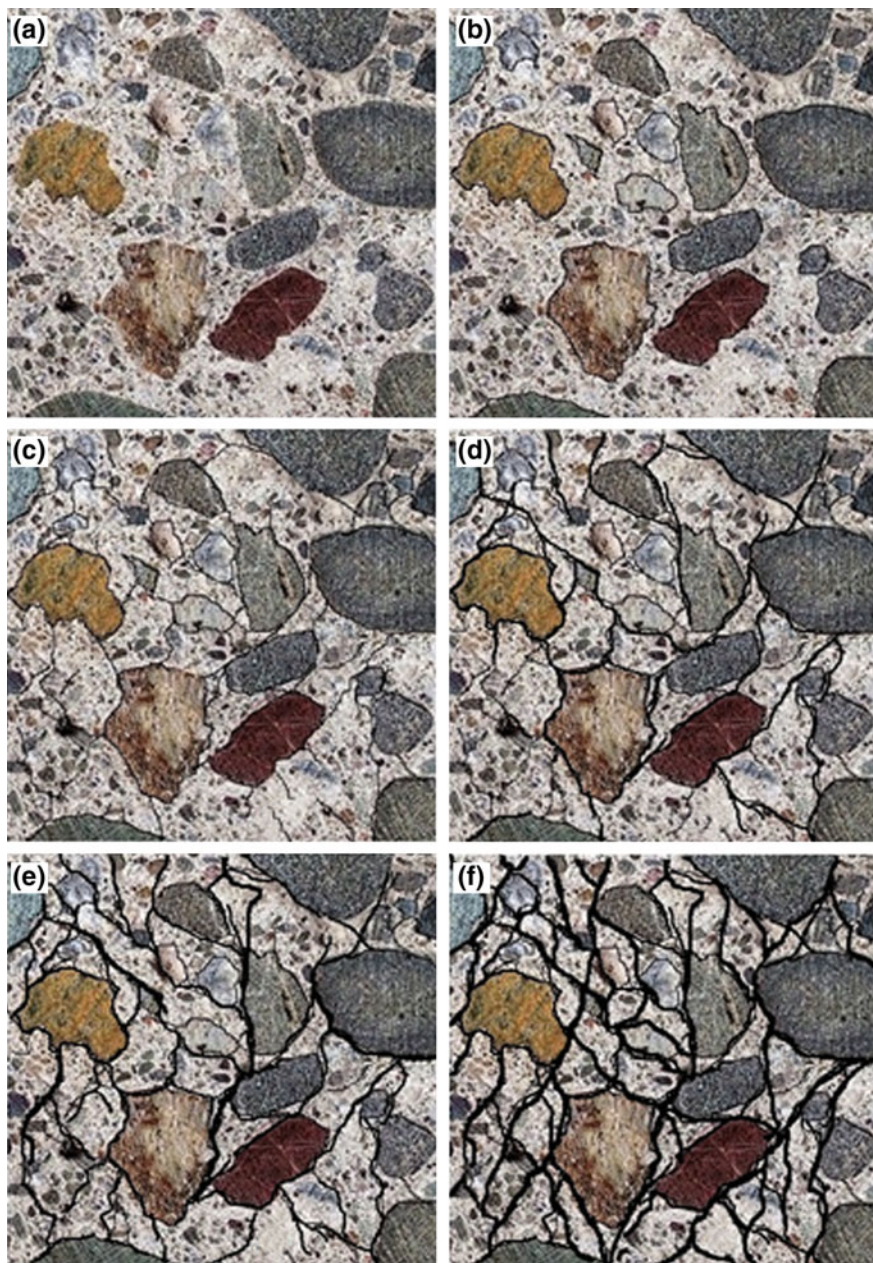
**Fig. 1.10** Concrete response at different stress levels—The figure schematically shows a stress-strain response exhibited by concrete at various stages of uniaxial stress conditions, e.g. compressive and tension loading conditions. When concrete is compressed to about 30 % of its ultimate strength (stage A), the response is linear-elastic; followed by a slight deviation in the response when the stress level is maintained in a range of 30–50 % of the ultimate concrete compressive strength (stages A to B). At a stress level of 75 % of the ultimate compressive strength (stage C); the concrete shows a significant decline in the slope of the stress-strain curve and it possesses a highest value of the volumetric strain at this stage. Thereafter (stages D to F), it exhibits a sharp change in the slope of the curve and it generally fails to support any further loading. It is accompanied by strain-softening after reaching stage F. In contrast, when subjected to the tensile loading, the concrete failure is brittle and it occurs abruptly as soon as the strain reaches its limiting value of 0.00014. Nevertheless, the concrete response under the tension is linear-elastic. The tensile strength of the concrete generally varies in a range of 6–12 % of its ultimate compressive strength

rate of the loading; the geometric dimensions of the sample (particularly its height to the diameter ratio); the moisture state; the aggregate type (crushed or rounded) and their properties; the air content in the mix; aggregate gradation, and the degree of hydration. In light of so many factors influencing the concrete strength, the testing procedures have been standardized by different agencies, such as ACI, ASTM, BIS, etc. to ensure reproducibility of the test results produced by different technicians.

Under the standard test conditions, the concrete exhibits a linear-elastic behavior when stressed to a stress level of about 30 % of the ultimate compressive strength. It appears that the microcracks in the interfacial transition zone of the concrete remain undisturbed when it is stressed up to 30 % of its ultimate compressive strength and for a stress level higher than this level, the microcracks present in the interfacial transition zone of the concrete extends in length because of the stress concentration prevailing at the crack tips. Nevertheless, these cracks confine themselves to the interfacial transition zone, and did not run into the mortar matrix. Until this point, the crack propagation in the interfacial transition zone remains more or less stable under the prevailing stress conditions in the concrete specimen. Figure 1.11 demonstrates different stages of the crack formation in the concrete matrix, their extension, widening and further progress into adjoining regions in the hydrated cement matrix, and finally into the concrete mass. Figure 1.10 depicts the corresponding stress-strain response of the concrete in compression. Various stages shown in Fig. 1.11 are schematically depicted in the Fig. 1.10, by marking various key points, such as A, B, C, etc. on the curve.

When the stress level in the concrete specimen is raised from 30 to 50 % of the ultimate concrete compressive strength and is maintained between these two levels, the shape of the stress-strain response starts deviating from the linear-elastic response exhibited earlier. This deviation in the stress-strain response can be attributed to the extension of the existing cracks in the interfacial transition zone to the adjoining mortar matrix under the increasing stress level. And, when it reaches about 75 % of the ultimate concrete compressive strength (the stage C; Figs. 1.10 and 1.11), the available internal energy in the system exceeds the crack-release energy required to initiate the cracking. This process results in a rapid growth of the cracks and subsequently, leads to the unstable propagation of the cracks into the adjoining areas of the concrete specimen. The stress level corresponding to this stage is called as *critical stress*. At this stress level, the concrete possess a highest ever volumetric strain and a slight increase in the magnitude of the stress beyond this point results in a reversal of the direction of the volumetric change. It is accompanied by a sudden volumetric expansion of the concrete specimens, followed by its crushing. It generally happens at a stress level near or at the peak value of the compressive strength exhibited by the concrete.

The concrete stress-strain response shows a gradual increase in curvature when it is stressed gradually from 75 % of the ultimate concrete compressive strength to its 90 % stress level (the stages D to F; Figs. 1.10 and 1.11), and thenceforth, it bends sharply and, finally, descends until the specimen is broken down. This point defines the ultimate compressive strength of the concrete specimen. The value of the



◀ **Fig. 1.11 Concrete behavior under stress**—The figure schematically shows a progressive development of the microcracks already existing in the interfacial transition zone in the concrete (a and b), their extension (c), widening and further progress into the adjoining areas in the concrete (d–f). A very thin layer of separation around the surface of the coarse aggregates in concrete exists from the day one after its casting. Figure 1.11 (a and b) schematically shows a very thin layer of discontinuity (ITZ) at the surface of coarse aggregates (also, see Fig. 1.8). It is approximately 10–50  $\mu\text{m}$  in thickness, mostly invisible to the bare eye. When the concrete is stressed to about 30 % of its ultimate compressive strength, these microcracks extend and widen in thickness, but remains confined to the ITZ (c). Concrete exhibits a near linear-elastic response under compression (also, see Fig. 1.10). And, when it is stressed to a level of 30–50 % of the ultimate concrete compressive strength, the cracks start extending to the adjoining mortar, but remains stable (d) and the concrete response starts deviating from the linear one, exhibited earlier. At a stress level of 75 % of the ultimate strength; these cracks grow, further widen, and progress into the mortar matrix with a release of the energy in excess of the crack-release energy of the concrete (e). At this stage, the concrete possesses a maximum value of the volumetric strain. Thereafter, it generally fails to support any further loading and is accompanied by the strain softening response

crushing strain remains more or less same for all types of concrete, whether a normal or the high strength concrete. However, the shape of the stress-strain curve becomes steeper around a strain value of 0.002 as the grade of the concrete (representing its characteristics compressive strength) is improved, for instance from M25 to M30, and so on.

Unlike the concrete subjected to the compressive stresses, the cracks present in the interfacial transition zone and the mortar matrix grow and extend rapidly to the adjoining areas in the concrete, when subjected to the tensile stresses and thereby leading to a sudden failure of the concrete [Shah and Sankar (1987)]. It is observed that by and large, the ratio of the uniaxial concrete tensile strength and its compressive strength ranges from 6 to 12 %. Accordingly, most of the concrete elements in practice are designed under the assumption that the concrete would resist the compressive stresses arising in the member and the tensile stresses are either taken care of by some external means, like reinforcing it with a material having a high tensile strength, such as steel rebars, etc. provided in the identified tensile zones of the member; or by using and mixing discrete steel and/or synthetic fibers randomly but uniformly in the concrete mass; or by pre-stressing the member using tendons at some designated locations along its length that neutralizes the affect of the tensile stresses arising on account of the external loading, etc. in the structural member.

Out of these techniques, reinforcing the tensile zone of the concrete members using conventional longitudinal rebars and employing high strength steel cables/tendons for pre-stressing purpose have been standardised and codified in the past by different bodies, such as ACI 318 (2008), IS 456 (2000), etc. for ensuring a uniform design practice across different designers, despite the fact that the use of fibers as a reinforcing material was explored much earlier than the other techniques; but somehow, their routine use in various applications did not become widespread. However, the recent developments in the fiber reinforcement technology, the material models, the testing methods and understanding of the mechanics behind the strength improvement exhibited by the concrete containing fibers have given a big boost to the use of material for various structural applications in recent years.

## 1.5 Fiber Reinforced Concrete

The use of fibers in the (lime) concrete as a reinforcing medium is the earliest known technique. The fibers in various forms, such as natural fibers, etc. were primarily used to increase the load carrying capacity of members. Their use dates back to the Roman period (300 BC–476 AD), wherein the ancient concrete was found to contain fibers. Straw reinforced mud bricks were found at a number of ancient sites in the Middle East dated back to approximately 10,000 years ago. The indigenous inhabitants in the USA were using the sun dried adobe bricks, believed to be made using a mixture of sand, clay and the straw.

In recent years, the first patent for the fiber reinforced concrete was filed in California (1874) by A. Bernard. A patent by H. Alfson in France (1918) was followed by G.C. Martin in California (1927) for the pipes manufactured using the steel fiber reinforced concrete. A process was patented by H. Etheridge (1931) regarding the use of the steel rings to address the anchorage of steel fibers. The widespread applications of the material in the routine construction practice however were hindered by their high costs, poor testing facilities and most importantly, the rapid parallel development of using concrete reinforced with the steel bars and cables. It was not until the experiments of James Romualdi (1962) that a clearer understanding of properties of the steel fiber reinforced concrete (SFRC) emerged. The development of SFRC continues and in more recent years, extensive research efforts in this direction are aimed to frame guidelines regarding the testing and design methods using the steel fibers alone or along with the synthetic fibers. The following section briefly describes the established reinforcing mechanism of the steel fibers in concrete.

It is well known that concrete is a quasi-brittle material with a low strain capacity, especially under the tensile stress conditions. The presence of the cracks both in the interfacial transition zone and the mortar matrix of concrete is a single most factor responsible for the insignificant tensile strength exhibited by it. Figure 1.11 presents, schematically, the development and the transformation of the microcracks existing in the transition zone of the concrete into a system of major cracks that led to the strain softening behavior at higher strains and finally, the failure of the concrete when it is stressed to about 90 % of its ultimate compressive strength. However, it is an established fact by now that when the short and discrete fibers are mixed into the concrete randomly, but uniformly, throughout the concrete mass, it exhibits a better performance not only under static and quasi-statically applied loads, but also under fatigue, shock, and impulsive loadings. These fibers are found to be more effective when the tensile strength of the fibers used in the concrete mix is comparable to the mortar matrix strength. It is reported that the short and discrete steel fibers are more effective in improving the brittle characteristics of the concrete than the synthetic fibers, etc. The random orientation and presence of the steel fibers throughout the concrete mass is a main contributor to the strength enhancement exhibited by the concrete in its hardened state.

When the short steel fibers are mixed in the concrete, these occupy the inter-particle spaces existing around coarse aggregates along with the hydrated cement paste. Figure 1.12 depicts a typical random distribution of the steel fibers in the concrete mix. Mostly, they surround a bulk of the coarse aggregates present in the mix and their distribution in the mortar matrix is generally observed to be random in nature.

This randomness of the fibers around coarse aggregates forms a web-like structural system around these aggregates, similar to a space truss, with these fibers acting as ties and the mortar matrix as their struts. The fibers embedded in the mortar matrix carries the tensile forces induced in the system; whereas, the concrete matrix carries compression as well as distributes and transfers the internal tensile forces to the fibers embedded in the concrete.

The enhancement in the mechanical properties of the concrete because of the fiber mixing can be attributed mainly to their localized reinforcing capability, as their presence in the mortar matrix around coarse aggregates in the concrete arrests the opening, widening and later on, extension of the microcracks already existing therein to adjoining areas in the concrete mass. Because of this, unlike the conventional concrete, the concrete prepared using randomly dispersed fibers at the time of mixing exhibits enhanced straining capacity, both under the tensile as well as compressive stresses, along with a significant value of the residual tensile



**Fig. 1.12** *Steel fiber reinforced concrete*—The short, discrete fibers (shown by the *dark lines*) are randomly dispersed in the concrete at the time of mixing and are present throughout the hydrated cement mortar in the mix. These fiber forms a spatial network around coarse aggregates; wherein, fibers act as ties of imaginary ‘space trusses’ and the mortar mix carries the compression, and also providing anchorage to the fibers. The interfacial transition zone (ITZ) in the concrete, which, otherwise controls the concrete strength properties becomes able to transfer the stresses across the line of discontinuities formed around coarse aggregates by this zone. It also prevents the extension, widening and progress of the microcracks already existing in the ITZ into the adjoining regions in the mortar and their further development in the concrete. The presence of the fibers significantly improves the quasi-brittle characteristics and tensile straining capability of the concrete



strength. Nevertheless, the tension straining capacity of the concrete is increased many times than its crushing strain by the fiber inclusion in the concrete mix.

The fibers present in the concrete does not arrest the formation of the microcracks in the interfacial transition zone and neither they are active till a stress level causing extension of the microcracks in the interfacial transition zone to the mortar matrix (Fig. 1.11c). Therefore, the concrete with and without the randomly dispersed steel fibers exhibits nearly an identical value of the first crack strength (both, for the direct tension and flexural strength). The fibers in the concrete actively participate in arresting the extension of the microcracks existing in the interfacial transition zone, their widening and their further progress into the mortar matrix after the formation of a first crack in the concrete. The internal cracking do occur similar to the normal concrete as shown in Fig. 1.11d–f, but their further progress from one aggregate to the adjoining one through the mortar matrix is significantly delayed by the presence of the steel fibers in the concrete mix. Because of their high tensile strength and anchorage into the mortar matrix, the fibers transfer the internal tensile stresses, induced in the concrete by virtue of the *Poisson's effect* and otherwise also, across the cracks developed in the concrete. This phenomenon significantly improves the ultimate crushing strain of the concrete from a normal value of 0.0035 to a value as high as 0.006, although its ultimate compressive strength increases marginally by this fiber inclusion in the concrete mass.

It is reported that the bond/pullout resistance, strength properties of the fibers and the mortar matrix play a substantial role in controlling the post-cracking behavior of the fiber reinforced concrete members. Because the strength mobilized in the fibers at various stress levels depends entirely on the pullout resistance of the fibers in the concrete and their mechanical properties.

The pullout behavior which is an indirect measure of the fiber slip, the fiber elongation and the fiber strengthening in the concrete is associated with three bond mechanisms, namely: (1) adhesion, (2) friction, and (3) mechanical anchorage. It is reported that the fiber embedment length into the mortar matrix, the fiber aspect ratio and their orientation with respect to the loading direction and the matrix strength greatly influences the pullout response of fibers. Nevertheless, the addition of the short steel fibers to the matrix also leads to an anisotropic behavior owing to their random distribution and orientation in the concrete. But, when the alignment of the fibers coincides with the principal stress in a flexural member, the contribution of the fibers to the material strength is more pronounced than otherwise is the case, because the alignment of the fibers along the direction of principal stress in the concrete bridges the crack surfaces effectively than otherwise. As the steel fibers possess much higher tensile strength and the elastic modulus than the synthetic fibers, they are found to be more effective in sharing the tensile forces in the mortar matrix and their further transmission to the adjoining concrete volume than the synthetic fibers.

Unlike the concrete with the steel fibers, the low elastic modulus of synthetic fibers did not allow them to form an efficient web-like structural system around coarse aggregates in the hardened concrete and consequently, they contribute less towards improving the post-cracking behavior of the member. This is the main

reason for a widespread use of the steel fibers in the practice over the synthetic fibers. However, the experimental investigation in recent years has established an innovative and efficient use of concrete manufactured by using both the steel fibers as well as synthetic fibers; wherein, the steel fibers in the concrete controls its residual tensile strength and the synthetic fibers controls the response of members near the peak load, permeability characteristics and its corrosion resistance.

Theoretically, it is better to provide steel fiber concrete only in the tensile zone of the member, but practically, it is a very cumbersome activity to do so. Using steel fiber concrete in the entire section of the member generally leads to an increased consumption of steel fibers in the member for a given moment demand of the member as the steel fibers are present both in the compression as well as the tensile zone of the member, but their full contribution towards the flexural strength augmentation can be realized only by providing them in the tensile zone; wherein, the fibers contribute maximum in increasing the concrete tensile straining capacity and the residual tensile strength. This fiber addition in the compression zone of the member gives negligible enhancement in the concrete compressive strength and the crushing strain in comparison to a significant enhancement in the residual tensile strength and the post cracking behavior.

It is important to note that the uniform presence of steel fibers in the entire concrete section also results in improvement in the material flexural strength, shear strength, impact and fatigue strength. As the fibers are short, discontinuous, and they rarely touch each other in the concrete mass, there exists no continuous conductive path for stray or induced currents or currents from electromotive potential between different areas of the concrete. This aspect of the SFRC also reduces, significantly, the corrosion potential in the sections made up of this material. Experience to date has shown that if a concrete is well compacted, and complies with the provisions of the design codes, such as ACI 318 (2008), BIS 10262, etc for the water-cement ratio, and then corrosion resistance of the fibers remains limited to surface skin of the concrete member only. This limited surface corrosion seems to exist even when the concrete specimens are placed in a highly saturated solution of chloride ions.

The research efforts in the past have now been consolidated in the form of guidelines with regards to the fiber specifications, its mixing in the concrete mix; methods of testing; constitutive laws and design guidelines. Nevertheless, guaranteeing the quality and performance of the steel fibers, and finally the steel fiber reinforced concrete (SFRC), is critical and the challenge confronted by engineers involved in the execution of projects using the SFRC is to unambiguously define the performance needed by the concrete so as to achieve the finished structure the operation that was assumed in design. The recent developments in control methods and techniques to get the content and the orientation of steel fibers in the concrete mix have given a big impetus to the use of SFRC in its structural applications with a confidence. A number of test methods have been developed in this regards using magnetic induction based methods and are used successfully in a number of projects. The Chap. 2 presents the details of various constitutive models developed for the SFRC so far in compression and tension.

## 1.6 Conventional Reinforced Concrete

Unlike steel fiber reinforced concrete section (SFRC), the concrete member with a conventional reinforcement generally uses a material having a high tensile strength, like steel, etc. in its identified tensile zone to meet the moment-demand. This type of reinforcement provided in the member is called as *rebars*. Unlike the SFRC, the brittle characteristics of concrete are not improved upon by this inclusion, but the overall flexural response of the concrete section transforms from a brittle to ductile one depending upon the percentage of the steel provided in the section. The short and discrete steel fibers are mixed in the concrete at the time of mixing and are present uniformly throughout the concrete volume in case of the SFRC; whereas, the rebars are provided continuously in an identified tensile zone of conventional flexural concrete members. The tensile zone exists below the neutral axis of a simply supported beam under the gravity loading conditions. In case of a continuous/redundant beam, the tensile zone exists above the neutral axis over the supports and it is below the neutral axis near the mid spans of the beam. The rebars function similar to the steel fibers used in the concrete in case of the SFRC. The rebars embedded in the concrete carries the tensile forces induced in the member through various bond mechanisms; whereas, the concrete matrix carries the compression as well as distributes and transfers the internal tensile forces to the rebars, which because of their high tensile strength provide the requisite tensile force in the section to meet the imposed moment demand in conjunction with the compressive force being mobilized in the concrete above the member neutral axis.

Unlike the SFRC members, the truss-action exists in the conventionally reinforced concrete members at the global level; wherein the concrete in the section simulates itself as struts of an imaginary truss system developed in the concrete flexural member, and the rebars present in the tensile zone of the member as its lower/tension chord members. This has been depicted in Fig. 1.13. In case of the SFRC, same sort of the truss mechanism operates at the local level, around coarse aggregates present in the hardened concrete because of the formation of a space-truss like structural system by the randomly present steel fibers in the concrete that act as ties an imaginary truss-systems and the hydrated mortar matrix in

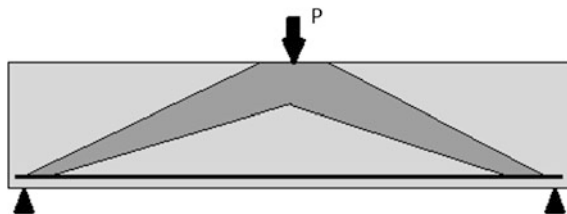


**Fig. 1.13** Truss-action mobilised in a RC beam—The concrete present in a RC beam simulates itself as struts (shown by a dark shaded area) of an imaginary truss system, generally between the two adjacent diagonal cracks, and the longitudinal rebars present in the tensile zone of the member as tension chord members

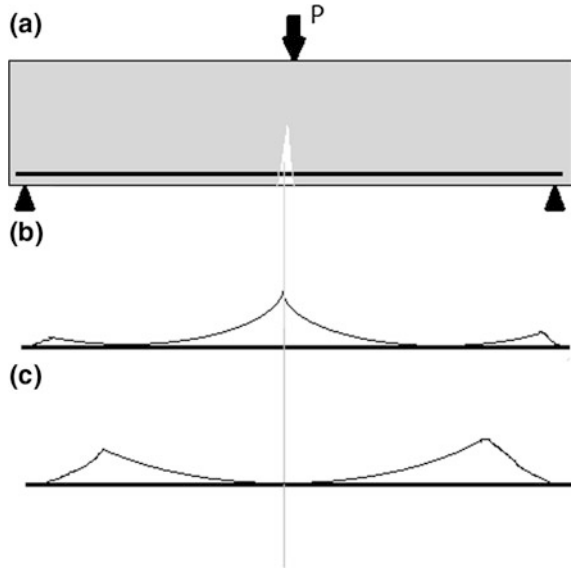
the concrete as their struts. Because of the existence of a truss-action in the conventional reinforced flexural members, these are able to transfer the applied loads to their support system. The continuous reinforcing bars in the concrete member placed on its tensile face provide the requisite tensile force needed to ensure the equilibrium.

The tensile stresses are induced below the neutral axis of flexural members under the gravity loading conditions. Once the internal energy stored in the member because of external loading exceeds the crack-release energy of the concrete, cracks start developing rapidly in the concrete. The prevailing tensile-strain conditions below the neutral axis of the member further exaggerate the problem. It leads to the failure of the member abruptly with the formation of the flexural tensile cracks unless it is reinforced suitably by some external means. The rebars provided in the tensile zone of the member take up the tensile forces through various bond mechanisms *viz.*: chemical adhesion, frictional resistance, mechanical interlock, etc. and subsequently, these rebars prevent the widening, and extension of the cracks towards the neutral-axis of the member under increasing load. If the bond between the rebars and the concrete became inadequate because of any reasons; it results in slippage of the rebars and leads to redistribution of the stresses in the member. It is generally accompanied by the crack formation in the tensile zone of the member.

At the flexural crack location, the tension is carried by the rebars alone; whereas in between the cracks, the concrete carries some tension depending upon the strain value; thereby relieving, though partially, the tension in the rebars present in the uncracked part of the concrete in between the adjacent flexural cracks formed in the member. The contribution of the concrete in the stress-sharing along with the uncracked concrete lying in between the adjacent cracks in a flexural member is known as tension-stiffening. This phenomenon has a significant effect on the effective member stiffness and also results in the fluctuation of the bond stress along the rebar length. Figure 1.14 depicts a reinforced concrete beam along with a typical profile of the stresses, *viz.* the tension and the bond stress, developed along the length of the tensile reinforcing bar embedded in its tensile zone. It is worth to note that the magnitude of the tensile force being developed in the member is highest at the location of the crack and this force, subsequently, gets transferred to the concrete surrounding the rebars in the tension zone of the member through various bond mechanisms. Figure 1.14c depicts a typical variation of the bond stress mobilised along the length of the rebars.

Unlike the SFRC sections, the concrete sections having a conventional longitudinal tension reinforcing bars behave differently depending upon the percentage of steel provided in the section. The SFRC section fails once the strain on its tensile face reaches the critical strain value. Normally, the design value of a surface crack-width dictates the critical value of the tensile strain permitted for an SFRC section. The fiber parameters, namely volume fraction and fiber aspect ratio, along with the concrete strength controls the limiting value of the strain and the corresponding permitted value of the residual tensile strength of the SFRC. Nevertheless, the failure of SFRC section can be controlled by selecting an appropriate combination of the fiber parameters. It can fail following a desirable 'ductile' failure mode

**Fig. 1.14** Schematic representation of the stress mobilisation in a typical rebar of RC member—**a** A typical flexural crack developed at the point of maximum moment in the RC beam; **b** mobilisation of the tensile stress along the length of a rebar and **c** the bond stress mobilized along the length of rebar after the formation of the crack in the RC member



or in a brittle mode of failure through fiber fracturing. In both cases, the failure always occurs with respect to the tension. However, in case of the reinforced concrete (RC) sections, the failure always occurs with respect to the compression, generally by crushing of the concrete. However, it is important to note that the section can be designed to fail either through yielding of the rebars or through the crushing of the concrete by appropriate selection of the reinforcement. But in the former case, the failure finally occurs through concrete crushing taking place in the region of maximum moments. In this case, the percentage of rebar area plays a crucial role in controlling the failure mode. When it is kept less than the critical value, the section fails in a ductile manner; otherwise, it occurs abruptly once the strain in the compressive face of the section reaches the concrete crushing strain ( $\approx 0.0035$ ). The beam in the former case is called as an under-reinforced section and in the latter case; it is called as an over-reinforced section. The critical value of the longitudinal tensile steel area that distinguishes these two states is known as the balanced-state and the area of the longitudinal tensile steel provided to achieve this state is a balance-state percentage tensile area.

When the section is reinforced with a longitudinal steel area equal to that required in its balanced state, the strain in the compression face of the member reaches its limiting value simultaneously as the strain in the rebars provided in the tension zone of the beam approaches its yield strain. The failure of such a section occurs by simultaneous initiation of the concrete crushing and the yielding of the longitudinal tensile reinforcement in the section. Whereas, in case of an under-reinforced RC section, a slight increase in the moment causes the rebars to yield and these elongate significantly without any increase in stress. The marked increase in the tensile strain causes the neutral axis in the section to shift upwards,

thereby causing a reduction of the concrete area in compression. As the total tensile force below the neutral axis remains constant at its peak value ( $=A_{st} f_y$ ), therefore in order to maintain the equilibrium, the stress in the concrete starts increasing. Once it touches the material ultimate strength, crushing of the concrete at the extreme compression face of the section occurs. Simultaneously, this process is accompanied by the formation of wider and deeper flexural cracks in the section along with an increase in the beam curvature and the corresponding deflections. It is to be noted that the corresponding increase in the moment capacity of the section in this process is marginal, being attributed only to a small increase in the lever arm that occurs because of an upward shifting of the neutral axis in the section.

Although the RC beam section is able to maintain the equilibrium by mobilizing the strength of the rebars and the concrete strength, but the high value of the strain prevailing at the rebar level in case of under-reinforced sections fails to prevent the opening and extension of the microcracks in the concrete; their subsequent widening and further progress to the relatively less strained area of the concrete. These microcracks originating at different interfacial transition zones in the concrete volume finally join each other and led to the formation of flexural cracks on the tensile face of the RC member. Nevertheless, it normally happens at the point of the maximum bending moment in the member.

Unlike the under-reinforced RC sections, the beam with a longitudinal tensile steel area more than the tensile steel area required for the balanced-state area undergoes relatively less straining of its tensile face and this, consequently, exhibits less cracking. Nevertheless, the member undergoes an abrupt brittle failure when the strain on its compression face reaches the limiting strain value. This type of failure is termed as 'compression failure'. As the limit state of collapse reached in an over-reinforced beam, because of a higher tensile steel area (more than the balanced-state area) in the section, the stress in longitudinal rebars remains more or less in the elastic range throughout the loading history and it increases proportional to the strain prevailing in the section; whereas, the stress in the concrete did not follow a similar trend owing to the material nonlinearity exhibited by the concrete at a strain value higher than 0.002. Therefore, in order to maintain the equilibrium, the concrete area under the compression has to increase, and that happens by lowering of the neutral axis in the section as the section tries to maintain the equilibrium. Unlike a under-reinforced sections, the 'distress signals' in the over-reinforced beam sections like cracks, curvature and deflections remains silent right up to the failure. Low strain values in the section are responsible for a silent nature of the section failure and simultaneously, it results in a section with inherently low ductility. Because of this, the concrete beams having a conventional tension steel area more than a value required to achieve the balanced-state conditions are always avoided in the practice. The mathematical models for proportioning RC beams have been developed and these are well documented in the published literature. The reader is advised to refer to the standard texts in this regards.

## References

- American Concrete Institute (ACI) (2008) Building code requirements for reinforced concrete. ACI Standard 318-08, Detroit
- Bentur A, Alexander MG (1995) A review of the work of the RILEM TC 159-ETC: engineering of the interfacial transition zone in cementitious composites. *Mater Struct* 33(2):82–87
- Bureau of Indian Standards (BIS) (2000) Plain and reinforced concrete—code of practice. IS 456 (4th rev.), New Delhi, India.
- Hsu TTC, Slate FO (1963) Tensile bond strength between aggregate and cement paste or mortar. *J Am Concr Inst Proc* 60(4):465–486
- Hsu TTC, Slate FO, Sturman GM, Winter G (1963) Microcracking of plain concrete and the shape of the stress-strain curve. *J Am Concr Inst Proc* 209–224
- Maso JC (1996) Interfacial transition zone in concrete, RILEM report 11. E & FN Spon, London
- Shah SP, Sankar R (1987) Internal cracking and strain softening response of concrete under uniaxial compression. *ACI Mater J* 84(3):200

## Chapter 2

# Material Models

Concrete is a quasi-brittle material and it possesses a low tensile strain capacity. Though it exhibits a good compressive strength and a significant crushing strain value, but the presence of the microcracks in the interfacial transition zone and the mortar matrix reduces its tensile strength virtually to a zero. When the compressive stress in the concrete specimen reaches the threshold limit (about 75 % of the concrete compressive strength), the concrete undergoes dilation and exhibits a strain softening after reaching the peak/ultimate strength. However, the brittle characteristics of the concrete can be improved considerably by using and dispersing the short and discrete fibers, uniformly, throughout the concrete mass at the time of mixing. The concrete reinforced internally by means of the short and discrete steel fibers is called as steel fiber reinforced concrete (SFRC). It is an experimentally established fact that the concrete after the addition of steel fibers exhibits a better performance not only under static and quasi-statically applied loads, but also under fatigue, shock, and impulsive loadings (ACI 1993; Robins et al. 2002; Barros et al. 2005; Marco et al. 2009; Chalioris 2013; Singh 2015). Nevertheless, the random presence of the steel fibers, *albeit* uniformly, throughout the concrete mix and their relatively higher tensile strength in comparison to the hydrated cement paste in the concrete is a main contributor to the strength enhancement exhibited by the SFRC. The Chap. 1 described the microstructure of the concrete along with various factors that affect it and explains how it plays an important role in controlling the stress-strain response of the concrete under a tension and compressive type of loading. The stability of the concrete macrostructure and the consequential improvement in various concrete properties that the inclusion of the fibers in the mix would bring in was also described. The present chapter discusses various models developed to simulate the compression and tensile behavior of the SFRC. It also presents a forward analysis approach to determine the value of the fiber parameters ( $l/d$  and  $V_f$ ) and the concrete grade required to achieve a desired value of the residual-tensile strength value of SFRC.



## 2.1 SFRC Constitutive Models

A constitutive model is a set of expressions that describe the response of a material when it is stressed, externally or internally. These expressions constitute an essential component of analysis models to predict the member response under different loading conditions. A number of constitutive models have been proposed by different researchers in the recent past. The most prominent among them are those proposed by Mohamed and Victor (1994), RILEM (2002), Barros et al. (2005), Soranakom and Mobasher (2007, 2009), Chalioris (2013). These models are used to develop various design methods for proportioning SFRC beams, but are convenient to use only in cases when limited tensile parameters are known as a prerequisite or at the start of the analysis. Because most of these models rely heavily on the tensile stress distributions determined through the experimental testing of the standard test specimens or some empirical expressions. The design procedures so developed always possess inherent flaws on account of the assumptions taken while developing the empirical relations or testing procedures. Generally, a fixed rectangular stress distribution for the compression block is used in some of the existing models that do not allow the designer to use a particular stress–strain distribution when the failure is reached before the ultimate compressive stress is reached in the concrete. However, the model proposed by Singh (2015) is more systematic and easier to use in the analysis and design of SFRC sections than the previous models. It requires various fiber parameters, such as aspect ratio ( $l/d$ ), volume fraction ( $V_f$ ), fiber shape and the characteristics compressive strength of the concrete to determine analytically the residual tensile strength of SFRC unlike previous models that requires input from experimental investigations to start the analysis. The following sections present the details of the compression and the tension constitutive material model of SFRC.

### 2.1.1 Compressive Model

Concrete being a heterogeneous material is not able to provide a resistance to the tensile forces, although it exhibits a significant strength in compression. Concrete's inability to provide resistance to tensile forces is mainly due to the existence of a weak interfacial transition zone around coarse aggregates present in the concrete mass. The interfacial transition zone in concrete acts as a bridge between the coarse aggregates and the surrounding hydrated cement paste (mortar matrix) in concrete and is an only medium to transfer the stresses across different phases of the concrete. The presence of voids and other microcracks in the interfacial transition zone do not permit an effective stress transfer across its thickness and, thereby, leads to the reduction in the load carrying capacity of the concrete irrespective of the load type. However, a significant improvement in the post-peak compressive behavior is reported in the published literature when short fibers are randomly mixed in the

concrete mass, although the peak compressive strength of the concrete is marginally increased by the fiber inclusion in the mix (ACI 1993; Mohamed and Victor 1994; Robert et al. 1987; Lini et al. 1998; Marco et al. 2009; Kang 2011; Michels et al. 2013).

The contribution of fibers is most apparent in the post-peak region in the case of the SFRC, where the response is described by a relatively less steep decaying stress-strain response. Once the matrix cracks under induced tension, the debonding and pulling out of the fibers from the concrete dissipates energy, thereby, leading to a substantial increase in the post-cracking characteristics. Figure 2.1 shows a typical stress-strain response exhibited by SFRC specimen in compression when it is reinforced by the steel fibers with different aspect ratio.

Similar to the normal concrete, the SFRC exhibits a linear-elastic behavior up to a stress level of 30 % of the ultimate concrete strength in compression. At this stage, the internal microstructure of the concrete remains more or less stable. However, when the stress level in the specimen is increased gradually to 50 % of the ultimate concrete compressive strength, the stress-strain response starts deviating from the linearity. The initiation of the nonlinearity in the response of the concrete specimen mainly happens because of the internal extension of the microcracks present in the interfacial transition zone of the concrete to the adjoining regions.

After reaching a stress level of 50 % of the ultimate concrete compressive strength, the steel fibers present in the concrete matrix get activated and delays the extension of the microcracks in the interfacial transition zone to the surrounding mortar matrix. This all happens because of the local reinforcing capability of the steel fibers which arrests the crack widening due to their anchorage into the hydrated cement paste adjoining to the coarse aggregates. However, its effect on the

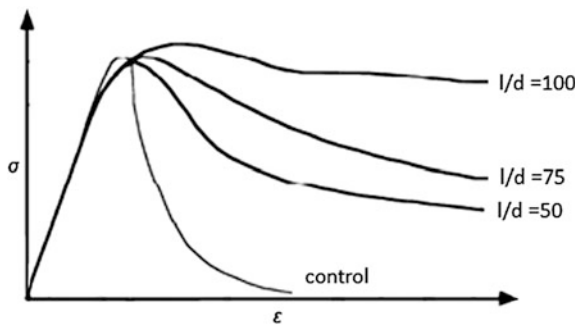


**Fig. 2.1** A typical stress–strain response of SFRC under compressive—The local reinforcing capability of steel fibers present in the mortar matrix and the web-like structural network formed by these fibers around the surfaces of coarse particles in the mix significantly enhances the post-cracking characteristics of the concrete. The extent of improvement depends upon the fiber parameters considered in the mix *viz.*: the fiber aspect ratio ( $l/d$ ) and the volume fraction ( $V_f$ ). Higher the value of the fiber parameters ( $V_f$  or  $l/d$ ) adopted in the design more is the improvement in the post-peak characteristics of the SFRC

shape of the compression stress-strain response remains insignificant and in the pre-cracking stage, therefore, the stress-strain response exhibited by the plain concrete can be used as such in the design, etc. without affecting the final results.

The effect of the steel fibers become significant and visible on the stress-strain response only after the stress level in the specimen is increased beyond the threshold level of a normal concrete i.e. 70 % of the ultimate concrete compressive strength. At this stage, the tensile strength of the fibers surrounding coarse aggregates in the concrete mobilizes and prevents the extension, and widening of the microcracks existing in the interfacial transition zone and their subsequent progress to the adjoining regions of the hardened concrete. This phenomenon considerably improves the post-cracking behavior of the SFRC.

It is reported that SFRC is able to sustain a compressive strain value of 0.005–0.009 on failure and the corresponding failure stress improves to about  $0.95\sigma_{cu}$  from a value of  $0.85\sigma_{cu}$  taken for a normal concrete, where  $\sigma_{cu}$  is concrete cylinder strength. This value of the concrete strength works out to be 0.75 times the cube compressive strength. The strength of concrete is a maximum load attained during the loading process under uniaxial compression conditions and it is determined as per the provisions of IS 516 (1959) wherein; 150 mm standard cubes are tested in the strain-controlled loading after 28 days of the water curing period. The prescribed uniform strain rate for the testing is 0.001 mm/mm per minute. As the concrete exhibits considerable variation in the test results, it must be reported as a characteristic (5-percentile) and mean values; normally, expressed as the concrete characteristics compressive strength ( $f_{ck}$ ).

The design compressive stress of SFRC, therefore, can be adopted as  $0.5f_{ck}$  by applying a partial safety factor of 1.5 to the stress value of  $0.75f_{ck}$ , where the  $f_{ck}$  is the characteristic compressive strength of the concrete. The maximum value of the stress is reached at a strain approximately equal to 0.002 similar to the plain concrete and thereafter; an increase of the strain is accompanied by a drop of the stress. Nevertheless, the rate of drop of the compressive strength of SFRC in the post-peak range is relatively smaller than the plain concrete. Equation 2.1 gives the design compressive stress ( $f_c$ ) of SFRC corresponding to any strain value  $\epsilon$ ,  $<0.004$ . The design value of the strain for SFRC in compression is 0.004.

$$f_c = \begin{cases} 0.5f_{ck} \left[ 2 \left( \frac{\epsilon}{0.002} \right) - \left( \frac{\epsilon}{0.002} \right)^2 \right], & \epsilon < 0.002 \\ 0.5f_{ck} & 0.002 \leq \epsilon \leq 0.004 \end{cases} \quad (2.1)$$

### 2.1.2 Tension Model

Concrete is not normally designed to resist direct tension due to its low tensile strain capacity. However, tensile stresses do develop in concrete members as a result of flexure and/or principle tensile stresses arising in the member from a multi-axial state of stress caused by external loading. For any structural member, therefore, it is

mandatory to possess adequate compressive as well as tensile strength to perform satisfactorily.

The low tensile strength of concrete is due to the presence of a weaker zone of separation—interfacial transition zone—mainly around coarse aggregates at their interface with the surrounding hydrated cement matrix. The microcracks in the interfacial transition zone propagate rapidly under tension and that happens at a much lower stress level in comparison to the case where the load is compressive in nature. Concrete cracks once the strain (longitudinal or lateral strain arising from Poisson's effect) exceeds its limiting tensile strain capacity. Once that happens, the subsequent concrete failure is brittle in nature and it occurs abruptly within no times. The value of the limiting tensile strain in concrete is reported to range from 0.0001 to 0.0002. The value of the cracking tensile strength for the SFRC can be taken similar to the value  $[=0.7\sqrt{f_{ck}}$  in MPa] reported for the plain concrete, because the fibers in the SFRC activate only after the concrete cracks.

Unlike a plain concrete, the SFRC exhibits a significant residual-tensile strength because of the contribution of the fibers embedded in the hardened concrete, although its first cracking strength is almost same as that of a plain concrete. The SFRC member, however, during the loading process undergoes a considerable deformations and cracking before the failure. This all happens because of the fibers present uniformly in the concrete volume, almost in every possible direction that bridge the crack surfaces in the concrete member. But, this improved response exhibited by SFRC is greatly influenced by the amount of the fibers crossing the crack, their pullout behavior and the strength properties. The pullout behavior, which is an indirect measure of the fiber slip and the fiber elongation in the SFRC, is associated with the three identified bond mechanisms: namely, (1) adhesion, (2) friction, and (3) mechanical anchorage. It is an experimentally established fact that the fiber embedment length, the fiber orientation with respect to the loading direction and the matrix strength plays a significant role in defining the pullout response of the fibers embedded in the concrete (Kullaa 1992; Karayannis 2000; RILEM 2002; Gettu et al. 2005; Soranakom and Mobasher 2007, 2009; Hameed 2013; Michels et al. 2013). The fibers, usually, aligned in the direction of the loading are more effective in transferring the tensile force across the crack width than otherwise is the case. Fibers having an inclination of more than  $60^\circ$  contribute as little as 10 % of the case where these fibers are oriented along the loading axis.

This unique behavior exhibited by the SFRC permits an analyst to generate a stress-crack opening  $[\sigma-w]$  relationship and/or a stress-strain  $[\sigma-\epsilon]$  response for a SFRC member over a wide spectrum of the strain values and/or displacements. An  $\sigma-w$  relationship basically describes the stresses ( $\sigma$ ) carried by the steel fibers across a tension crack in the SFRC as a function of the crack-width/opening ( $w$ ). This procedure is known as 'fictitious crack approach' and was first suggested by Hillerborg et al. (1976). The fiber parameters ( $V_f$ ,  $l/d$  and the fiber shape) used in concrete mix play a significant role to the shape of an  $\sigma-w$  curve exhibited by SFRC. In addition, the casting process used to pour an SFRC into the moulds also has a considerable effect on orientation of the steel fibers in the member (Toutanji and Bayasi 1998; Swamy and Stavrides 1976; Stähli et al. 2007). In case, the fibers

get aligned along the tensile stress trajectories in the member during the pouring, these are more effective in transferring the stress across the cracked surfaces than otherwise would be the case. This generally happens near the surfaces of mould, where the steel fibers tend to align themselves parallel to the external surface of a mould. Studies on the fresh-state properties of SFRC in the past (Romualdi and Mandel 1964; Stroeven 1979; Soroushian and Lee 1990; Akkaya et al. 2000; Gettu et al. 2005; Dupont and Vandewalle 2005; Stähli et al. 2008) have confirmed this phenomenon, reported it as *wall-effect* in the published literature. Figure 2.2 schematically shows the wall-effect observed in the SFRC during the placement and compaction operations.

Two reasons have been identified for this preferential orientation of the steel fibers in the concrete—(a) the wall-effects that depend on the geometry of the formwork/mould; (b) the flow of concrete, which depends on the rheological properties of the material, the geometry of the formwork and the casting procedure. Because cementitious material flows only if a stress higher than a critical value is applied to ensure the movement of the concrete. The pumping force exerted to ensure the concrete movement tends to align the fibers in the direction of the flow. Even though the wall-effect has a local nature and it should not have a significant influence in the structural response of a big structural element, but the restrictions imposed by the rigid surfaces of the moulds can affect the post-cracking response of smaller specimens generally used in the laboratory testing. For example, Gettu et al. (2005), Torrents et al. (2012) have verified the wall-effect and observed a

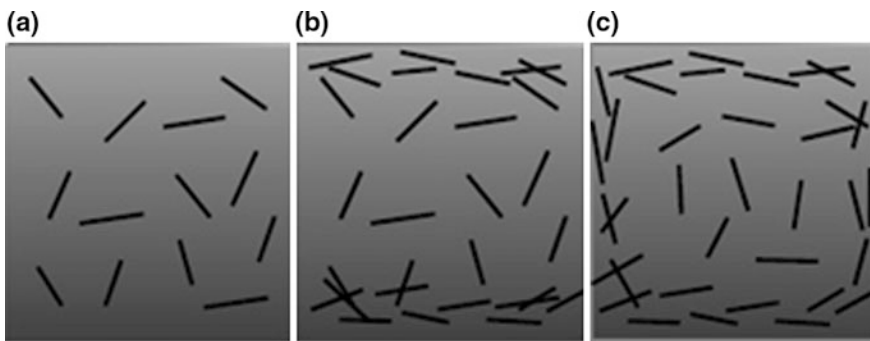


**Fig. 2.2** *Wall-effect*—The figure illustrates how the orientation of steel fibers in a concrete volume is affected by the presence of boundaries, e.g. surfaces of moulds, etc. If the SFRC is subjected to no restrictions, the fibers are distributed randomly and no preferential orientations occur (see **a**). This type of boundary free zone usually occurs in the middle part of beams, etc. However, if it is to be poured between two surfaces (top and bottom surfaces), shown in (**b**), the fibers near the boundaries will tend to align themselves parallel to the surfaces. This effect is more noticeable as the SFRC volume becomes exposed to more boundaries, as shown in (**c**). The **b** shows the beneficial effect of this phenomenon, especially for flexural members wherein the fibers oriented along the bottom (tensile) face are more effective in resisting the applied moments. Interestingly, the random presence of the fibers near the middle of the concrete volume (**a**) contributes towards the shear capacity of the section

preferential orientation of the steel fibers in the perpendicular plane to the casting direction caused by the vibration of the small beams ( $150 \times 150 \times 700$  mm).

Therefore, the tensile response of SFRC expressed either in the form of  $\sigma$ - $w$  (see Fig. 2.3) or  $\sigma$ - $\epsilon$  relationship (see Fig. 2.4) must be determined through an experimental testing that must take care of and consider all those factors that may affect the response at the time of their casting. It can be ensured by employing a pouring/casting method in the actual construction that is identical with the technique used while preparing the test specimens (prisms and tensile block). RILEM and other agencies has standardised the methods and procedure that require results of the uniaxial tensile test and the bending tests to determine the values of various key parameters to define a tensile-constitutive relationship of SFRC.

The stress-crack width [ $\sigma$ - $w$ ] response of SFRC specimen shown in Fig. 2.3 indicates that once the matrix fails in tension (end of the phase-1), it leads to the formation of a number of cracks in the concrete, though fine in crack-widths, but the fibers present there bridge the cracks and ensure transfer the tensile forces across the crack-width in the specimen. This composite action is responsible for sustenance of the load carrying capacity of SFRC, in the phase-2 of the response curve.

Figure 2.3 also depicts a typical phase-3 of the response exhibited by the SFRC that represents the strength contributed by the fibers alone in tension. Because of the wide cracks formed in this phase, the concrete did not contribute significantly towards the strength. Fibers crossing the crack try to stabilize the member by a

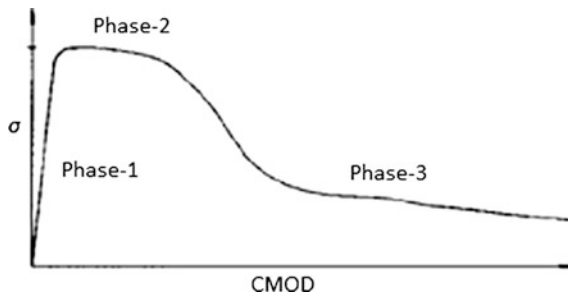


**Fig. 2.3** SFRC stress-crack width ( $\sigma$ - $w$ ) response in tension—The local reinforcing capability of steel fibers present in the mortar matrix depends entirely on their pullout response. The uncracked response shown in the phase-1 in the figure is always elastic-linear in nature. The fibers in hardened concrete get activated only after the formation of the cracks in the member (phase-2). Once that happens, the concrete residual strength in this phase is coming from the composite action that exists between the concrete and the fibers. The crack-mouth-opening-displacement (CMOD) continuously increases with almost at a constant stress level exhibited by the SFRC member. The crack width is usually very fine in the phase-2 that increases at a rapid rate at the end of the phase, followed by a further increase in the crack widths, but that is generally accompanied by a stress reduction phenomenon. Usually, the crack width of already developed cracks in the specimen increases in the phase-2 with a formation of new ones. The phase-3 in the figure shows the contribution of the fibers alone that are anchored into the hydrated cement matrix in the concrete, in the load sharing at the end of the phase-2. The cracks then become wide enough to cause a drop in the strength exhibited by SFRC

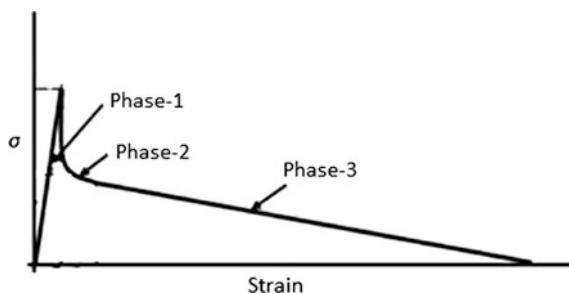


**Fig. 2.4** A typical stress-strain response of SFRC in tension—A drop-down response exhibited by SFRC in tension, i.e. linear-elastic up to the first cracking, followed by a sudden drop of strength in the post-cracking range which, later on, diminishes to zero at very high strain, usually at 0.04

variety of bond mechanisms. During this process, a number of new cracks also form in the concrete and those already developed in the SFRC grow continuously and widen under the increasing load.

During the third phase, however, the SFRC exhibits a reduction in the load carrying capacity. Generally, the fibers in the concrete start pulling-out from the matrix and/or fracturing depending upon the fiber-type, their aspect-ratio and the volume-fraction used in the mix. It eventually leads to the failure of the member once the applied load exceeds the tensile strength contributed by the fibers. It can occur in the fiber-pullout mode or fiber-fracture mode depending upon the fiber aspect ratio. The failure in the fiber pullout mode is always ductile in nature; whereas it occurs abruptly in case of a fiber fracture mode. It must therefore be avoided to occur by an appropriate selection of the fiber aspect ratio in the concrete mix.

The Fig. 2.4 shows a typical stress-strain ( $\sigma$ - $\epsilon$ ) response exhibited by SFRC in tension. Like the stress crack-width response [ $\sigma$ - $w$ ], it also consists of three parts, denoting a contribution from the concrete alone (phase-1), initiation of a composite action; wherein, the mortar matrix and the steel fibers embedded in it are providing the requisite resistance (phase-2) and followed by the contribution from the steel fibres alone (phase-3).

In the phase-1, the tensile stress-strain ( $\sigma$ - $\epsilon$ ) response exhibited by SFRC is linear-elastic in nature and generally, no cracking occurs in the specimen. The geometry of fibers usually has no influence on the load-carrying capacity at this stage. The fibers virtually remain silent till the formation of the first crack in the specimen, which normally formed at a strain value of 0.00014. The maximum value of the tensile stress in the specimen therefore is only related to the strength exhibited by the concrete. The Hooks law governs the stress-strain response of SFRC in this phase. The strain value corresponding to the strength exhibited by the material can be determined from the concrete strength and its elastic modulus. The end of the phase-1 signifies the onset of cracking and activation of the fibers in the SFRC.

Cracking initiates in the concrete, in the phase-2, which results in a sharp drop in the stress value. It is generally accompanied by the first major deviation from the linearity of the stress-strain response exhibited by SFRC member. As the crack-width is usually fine in this phase, a composite action still exists between the steel fibers and the concrete. However, the composite action quickly vanishes as the new cracks form in the section and those already existing there have started widening under the increasing strain. By the end of phase-2, the cracks are well established and wide enough (0.1–0.2 mm) to cause a complete loss of the contribution from the concrete part. Most of the fibers in the SFRC have exceeded their peak loads at this stage and they begin to slip at more or less constant loads.

Phase-3 starts with the formation of a system of well-defined cracks in the concrete. The fibers resisting the openings, caused by the crack formation, are doing so primarily through the fiber-pullout. Naturally, not all fibers that cross the crack contribute towards the strength, since many of them are not sufficiently anchored in the adjoining mortar mix. This mainly happens due to the random orientation of the fibers in the concrete. It is also expected that the residual-tensile strength exhibited by SFRC at this stage should theoretically remain constant if all the fibers that cross the crack surface were aligned in the load direction. But as a substantial number of fibers are inclined due to their random presence in the mix, they will not contribute in a similar way as the fibers would do, which are aligned in the direction of loading. With the increasing crack opening, however, the contribution from the inclined fiber will also increase as they straighten themselves under the tensile stress in the member. This process results in the drop of the effective stress across the crack during the middle stage of phase-3. Eventually, with increasing crack opening, most fibers will pull out with no residual force. This usually happens after a strain of 0.040.

A typical stress-crack opening relationship and stress-strain response exhibited by SFRC specimen is shown in Figs. 2.3 and 2.4, respectively, can be simplified for the analysis and design purpose of SFRC members. Three types of simplified relationships *vis-a-vis* Multilinear, Bilinear and Drop-constant relationship were suggested by different researchers in the past. These simplified versions of the relationship, help to simplify the analysis and obtain a satisfactory solution. Any one out of these simplified models can be selected depending upon the value of the limiting-strain adopted in the design.

### 2.1.2.1 Multi-linear Relationship

The experimental stress-strain ( $\sigma$ - $\epsilon$ ) response of SFRC generally consists of first a descending part after the first crack forms in the SFRC, then a slow descending and finally, a descending that occurs at a rapid pace. Nevertheless, the response of the SFRC in the pre-cracking range is always elastic-linear in nature. Figure 2.5 shows a typical multilinear constitutive tension model for an SFRC; a simplified representation of actual stress-strain response shown in Fig. 2.4. In this model, a very realistic representation of the stress-crack opening relationships can be obtained and



it is best suited in cases where an study demands an analysis over a large range of strain values, lasting up to a value of 0.040, and for this to happen, the SFRC must contain fibers with a volume fraction of more than 1.25 % and having an aspect ratio sufficiently large to ensure a ductile behavior. The strain value corresponding to the point-B, shown in the Fig. 2.5, depends entirely on the fiber parameters used in the concrete mix and it must be evaluated from the experimental studies conducted on SFRC for a given set of the fiber parameters. The crack-width corresponding to the range shown from the point-C to the point-D in the Fig. 2.5 becomes large enough to cause the fiber pullout from the mortar matrix and it results in a rapid decline in the effective stress transfer across the cracks. Usually in the range C–D, very wide cracks appeared in the specimen.

### 2.1.2.2 Bilinear Relationship

A bilinear model is a further simplified version of the multilinear constitutive relationship given in the previous section. In this model, the range from the point-C to the point-D, shown in Fig. 2.5 that usually results in a rapid loss of the strength after the formation of wide cracks in the specimen, is ignored in the analysis. This model provides a reasonably good representation of the measured SFRC behavior, when the crack-width is a prime limit-state of the adopted design procedure. A typical bilinear model for SFRC is shown in Fig. 2.6. In this model, a total of four material parameters are required to describe the stress-strain response and the corresponding stress-crack opening relationship of the material. The value of the mobilized stress and the strain value corresponding to the point-B are determined through an experimental testing; whereas, the values corresponding to the point-C are usually dictated by the limit-state criterion adopted in the design with respect to the crack-width at ultimate state. The stress at this stage (point-C) denotes the design value of the residual-tensile strength of SFRC corresponding to a permitted crack opening. Similar to the model described in the previous section, the stress

**Fig. 2.5** SFRC multi-linear model—It consists of a set of idealised straight lines joining each other at characteristics key points (A, B, C, and D) of an actual stress-strain response of SFRC. Nevertheless, the shape of the stress-strain response of the material is greatly influenced by the casting procedure used for the SFRC

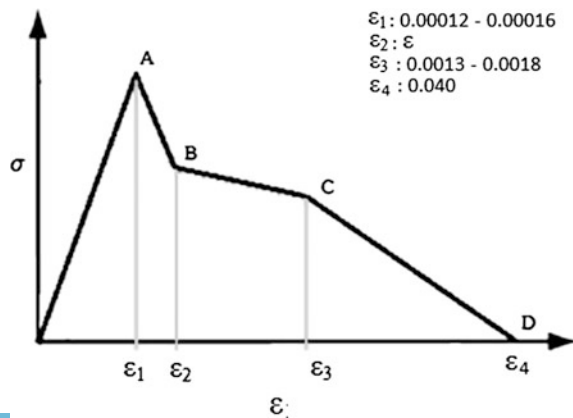
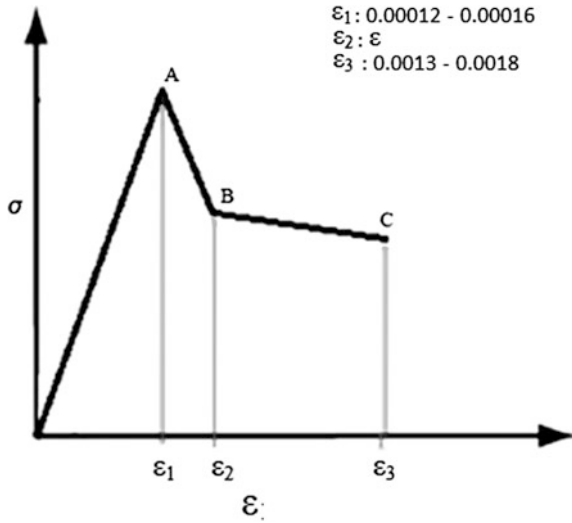


**Fig. 2.6 SFRC bilinear model**—It consists of a set of idealised straight lines joining each other at characteristics key points (A, B, and C) of an actual stress-strain response of SFRC

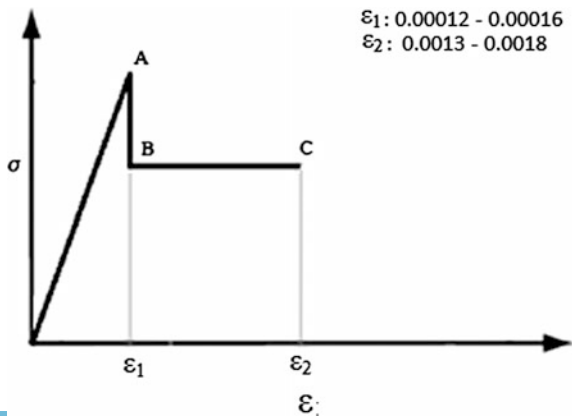


value (at the point C) can be determined either by conducting the standard tests on the SFRC specimens or it can be determined from the material analytical models. One such model is described in the next section that considers the randomness of the steel fibers in the concrete and requires concrete compressive strength ( $f_{ck}$ ), fiber aspect ratio ( $l/d$ ) and fiber volume fraction ( $V_f$ ) as an input parameter for estimation of the residual tensile strength of SFRC.

**2.1.2.3 Drop-Constant Relationship**

An even more simple representation of the stress-strain relationship for SFRC which has obvious advantages from a design point of view is shown in Fig. 2.7. It

**Fig. 2.7 SFRC drop-constant model**—It consists a line describing the elastic response of a set of idealised straight lines joining each other at characteristics key points (A, B, and C) of an actual stress-strain response of SFRC



is called as drop-constant relationship. Unlike the bilinear model, it needs only the value of the residual tensile strength of the SFRC corresponding to the point B or C shown in the model, which are virtually same on account of the assumption, along with the corresponding values of the strain. The strain value at the point-C in the model can be taken from the permitted value of the crack-width considered in the design. The strain value corresponding to the point A or B shown in the model is the limiting concrete strain that causes the formation of the first crack in the specimen when subjected to a tensile force.

It is important to note that the ultimate flexural capacity of an SFRC member remains practically unaffected, if instead of multilinear or bilinear model, a drop-constant model is adopted in the analysis. This is because of the fact that before the strain in the concrete section reaches the limiting concrete tensile strain especially during the first-time loading; a small part of the concrete existing below and close to the section neutral axis remains uncracked and effective in the flexural member. The magnitude of the resulting tensile force contributed by the small uncracked portion of the concrete and the corresponding internal moment is negligibly small and it can be safely neglected in the design calculations without affecting the accuracy of the results. In case, the loading is done on a previously loaded beam, it is possible that prior overloading may have caused the tensile cracks to penetrate deep enough to effectively eliminate the little contribution coming from the previously uncracked concrete portion of the section. Hence, the assumption to consider a constant value of the residual design tensile strength after the formation of the first crack is satisfactory and appears to be realistic. It also helps, simultaneously, to simplify the calculations and final expressions considerably. This is the reason that design engineers usually prefer material constitutive models that results in conservative estimation of the member capacity in a short time.

## 2.2 Analytical Tensile-Constitutive Model Based upon Drop-Constant Relationship

Consider SFRC containing short and discrete steel fibers dispersed randomly in the concrete mix at the time of mixing. It is assumed that these are present uniformly throughout the concrete mix. Figure 2.8a depicts one such steel fiber embedded in the concrete. It is in equilibrium under the induced pullout force ( $F$ ). The length and diameter of the fiber is  $l$  and  $d$ , respectively; thereby giving a fiber aspect ratio of  $l/d$ . The ultimate tensile capacity of an SFRC can be estimated by multiplying the number of fibers ( $n$ ) crossing the unit area of the crack and the average bond resistance ( $\tau_b$ ) being mobilized on the surface of the fiber.

Volume-fraction ( $V_f$ ) is used to quantify the number of fibers in the SFRC and it is normally expressed as a percentage of the concrete volume. This parameter is used to prescribe dosages of the steel fibers to be mixed in the concrete to get a desired performance, both in the fresh as well as the hardened state. Equation 2.2

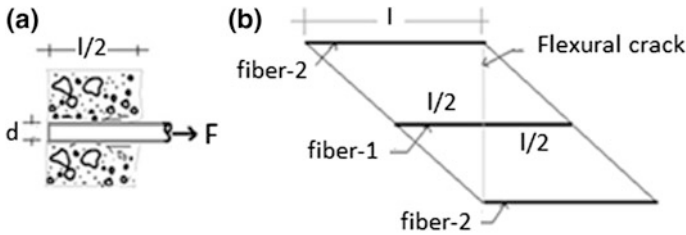


**Fig. 2.8** *Fiber embedment length*—The effectiveness of the steel fibers in load sharing depends upon the embedment length they have with the hydrated cement paste. Fibers having embedment length less than the critical value (e.g. Fiber-2) will simply pullout from the paste and contribute nothing towards the load sharing. And, the fibers, for instance Fiber-1, possessing an adequate embedment length is responsible for the residual flexural and/or tensile strength exhibited by the SFRC

gives an equivalent number of fibers ( $n$ ) crossing a unit area of the crack, where  $d$  is the diameter of the fiber.

$$n = \frac{4V_f}{\pi d^2} \tag{2.2}$$

Figure 2.8b shows a group of fibers crossing a vertical flexural crack. The fibers are assumed to be aligned perpendicular to a typical flexural crack and are contained within a quadrilateral domain, which represents all the possible fiber arrangements across the crack. Out of all such fibers in the domain, the fiber-1 lying at mid height of the quadrilateral domain with a pull-out length of  $l/2$  will be most effective in transmitting tensile force across the crack; whereas, the fibers lying above or below this height will have a higher probability of being pulled-out from the concrete as they have an inadequate value of embedment length, which varies from zero (shown at the top/bottom face, e.g. Fiber-2) and is equal to  $l/2$  for the fibers laying at the mid height of the domain (e.g., Fiber-1).

The force ( $F_{tp}$ ) required to pull-out a fiber (e.g. like a Fiber-1), with an average value of the embedment length of  $l/2$  from the concrete can be estimated from Eq. 2.3. In this equation, the average mobilized interfacial shear stress ( $\tau_b$ ), in MPa, at the surface of a plain straight fiber can be taken from a lower bound empirical equation:  $0.75\sqrt{f_{ck}}$ , where  $f_{ck}$  is concrete characteristic compressive strength, taken in MPa. The shape of the fiber has a significant effect on this strength value (Šalna and Marčiukaitis 2003; Shaurya 2015) and, accordingly, it should be multiplied by a suitable factor depending upon the fiber shape.

$$F_{tp} = \tau_b \pi d \frac{l}{2} \tag{2.3}$$

The total pull-out tensile strength ( $\sigma_{tp}$ ) contributed by all such fibers in the direction of the load and those crossing the unit crack area can be determined by

multiplying Eqs. 2.2 and 2.3. The final expression of the residual tensile strength mobilized in the fiber pullout failure mode is given in Eq. 2.4.

$$\sigma_{tp} = \frac{F_{tp}}{1} = 2\gamma_o\gamma_d\gamma_l \left( \tau_b V_f \frac{l}{d} \right) \quad (2.4)$$

In Eq. 2.4, the constants  $\gamma_o$ ,  $\gamma_d$  and  $\gamma_l$  denote the effect of fiber orientation with respect to the loading axis; fiber dispersion along the length and the width of the flexural member caused during the concrete compaction and placement operations; length factor  $\gamma_l$  takes into account the nonlinear distribution of the bond stress along the length of the fiber, respectively. It is an experimentally established fact that the effect of the fiber orientation on the pull-out strength is insignificant, if the fibers are aligned at an orientation-angle up to  $30^\circ$  with respect to the loading. A reduction as high as 60 % in the strength was observed; when the orientation of the fibers is kept more than  $40^\circ$  and up to  $60^\circ$  for various fiber lengths. The fibers with an orientation angle of more than  $60^\circ$  will contribute as little as 10 % (Robert et al. 1987; Gettu et al. 2005; Kang 2011; Soranakom and Mobasher 2007, 2009; Michels et al. 2013). The fiber pull-out behaviour becomes increasingly more influenced by the mechanical properties of the steel fibers embedded in concrete than the strength of the matrix as the fiber orientation angle increases with respect to the loading axis.

The weighted average value of  $\gamma_o$  was found to be 0.8 based upon the strength reduction reported in the past investigations. Probability analysis indicates that the value of  $\gamma_d$  can be taken as 0.5 because the fibers have equal probability to align themselves along the two plan dimensions of the member during the placement and compaction of the concrete mix. The value of the length factor  $\gamma_l$  can be taken as 0.5 for the fiber length  $l$  less than its critical length  $l_c$ ; otherwise this value is  $(1 - 0.5 l/l_c)$  (Karayannis 2000). Therefore, the total pullout tensile strength ( $\sigma_{tp}$ ) of plain straight fibers crossing the unit area of a crack of in the SFRC member can be simplified to Eq. 2.5 and it must be multiplied by a suitable fiber-shape factor depending upon the fiber types. The shape factor for the hooked-end fibers and the wavy-fibers are reported as two and three, respectively (Malik 2014; Shaurya 2015; Nadda 2015).

$$\sigma_{tp} = 0.3V_f \frac{l}{d} \sqrt{f_{ck}} \quad (2.5)$$

The second failure mode in which an SFRC specimen could fail is a fiber-fracturing mode; wherein the fibers embedded in concrete get fractured at collapse. This type of failure usually occurs when fibers are long enough to shift the failure from a pullout mode to the fracture mode. In such cases, the pullout resistance of the fibers become more than their yield strength because of their longer embedment length, thereby resulting in a high bond strength for a given fiber diameter. The residual-tensile strength ( $\sigma_{tf}$ ) for such cases can be estimated by multiplying the design yield strength ( $f_y$ ) of the steel fiber (diameter,  $d$ ) with their total cross-section area crossing the crack. Equation 2.6 gives a force over the unit crack area ( $\sigma_{tf}$ ) required to cause yielding of fibers embedded in the concrete and

their subsequent fracturing that happens suddenly soon after the fiber yielding; the steel fibers possess a low percentage elongation. A partial safety factor of 1.15 is used in Eq. 2.6 to take care of the variation of strength properties of material from their nominal values.

$$\sigma_{f_f} = 0.87f_y \left( n\pi \frac{d^2}{4} \right) = 0.87f_y V_f \quad (2.6)$$

The length of the fibers embedded in concrete at which the bond stress mobilized on the surface of steel fibers becomes equal to their yield strength is called as critical length. The value of the fiber critical aspect-ratio  $(l/d)_c$  can be determined by equating Eqs. 2.5 and 2.6. If the actual fiber aspect-ratio  $(l/d)$  in an SFRC is kept less than its critical value  $(l/d)_c$ , the failure always occurs in the fiber pullout mode; otherwise, it will happen in a fiber-fracture mode. Equation 2.7 gives a simplified expression for the critical fiber aspect ratio. The value given in Eq. 2.6 should be multiplied with a factor of 0.2 ( $=\gamma_o\gamma_d\gamma_l$ ) to consider the effect of the fiber orientation and its distribution in the SFRC before it is equated with Eq. 2.5; it is given below:

$$\begin{aligned} 0.3\sqrt{f_{ck}}V_f \frac{l}{d} &= 0.2 \times 0.87f_y V_f \\ \Rightarrow \left( \frac{l}{d} \right)_c &= \frac{0.174f_y}{0.3\sqrt{f_{ck}}} = \frac{0.58f_y}{\sqrt{f_{ck}}} \end{aligned} \quad (2.7)$$

The design tensile strength  $\sigma_t$  of a concrete with randomly distributed short and discrete plain-straight steel fibers can be taken from the Eq. 2.8, corresponding to any strain value  $\varepsilon < \varepsilon_t$  (=limiting value of the tensile strain considered in the design of SFRC member based upon the permitted crack-width). This value can be adopted from an experimental stress-crack opening relationship of SFRC. In the absence of such data, however, this value can be taken as 0.015. The failure of SFRC can take place by pullout of the fibers or by fiber fracturing depending on whether the fiber aspect ratio is kept more than the critical value given in Eq. 2.7 or not. The value of the corresponding design residual-tensile strength ( $\sigma_t$ ) of SFRC should be taken as a least of  $\sigma_{tp}$  and  $\sigma_{tf}$ , respectively, as is given in Eq. 2.8.

$$\sigma_t = \begin{cases} 5000\varepsilon\sqrt{f_{ck}}, & \varepsilon \leq 0.00014 \\ 0.3\sqrt{f_{ck}}V_f \frac{l}{d}, & 0.00014 < \varepsilon \leq \varepsilon_t(=0.015) \end{cases} \quad \text{For } \frac{l}{d} < \left( \frac{l}{d} \right)_c \quad (2.8)$$

$$\sigma_t = \begin{cases} 5000\varepsilon\sqrt{f_{ck}}, & \varepsilon \leq 0.00014 \\ 0.87f_y V_f, & 0.00014 < \varepsilon \leq \varepsilon_t(=0.015) \end{cases} \quad \text{For } \frac{l}{d} \geq \left( \frac{l}{d} \right)_c$$

Figure 2.9 shows a normalised tension-constitutive material model for SFRC. It is based upon the constitutive model, given in Eq. 2.8 and considers both types of the material failures depending upon the value of the fiber aspect ratio taken in the

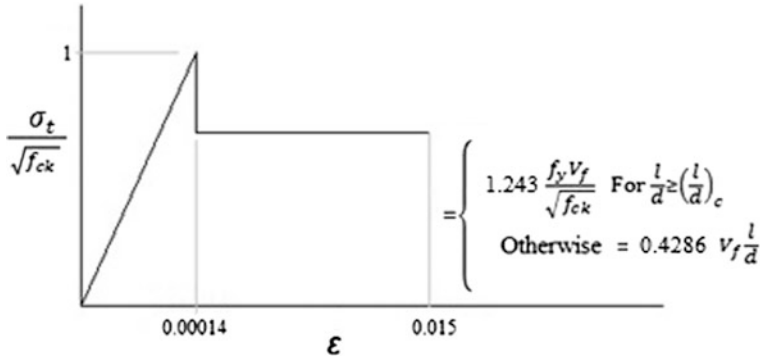


**Fig. 2.9** SFRC tension constitutive model (with short, plain steel fibers)—A drop-down model for SFRC in tension, i.e. linear-elastic up to the first cracking, followed by a sudden change in the post-cracking strength, occurring once the strain in the matrix touches the limiting tensile-strain capacity of the concrete and thereafter, it exhibits a plastic response up to the limiting tensile straining capacity of the SFRC. The extent of the *drop* or the *rise* in the post-cracking strength exhibited by SFRC depends entirely on the fiber-parameters used in the mix. When the combination of  $V_f$  and  $l/d$  in the concrete is more than the critical value of the fiber-index ( $=\sigma_t/f_{ck}$ ), it shows a rise of the post-cracking strength and the SFRC exhibits a ‘strain-hardening’; otherwise, it will show a ‘strain softening’ upon cracking. For fibers of any other shape, the residual tensile strength value shown in the figure should be divided by the corresponding ‘shape factor’—two for hooked-end fibers and three for wavy ones

production of SFRC. It is important to note that the fiber parameters ( $l/d$  and  $V_f$ ) play an important role in fixing the failure mode of SFRC. It can fail by exhibiting either a strain-hardening response or a strain-softening response in its post-cracking range.

The Fig. 2.9, and the constitutive model given in Eq. 2.8, indicate that the contribution from the steel fibers activates in an SFRC member only after the tensile strain in the concrete reaches its limiting value and afterwards, the stress drops or rises suddenly to a new value depending upon the fiber parameters: namely, the fiber aspect ratio ( $l/d$ ), volume fraction ( $V_f$ ), their shape and the concrete compressive strength ( $f_{ck}$ ) adopted in the design of an SFRC member. The strength exhibited by SFRC in its post-cracking range at some prescribed value of the crack opening ( $w$ ) is termed as a residual-tensile strength ( $\sigma_t$ ). Normally, the value of the permitted crack opening ( $w$ ) is decided based upon the results of the standard bending tests. The next section presents details of such procedures recommended by various design guidelines. If this value of the strength in its post-cracking stage is reported to be more than the first crack strength, the SFRC is termed as strain-hardening material; otherwise, it will act as a strain-softening material. Equations 2.9 and 2.10 give expressions for estimating the values of the fiber-parameters necessary to ensure a SFRC post-cracking response in the strain-softening or the strain-hardening mode for a given set of  $f_y$  and  $f_{ck}$  values considered in the design.

The values of the fiber-parameters ( $V_f$  and  $l/d$ ) that define the transition of the post-cracking behavior of SFRC from a ‘strain-softening’ to the ‘strain-hardening’

can be determined by equating the strength values given by Eq. 2.8 with the cracking tensile strength ( $\sigma_{cr}$ ). It is given in Eq. 2.9 for an SFRC prepared using short, plain fibers, but it must be divided by the corresponding fiber-shape factor of two and three for the hooked-end and the wavy fibers, respectively. If the value of the volume fraction ( $V_f$ ) or the fiber aspect ratio ( $l/d$ ) to be adopted in the concrete mix is kept less than the value given in the Eq. 2.9, the SFRC will exhibit a strain-softening in its post-cracking range; otherwise, it will lead to the strain hardening.

$$0.3\sqrt{f_{ck}}V_f\frac{l}{d} = 0.7\sqrt{f_{ck}} \quad \text{For } \frac{l}{d} < \left(\frac{l}{d}\right)_c \quad (2.9)$$

$$\Rightarrow V_f(l/d) = 2.33$$

Equations 2.7 and 2.9 can be combined to get a value of the volume fraction ( $V_f$ ) that would lead to strain-hardening response of SFRC. If the fiber aspect-ratio ( $l/d$ ) in the concrete mix is kept less than its critical value (as given in Eq. 2.7), a value of the volume fraction ( $V_f$ ) taken more than the value, given in Eq. 2.10, always give a strain-hardening response in the material post cracking range.

$$V_f \geq 4.0 \frac{\sqrt{f_{ck}}}{f_y} \quad (2.10)$$

Equations 2.9 and 2.10 indicates that if the fiber aspect ratio ( $l/d$ ) in the SFRC is kept less than its critical value ( $(l/d)_c$ ); then, the selected value of the fiber aspect ratio ( $l/d$ ) and the volume fraction ( $V_f$ ) used in the concrete mix only controls the post-cracking behaviour of the SFRC. Otherwise, the material properties, such as the characteristic compressive strength ( $f_{ck}$ ) of concrete and the yield strength ( $f_y$ ) of the steel fibers plays their part in controlling the residual tensile strength ( $\sigma_r$ ) and the post cracking response of SFRC. Nevertheless, the SFRC in the latter case will exhibit a brittle failure with the specimen failing in the fiber-fracturing mode and it must be avoided in practice as the impending failure is silent in nature and occurs suddenly without giving any warning and time to escape.

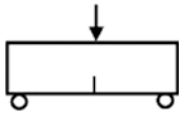
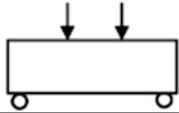

### 2.3 Experimental Characterization of the Tensile Response

Most of the design guidelines use bending tests to characterize the post-cracking response of the SFRC and in determining the other key parameters needed to define its constitutive-tensile model. Table 2.1 gives a brief of different loading-setups and the specimen sizes recommended by several guidelines in this regards.

The uniaxial test is the most direct method to obtain a stress-crack opening [ $\sigma$ - $w$ ] relationship of the SFRC, particularly for deciding the value of the safe stress



**Table 2.1** Test methods in use for the characterization of the post-cracking behavior of SFRC

Test	Specimen size (mm)	Loading-setup	Standard
3-point bending test	600 × 150 × 150		RILEM TC 162-TDF (2002) and EN 14651:2005
4-point bending test	600 × 150 × 150		CNR-DT 204 (2006)
Uniaxial tensile test	150 Φ × 150		RILEM TC 162-TDF (2002)

to be considered in the design of SFRC members at the service load and to check the adequacy of the section at ultimate load. It is an accepted practice to obtain the characteristic and the design tensile strengths, independently, through analytical models, code prescriptions or the standard testing methods intended for a plain concrete.

The bending tests are accepted procedure to develop a stress-strain ( $\sigma$ - $\epsilon$ ) relationship of the material from a load-displacement response exhibited by the standard SFRC flexural member. This process is known as inverse analysis [Tlemat et al. (2006)]. In contrast to the direct tension tests, this process is easier to use as they require measured load-displacement or moment-curvature responses obtainable with minimal testing complexities than those associated with the procedures requiring results from the direct tensile tests. The four-point or three-point bending tests are prescribed by most of the guidelines to obtain a load-displacement response of the specimens.

Idealised tensile stress-strain constitutive relationships are suggested for the SFRC by most of the guidelines that uses the results from a deformation-controlled beam-bending tests, conducted on a standard specimens to determine the peak and post-cracking stresses. In the suggested procedures, generally, the strains corresponding to the stresses were empirically estimated as fixed values. Nevertheless, this type of the procedure is not free from the inherent flaws; the accuracy of the tensile stress-strain response depends greatly upon the precision with which an analyst determines the load at the initiation of the crack on a measured load-deflection response in addition to the assumptions made for the calculation of the post-cracking strength. Moreover, the results from these bending tests are highly dependable on the beam size, the casting method and the loading-setup. It is important to note that because of so many factors influencing the flexural response, the results from these tests shows a large scatter. This may be attributed to the

amount of fibers and their distribution in the cracked section and to minimize it, the use of a three-point bending test conducted on a standard specimen with a central notch is recommended by most of the standard testing guidelines. The central notch at the point of the maximum bending moment is recommended to fix the position of the failure plane in an SFRC Beam specimen. The following sections describe in detail different test procedures prescribed by various guidelines.

### 2.3.1 RILEM TC162-TDF (2002) Procedure

This guideline prescribes a three-point bending test conducted using a simply supported notched-beam to obtain various key-parameters of the SFRC tensile stress-strain relationships. The beam specimen of  $150 \times 150 \times 600$  mm (an effective span of 500 mm) with a central notch is recommended for this purpose. The unnotched depth of the beam specimen should be kept as  $125 \text{ mm} \pm 1 \text{ mm}$  with a 5 mm wide or less notch at its mid span. The dimensions of the specimen shall not vary by more than 2 mm on all sides. It is also recommended that the difference in the overall dimensions on opposite sides of the specimen shall not be greater than 3 mm. The device for measuring the specimen dimensions should have an accuracy of 0.1 mm.

The guidelines did not recommend the use of the prescribed beam size for a beam having steel fibers longer than 60 mm and made using aggregates larger than 32 mm. It is required that the concrete should be compacted by means of external vibration only; however, in the case of a self-compacting steel fiber concrete, the mould shall be filled in a single pour and levelled off without any compaction. The concrete specimens shall be cured in the moulds for 24 h after the casting, at  $(27 \pm 2) ^\circ\text{C}$ , either under polyethylene sheeting or at not less than 95 % relative humidity. The specimens are then demoulded between 24 and 48 h after the casting and cured for a further period until preparation for testing. Testing shall normally be performed at 28 days (or at any other specified age of the specimen).

The steel rollers with a diameter of  $30 \text{ mm} \pm 1 \text{ mm}$  shall be used to support the beam at its ends and also, at the load-point on its top face. These shall be capable of rotating freely around their axis. The device used for measuring the load and the mid-span deflection, and crack-mouth-opening displacement (CMOD) in the test setup must have a least count of 0.1 kN and 0.01 mm, respectively. The notch CMOD measuring system should be installed along the longitudinal axis at the mid-width of the test specimen, so that the distance between the bottom face of the specimen and the axis of the measuring system is 5 mm or less.

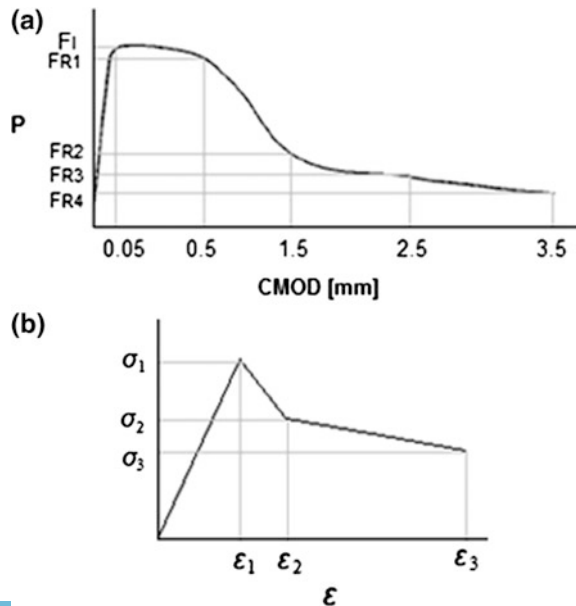
The loading should be applied so that the measured midspan-deflection of the specimen increases at a constant rate of 0.2 mm/min until the specified final deflection is reached that normally is taken as 3 mm. The value of the load and the beam midspan-deflection should be recorded continuously. It is important to note that if the crack forms outside the notch, the test has to be rejected and it should be performed on a fresh beam specimen. When the test is executed by means of

CMOD control, the machine shall be operated in such a manner that the CMOD increases at a constant rate of 50  $\mu\text{m}/\text{min}$  for CMOD from 0 to 0.1 mm, followed by a constant rate of 0.2 mm/min until the end of the test. The test results are obtained in the form of load-crack opening response of the specimens. Later on, this test data can be converted into the stress-strain response of SFRC using a set of the empirical relations. A typical response of the SFRC in the form of a load-crack opening displacement and the recommended format of the stress-strain response is shown in Fig. 2.10.

The residual tensile strengths  $F_{Ri}$ , shown in Fig. 2.10a, are key-parameters characterising the post-cracking behavior of SFRC. The value of these parameters can be determined by following the testing procedure described above and using Eq. 2.11. The load  $F_L$ , is a load corresponding to the limit of proportionality exhibited by the test specimen. It can be taken as a load corresponding to the 0.5 mm midspan-deflection ( $\delta$ ) or a CMOD value of 0.05 mm. It is important to note that the load-deflection response of the member is linear-elastic up to the load  $F_L$  and it may or may not be accompanied by the crack formation; therefore either of these two values can be adopted as the limit of proportionality.

Similar to the value of  $F_L$ , the residual-tensile strengths,  $F_{R1}$  and  $F_{R4}$ , respectively, are fixed as a load value corresponding to the specified value of the CMOD or the mid-span deflection measured in the prescribed bending test.  $F_{R1}$  is a load value corresponding to the CMOD of 0.5 mm or a deflection value of 0.46 mm. The value of this residual stress can be less or higher than the value determined corresponding to the  $F_L$ . The residual stress value,  $F_{R4}$  is measured at a CMOD of 3.5 mm or a

**Fig. 2.10** SFRC tension constitutive model recommended by RELIM—**a** load-crack opening displacement response; **b** a stress-strain response. The load-CMOD response of the material can be obtained following the procedure prescribed by EN 14651:2005



deflection value of 3.00 mm. Generally, this value of the residual-stress represents the strength of SFRC specimen corresponding to the ultimate state.

The guideline has proposed a strain value of 0.025 at the ultimate state by taking the characteristic length  $l_{cs}$  equal to the height of the neutral axis (=140 mm) in the specimen, taken at the point where the CMOD is measured. It gives a strain value of  $(3.5/140) = 0.025$  for a CMOD of 3.5 mm. This is the inherent flaw in the model as the depth of the neutral axis depends on the fiber parameters, such as the fiber-aspect ratio ( $l/d$ ), the volume fraction ( $V_f$ ) and the concrete compressive strength. However, because of the simplicity and familiarity of the testing procedure, it is used in practice more commonly than any other method.

$$\sigma_{Ri} = \frac{3F_{Ri}L}{2bh_1^2} \quad (2.11)$$

In Eq. 2.11,  $L$  is an effective span of the beam specimen ( $B \times D$ ). The parameter  $h_1$  denotes a distance from the top of the notch provided in the beam specimen to its top face. The parameter  $F_{Ri}$  is a load recorded at  $CMOD_i$  or midspan-deflection ( $\delta_{Ri}$ ) during the beam testing (see Fig. 2.10). The values of stresses  $\sigma_i$  shown in Fig. 2.10 can be determined from a set of expressions given in Eqs. 2.12–2.15.

$\sigma_1 = 0.7Y\sqrt{f_{ck}}(1.6 - D)$ MPa; Where,  $D$  (in ‘m’) is the depth of the beam specimen and the value of constant

$$(Y) = 0.75 \quad \text{for } f_{ck} < 45 \text{ and it is } 0.85 \quad \text{for } f_{ck} > 50. \quad (2.12)$$

$$\varepsilon_1 = \frac{\sigma_1}{5000\sqrt{f_{ck}}} \quad (2.13)$$

$$\sigma_2 = 0.45f_{R1}k_h \text{ MPa}; \quad \varepsilon_2 = \varepsilon_1 + 0.0001 \quad (2.14)$$

$$\sigma_3 = 0.37f_{R4}k_h \text{ MPa}; \quad \varepsilon_3 = 0.025 \quad (2.15)$$

In Eqs. 2.14 and 2.15,  $k_h$  is a beam-depth factor and it reflects the effect of the specimen size on the SFRC strength properties. The value of the factor can be calculated from Eq. 2.16. Nevertheless, the equation is applicable for a beam-depth of 125–600 mm only. This apparent specimen size-effect is not yet fully understood as of now and further investigations are going on in order to identify whether this is arising due to a discrepancy of the material properties between different batches, or to the size-effect intrinsic to the procedure, or a combination of these parameters. Accordingly, it is strictly recommended in the guidelines that the depth of the beam specimen must lie in the prescribed range.

$$k_h = 1 - 0.6 \frac{D \text{ (in cm)} - 12.5}{47.5} \quad (2.16)$$

It is important to note that the maximum crack-width in the test specimen at the ultimate limit state is restricted to 3.5 mm so as to ensure a sufficient anchorage

capacity for the steel fibers present in the concrete. However, if crack-widths larger than 3.5 mm are expected to form at collapse or are used in the design, the residual-tensile strength corresponding to that crack-width and the value measured during the bending test has to be used to calculate the value of the stress  $\sigma_3$ . It is also recommended by the design guideline that this value, which replaces  $F_{R4}$  in Eq. 2.15, should not be lower than 1 MPa; if it is coming less than 1 MPa, the mix proportions of SFRC should be altered to get the value more than that required.

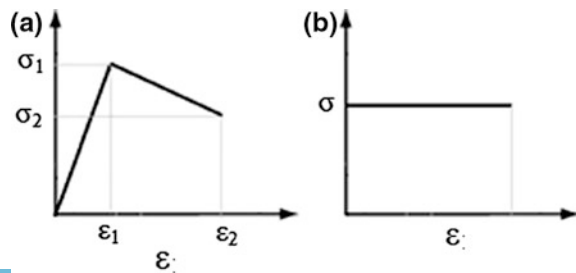
### 2.3.2 CNR-DT 204 (2006) Guidelines

The Italian National Research Committee published a set of design guidelines (CNR-DT 204) in the year 2006. This prescribes a set of rules for proportioning and construction of SFRC members. Unlike the RELIM guidelines, it has given two different types of material models describing the tensile behavior of SFRC member: namely, (a) the linear-elastic model and (b) the plastic-rigid model, as shown in Fig. 2.11. The linear post-cracking behavior differentiates between the strain-hardening and strain-softening materials. In case of strain-hardening response, the slope of the curve in the post-cracking range (after onset of the strain  $\varepsilon_1$ ) increases with an increase in the strain-value, while it reduces in the strain-hardening response. These models are expressed in terms of  $\sigma$ - $\varepsilon$  and  $\sigma$ - $w$  relationships.

The linear-elastic model can be used to proportion SFRC beams, both at the ultimate limit state and the serviceability limit state of the design procedure, but the plastic-rigid model is recommended to be used only in case of the ultimate limit state. Unlike the RELIM guidelines, use of the four-point bending tests and uniaxial tensile test is prescribed to obtain the  $\sigma$ - $\varepsilon$  and  $\sigma$ - $w$  relationships. The tests should be carried out as per the provisions of the Italian standards UNI 11039 (2003) and UNI 11188 (2004), respectively.

The post-cracking strength of SFRC is defined on the basis of either the point-values ( $f_i$ ) taken corresponding to a specified nominal value of the crack-opening ( $w_i$ ), or on the mean-values ( $f_{eqi}$ ) calculated for assigned intervals of the crack-opening. Unlike the RELIM guidelines, the crack opening is taken as the displacement between the two points at the notch-tip ‘CTOD’ caused after the

**Fig. 2.11** SFRC stress-strain ( $\sigma$ - $\varepsilon$ ) response recommended by the CNR-DT 204—  
**a** A linear-elastic response;  
**b** a plastic response



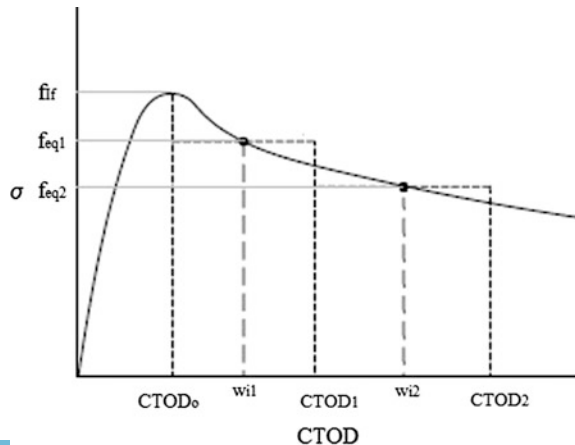
formation of a crack instead of the crack-mouth opening displacement (CMOD) considered by the RILEM (2002). The selection of the residual-tensile strength on the basis of the crack-width is important as the SFRC loses its load carrying capacity significantly with an increase of the crack opening. A high value of the crack opening in an SFRC member leads to a complete loss of the fiber anchorage, thereby resulting in a drop of the strength values with the increasing crack-width. The guidelines permit the analyst to select the design stress depending upon the crack-width taken either from the fiber anchorage considerations or the serviceability criterion. The Eqs. 2.17 and 2.18 gives the mathematical expressions derived using the equilibrium conditions of a rectangular section under bending to determine the key parameters of the linear-elastic model (see, Fig. 2.11a).

$$\sigma_1 = 0.45f_{eq1} \quad (2.17)$$

$$\sigma_2 = k \left[ \sigma_1 - \left( \frac{w_u}{w_{i2}} \right) (\sigma_1 - 0.5f_{eq2} + 0.2f_{eq1}) \right] \geq 0 \quad (2.18)$$

In Eqs. 2.17 and 2.18,  $f_{eq1}$  and  $f_{eq2}$  are the SFRC post-cracking equivalent strengths considered in the serviceability and the ultimate limit states, respectively. The parameter  $w_{i2}$  is the mean value of the crack opening (in the intervals 'CTOD<sub>1</sub> and CTOD<sub>2</sub>') where  $f_{eq2}$  is evaluated from the  $\sigma$ - $w$  response of SFRC. The parameter  $w_u$  denotes the crack-width at the ultimate state, generally taken as 3 mm for a structural element in bending, and 1.5 mm when it is subjected to tension. The values of  $f_{eq1}$  and  $f_{eq2}$  can be determined from the test results (Fig. 2.12 depicts a typical curve) of the four-point bending test conducted in accordance with the UNI 11039 (2003). It is important to note that the CTOD<sub>1</sub> is a permitted value of the crack-width corresponding to the serviceability limit state; whereas the CTOD<sub>3</sub> is a value of the crack-width at the ultimate limit state. The value of the CTOD<sub>2</sub> can be selected arbitrarily depending upon the desired performance level. In Eq. 2.18,  $k$  is

**Fig. 2.12**  $\sigma$ - $w$  response—It can be obtained using the 4-point bending test or axial tension testing of SFRC standard specimens, conducted in accordance of UNI 11039 (2003) and UNI 11188 (2004), respectively



a coefficient taken equal to 0.7 for the specimens fully subjected to the tensile stresses and it is equal to 1 in all other cases of loading.

In case of the plastic model (Fig. 2.11b), Eq. 2.19 can be used to determine the stress ( $f_{tu}$ ) at the ultimate state. This expression is derived using the equivalence of the moment capacity of the SFRC rectangular section considering the plastic-tensile response with a peak stress-value ( $f_{tu}$ ) and an imaginary rectangular section with a linear-elastic stress distribution. The stress  $f_{cq2}$  is the peak value of the stress is taken in the elastic stress distribution.

$$\sigma = f_{tu} = \frac{f_{eq2}}{3} \quad (2.19)$$

Figure 2.12 shows a typical  $\sigma$ -w response of the SFRC, obtained experimentally to evaluate different key-parameters of the material constitutive model. It is important to note the linearity of the  $\sigma$ -w response, especially in its post-cracking range. This characteristic of the response exhibited by the SFRC in the post-cracking range of the stress-crack width ( $\sigma$ -w) curve is used to derive and simplify the expression of the post-peak strength ( $\sigma_2$ ), given in Eq. 2.18.

It is important to note that the parameter ( $f_{eq}$ ) used in the CNR-DT-204 is better to use over the parameter ( $f_R$ ) adopted by the RILEM (2002) guidelines for developing the tensile constitutive model of SFRC. Some studies in the past, such as Barros et al. (2005) are supporting the use of the parameter ( $f_{eq}$ ) instead of ( $f_R$ ). This is because of the fact that the former parameter represents the energy-absorption capacity of the material up to a certain deflection exhibited by the SFRC member; whereas, the parameter ( $f_R$ ) corresponds to the stress associated with the force at a certain deflection level, which is more susceptible to the local irregularities of the load-displacement curve than the energy absorption capacity which is a measured of the area of the load-displacement response curve. As the procedure adopted by the CNR-DT-204 is based upon the equivalent strength values, it is essential to evaluate the post-cracking strength of the material by using the recommended value of the limiting crack-width, which has a significant effect on the toughness. The wider cracks could be highly detrimental to the strength and may also cause a significant reduction of the material toughness.

In case of a strain-hardening response, the SFRC section exhibits a set of multiple cracking that develops with the increasing load and the average strain-value may be obtained directly from the experimental tests. Nevertheless, the ultimate strain value for this type of the material response is limited to 0.010; whereas, in case of a strain-softening response, there appears only one main crack in the section usually at the point of the maximum moment in the section.

The ultimate strain for a strain-softening response is related to the crack-width appeared in the section at the ultimate state ( $w_u$ ) and the equivalence should be carried out by means of a characteristic length ( $l_{cs}$ ). The value of  $l_{cs}$  should be determined from the minimum of the average crack spacing ( $s_{rm}$ ) observed in the

tests and the height of the neutral-axis ( $h_2$ ). However, the ultimate tensile strain in the section for this case is limited to 0.020 and there is also an upper limit [ $w_u = \epsilon_u \cdot l_{cs} \leq 3.0$  mm] on the value of the crack-width ( $w_u$ ) formed in the specimen at the ultimate load.

### 2.3.3 fib Model Code (2010)

The fib (*Fédération Internationale du Béton*), similar to the CRN-DT 204 guidelines, has also recommended two different types of constitutive relationships to model for the tensile behavior of SFRC in its updated version (MC2010) of the CEB-FIP Model Code 90; namely, the linear-postcracking behavior and the plastic-rigid behavior. Figure 2.11 depicts these two types of the SFRC material model. Interestingly, SFRC can exhibit a strain-softening or strain-hardening response depending upon the fiber parameters taken in the design of SFRC mix. The key parameters ( $f_{fts}$  and  $f_{ftu}$ ) in both the models are defined by means of the residual flexural-tensile strengths, determined from a set of the test results, conducted under the three-point load bending conditions in accordance with the provisions of EN 14651 (2005).

The parameter  $f_{fts}$  represents the residual-tensile strength of SFRC. It is defined as the post-cracking strength of the material corresponding to the crack-opening displacement ( $w$ ) considered in the serviceability limit state; whereas,  $f_{ftu}$  is value of the ultimate value of the residual-tensile strength corresponding to the maximum permitted value of the crack-opening displacement ( $w_u$ ) of SFRC in the design. For the rigid-plastic model, the value of ( $w_u$ ) is prescribed as 2.5 mm and that for the linear-elastic model, it depends on the ductility level adopted in the design, but it should not exceed 2.5 mm. The expressions to determine the parameters  $f_{fts}$  and  $f_{ftu}$  are given in Eqs. 2.20 and 2.21.

$$f_{fts} = 0.45f_{R1} \quad (2.20)$$

$$f_{ftu} = k \left[ f_{fts} - \left( \frac{w_u}{CMOD_3} \right) (f_{fts} - 0.5f_{R3} + 0.2f_{R1}) \right] \quad (2.21)$$

In Eq. 2.21,  $k$  is a fiber orientation-factor considered in the design. This factor equals one for an isotropic fiber distribution. However, the value can be taken lower or higher than one, if favourable or unfavourable effects are experimentally verified on the real-scale structural elements. Equation 2.11 is used to compute the value of the parameters ( $f_{R1}$  and  $f_{R3}$ ) taken in the Eqs. 2.20 and 2.21.

The fib Model Code has specified a strain-level for the identification of strain-hardening or strain-softening response exhibited by SFRC in its post-cracking range. It will be a strain-hardening, if it occurs at an ultimate tensile strain value of 0.010; otherwise, the material is considered as of strain-softening nature. For a SFRC exhibiting a strain-softening response, the  $\sigma$ - $\epsilon$  diagram is



defined by identifying the crack-width ( $w$ ) appearing in the section and the corresponding characteristic length ( $l_{cs}$ ) of the structural element. Therefore, the corresponding value of the strain can be expressed as  $\varepsilon = w/l_{cs}$ . The value of  $l_{cs}$  is a minimum of the average crack spacing ( $S_{rm}$ ) or the distance between the neutral axis and the tensile face of the cross section ( $h_2$ ).

In case of the beam section with conventional rebars; the parameter  $h_2$  is evaluated in the cracked-phase assuming no tensile strength of the SFRC, similar to the conventional RC sections, and for a load configuration corresponding to the serviceability state of crack-width and spacing. However, the value of  $h_2$  is assumed equal to the height of the beam-section in case of a SFRC beam section without conventional tensile reinforcement. Therefore, the ultimate crack-width  $w_u$  be calculated as  $w_u = l_{cs} \cdot \varepsilon_u$ . The ultimate strain  $\varepsilon_u$  equals 0.020 for variable strain distribution along the cross section and it is 0.010 for uniform tensile strain distribution along the cross-section.

For a SFRC exhibiting a strain-hardening response, however, the parameter ( $l_{cs}$ ) is not necessary. The  $\sigma$ - $\varepsilon$  diagram is defined by assuming the stain at ultimate ( $\varepsilon_u$ ) equal to 0.020 for a variable-strain distribution along the depth of the section (e.g., beams) and by taking it equals to 0.010 for the uniform tensile-strain distribution along the cross section (e.g. axial tension case). It is important to remark that the ultimate crack-width  $w_u$  required in estimating the parameter  $f_{tu}$  may be calculated using relationship:  $w_u = l_{cs} \varepsilon_u$ .

### Example 2.1

*Standard prisms of  $150 \times 150 \times 750$  mm were cast using SFRC. It contains short steel hooked-end fibers (0.5 mm diameter and 30 mm long) with a fiber volume fraction of 1 %. The sample size was 6 units and these were tested under a standard 3-point loading conditions, with an effective span of 500 mm, following a standard testing procedure. Table 2.2 gives the results from the test taken at various prescribed CMOD values. The results from the standard 150 mm concrete cubes indicate that the SFRC possesses a 28 days compressive strength of 42.58 MPa.*

Based upon the test data, the tension constitutive model of the SFRC can be derived using the applicable equations, given in the previous sections:

**Table 2.2** Test results of a 3-point bending test

S. No.	The stress values (MPa) corresponding to the CMOD of			
	0.05 mm	0.5 mm	2.5 mm	3.5 mm
	$f_L$	$f_{R1}$	$f_{R3}$	$f_{R4}$
1	9.14	13.53	9.60	3.09
2	7.20	10.03	6.72	2.98
3	7.09	10.60	6.17	2.67
4	7.55	11.79	6.40	2.71
5	7.49	10.11	6.56	2.88
6	6.76	9.48	6.08	2.15
Average value	7.51	10.92	6.92	2.75

- **RELIM model** (Eqs. 2.12–2.15)

The value of the shape factor,  $k_h = 0.9684$

$\sigma_1 = 4.97$  MPa,  $\varepsilon_1 = 0.000152$

$\sigma_2 = 4.76$  MPa,  $\varepsilon_2 = 0.000252$

$\sigma_3 = 2.42$  MPa,  $\varepsilon_3 = 0.025$

- **fib model** (Eqs. 2.20–2.21)

$f_{ts} = 4.914$  MPa,  $\varepsilon_1 = 0.00015$

$f_{tu} = 1.276$  MPa,  $\varepsilon_2 = 0.025$

- **Ultimate tensile strength** (Eq. 2.8)

$$\sigma_u = 2 \times 0.3 \times V_f \times \frac{1}{d} \sqrt{f_{ck}} = 2.35 \text{ MPa}, \varepsilon_u = 0.015$$

- **CNR-DT 204 (2006)** (Eqs. 2.17–2.18)

$$f_{eq1} = \frac{10.92 + 7.51}{2} = 9.215 \text{ MPa} \quad \text{for } w_{11} = \frac{0.05 + 0.5}{2} = 0.275 \text{ mm}$$

$$f_{eq2} = \frac{6.92 + 7.51}{2} = 4.835 \text{ MPa} \quad \text{for } w_{21} = \frac{2.5 + 3.5}{2} = 3.0 \text{ mm}$$

$f_{ts} = 4.146$  MPa,  $\varepsilon_1 = 0.00015$

$f_{tu} = 0.5945$  MPa,  $\varepsilon_2 = 0.020$

Knowing the key points of the stress-strain response (see, Figs. 2.9, 2.10 and 2.11), the flexural capacity of SFRC member can be computed using the equations of statics (see, Chap. 3 for details).

## References

- Akkaya Y, Picka J, Shah SP (2000) Spatial distribution of aligned short fibers in cement composites. *J Mater Civil Eng* 12(3):272–279
- American Concrete Institute (ACI) (1993) ACI 544.4R–88: Design considerations for steel fiber reinforced concrete
- Barros JAO et al (2005) Post-cracking behaviour of steel fibre reinforced concrete. *Mater Struct* 38:47–56
- CNR DT 204 (2006) Guide for the design and construction of fiber-reinforced concrete structures. National Research Council, Rome
- CEB-FIB (2010) Model code—first complete draft, vol. 1. *FIB Bull* 55:1–318

- Chalioris CE (2013) Analytical approach for the evaluation of minimum fibre factor required for steel fibrous concrete beams under combined shear and flexure. *Constr Build Mater* 43: 317–336
- Dupont D, Vandewalle CL (2005) Distribution of steel fibres in rectangular sections. *Cem Concr Compos* 27:391–398
- EN 14651:2005 Test method for metallic fibered concrete—measuring the flexural tensile strength (limit of proportionality (LOP), residual)
- Hameed R (2013) Bond stress-slip behaviour of steel reinforcing bar embedded in hybrid fiber-reinforced concrete. *KSCE J Civil Eng* 17(7):1700–1707
- Hillerborg A, Modéer M, Petersson P (1976) Analysis of crack formation and crack growth in concrete by means of fracture mechanics and finite elements. *Cem Concr Res* 6:773–780
- Gettu R, Gardner DR, Saldívar H, Barragán BE (2005) Study of the distribution and orientation of fibers in SFRC specimens. *Mater Struct* 38:31–37
- Kullaa J (1992) Constitutive modelling of fibre-reinforced concrete under uniaxial tensile loading. *Rakenteiden Mekaniikka* 25(4):24–49
- Kang ST (2011) The effect of fibre distribution characteristics on the flexural strength of steel fibre-reinforced ultra high strength concrete. *Constr Build Mater* 25:2450–2457
- Karayannis CG (2000) Analysis and experimental study for steel fibre pullout from Cementitious matrices. *Adv Compos Lett* 9(4):243–255
- Lini TY, Paramasivam P, Lee SL (1998) Behaviour of reinforced steel-fiber-concrete beams in flexure. *J Struct Eng* 113(12):2439–2458
- Marco DP, Giovanni P, Lucie V (2009) Fibre reinforced concrete: new design perspectives. *Mater Struct* 42:1261–1281
- Malik C (2014) Development of flexural-stress block for steel fibre reinforced concrete members. M. Tech. thesis, Guru Nanak Dev Engineering College, Ludhiana, India
- Mohamed M, Victor CL (1994) Flexural strength of fiber cementitious composites. *J Mater Civ Eng* 6(3):390–406
- Michels J, Christen R, Waldmann D (2013) Experimental and numerical investigation on post cracking behaviour of steel fiber reinforced concrete. *Eng Fract Mech* 98:326–349
- Nadda G (2015) Flexural stress block development for hybrid-fibre reinforced concrete members. M. Tech. thesis, Guru Nanak Dev Engineering College, Ludhiana, India
- Robert JC et al (1987) Inelastic behaviour of reinforced fibrous concrete. *J Struct Eng* 113(4): 802–817
- Robins P, Austin S, Jones P (2002) Pull-out behaviour of hooked steel fibres. *Mater Struct* 35: 434–442
- Romualdi JP, Mandel JA (1964) Tensile strength of concrete affected by uniformly dispersed and closely spaced short lengths of wire reinforcement. *J Am Concr Inst* 61:657–672
- RILEM TC 162-TDF: Test and design methods for steel fibre reinforced concrete (2002) Design of steel fibre reinforced concrete using the  $\sigma$ -w method: principles and applications. *Mater Struct* 35:262–278
- RILEM TC 162. TDF (2002) Test and design methods for steel fibre reinforced concrete: bending test. *Mater Struct* 35:579–82
- Šalna R, Marčiukaitis G (2003) Influence of fiber shape on the strength of steel fiber reinforced concrete. In: 10th International conference on modern building materials, structures and techniques, pp 763–767
- Shaurya S (2015) Effect of different types of steel fibers on flexural response of SFRC beams: experimental investigations. M. Tech. thesis, Guru Nanak Dev Engineering College, Ludhiana, India
- Soranakom C, Mobasher B (2007) Closed-form solutions for flexural response of fiber-reinforced concrete beams. *J Eng Mech* 133(8):933–941
- Soranakom C, Mobasher B (2009) Flexural design of fiber-reinforced concrete. *ACI Mater J* 106 (5):461–469
- Soroushian P, Lee C-D (1990) Distribution and orientation of fibers in steel fiber reinforced concrete. *ACI Mater J* 87(5):433–439

- Singh H (2015) Flexural modelling of steel-fibre-reinforced concrete member with conventional tensile rebars. In: Proceedings of the ICE—structures and buildings, vol 169 (SB1), pp 44–56
- Stahli P, Custer R, Van MJGM (2008) On flow properties, fibre distribution, fibre orientation and flexural behaviour of FRC. *Mater Struct* 41(1):189–196
- Stähli P, Sutter M, van Mier JGM (2007) Improving the mechanical properties of HFC by adjusting the filling method. Proceeding of RILEM fifth international workshop on high performance fibre reinforced cement composites (HPFRCC5). Mainz, Germany, pp 23–30
- Stroeven P (1979) Morphometry of fibre reinforced cementitious materials, Part II: Inhomogeneity, segregation and anisometry of partially oriented fibre structures. *Mater Struct* 12:9–20
- Swamy RN, Stavrides H (1976) Influence of the method of fabrication on strength properties of steel fibre concrete. *Mater Struct* 52(9):243–253
- Torrents JM et al (2012) Inductive method for assessing the amount and orientation of steel fibers in concrete. *Mater Struct* 45:1577–1592
- Toutanji H, Bayasi Z (1998) Effect of manufacturing techniques on the flexural behaviour of steel fiber-reinforced concrete. *Cem Concr Res* 28(1):115–124
- Tlemat H, Pilakoutas K, Neocleous K (2006) Modelling of SFRC using inverse finite element analysis. *Mater Struct* 39:221–233
- UNI 11188 (2004) Design, production and control of steel fiber reinforced structural elements
- UNI 11039 (2003) Concrete reinforced with steel fibers; (1a) Part I: Definitions, classification and designation; (1b) Part II: Test method to determine first cracking strength and ductility indexes

## Chapter 3

# Design of SFRC Flexural Members

SFRC is a modified form of concrete wherein short and discrete steel fibers are dispersed in the concrete ingredients at the time of mixing. The hardened product unlike a plain concrete possesses improved mechanical properties with an enhanced post-cracking tensile resistance and the toughness. This is happening because of the random distribution and orientation of the fibers in concrete caused at the time of mixing and its placement. When the alignment of the fibers coincides with the principal stress in a flexural member, the contribution of the fibers to the material strength is more pronounced than the case is otherwise. The fibers aligned along the direction of the principal stress in a member bridges the crack surfaces effectively and leads to a substantial increase in the ultimate tensile/flexural strength of SFRC member. The improved tensile-force carrying capacity of the concrete enables the designers to rely on the tension capacity of SFRC alone. Nevertheless, this improvement depends heavily on the pouring methods and the procedure used in the SFRC placement and its compaction in the moulds.

Unlike the conventional reinforced concrete flexural members, the failure of an SFRC member takes place when the strain on its extreme tensile face exceeds the ultimate strain value, thereby leading to either fiber pullout or fiber fracture depending upon the fiber aspect ratio used in the concrete mix. However, it can be made to fail by crushing of the concrete similar to the conventionally reinforced concrete members, when the steel bars and the steel fibers are used together to reinforce it. The inclusion of conventional rebars in the tensile zone of SFRC member reduces the strain, drastically, on its tension face and results in reduction of the crack-widths significantly. The relatively fine crack-widths aided by the discontinuous nature of the short steel fibers in the SFRC lead to a substantial reduction in the probability of the corrosion initiation. As a result, the material offers a viable option to design and optimize conventional RC flexural sections with an enhanced ductility, durability and toughness (Singh 2015; de Renaud et al. 2012; Giuseppe and Maria 2008; RILEM 2001, 2002, 2003). The present chapter discusses the design concepts and a systematic procedure to proportion flexural members using SFRC as a construction material, along with the other methods prescribed by different guidelines and design codes for this purpose.

### 3.1 Structural Design—Concept

The basic aim of a structural design is to proportion and select various dimensions of the constituent members of the structural system and their other parameters, such as materials, shape, construction technique, etc. so that it should fulfil its intended purpose with an adequate safety, serviceability and economy. Safety implies that the probability of collapse of a structural system and/or its constituent members is acceptably low, not only under the normal loads encountered during the routine occupation but also under abnormal overloads caused in the events of extremities, such as seismic activities, impacts, explosions, and consequences of human errors, to an extent disproportionate to the original design of members, etc.; whereas, the serviceability implies that the structural system perform satisfactorily under the service loads, without causing any discomfort to the occupants from the excessive deflections, vibrations, loss of durability and the possible damage to different members of the structural system because of the inadequate member sizes, etc. It is worth to note that the serviceability requirements are directly linked to the safety and economy of the structural system, e.g. the crack-width more than the permitted value may leads to an increased vulnerability of the reinforcing bars to the corrosion that could, over a period of time, lead to the strength degradation of the member, caused by the reduced effective tensile-steel area in beams. It is therefore a general practice to use safety margins in the design against the risk of failure, both in terms of collapse and unserviceability. A high value of these margins in the design is generally associated with an increased cost of the structure. The engineer should therefore judiciously choose a value of the safety margins by weighing the increased cost of the structural system on account of using higher safety margins against the potential losses that could result from any possible damage and/or unserviceability. The multiple partial safety factors are prescribed by different design guidelines, such as ACI 318 (2008), BIS 456 (2000), etc. to get the design load and safe carrying capacity of structural members. These prescribed values of the factors help ensure a uniform safety margins in the design irrespective of the design engineer. Nevertheless, the engineer can use the partial safety factors other than those specified by the design codes, based upon their wisdom and requirements of the structural member/system. Generally, these are recommended based upon experience, tradition, engineering judgement and the past performance studies to get a safe value of the stresses from the material ultimate strength exhibited under different stress-conditions, such as axial tension, axial compression, bending, shear, and/or their combinations giving different sets of the interactive phenomenon among two or more states of stresses. A separate set of factors is prescribed by different codes to meet the serviceability criterion. Generally, the partial safety factor with regards to the material allows the designer to consider the uncertainties related to the material strengths, member dimensions, assumptions in the analysis and design, etc. whereas; the factors with regards to the load take care of uncertainty and randomness associated with the load, and its possible variation over a period of time. In brief, the design must aim to achieve a design resistance of the

different members, and structural system as a whole, using the prescribed material partial safety factors greater than or at the worst, equal to the maximum load effects obtained by using the load partial safety factors and simultaneously, it must meet the serviceability requirements. It is generally required that a structural design must aim to achieve following fundamental requirements:

- The structural system must be able to sustain all actions expected to occur during the expected lifespan and perform satisfactorily as per the design philosophy.
- The structural system should have a structural form which has a low sensitivity to the hazards considered or anticipated to occur during the expected lifespan.
- The structural system must be able to survive the accidental removal/damage of some individual member.
- It should guarantee an adequate durability in order to control the maintenance costs.

The material characteristics and its response to the loading play an important role in a design process. Because the structural member is subjected to a variety of stresses while transferring the applied load to an identified support-system and during this process, it undergoes both elastic and plastic deformations depending upon the load level. If the stress level in a member exceeds a certain value defining the material nonlinearity, the member may start behaving inelastically. Nevertheless, it can be made to behave elastically by selecting an appropriate value of the safe stress. The working stress method is one such approach wherein the member is designed to operate within an elastic range of the material constitutive law. The design engineer decides about the extent the member(s) of a structural system should undergoes elastic or plastic deformations while performing their assigned duty to safely transfer the induced forces to the supporting-system. The material constitutive relationships as prescribed by the design guidelines or established by experimental studies and testing helps the designer to proportion the structural member(s) to meet the moment/shear demand imposed by the loading. It is, therefore, essential that the designer must possess adequate knowledge about the material characteristics going to be used in the construction and their failure envelop describing the safe design stresses. The following section describes a typical flexural response exhibited by SFRC member under the increasing load and ways to control the material behavior through designing. This will help the analyst to select an appropriate value of the stress level required to achieve a desired member response.

## 3.2 Flexural Responses of SFRC Members

The general flexural response of SFRC members is now well understood. Like conventional RC sections, the SFRC flexural member behaves differently after the formation of the cracks, especially at high strains. Before the formation of cracks, the flexural members cast using SFRC and those with conventional longitudinal tensile

reinforcing bars behave more or less in a similar way. Steel fibers in the SFRC members and the reinforcing bars in case of RC sections activate only after the formation of cracks that leads to deviation from the linear-elastic behavior exhibited by the member before the crack formation. In general, the flexural response of SFRC members can be classified into four phases: namely, (1) Uncracked phase; (2) Linear-elastic cracked phase; (3) Non-linear cracked phase; and (4) Fiber pullout/fracturing phase. Figure 3.1 depicts various identified phases so far and the corresponding stress-profiles plotted along the depth of an SFRC flexural member.

### 3.2.1 Uncracked Phase

In the early stages of the loading, the applied moment is less than the cracking moment of the section. No cracks develop in the section at this stage and the entire section is effective in resisting the applied moment. It usually happens, when the

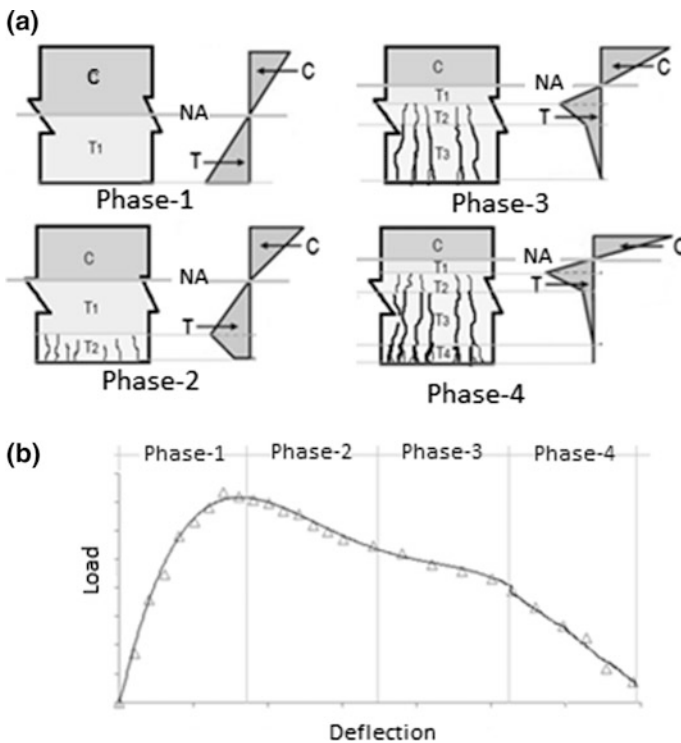


**Fig. 3.1** Load-deflection response of SFRC flexural members—A schematic representation of the flexural response exhibited by an SFRC-beam section along with a stress distribution profile along the beam depth (a). It also shows different identified phases of the flexural response earmarked on a typical load-deflection plot/response of SFRC member (b)



tensile strain caused by the loading is less than the limiting tensile strain of the concrete. Figure 3.1a shows a typical SFRC beam section in the region of maximum moment, in the phase-1 of the loading (see, Fig. 3.1b). The region C and T<sub>1</sub>, shown in the figure, represents the compressive zone and the tensile zone of the SFRC section. The distribution of the strain and the corresponding stresses can be assumed to be linear along the beam depth and the both parameters are related to each other through the *Hooke's* law. The beam section can be made to behave/operate in this phase if it is ensured that the maximum stress in the section remains less than the tensile strength of the SFRC; it generally correspond to the limit of proportionality of the material. In other words, when the maximum value of tensile strain in the section remains less than the limiting tensile strain, the slope of a load-deflection response curve exhibited by the member remains linear up to the limit of proportionality and thereafter, it deviates from the linearity at the end of this phase. There is no cracking in the tensile zone of the beam section and the maximum tensile stress is usually reached at the end of the phase. It is important to note that the fiber geometry and their mechanical properties have no influence on the load carrying capacity of the SFRC in this phase. It is a function of the concrete compressive strength only but the presence of the steel fibers in the concrete section helps to avoid the sudden failure of the beam that would otherwise occur in a beam cast using a plain concrete. The linear-elastic theory can be used to design the beam section. Nevertheless, the section meets the serviceability requirement with regards to the crack-widths as the strain-values prevailing on the tensile face of the section are abysmally small.

### 3.2.2 *Linear-Elastic Cracked Phase*

At the end of the uncracked phase, the straining of material usually becomes large enough to cause strain values higher than the limiting tensile straining capacity of the concrete; thereby leading to the formation of flexural cracks on its tension face. With increasing load, these cracks widen and propagate gradually towards the neutral-axis of the beam.

Figure 3.1a shows an SFRC beam section in the phase-2 of the loading. It is important to note that a plain concrete section becomes ineffective in resisting the tensile stresses in this phase; whereas in case of the SFRC, the tensile stresses resisted by the concrete prior to the cracking are transferred to the steel fibers, which bridges the cracked surfaces effectively in the entire cracked tension zone of the beam. The section continues to provide the requisite tensile strength needed to support the load similar to a conventionally reinforced concrete section, wherein the tensile stresses after cracking are transferred to the reinforcing bars through various bond mechanisms. However, this phenomenon results in upward shifting of the neutral-axis in the section; thereby causing an increase in the curvature at the higher loads.

Generally, this is associated with the formation of a large number of hairline-fine cracks, all distributed over the tension face of the beam section. The maximum crack-width normally varies from 0.1 to 0.3 mm in this phase. As the value of the crack-width constitutes an important serviceability limit in the design, especially, for an SFRC beam section wherein the residual-tensile strength also depends upon the extent of the crack-opening; it is therefore mandatory to conform to the applicable guidelines with regards to the crack-width, etc. while designing a SFRC section. Higher the width of the crack-opening, the lesser will be the residual tensile strength of the material, and vice versa. Because of the formation of relatively small crack-widths in the SFRC sections, the linear-elastic theory (especially, for a section in the phase-1) and the cracked-transformation section concept (for a section in the phase-2) can be used to derive expressions for stresses in the section under the service loading conditions. It is presumed that the reader is familiar with the simple theory of bending and it can be extended easily to the SFRC beam sections in the analysis. But, it is important to note that beam section designed at the ultimate limit state under the applicable factored loads must be checked for the serviceability under the service load, especially with respect to crack-widths, deflection, etc.

### 3.2.3 Non-linear Cracked Phase

With increasing load, the deflection behavior of the SFRC flexural member changes from an elastic to more or less elastic-plastic. It is generally associated with the deflection softening response with the formation of a plastic hinge, developing in the region of maximum moments in the beam. The hairline-fine cracks formed in the phase-2 start widening and it occurs rapidly. In this phase, three distinct regions exist in the tension zone of an SFRC beam, marked  $T_1$ ,  $T_2$ , and  $T_3$  in Fig. 3.1a. The region  $T_1$  in the beam section remains crack free and small hairline cracks do form in the region  $T_2$  because of the strain values which exceeds the limiting straining capacity of the material at the boundary of the  $T_1$ . Most of the steel fibers in the tensile zone  $T_3$  of the beam section exceed their peak loads and begin to slip at more or less constant loads. It is important to note that fibers in the SFRC get activated at very low slip values and a crack opening of as low as 0.1 mm. In the zone  $T_3$  of the section at this phase, the fibers with a long embedment length are still capable to carry additional load, *albeit* with increasing slip. However, the steel fibers with a smaller embedment length in the concrete start pulling out from the matrix. The steel fibers resisting the opening and widening of already developed cracks in the section are doing so primarily through the fiber-pullout mode. Nevertheless, not all steel fibers that cross the crack provide resistance, since many of them are not sufficiently anchored into the adjoining cement matrix in the SFRC; the fibers with adequate anchorage length participate in this process. This is generally accompanied by a drop in the load carrying capacity of the member as depicted in load-deflection plot (see Fig. 3.1b). The residual-tensile strength exhibited by the SFRC should theoretically be expected to remain constant if all the

fibers were aligned in the load direction. But due to the random presence and orientation of the fibers in the matrix, a substantial amount of fibers in the concrete are relatively less activated than the fibers which are aligned along the principal stress trajectories in the member, resulting in the further drop in the load carrying capacity. With the increasing crack-opening, however, the inclined fibers across the cracked surface will crush the concrete lying in-between the fiber and the crack surface as they try to straighten out under the increasing tensile stresses. Subsequently, these fibers reengage themselves in the load transfer process across the crack. This process always leads to a nonlinear response that the SFRC flexural members would exhibit in this phase. Nevertheless, the value of the residual-tensile stress of SFRC can be prevented from dropping to zero by limiting the strain value on the extreme tensile face of the SFRC flexural member to a permissible value determined experimentally through the fiber pullout response.

It is important to note the SFRC flexural members generally exhibit a linear relationship between the strain ( $\epsilon$ ) and the maximum deflection ( $\delta$ ). Following equation can be used to derive the strain value from the deflection values observed during the testing.

$$\delta = 72.4\epsilon + 0.02$$

The behavior of an SFRC beam in the nonlinear phase depends on the fiber parameters ( $V_f$  and  $l/d$ ) in addition to the compressive strength of the concrete. A parameter called as ‘fiber-index’ ( $\beta$ ) is used to quantify the residual-tensile strength of the SFRC. It should be used to check the state of the strain value prevailing on the extreme tension face of the beam section in the ultimate state. The fiber-index ( $\beta$ ) is a ratio of the residual tensile strength of the SFRC to its 28 days compressive strength at a prescribed value of the crack width ( $w$ ). It can be used conveniently to proportion the beam. The procedural details of the method are given in the next section.

The inclusion of the conventional longitudinal reinforcing bars in the section can significantly enhance the ductility of SFRC members; the conventional reinforcing bars can sustain very high tensile strains (the ultimate strains usually ranges from 0.12 to 0.2) in comparison to the SFRC. This mainly happens because of the composite action that would come into play in the member, which leads to the transfer of the tensile forces from SFRC to the embedded rebars in the tensile zone of the section.

The ultimate tensile strain and the compressive strain of SFRC range between 0.015–0.020 and 0.0035–0.0070, respectively. Therefore, irrespective of the value of the fiber-index ( $\beta$ ) and the conventional rebars percentage ( $p_t$ ), the final collapse of the member is always caused by the crushing of the concrete at the extreme compression face of the beam, regardless of whether conventional rebars have yielded or not, *albeit* it is accompanied by the wide and deep cracks formed on the tensile force of the beam in the absence of the conventional rebars at the ultimate state. It is therefore highly desirable that the SFRC-beam section must be proportioned to operate in the phase-2 in its routine use at the service load and the phase-3,

occasionally, at/near the ultimate load. The value of the permissible tensile stress (fiber index,  $\beta$ ) should therefore be selected from the permitted crack-width (CMOD) in the SFRC section based upon, both, the serviceability criterion and the strength criterion. And every attempt should be made to limit the crack-width at ultimate state to a value required to meet the permitted value of the residual strength of the material.

### 3.2.4 *Fiber Pullout/Fracturing Phase*

With the increasing crack-opening, most of the steel fibers in the concrete will, eventually, either get fractured or completely pulled out from the matrix depending upon their aspect ratio; thereby, leading to the formation of a new zone  $T_4$  in the tension zone of the SFRC beam section. This is depicted in the phase-4 of Fig. 3.1a. In this phase, the cracks are wide enough to wipe out the fibers from the concrete matrix. The concrete near the tensile face of the SFRC members virtually carries no tensile stress and it leads to a significant reduction of the effective area of the tension zone. This process results in an upward shifting of the neutral-axis of the beam under increasing load levels and is generally accompanied by large deflections that the beam exhibits because of increasing curvature in this phase of the loading. However, the beam continues to support the load because of some fibers which are still engaged near the neutral-axis in the beam tensile zone. An attempt should be made that a SFRC beam section never enter this phase by making use of suitable safety factors while designing. If design constraints warrant otherwise, then crack width should be controlled by using conventional reinforcing bars in the tension zone of the section.

### 3.3 Analysis at Ultimate Limit State

Any structural member and/or system have to be safe at various ultimate limit states as well as it should be serviceable in its routine use. At ultimate limit state, the load levels are those corresponding to the impending failure of the structure while these are corresponding to the day-to-day service loads in the serviceability limit state. It is therefore mandatory to check the safety of structures at the load levels that may cause their failure under the anticipated factored loads. At the ultimate limit state, an SFRC beam section should be designed to operate in the phase-2 or phase-3. Usually, the residual-tensile stress exhibited by SFRC in the phase-3 of the load-deflection response of the member is taken as design stress at the ultimate limit state. But the section so designed must be checked for the serviceability limits, especially for the crack-widths as the maximum value of crack-width controls the residual tensile strength as well as it affects the serviceability criteria.

The stress-profile model is the most commonly adopted method to capture the flexural capacity of members. This approach is simple to understand and uses conventional principles of the flexural mechanics. Moreover, it could be incorporated easily into a design rationale similar to that used for conventionally reinforced concrete members. The starting point of the method is to assume a stress-profile for the member, both in tension and compression, depending upon the material characteristics. A linear-strain distribution is usually assumed along the depth of the flexural member. This condition is mostly met in practice for the flexural members having a span/depth ratio of more than 2.5; otherwise, the distortions caused by the shear should be considered in the analysis. The material constitutive model defines the relationship between the strain values and the corresponding stresses mobilized at various points along the member depth. The stresses can be used to estimate the magnitude of the section forces (namely, compression and tensile) acting above and below the member neutral axis; the integration of the stress function used in the material constitutive model gives the resultant force and its point of application. The material constitutive models, described in the Chap. 2, can be used for this purpose. Once the value of the neutral-axis of the section is known from the equilibrium conditions, it can be used to predict the flexural capacity of the member and the corresponding value of the crack-width at the ultimate state.

A SFRC rectangular beam section having width ( $B$ ) and depth ( $D$ ) is considered. The quantity of the steel fibers in the beam section is expressed by means of a parameter, called as *volume fraction* ( $V_f$ ), which defines the ratio of the volume of the steel fibers present in the section to the concrete volume. Steel fibers with an aspect ratio ( $l/d$ ) are considered to be randomly distributed and presented uniformly in the entire section. The effect of the fiber orientation with respect to the loading axis and their alignment along the span and the width of the member are incorporated in the model through the material tensile-constitutive model, described in the Chap. 2.

Conventional longitudinal steel rebars having a cross-sectional area ( $A_{st}$ ) are also considered to be present in the beam section at a distance ( $d'$ ) from its bottom face for a sake of completeness. By putting a zero value of tensile steel areas ( $A_{st}$ ), the model can be used for the analysis of a SFRC beam section; otherwise, it gives results for the SFRC section reinforced using conventional steel bars. Figure 3.2 gives a schematic representation of the beam section along with the stress-profile adopted in the present analysis.

Cracking initiates in an SFRC member once the principal tensile stresses caused by the external loading exceed the material limiting tensile strength. This phenomenon causes the neutral-axis in the member to move towards its compressive face. In such a scenario, the equilibrium of the section is predominantly maintained by the pullout resistance of the fibers bridging the cracks below the section neutral-axis and the compressive force being mobilized above the neutral-axis (the phase-3 of the load-deflection response). The residual-tensile strength of SFRC required for maintaining the equilibrium of the beam section after the cracking can

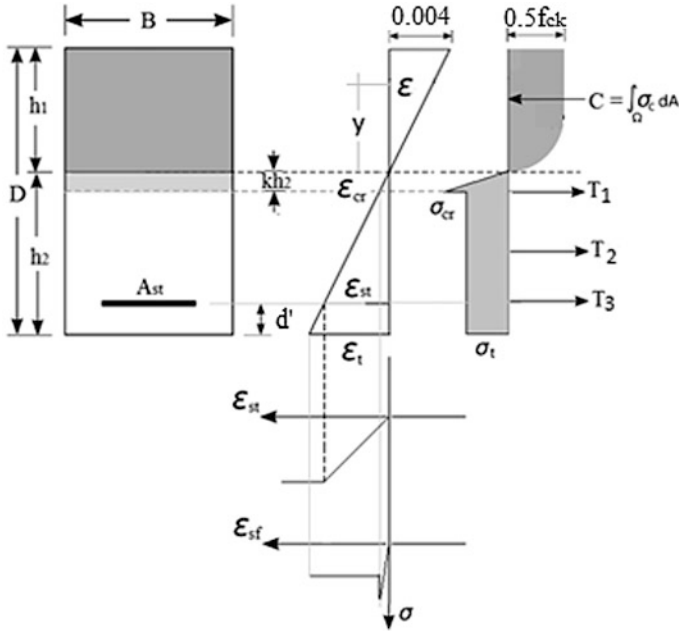


**Fig. 3.2** *Stress-profile model*—A schematic representation of an SFRC-beam section reinforced with the conventional longitudinal reinforcement on its tensile zone. It also shows the strain and stress distribution along the beam depth along with the tension-constitutive relationships of conventional rebars and SFRC. The local reinforcing capability of the steel fibers present in the mortar matrix significantly enhances the post-cracking characteristics of the concrete. The residual-tensile strength of the SFRC and that mobilized in rebars contributes towards the flexural strength of the SFRC members. Nevertheless, the extent of improvement depends upon the fiber parameters considered in the concrete mix viz: fiber aspect ratio ( $l/d$ ) and volume fraction ( $V_f$ )

be taken from the constitutive tension model described in the previous chapter. However, in the case of an SFRC flexural member having conventional longitudinal tensile reinforcement in its tensile zone, the tensile strength of the rebars will also mobilize and contribute in controlling the position of the neutral-axis in the section depending upon the strain-value prevailing at the level of the rebars in addition to the contribution from the steel fibers present in its tensile zone.

Knowing the radius of curvature,  $r$  ( $=\epsilon/y$ ) of the beam, the strain ( $\epsilon$ ) at any level ( $y$ ) from the neutral-axis of the beam can be determined. This is based on the fact that the plane section normal to the beam-axis remains plane after bending for a member having a *span/depth ratio* of more than 2.5. This concept can be used easily to develop a relationship between the position of the neutral-axis (defined by  $h_1$  and  $h_2$ ) in the beam section and the extreme strain values prevailing at the beam

top face ( $\epsilon_{cu}$ ) and the beam bottom faces ( $\epsilon_t$ ) and/or strain at the level of the rebars ( $\epsilon_{st}$ ). The summation of  $h_1$  and  $h_2$  denotes the depth ( $D$ ) of the section. This relationship is given in Eq. 3.1.

$$r = \frac{\epsilon_{cu}}{h_1} = \frac{\epsilon_t}{h_2} = \frac{\epsilon_{st}}{(d - h_1)} = \frac{\epsilon_{st}}{(h_2 - d')} \quad (3.1)$$

The Eq. 3.1 can be simplified to determine the depth of the neutral axis ( $h_1$ ) in the beam. The values of  $(h_1/D)_b$  and  $(h_2/D)_b$  define the position of the neutral axis in the balanced-state, when the strain values at the top face of the beam ( $\epsilon_{cu}$ ) and at the level of the tensile steel ( $\epsilon_{st}$ ) in the beam reached, simultaneously, their extreme limits [see, Chap. 2 for details]. Equation 3.2 gives the position of the neutral axis in the balanced state of the SFRC beam. It can be determined using the similarity of the strain triangles existing above and below the neutral-axis of the beam section.

$$\left(\frac{h_1}{D}\right)_b = \left(\frac{\epsilon_{cu}}{\epsilon_{cu} + \epsilon_{st}}\right) \frac{d}{D} \quad \text{and} \quad \left(\frac{h_2}{D}\right)_b = \left(\frac{\epsilon_{st}}{\epsilon_{cu} + \epsilon_{st}}\right) \frac{d}{D} \quad (3.2)$$

Similarly, the depth of the uncracked concrete zone ( $kh_2$ ) existing in the beam section below its neutral axis can be determined using Eq. 3.1. This zone extends from the neutral axis to a depth where tensile stress in the section becomes equal to the limiting tensile strength ( $\sigma_{cr}$ ) of the concrete. The similarity of the strain diagrams shown in Fig. 3.2 can be used to find the value of the constant ( $k$ ) and it is given in Eq. 3.3.

$$k = \frac{\epsilon_{cr}}{\epsilon_t} \quad (3.3)$$

The principle of statics [ $\int_A \sigma \partial A = 0$  and  $\int_A \sigma y \partial A = M$ ] can be used to calculate the actual position of the neutral-axis in the SFRC beam section and the corresponding moment capacity ( $M_u$ ). The expanded version of these two expressions is given below:

$$\int_{h_2}^{h_1} \sigma B \partial y = Br \int_{h_2}^{h_1} \sigma \partial \epsilon = 0 \quad (3.4)$$

Equation 3.4 indicates that the position of the neutral-axis in a beam section is such that the integral vanishes for any assumed stress distribution along its depth. This means that the actual position of the neutral-axis of the beam can be determined by equating the areas of the compression zone (C) and the SFRC tension-stress block (a sum total of  $T_1$  and  $T_2$ ) along with the contribution from the conventional reinforcing rebars ( $T_3$ ) present in the section, i.e.

$$C = T_1 + T_2 + T_3$$

$$\text{Or } 0.4167f_{ck} h_1 B = \frac{1}{2} \sigma_{cr} k h_2 B + \sigma_t (1 - k) h_2 B + \sigma_{st} A_{st} \quad (3.5a)$$

$$\Rightarrow \frac{h_1}{h_2} = \frac{0.5 \sigma_{cr} k + \sigma_t (1 - k) + \sigma_{st} p \left( \frac{D}{h_2} \right)}{0.4167 \xi f_{ck}} \quad (3.5b)$$

$$\text{and, } h_1 + h_2 = D \quad (3.5b)$$

Equation 3.5 indicates the actual position of the neutral-axis in the beam section. Equations 3.5a and 3.5b can be used together to find actual values of the section neutral-axis. It is pertinent to note that the position of the neutral-axis depends entirely on the material properties of the SFRC and the extent to which the stress in the conventional longitudinal rebars are mobilized under a given loading condition. A simplified form of equation the 3.5 is given in Eq. 3.6.

$$\xi \frac{h_1}{D} = \left( \frac{2.38\beta + 2.4\gamma\omega}{1 + 2.38\beta} \right) \text{ and } \frac{h_2}{D} = \left( 1 - \frac{h_1}{D} \right) \quad (3.6)$$

In Eq. 3.6, the parameter ( $\beta$ ) is a fiber-index of the SFRC that denotes the ratio of the material residual-tensile strength to its 28 days compressive strength corresponding to some specified crack-width; whereas, the constant ( $\omega$ ) is a reinforcement-index [ $= (A_{sr}/BD) f_y/f_{ck}$ ] and ( $\gamma$ ) is a constant which describes the extent to which the stress in the conventional longitudinal tensile reinforcement bars, having yield strength ( $f_y$ ), is mobilized under the prevailing strain condition in the member. The value of the stress-mobilization factor ( $\gamma$ ) for the conventional reinforcing bars at different strain values in excess of the elastic strain are given in Table 3.1. These values have been derived based upon the constitutive relationship prescribed by the IS 456 (2000) for the cold worked deformed bars. Otherwise, these values can be obtained from IS 456 (2000) as given therein in the clause 38.1.e. The parameter ( $\xi$ ) in Eq. 3.5 and 3.6 represents the effect of the steel fiber inclusion in the concrete on its crushing strain; it raises from 0.0035 (for a plain concrete) to 0.004 (for a SFRC). The value of the parameter ( $\xi$ ) is unity for the SFRC and it is 0.86 for the plain concrete.

Equations 3.2 and 3.6 can be used to ascertain the state of the strain prevailing in the beam section and an attempt should be made to keep ( $h/D$ )-ratios well within the limits prescribed by Eq. 3.2; otherwise, the failure will take place by over-straining of the material. In the case of SFRC, the resulting failure is brittle in nature. It takes place abruptly by crushing of the concrete in the beam in case it is reinforced using conventional rebars in its tensile zone. In both cases, the failure is generally

**Table 3.1** Values of stress-mobilization factor ( $\gamma$ ) for reinforcing rebars

Strain	<0.00144	0.00144	0.00154	0.00174	0.00214	0.00244	≥0.0038
Factor ( $\gamma$ )	$\varepsilon E / f_y$	0.70	0.74	0.78	0.83	0.85	0.87



accompanied by the formation of wide cracks on the beam tensile face. It is important to note that the SFRC beam without conventional longitudinal reinforcing bars can lose its tensile capacity in case the flexural cracks became wide enough to wipe out the contribution of the steel fibers lying in the section tension zone. The presence of conventional rebars prevents the sudden loss of flexural capacity even if these are provided in a small dosage.

Similarly, the moment capacity ( $M_u$ ) of the SFRC beam section can be determined using the equation of statics. This is given in Eq. 3.7. The term C in the expression represents the compressive force mobilized above the neutral-axis in the concrete; whereas,  $T_1$ ,  $T_2$  and  $T_3$  denote the tensile resistance of the uncracked portion of the concrete existing below the neutral-axis, the residual-tensile strength of the SFRC and the tensile force mobilized in the longitudinal rebars, respectively. The magnitude of the forces being induced in different zones of the SFRC beam section can be determined by integrating their respective stress-block areas. Figure 3.2 schematically depicts the process to find the magnitude of these forces.

$$M_u = C(0.5833h_1) + T_1 \left( \frac{2}{3}kh_2 \right) + T_2 \left[ h_2 - \frac{(1-k)h_2}{2} \right] + T_3(h_2 - d') \quad (3.7)$$

Equation 3.7 can be simplified to a non-dimensional form as given in Eq. 3.8 by substituting the values of  $C_1$ ,  $T_1$ ,  $T_2$  and  $T_3$ .

$$\frac{M_u}{f_{ck}BD^2} = \left[ 0.24\xi \left( \frac{h_1}{D} \right)^2 + \left( \frac{h_2}{D} \right)^2 \left\{ \alpha\beta + 0.5\beta + \gamma\omega \left( \frac{D}{h_2} \right) \left( 1 - \frac{d'}{D} \frac{D}{h_2} \right) \right\} \right] \quad (3.8)$$

In Eq. 3.8,  $\alpha$  denotes a constant that considers the contribution of the uncracked concrete existing below the neutral-axis of the SFRC flexural member. Equation 3.9 gives a simplified expression to find the value of this constant. It is important to note that the value of the constant ( $\alpha$ ) depends entirely on the physical properties of the SFRC, such as the cracking tensile strength ( $\sigma_{cr}$ ) and the residual-tensile strength ( $\sigma_r$ ) of SFRC. The parameter ( $k$ ) in the expression depends upon the ratio of the concrete cracking-strain ( $\varepsilon_{cr}$ ) and ultimate tensile strain ( $\varepsilon_t$ ) adopted in the design of an SFRC beam section. The value of the parameter ( $k$ ) normally ranges from 0.0075 to 0.01. In practice, the value of the cracking-strain can be taken identical to that of a plain concrete (=0.00015) and the value of the ultimate strain in tension should be adopted corresponding to the permitted crack-width at the ultimate limit state. It can be taken as 0.015 for SFRC in case the crack-width is not specified or SFRC experimental stress-CMOD response is unknown.

$$\alpha = \left[ \frac{1}{3} \left( \frac{\sigma_{cr}}{\sigma_r} \right) k^2 - \left( \frac{k^2}{2} \right) \right] \quad (3.9)$$

Generally, the value of ( $k$ ) is too small to affect the overall analysis results. It is therefore always safer to ignore the contribution of the uncracked concrete existing

below the neutral-axis. Accordingly, the value of the constant ( $\alpha$ ) can be ignored during the analysis without affecting the accuracy of the results. This process results in further simplification of Eq. 3.8; it is given in Eq. 3.10.

$$\frac{M_u}{f_{ck}BD^2} = \left[ 0.24\xi \left( \frac{h_1}{D} \right)^2 + \left( \frac{h_2}{D} \right)^2 \left\{ 0.5\beta + \gamma\omega \left( \frac{D}{h_2} \right) \left( 1 - \frac{d'}{D} \right) \right\} \right] \quad (3.10)$$

In Eq. 3.10, the fiber-index ( $\beta = \sigma_t/f_{ck}$ ) is a ratio of the residual-tensile strength of the SFRC at some specified crack-width ( $w$ ) and its 28 days compressive strength. An expression for estimating the value of the SFRC residual tensile strength ( $\sigma_t$ ) is given in Eq. 2.8 or it can be obtained from the SFRC experimental stress-CMOD response for a prescribed value of the crack-opening. The depth-ratio ( $d'/D$ ) defines the position of the conventional longitudinal tensile rebars in the flexural member from the section bottom face. The position of the neutral-axis ( $h/D$ ) in the beam section can be determined from Eq. 3.6. The limiting strain values for the SFRC in compression ( $\epsilon_{cu}$ ) can be adopted at 0.004; while for the steel rebars (Fe415 grade), this value ( $\epsilon_{st}$ ) can be taken as 0.0038. Accordingly, Eq. 3.1 can be simplified to Eq. 3.11 in term of the depth-ratio ( $d'/D$ ) and the position of the neutral-axis ( $h_1/D$  and  $h_2/D$ ) in the beam section.

$$0.95 \left( \frac{h_1}{D} \right) = \left( \frac{h_2}{D} - \frac{d'}{D} \right) \quad (3.11)$$

By substituting the values of ( $h/D$ )-ratio from Eq. 3.6 in the Eq. 3.11, a simplified expression can be obtained in terms of the fiber-index ( $\beta$ ) and the reinforcement-index ( $\omega$ ). Equation 3.12 gives the final expression giving a relationship between these two parameters in the balanced-state ( $\beta_c$  and  $\omega_c$ ) of the beam and the value of the depth-ratio ( $d'/D$ ) adopted in the design.

$$\beta_c = \left[ \frac{1 - 4.076\omega_c - \left( \frac{d'}{D} \right)}{2.26 + 2.38 \left( \frac{d'}{D} \right)} \right] \quad (3.12)$$

The critical combinations of ( $\beta$ - $\omega$ ) values for different depth-ratio ( $d'/D$ ) of the conventional tensile rebars in a flexural member are shown in Fig. 3.3. If the fiber-index ( $\beta$ ) and the reinforcement-index ( $\omega$ ) values are taken in a manner that these two values fall in the area enclosed by the graph-axis and the straight line plotted for different depth-ratio ( $d'/D$ ) of the longitudinal tensile rebars, the impending section failure is always ductile one, taking place by yielding of the tensile rebars. The figure also indicates that the longitudinal tensile rebars if placed closed to the bottom face of a SFRC flexural member give a relatively wide spectrum of the ( $\beta$ - $\omega$ ) values to choose from than the case when the rebars are placed nearer to the neutral-axis of the member. It is interesting to note that the quantity of the conventional reinforcing rebars in the SFRC beam section can be reduced by increasing the fiber content ( $V_f$ ) in the section, and vice versa. In case,

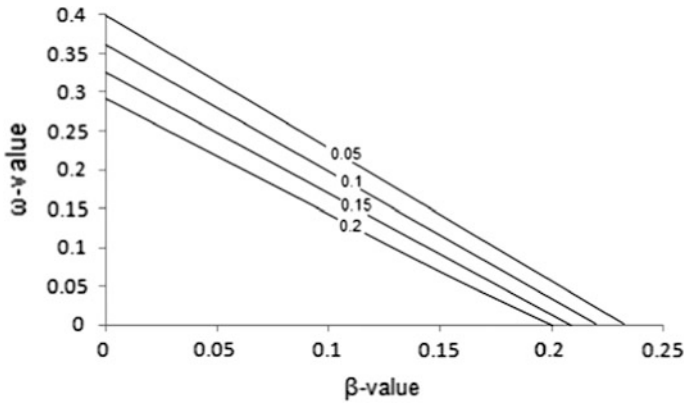


**Fig. 3.3**  $\beta$ - $\omega$  values for different depth-ratio of the conventional tensile rebars in SFRC flexural member—The chart can be used to select an appropriate combination of the fibre-index ( $\beta$ ) and reinforcement-index ( $\omega$ ) in the beam section to ensure that it should behave in a ductile manner. If the selected value of the fiber-index and reinforcement-index falls in the area shown in the figure, the impending failure is ductile in nature

the ( $\beta$ - $\omega$ ) values selected during a design process fall outside the critical envelop shown in Fig. 3.3, the flexural member always fails by crushing of the concrete lying near its compression face. It generally occurs abruptly and without giving any warning.

The fiber aspect ratio ( $l/d$ ) for the steel fibers to be used in concrete mix should be selected corresponding to the fiber-pullout failure mode; wherein, the fiber aspect ratio is kept less than its critical value (see, Eq. 2.7), and vice versa for the other mode of failure. It is always better to proportion the SFRC beam section in the fiber pullout mode as it results in a section failure in the ductile mode with an ample warning time, unlike a failure in the fiber-fracture mode which is sudden and brittle in nature. Although quantity of the fibers required in the later case is less but it will require the fibers long enough to provide a fiber aspect ratio higher than the corresponding critical fiber aspect ratio. Equation 3.13 gives a simplified expression for the value of the fiber-index ( $\beta$ ) in the fiber-pullout failure mode. This equation is applicable for the plain-straight fibers having quantity/dosage expressed by means of fiber volume fraction ( $V_f$ ) and fiber aspect ratio ( $l/d$ ); it has been obtained by substituting the value of the residual tensile strength of SFRC (see, Eq. 2.8) and its characteristics strength ( $f_{ck}$ ).

$$\beta = \frac{0.3V_f(l/d)}{\sqrt{f_{ck}}} \quad (3.13)$$

Equation 3.10 can be used to generate a set of design charts for proportioning SFRC beam sections for different design constraints. The Figs. 3.4, 3.5 and 3.6 have been plotted for a commonly used depth-ratio ( $d'/D$ ) of 0.05, 0.10, and 0.15 in

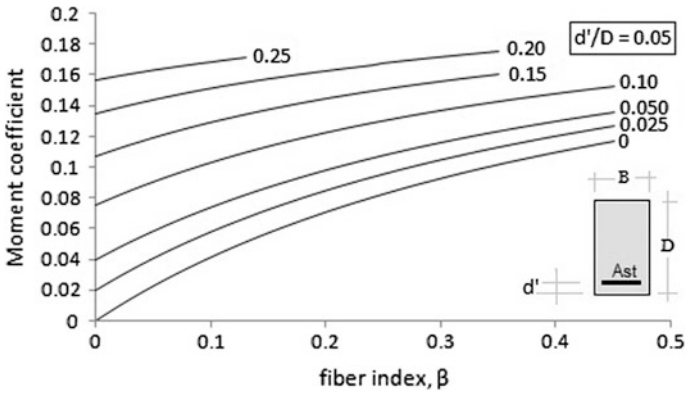


**Fig. 3.4** *Moment coefficient variation of SFRC beam with the fiber-index*—The chart can be used to select an appropriate combination of the fiber-index ( $\beta$ ) and reinforcement-index ( $\omega$ ) in the beam section to ensure that it should behave in a ductile manner and simultaneously meets the moment demand. It indicates that beam section needs higher fiber dosage at low values of  $\omega$ -values, and vice versa to meet a given moment demand

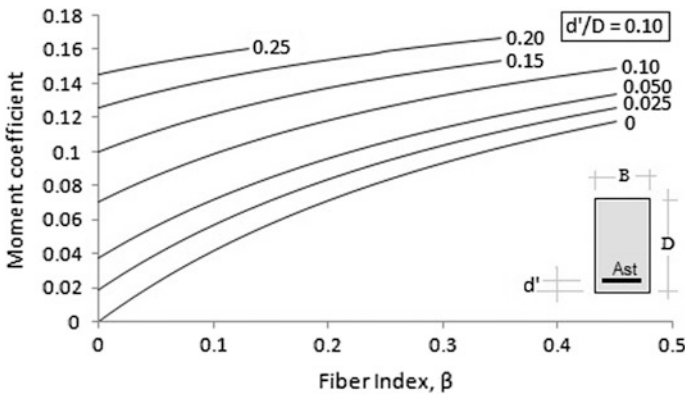


**Fig. 3.5** *Moment coefficient variation of SFRC beam with the fiber-index*—The chart can be used to proportionate SFRC beam section reinforced with conventional rebars at a depth-ratio of 0.10. The comparison of charts, given in Figs. 3.4 and 3.5, shows that the beam section needs a higher percentage of reinforcing steel if these are placed nearer to the neutral-axis (i.e. higher value of the depth-ratio)

routine practice. The value of the constant ( $\gamma$ ) has been adopted corresponding to the strain-value prevailing in the section at the time of analysis; therefore, these charts can be used as a design-aid for a SFRC flexural member reinforced using conventional reinforcing bars in its tensile zone.



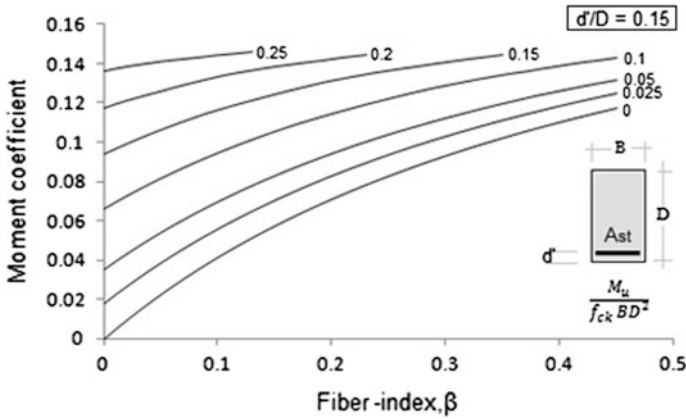


**Fig. 3.6** Moment coefficient variation of SFRC beam with the fiber-index—The chart can be used to proportionate a SFRC beam reinforced with conventional rebars at a depth-ratio of 0.15. The beam section designed at a higher value of depth-ratio requires relatively higher fiber dosage for a given value of tensile steel area, and vice versa. However, it is always better to use a minimum percentage of tensile steel rebars in the tensile zone of the SFRC beams as this helps to reduce the tensile strain drastically and the consequential crack-width. Nevertheless, the use of a ( $\beta$ - $\omega$ ) combination meeting the requirement of a balanced-state section is always a good choice to opt for the design

### 3.4 Design of RC Sections

The flexural model (Eq. 3.10) developed in the previous section can be used also to predict the ultimate capacity of the rectangular concrete sections having conventional longitudinal rebars as their alone tension reinforcement. It is important to note that the concrete beams always fail by crushing of the concrete lying in their extreme compression face, irrespective of the amount of the reinforcement provided in its tensile zone, both in the conventional RC sections as well as SFRC sections. This happens because of the lower straining capacity of the concrete, both in the compression (0.0035 for a plain concrete and 0.004 for the SFRC) and the tension (0.00015), in comparison to the rebars (0.12) and the SFRC (0.015). The figures shown in the brackets are the generally accepted values of the limiting strain values of the respective material. The strain values indicate that the plain concrete fails relatively earlier than the SFRC, and it accordingly provides a smaller compressive resistance than the SFRC. The magnitude of the compressive resistance above the section neutral-axis can be determined by integrating the area of the stress-strain response exhibited by the concrete. The ratio of the compressive resistance provided by the plain concrete and the SFRC comes to be 0.86. Therefore, the first term in the expression (Eq. 3.10) showing the contribution of the compressive zone in a beam towards its flexural capacity must be multiplied by a factor ( $\xi$ ) of 0.86 to get the actual capacity of RC sections. Nevertheless, the value of this factor ( $\xi$ ) is unity for an SFRC section. The simplified expression for this purpose is shown in Eq. 3.14 by taking the value of the fiber-index ( $\beta$ ) as zero for an RC section.

$$\frac{M_u}{f_{ck}BD^2} = \left[ 0.24\xi \left(\frac{h_1}{D}\right)^2 + \left(\frac{h_2}{D}\right)^2 \left\{ 0.5\beta + \gamma\omega \left(\frac{D}{h_2}\right) \left(1 - \frac{d'}{D} \frac{D}{h_2}\right) \right\} \right] \quad (3.14)$$

$$\frac{M_u}{f_{ck}BD^2} = \left[ 0.2064 \left(\frac{h_1}{D}\right)^2 + \gamma\omega \left(\frac{D}{h_2}\right) \left(1 - \frac{d'}{D} \frac{D}{h_2}\right) \left(\frac{h_2}{D}\right)^2 \right]$$

The value of the neutral-axis coefficients ( $h_1/D$ ,  $h_2/D$ ) can be determined using a set of simplified expression given in Eq. 3.15 for the RC sections for any given value of the reinforcement-index ( $\omega$ ). In this equation, the value of the neutral-axis coefficient determined from Eq. 3.6 has been divided by  $\xi$  ( $= 0.86$ ) for a RC beam section. The value of the fiber-index for a RC section is zero. The strain-compatibility method can be used to arrive at the exact value of the neutral-axis coefficients ( $h_1/D$  and  $h_2/D$ ) for the beam sections having a value of the reinforcement-index ( $\omega$ ) of more than 0.2, representing an over-reinforced beam section. It can be easily verified that the RC beam always behave as an over-reinforced section, if the value of the reinforcement index ( $\omega$ ) is kept more than 0.2 in the design. The value of stress-mobilization factor ( $\gamma$ ) can be taken from Table 3.1 depending upon the value of the strain mobilized at the rebar level in the beam section.

$$\frac{h_1}{D} = 2.77\gamma\omega; \text{ and } \frac{h_2}{D} = \left(1 - \frac{h_1}{D}\right) \quad (3.15)$$

### Example 3.1

*A reinforced concrete beam of rectangular section has the cross-sectional dimensions of 300 mm × 600 mm. The beam is reinforced with 4 No.—25 mm diameter rebars in its tensile zone at an effective depth of 550 mm. Assuming M20 concrete and Fe 415 grade steel; compute the ultimate flexural capacity of the beam section.*

#### Solution

- Given: B = 300 mm, D = 600 mm, d = 550 mm,  $A_{st} = 1963 \text{ mm}^2$ ,  $f_y = 415 \text{ MPa}$ ,  $f_{ck} = 20 \text{ MPa}$
- The value of the reinforcement-index ( $\omega$ ) =  $\frac{1963 \times 415}{300 \times 600 \times 20} = 0.2263 > 0.2$ , thereby indicating that the section is over-reinforced in nature.<sup>1</sup>
- $d' = 600 - 550 = 50 \text{ mm}$
- $\frac{d'}{d} = \frac{50}{550} = 0.091$
- $\frac{d'}{D} = \frac{50}{600} = 0.0833$
- $\frac{d}{D} = \frac{550}{600} = 0.917$
- For a Fe415 steel grade, the limiting value of the neutral-axis coefficient ( $h_1/D$ ) = 0.479 ( $d/D$ ) = 0.439

<sup>1</sup>It can be proved that the value of the reinforcement-index ( $\omega$ ) > 0.2 always results in an over-reinforced beam section.

- As the section is over-reinforced ( $\omega > 0.2$ ); therefore, in order to determine the approximate position of the section neutral-axis (first trial), the value of the stress-mobilization factor ( $\Upsilon$ ) is taken as 0.87, corresponding to the known values of the stress ( $=0.87f_y$ ) mobilized in the tensile steel at the yield strain (Eq. 3.15)

$$\frac{h_1}{D} = 2.77\gamma\omega = 2.77 \times 0.87 \times 0.2263 = 0.5494 > 0.439$$

The first trial confirms that the section is over-reinforced. Therefore, the strain at the rebar level in the section can be determined using the strain-compatibility conditions. The equation for this purpose can be derived using the similarity of the strain triangles existing above and below the neutral-axis of the beam in terms of the limiting strain of the concrete in compression (i.e. 0.0035) and it can be used to calculate the strain in the rebars for a given value of the  $h_1/D$ . The value of the limit strain in concrete should be taken as 0.0035 ( $= 0.86 \times 0.004$ ) in case of a RC beam section. The equation is given below:

$$\epsilon_{st} = 0.0035 \left( \frac{D}{h_1} \frac{d}{D} - 1 \right) = 0.00234$$

The value of the rebar stress-mobilization factor ( $\Upsilon$ ) corresponding to this value of the strain is obtained as 0.8433 (from Table 3.1) and then, Eq. 3.15 is again used to find the new value of the neutral-axis position, expressed as  $h_1/D$ . This process is repeated till the difference between the new and the last obtained value becomes insignificant.

2nd cycle:

$$\frac{h_1}{D} = 2.77\gamma\omega = 2.77 \times 0.8433 \times 0.2263 = 0.5286 \quad (\text{Using Eq. 3.15})$$

$$\Rightarrow \epsilon_{st} = 0.002571 \Rightarrow \Upsilon = 0.8519 \quad (\text{Using Table 3.1})$$

3rd cycle:

$$\frac{h_1}{D} = 2.77\gamma\omega = 2.77 \times 0.8519 \times 0.2263 = 0.5340 \quad (\text{Using Eq. 3.15})$$

$$\Rightarrow \epsilon_{st} = 0.00251 \Rightarrow \Upsilon = 0.8510 \quad (\text{Using Table 3.1})$$

4th cycle:

$$\frac{h_1}{D} = 2.77\gamma\omega = 2.77 \times 0.851 \times 0.2263 = 0.5334 \quad (\text{Using Eq. 3.15})$$

$$\Rightarrow \epsilon_{st} = 0.002516 \Rightarrow \Upsilon = 0.8511 \quad (\text{Using Table 3.1})$$

The difference of the neutral-axis coefficients as obtained from the 3rd and the 4th cycle becomes approximately zero; therefore, the value determined at the end of the 4th cycle can be adopted as its true value. The value of the  $h_2/D$  is determined as  $0.4666(1 - 0.5334)$

The section flexural capacity can be determined using Eq. 3.14.

$$\frac{M_u}{f_{ck}BD^2} = \left[ 0.24 \times 0.86(0.5334)^2 + 0.8511 \times 0.2264 \times \frac{1}{0.4666} \times \left( 1 - \frac{0.0833}{0.4666} \right) (0.4666)^2 \right]$$

$$\frac{M_u}{f_{ck}BD^2} = 0.1326 \Rightarrow M_u = 286.06 \text{ kN m}$$

### 3.5 Design of SFRC Sections

The use of the flexural model (Eq. 3.10) developed in the previous section can be extended to predict the ultimate capacity of rectangular sections reinforced with the steel fibers alone. It is worthwhile to note that SFRC beams must be proportioned using the permitted value of the crack-width in the beam section; both at the serviceability and the ultimate limit states; the anchorage capacity of the steel fibers present in the concrete depends entirely on the crack-opening/width. A wide crack may lead to a premature section failure by the fiber pullout mode and it must be ensured that the selected value of the fiber aspect ratio must be kept less than then its critical value and it must be sufficiently large in comparison to the crack-width to prevent the premature failure in the fiber pullout. Most of the design guidelines put an upper limit of 3.5 mm on the maximum value of the crack opening in the beam section corresponding to the ultimate limit state. Eq. 3.16 gives a flexural capacity of SFRC members. It has been obtained from Eq. 3.10 by taking the contribution from the conventional steel bars as zero.

$$\frac{M_u}{f_{ck}BD^2} = \left[ 0.24 \left( \frac{h_1}{D} \right)^2 + 0.5\beta \left( \frac{h_2}{D} \right)^2 \right] \quad (3.16)$$

The value of the neutral-axis coefficients ( $h_1/D$ ,  $h_2/D$ ) can be determined using a set of simplified expression given in Eq. 3.17 for the SFRC beam sections, for any given value of the fiber-index ( $\beta$ ). The Fig. 3.7 shows the variation of the moment coefficient ( $M_u/f_{ck} B D^2$ ) and the crack-width coefficient ( $w/D$ ) against the fiber-index ( $\beta$ ) adopted in the design. This design chart has been plotted using Eqs. 3.16 and 3.17 and it can be used to estimate the flexural capacity of the SFRC beam section and the crack-width ( $w$ ) that is expected to develop on the tensile face of the member when subjected to a moment ( $M_u$ ).



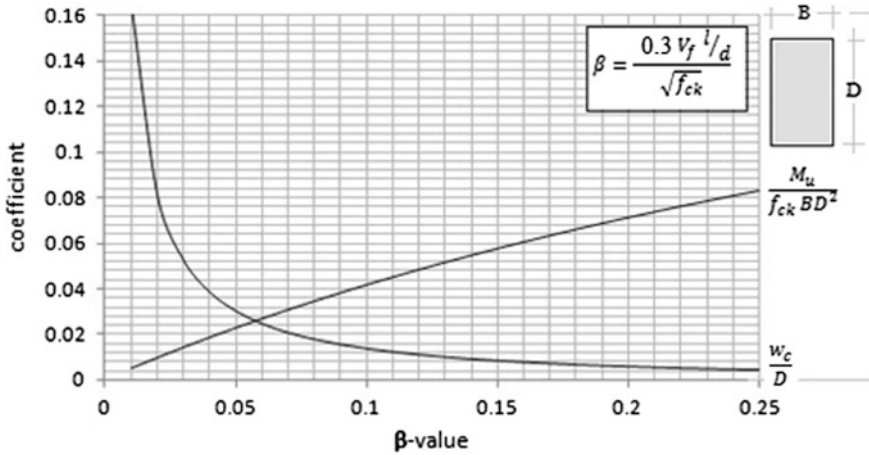


**Fig. 3.7** Moment coefficient and crack-width variation of SFRC beam with the fiber-index—The chart can be used to select an value of the fiber-index ( $\beta$ ) in the SFRC beam section to ensure that it meets the serviceability criterion (crack-width) and the ultimate strength limit states [Singh (2014)]

$$\frac{h_1}{D} = \left( \frac{2.38\beta}{1 + 2.38\beta} \right) \text{ and } \frac{h_2}{D} = \left( 1 - \frac{h_1}{D} \right) \tag{3.17}$$

It is important to note that the depth of the neutral-axis in an SFRC beam is a function of the fiber-index ( $\beta$ ) alone and the high value of the fiber-index indicate a higher tensile strength of the material. It is recommended that the fiber-index value less than 0.05 should never be used in the concrete mix/design as it results in very wide flexural cracks in the section.

The SFRC beam section will exhibit a strain-softening or strain-hardening response in its post-cracking range depending upon the fiber parameters ( $l/d$  and  $V_f$ ) and the concrete grade ( $f_{ck}$ ) taken in the design; the values of the fiber parameters can be used to determine the fiber-index ( $\beta$ ) for the design purpose. This value of the fiber index should be kept at least close to or higher than the balanced-state value ( $\beta_c$ ) to get an advantage of the strain-hardening; thereby giving enhanced member toughness; a desirable feature for any structural system designed to carry dynamic loading effects. Nevertheless, a SFRC member designed to exhibit a strain-hardening response produces relatively finer flexural cracks. Accordingly, a set of fiber parameters are determined to proportion the beam section in the balance state. Table 3.2 gives the various key-parameters required to achieve the balanced-state conditions in the design.

These values have been derived for the concrete crushing strain of 0.0040 and the ultimate tensile strain of 0.015 for SFRC. The values given in Table 3.2 should be modified in case the ultimate strains other than those used therein are taken in the design. The minimum quantity of the steel fibers to be added to the concrete mix



**Table 3.2** SFRC section-constants in the balanced state

Concrete limiting strains		$(h_1/D)_{\text{bal}}$	$\beta_c$	$\frac{M_u}{f_{ck}BD^2}$	$(V_f l/d)$ for plain straight fibers	
Compression, $\varepsilon_{cu}$	Tension, $\varepsilon_t$				Fiber pull-out mode	Fiber fracture mode
0.004	0.015	0.211	0.1123	0.0458	$0.375\sqrt{f_{ck}}$	$0.075\sqrt{f_{ck}}$

should conform to Eq. 2.9 in order to get the advantage of the material strain-hardening behavior.

### Example 3.2

An SFRC one-way slab with an effective span of 4.0 m is required to support a live load of 4 kN/m<sup>2</sup> along with a surface finish of 1 kN/m<sup>2</sup>. The hooked-end steel fibers are used in the M20 concrete to obtain the SFRC. The yield strength of the steel fibers is 1150 MPa. Suggest a suitable proportion of the steel fibers required in the concrete mix for this purpose.

### Solution

Assume an effective depth,  $d = 4000/25 \cong 160$  mm and an overall slab depth of 165 mm is adopted in the design.

Distributed load due to self weight of the slab =  $0.165 \times 25 = 4.125$  kN/m<sup>2</sup>  
 $\Rightarrow$  Total dead load =  $4.125 + 1 \approx 6$  kN/m<sup>2</sup> and, the factored load =  $1.5(6 + 4) = 15$  kN/m<sup>2</sup>

The factored bending moment  $M_u = (15 \times 4^2)/8 = 30$  kN m/m

And, the corresponding moment-coefficient =  $M_u/(f_{ck} BD^2) = 0.0375$

Equation 3.16 or Fig. 3.7 can be used to determine the value of the fiber-index ( $\beta$ ) required to provide a requisite strength of the slab, which is obtained as 0.09 in the present case. But, this value of the fiber-index is found to be less than the critical value ( $\beta_c$ ), given in Table 3.2 for the balanced-state of the SFRC beam section. It must therefore, be taken as  $\beta_c (=0.1123)$  to limit the tensile-strain to 0.015 on the extreme face of the slab section. The expression given in Eq. 3.13 can be used to get the values of the fiber-parameters corresponding to the adopted value of the fiber-index in the design. However, it is important to note that the fiber aspect-ratio finalised in the design should not exceed the critical fiber-aspect ratio to ensure a ductile response of the SFRC member under applied loading conditions. The critical fiber-aspect ratio  $(l/d)_c$  for the present example is found to be 75 [=  $(0.58 \times 1150)/(2 \times \sqrt{20})$ ]. A fiber shape factor of two has been used in following calculation for the hooked-end fibers considered in the mix design. Therefore, the maximum fiber-aspect ratio must be limited to 75 to ensure a ductile post-cracking behavior of the SFRC member and to avoid the fiber fracturing at ultimate state.

$$\beta = \frac{0.3V_f(l/d)}{\sqrt{f_{ck}}} = \frac{0.3 \times 2 \times V_f(l/d)}{\sqrt{20}} = 0.134V_f(l/d)$$

By equating the value of the fiber-index ( $\beta$ ) adopted in the design (say =0.12) with an expression simplified for the present case (as given above), a suitable combination of the fiber volume fraction ( $V_f$ ) and the fiber aspect-ratio ( $l/d$ ) can be obtained to provide the requisite flexural strength to the SFRC slab. It is given below:

$$\Rightarrow V_f (l/d) = 0.9$$

By using the above expression, a suitable dosage of the fibers with a maximum permitted value of the aspect ratio, limited to 75 or as determined from the workability considerations, can be determined to obtain M20 concrete mix. The workability requirements and other compaction/placement constraints of the concrete mix can change the value of the fiber parameters, such as  $l/d$  and  $V_f$ , determined from the strength considerations. It is worth to note that the improper workability or difficulty to place the SFRC properly in the moulds could drastically change its strength properties.

Table 3.3 lists different possible combinations of the fiber aspect ratio ( $l/d$ ) and the corresponding fiber volume fraction ( $V_f$ ) required to produce SFRC. It is given both for the fiber indexes of  $\beta = 0.09$  and 0.12 for a comparison purpose. It is however recommended to use values corresponding to the fiber-index ( $\beta$ ) = 0.12 only.

The minimum value of the fiber volume fraction ( $V_f$ ) required to get the advantage of the strain-hardening in the slab can be determined from Eq. 2.10; it is found as 1.5 % for the present case. It is therefore advisable to select the minimum dosage of the steel fibers having aspect ratio of 60 or less to get the benefit of the strain-hardening; the SFRC with a strain-hardening response exhibits fine cracks well scattered over the member tension face unlike the strain-softening material which undergoes a few wide to very wide cracks at the ultimate load.

A value of the fiber index higher than 0.12 can also be adopted in the design, if limiting the crack-width to some value is a major design constraint, but it generally requires a very high dosage of the volume fraction in the concrete to produce SFRC, which can significantly affect the flow characteristics and workability of the mix. In such cases, it is better to provide conventional longitudinal tensile steel reinforcing

**Table 3.3** Design options to select an appropriate combination of fiber-parameters at  $\beta = 0.09$  and 0.12

Aspect ratio, $l/d$	Volume fraction, $V_f$ (%)		Corresponding weight of the steel fibers ( $\text{kg/m}^3$ )	
	$\beta = 0.09$ (required)	$\beta = 0.12$ (adopted)	$\beta = 0.09$ (required)	$\beta = 0.12$ (adopted)
50	1.35	1.80	106	142
60	1.12	1.50	88	118
70	0.96	1.29	76	102
75	0.90	1.20	71	95

bars in the tensile zone of the beam section along with the steel fibers to further optimize the structural member.

The values of the section neutral-axis coefficients ( $h_1/D$  and  $h_2/D$ ) corresponding to the adopted value of the fiber-index ( $\beta$ ) = 0.12 are calculated from Eq. 3.17. These are given below:

$$h_1 / D = 0.2221 \text{ and } h_2 / D = 0.7778$$

Equation 3.16 can be used to find the corresponding value of the ultimate flexural capacity ( $M_u$ ) of the SFRC slab section; it is given below:

$$\frac{M_u}{f_{ck}BD^2} = \left[ 0.24 (0.2221)^2 + 0.5 \times 0.12 (0.7778)^2 \right] = 0.0481$$

Therefore, the SFRC slab possesses a moment of resistance ( $M_u$ ) = 38.51 kN m > 30.0 kN m; indicating that the selected dosage of the steel fibers at an appropriate value of the fiber aspect ratio, given in the Table 3.3, can achieve the requisite moment-demand of the SFRC slab. The value of the crack-width that would appear in the section at the ultimate moment/load can be found out using the design chart given in Fig. 3.7. It is obtained as 0.66 mm (=0.004 × 165); thereby indicating that the adopted section also meets the serviceability criterion.

### Example 3.3

*A rectangular SFRC beam has cross-sectional dimensions of 300 mm × 600 mm. Assuming M20 concrete and Fe 415 grade steel, design a suitable dosage of the hooked-end steel fibers required to provide an ultimate flexural capacity ( $M_u$ ) of 287 kN m, alone or along with the conventional reinforcing bars in its tensile zone. The yield strength of steel fibers is 1150 MPa.*

### Solution

- Given: B = 300 mm, D = 600 mm, Take d = 550 mm,  $f_y = 415$  MPa,  $f_{ck} = 20$  MPa,  $M_u = 287$  kN m

And, the corresponding moment-coefficient =  $M_u/(f_{ck} BD^2) = 0.1329$

Equation 3.16 or Fig. 3.7 indicate that SFRC section alone is not sufficient to provide a requisite flexural strength to the beam as the value obtained from the figure falls outside the range shown therein. It will, therefore, suffice if the SFRC beam section is proportioned in its balance state and the remaining value of the flexural capacity is achieved by providing conventional reinforcing steel bars in the tension zone of the section. The balanced-state parameters of an SFRC rectangular beam section are given in Table 3.2. The value of the fiber-index ( $\beta_c$ ) = 0.1123 and the corresponding moment coefficient (=0.0458) can be used to find the balanced flexural capacity ( $M_{ub}$ ) of the section.

$$M_{ub} = 0.0458 \times 20 \times 300 \times 600^2 = 99 \text{ kN m}$$

The balance flexural capacity ( $M_{u1}$ ) required to be provided by the conventional longitudinal tensile rebars =  $287 - 99 = 188 \text{ kN m}$

Therefore, the approximate value of the tensile steel,

$$\begin{aligned} A_{st} &\cong \frac{M_{u1}}{0.87f_y d} \\ &= 941.76 \text{ mm}^2 \end{aligned}$$

Use 3 No.-20 diameter in the tensile zone of the beam with a following set of the depth ratios.

- $\frac{d'}{d} = \frac{50}{550} = 0.091$
- $\frac{d'}{D} = \frac{50}{600} = 0.0833$
- $\frac{d}{D} = \frac{550}{600} = 0.917$
- The value of the reinforcement-index ( $\omega$ ) =  $\frac{3 \times 314 \times 415}{300 \times 600 \times 20} = 0.1086$
- For Fe 415 steel, the limiting value of the neutral-axis ( $h_1/D$ ) = 0.479 ( $d/D$ ) = 0.439
- Assuming an under-reinforced section; thereby taking  $\gamma = 0.87$  (using Eqs. 3.6 and 3.15)

$$\begin{aligned} \frac{h_1}{D} &= 0.392 < 0.439 \text{ and} \\ \frac{h_2}{D} &= 1 - 0.392 = 0.608 \end{aligned}$$

The section is under-reinforced. The rebar mobilization factor, therefore, can be taken as 0.87 from the Table 3.2, as the strain at the level of the rebar in the section is 0.005357 ( $>0.0038$ ). The strain at the rebar level in the SFRC was determined using following strain-compatibility condition.

$$\epsilon_{st} = 0.004 \left( \frac{D}{h_1} \frac{d}{D} - 1 \right) = 0.005357$$

It is interesting to note that the strain at the level of the longitudinal rebars in the beam section increases to 0.01065, when the beam is cast using the plain concrete (as in the conventional RC sections) instead of the SFRC. This increase in the strain is of the order of approximately 100 %. Therefore, an RC section is expected to have wider cracks on its tensile face in comparison to an equivalent SFRC section

because of a higher strain value prevailing at the rebar level in the former case. The strain at the rebar level in a beam section is an indirect measure of the crack-width.

The flexural capacity of the SFRC beam having conventional longitudinal tensile rebars in the section can be determined using Eq. 3.10.

$$\begin{aligned} \frac{M_u}{f_{ck}BD^2} &= \left[ 0.24 \left( \frac{h_1}{D} \right)^2 + \left( \frac{h_2}{D} \right)^2 \left\{ 0.5\beta + \gamma\omega \left( \frac{D}{h_2} \right) \left( 1 - \frac{d'D}{Dh_2} \right) \right\} \right] \\ &= 0.1436 > 0.1329 \quad (\text{OK}) \\ M_u &= 0.1436 \times 20 \times 300 \times 550^2 = 310,000,000 \text{ N mm } (=310 \text{ kN m}) \end{aligned}$$

The dosage of the steel fibers required in the beam section can be determined using Eq. 3.13 for an adopted value of the fiber-index  $\beta_c$  ( $=0.1123$ ) for a balanced section. Nevertheless, the fiber aspect-ratio finalised in the design should not exceed the critical fiber-aspect ratio. The critical fiber-aspect ratio  $(l/d)_c$  for the present example is determined as 75 [ $=(0.58 \times 1150)/(2 \times \sqrt{20})$ ]. A fiber shape factor of two has been used in the following calculation for the Hooked-end fibers adopted in the present case. The maximum fiber-aspect ratio therefore should be limited to 75 to avoid the fiber fracturing at the ultimate state.

$$\begin{aligned} \beta &= 0.1123 = \frac{0.3V_f(l/d)}{\sqrt{f_{ck}}} = \frac{0.3 \times 2 \times V_f(l/d)}{\sqrt{20}} = 0.1342V_f(l/d) \\ \Rightarrow V_f(l/d) &= 0.84 \end{aligned}$$

Table 3.4 shows a set of different dosage ( $V_f$ ) of the hooked-end steel fibers that can be used to achieve the required section flexural capacity of 310 kN m ( $>287$  kN m) along with the 3 No. of 20 mm diameter longitudinal tensile rebars provided at an effective cover of 50 mm from the bottom face of the beam. The fiber length and its diameter can be taken corresponding to the volume fraction ( $V_f$ ) adopted for the mix.

However, the design specifications listing the fiber parameters, e.g. the fiber aspect ratio  $(l/d)$  and its volume fraction ( $V_f$ ) required to get a desired performance should be freezed based upon the results of an experimental investigations carried out to see the influence the effect of fiber parameters on the flow characteristics and other fresh concrete properties.

**Table 3.4** Design options to select an appropriate combination of fiber-parameters

Aspect ratio, $l/d$	Volume fraction, $V_f$ (%)	Steel fibers dosage ( $\text{kg/m}^3$ )
50	1.68	135
60	1.40	112
70	1.20	96
75	1.12	88

### 3.6 Variation of $M_u$ with the Fiber-Parameters ( $V_f$ and $l/d$ ) and Reinforcement-Index

This section presents the influence of the fiber parameters, expressed as fiber-index ( $\beta$ ), and the reinforcement-index ( $\omega$ ) on the flexural capacity ( $M_u$ ) of an SFRC section. The fiber-index ( $\beta$ ) is a measure of the residual-tensile strength of the SFRC. A high value of the index indicates a higher section flexural capacity. Equation 3.13 indicates that it increases with an increase in the value of the volume fraction ( $V_f$ ) and a fiber aspect ratio ( $l/d$ ) used in the concrete mix. The compressive strength of concrete marginally affects the value of the fiber-index. An SFRC beam, therefore, designed at a higher value of the fiber-index is expected to possess a more flexural capacity. The addition of the conventional longitudinal reinforcing bars in the tensile zone of the beam tends to increase it further. But the overall improvement in the flexural capacity contributed by the steel fibers in the concrete and the longitudinal reinforcing bars is not additive in nature and consequently, it cannot be obtained by just superimposing the flexural capacities of the SFRC and RC sections. Figure 3.8 shows a typical variation of the flexural capacity of an SFRC section reinforced with the conventional longitudinal rebars in its tension zone, provided at a depth-ratio of 0.15. The figure shows that the flexural capacity ( $M_u$ ) of an SFRC member increases with an increase in the value of the fiber-parameters (both the fiber-content and the fiber aspect ratio) in the concrete mix for different concrete grades/strength, represented by fiber-index ( $\beta$ ), and for all values of the reinforcement-index ( $\omega$ ). However, the rate of the gain in the flexural capacity diminishes very fast at a high

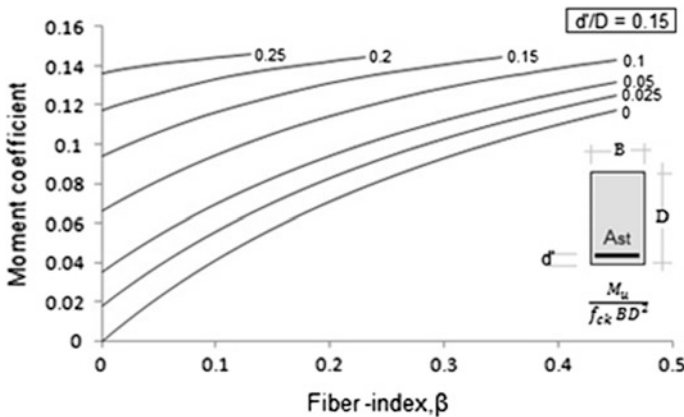


**Fig. 3.8**  $M_u$ - $\beta$ - $\omega$  interaction in an SFRC flexural member—The chart indicates that moment capacity ( $M_u$ ) of a SFRC section increases with an increase of either the fiber-index ( $\beta$ ) or reinforcement-index ( $\omega$ ) or both. It is interesting to note that percentage of conventional longitudinal steel reduces with the increase of the fiber-index ( $\beta$ ) and, vice versa is also true. If the values of the fiber-index and reinforcement-index are selected from the curve, the impending section failure is ductile in nature [Singh (2015)]

value of either the fiber-index or the reinforcement-index, and/or both. This happens because of the lowering of the neutral-axis in the section caused by the addition of a high dose of the fiber-content in the concrete mix and/or the high percentage of the longitudinal rebars provided in the tension zone of the section. This lowering of the neutral-axis in the section results in the delayed straining of the longitudinal rebars present therein. It is equally possible that it may prevent the yielding of the tensile reinforcing bars in beam sections, especially when the section has been designed with a large value of the fiber-index. Consequently, the contribution of these longitudinal rebars towards the flexural capacity of an SFRC section diminishes very fast at higher values of the fiber-index.

A similar phenomenon happens in the case of a heavily reinforced section, represented by a high reinforcement-index ( $\omega$ ) value, but with a relatively lower value of the fiber-index; wherein, the magnitude of the tensile stress mobilized in the longitudinal reinforcing bars reduces to an extent that the contribution of the induced tensile force in the rebars became insignificant towards the flexural capacity of the section. A graphical representation of this phenomenon occurring in an SFRC flexural member is shown in Fig. 3.9 that indicates the influence of fiber-index ( $\beta$ ) on the tensile stress mobilized in the reinforcing bars placed at 0.15D from the bottom face of the beam.

Interestingly, unlike the conventionally reinforced concrete beams, the SFRC beams offer an improved flexural behavior wherein an identical value of the flexural capacity can be achieved by selecting different combinations of ( $\beta$ - $\omega$ ) values in the

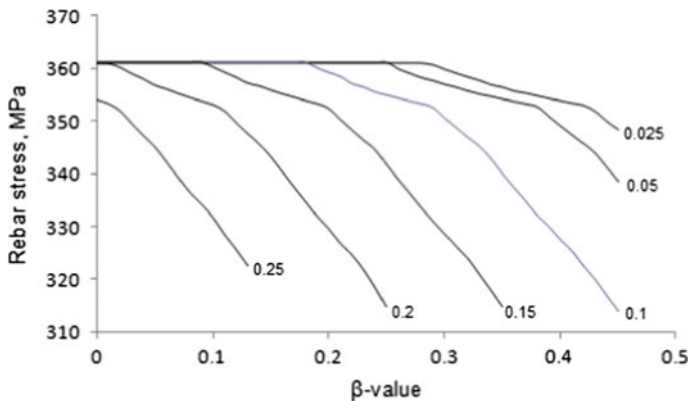


**Fig. 3.9** Effect of fiber-index on rebar stressing in a SFRC flexural member—The chart indicates that the stress in the longitudinal reinforcing rebars provided in tensile zone of a SFRC section dies down rapidly with an increase of either the fiber-index ( $\beta$ ) or reinforcement-index ( $\omega$ ) or both. This happens due to the delayed straining of the rebars caused by a relatively stronger tension zone of an SFRC section in comparison to the RC sections wherein the rebars get activated soon after the formation of a first crack in the concrete. In SFRC, the presence of the steel fibers in the concrete prevents the opening up of the cracks in the tension zone and in the case, these are formed, the fibers present there prevent them from widening-up and slow down their further progress towards the neutral-axis; thereby delaying the mobilization of the rebar force



section. It is worthwhile to note that in case of the SFRC flexural members, it is possible to attain the same value of the flexural capacity either by providing a low percentage of the conventional longitudinal tensile reinforcement ( $\omega$ -value) in the section along with a matching but a relatively high dosage of the fiber content ( $\beta$ -value), and vice versa. There exist a large number of ( $\beta$ - $\omega$ )-combinations to choose during the design of SFRC members. This enables the designer to detail an SFRC beam section comfortably in case it requires a heavy tensile reinforcement area on its tensile zone to meet a high moment demand imposed by the given loading conditions. However, it must be ensured that the combination of ( $\beta$ - $\omega$ )-values so selected during the beam proportioning must conform to the conditions imposed by Eq. 3.12 or as given in the Fig. 3.3; otherwise, it is likely that the beam section will turn into an over-reinforced section that fail by the crushing of the concrete laying near the top face of the member, especially in the regions of maximum moments.

Table 3.5 presents the results from a case study conducted on a set of SFRC beams designed with the different combinations of the ( $\beta$ - $\omega$ ) values for an identical flexural capacity. In the design option-1, no conventional reinforcing bars ( $\omega = 0$ ) have been used in the beam section and the flexural capacity is solely because of a high dosage of the steel fibers present in the concrete; whereas in option-4, the flexural capacity is only coming from the conventional longitudinal reinforcing bars present on the tensile face of the beam section.

In option-2 and 3, both the steel fibers in the concrete as well as the longitudinal reinforcing bars on the tensile face of the beam section contribute towards the flexural capacity, represented in term of the moment-coefficient [ $M_u/f_{ck}BD^2$ ]. All beam specimens have been designed using the procedure suggested in the previous sections.

The SFRC member therefore, unlike the conventionally reinforced concrete beams, gives a wide spectrum of the design options to a designer to meet the detailing requirement of applicable design code along with enhanced post-cracking characteristics. The values given in the Table 3.5 have been worked out for the fiber pullout failure mode—a desirable characteristics of SFRC, over the fiber-fracture mode, which is brittle in nature and results in a sudden failure. It is, therefore, advisable that the fiber content and the corresponding value of the fiber aspect ratio should be kept as high in the concrete mix as permitted by the workability requirements and from the cost-benefit ratio considerations. Nevertheless, the fiber aspect ratio in the concrete mix must be kept less than the critical fiber aspect ratio to ensure a ductile failure at ultimate state.

**Table 3.5** Flexural capacity of a member at different combinations of ( $\beta$ - $\omega$ )-values

Moment coefficient $= \frac{M_u}{f_{ck}BD^2}$	Rectangular-SFRC beam (B × D)							
	Option-1		Option-2		Option-3		Option-4	
	$\beta$ -value	$\omega$ -value	$\beta$ -value	$\omega$ -value	$\beta$ -value	$\omega$ -value	$\beta$ -value	$\omega$ -value
0.10	0.340	0.000	0.285	0.025	0.130	0.100	0.000	0.165

### 3.7 Influence of the Fiber-Index and Reinforcement-Index on the Rebar-Straining

This section presents the influence of the fiber-index ( $\beta$ ) and reinforcement-index ( $\omega$ ) on the strain-values prevailing at the level of the longitudinal tensile rebars in a SFRC flexural member. The strain value calculated at the member tensile face or at the level of the longitudinal tensile reinforcing bars is an indirect measure of the crack-width ( $w$ ) appearing on the tensile face of the SFRC beam section; therefore, it can be used as a key parameter while designing and/or checking SFRC member for the serviceability limits.

Figure 3.10 indicates that the strain value at the level of the longitudinal reinforcing bars in the SFRC flexural member reduces drastically with a increase in the fiber-index ( $\beta$ ) in comparison to the beam section wherein no conventional reinforcing bars are provided ( $\omega = 0$ ). This reduction in the strain value at the level of the reinforcing bars in the beam section needs special attention, particularly when the beam has been provided with the conventional longitudinal tension rebars alone and is designed to operate near the balanced-state or as an under-reinforced section.

The inclusion of the steel fibers in the concrete used to cast the beam reduce, drastically, the rebar straining and could transform the RC section to an over-reinforced type beam; wherein, the failure occurs by concrete crushing and it is abrupt and sudden in comparison to a more ductile failure that would occur otherwise in case of an under-reinforced beam. Nevertheless, the energy absorption capacity of an over-reinforced flexural members is significantly less in comparison to equivalently designed under-reinforced beams. It is therefore highly advisable to check the status of the beam and an attempt should be made to select an appropriate

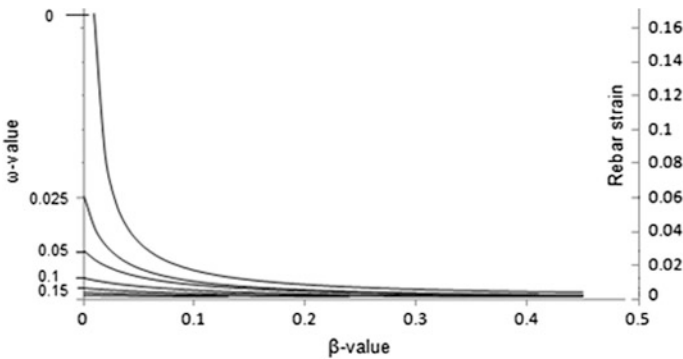


**Fig. 3.10** Effect of fiber-index and reinforcement-index on rebar-straining in a SFRC flexural member—The presence of steel fibers in quantities that give fiber-index value of more than 0.1 have a huge effect on the magnitude of the strain that a rebar would experience in a SFRC section. It can even change an otherwise under-reinforced RC section to an over-reinforced section when fibers are arbitrarily added to the concrete mix. It is therefore highly desirable to be very cautious while using the steel fibers in the conventionally reinforced beam sections

dosage of the steel fibers to keep the section under-reinforced. Figure 3.3 or Eq. 3.12 can be used to meet this requirement.

In case, the SFRC section is lightly reinforced using the longitudinal tensile reinforcing bars (e.g. with  $\omega = 0.025$ ), the tensile reinforcement in the section experiences a reduction of about 70 % in the rebar straining. This value of the reinforcement-index ( $\omega = 0.025$ ) corresponds to a tensile reinforcement steel area (fy415 grade steel) of 0.12 % for the M20 concrete mix. This happens because of the fibers in the concrete, which arrest the formation of the cracks and their subsequent widening and progress in the beam section. This process delays the straining and the consequential yielding of the reinforcing bars. The fibers are found to be most effective when the section has been designed with the value of the fiber-index in close vicinity of  $\beta_c$  (see, Table 3.2). The percentage of tensile steel in the section is immaterial as the large dosage of the fibers will not allow the rebars to contribute anything significant towards the flexural capacity. If the section has been designed with the fiber index ( $\beta$ )  $< \beta_c$  (especially, with a value less than 0.1), the presence of the longitudinal rebars in the section help to reduce the tensile strain on its extreme tensile face, which is a direct measure of the crack width opening that would be developed on the tension face of the section.

It is important to highlight that the inclusion of the conventional longitudinal reinforcing bars in the SFRC beam section enhances the effective tensile strength of the SFRC beam tensile zone. The presence of the rebars in the tensile zone of the SFRC member increases the effectiveness of the steel fibers as well. This mainly happens because of the reduction of the crack-width; the steel fibers and the longitudinal rebars in the section complement each other in arresting the initiation of cracks and their subsequent widening in the section. The enhanced tensile strength of the SFRC therefore causes the neutral-axis in the section to move downward and leads to further reduction of the strain on the extreme tension face of the beam. This trend is shown in Fig. 3.11 which indicates that there is a gradual downward movement of the neutral-axis ( $h_2/D$ ) in the beam section as the effective strength of the tensile zone, indicated by the fiber-index ( $\beta$ ), of a SFRC beam increases. The presence of the longitudinal rebars in the section also leads to the downward movement of the neutral-axis; higher the percentage of tensile steel in the section more rapidly it shifts the section neutral-axis towards the tensile face of the member.

With the increase in the concrete strength, however, this trend gets reversed and causes the upwards shifting of the neutral axis. But this upward movement of the neutral axis simultaneously increases the strain value at the bottom face of the member; thereby it may result in wider and deeper cracks in case of the SFRC designed with a low value of the fiber-index ( $\beta$ ). It is therefore always advisable to use a highest possible value of the fiber content along with a corresponding value of the fiber aspect ratio in the concrete mix, along with a compatible percentage of the longitudinal tension reinforcement. It will result in a more ductile beam section with enhanced flexural capacity and toughness as indicated in a typical moment-curvature curve (Fig. 3.13), reduced crack widths due to a relatively small strain values prevailing on the section tensile face and importantly, a saving of some part of the

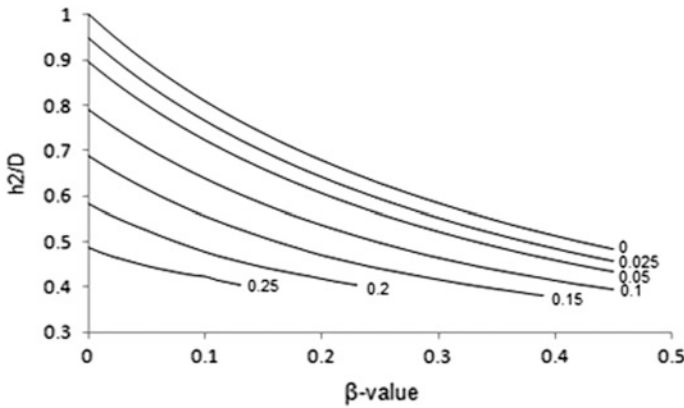


**Fig. 3.11** Effect of fiber-index on the position of the neutral-axis in a SFRC flexural member—The chart indicates the downward shifting of the neutral-axis in a SFRC with an increase of the fiber-index. This downward shifting of the neutral-axis lowers the tensile strain on the extreme face of the section thereby leading to the reduced crack-width

labour cost that otherwise will incur in the steel rebar cutting, bending and its fixation, etc. in case of the conventionally reinforced concrete beams.

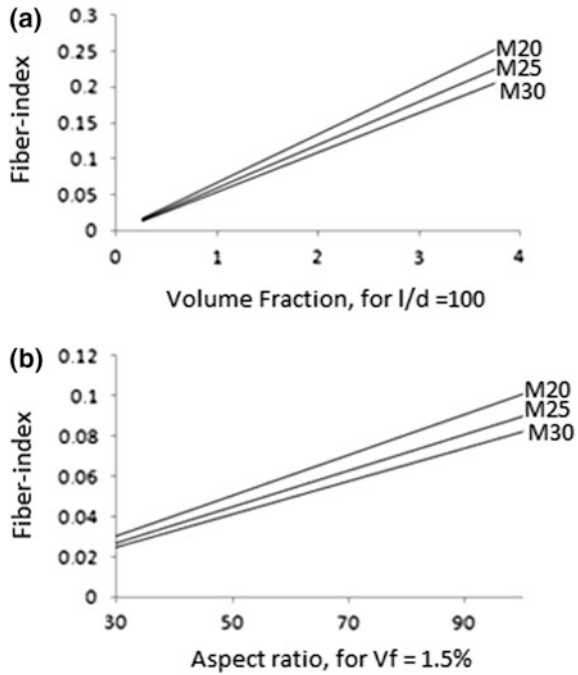
### 3.8 Influence of the Fiber-Parameters ( $V_f$ and $l/d$ ) on the Fiber-Index ( $\beta$ )

In the previous section, it is stated that the value of the fiber volume fraction ( $V_f$ ) and the fiber aspect ratio ( $l/d$ ) should be selected from the workability requirement and the concrete placement technique used at the time of casting. Improper selection of these two parameters in the SFRC gives either an inadequate post-cracking performance or leads to a harsh concrete mix that may be very difficult to handle and consequentially, it results in the poor residual-tensile strength and the post-cracking behaviour.

Figure 3.12a, b gives the variation of the fiber-index ( $\beta$ ) with the fiber-content ( $V_f$ ) and the fiber aspect ratio ( $l/d$ ) for different grades of the concrete. It indicates that the concrete grade has a pronounced effect on the fiber-index ( $\beta$ ) only at the higher value of the volume fraction ( $V_f$ ) and it becomes insignificant at the lower values. At a given value of the volume fraction, a low grade concrete (like, M20 mix) gives a higher value of the fiber-index in comparison to the high strength concretes, such as M25, M30, and so on. A low grade concrete, therefore, is better to use in the SFRC than the higher grade concrete mixes, if design calculations permits so. Moreover, in case of a higher concrete grade, using concrete to its full strength is not possible due to the limiting tensile strength of the SFRC, unless the effective tensile strength of the tension zone of the beam section is increased, either

**Fig. 3.12** Influence of fiber parameters on the fiber-index

—The chart indicates that the fiber-index value of SFRC is linearly related to the fiber aspect ratio or its quantity expressed by means of volume fraction irrespective of the compressive strength of the concrete. Low grade concrete, such as M20, gives a higher value of the fiber-index irrespective of  $V_f$  or  $l/d$  used in the concrete mix. The concrete grade did not have a significant influence on the fiber-index at the volume fraction ( $V_f$ ) normally used in practice, i.e. 0.75 % to the maximum value of 2 %



by using a higher fiber-content, expressed using ( $V_f$ ) and the corresponding fiber aspect ratio in the concrete or by means of additional longitudinal tensile reinforcing bars in the tensile zone of the beam. The comfortable mixing of the fibers in the concrete and its subsequent placement and handling will normally decide the maximum fiber dosage in the concrete that can be adopted in the design of a SFRC beam; experimental investigations are suggested to arrive at a workable combination of the fiber parameters required to achieve the desirable post-cracking performance and the comfortable handling of SFRC in its fresh state.

### 3.9 Moment-Curvature Response of SFRC Members

The moment-curvature response of a beam is a measure of its toughness or energy absorption capacity. The curvature denotes a change of the slope that a member undergoes upon loading. It can be conveniently measured from the linear strain distribution in the member section as a ratio of the summation of the compressive strain in the extreme concrete fiber ( $\epsilon_{cu}$ ) and the strain prevailing at the centroid of the reinforcing rebars ( $\epsilon_{st}$ ) or extreme tensile face ( $\epsilon_t$ ) of an SFRC section to the member depth ( $D$ ). It is worthwhile to note that the material constitutive relationship describing the material response upon loading plays a vital role in formulating the moment-curvature response of a flexural member. Because the stresses mobilized in

the compression zone and the tension zone of a member at various load levels defines the position of the section neutral-axis, which in turn controls the strain values at the top and bottom face of the member. The constitutive models of SFRC, given in the Chap. 2, can be used for this purpose along with the equations of statics to derive the corresponding value of the moment of resistance of a flexural member.

The response curve extending over a large strain values indicates higher member toughness. Generally, the addition of the steel fibers in the concrete enhances the beam toughness. This happens because of the bridging action of the steel fibers present in the concrete mass that prevents the widening of the cracks and their further progress toward the section neutral-axis, similar to the reinforcing mechanism exhibited by the conventional longitudinal reinforcing bars in a conventional RC section. The random presence of the fibers in the concrete simultaneously increases the crushing strain of the concrete from 0.0035 (for the plain concrete) to a value as high as 0.009 (for the SFRC) depending upon the fiber parameters adopted in the mix design. The results from a typical case study are presented in Table 3.6 to illustrate the improvement of the toughness caused by the fiber

**Table 3.6** Comparison of analytical and experimental value of the flexural capacity

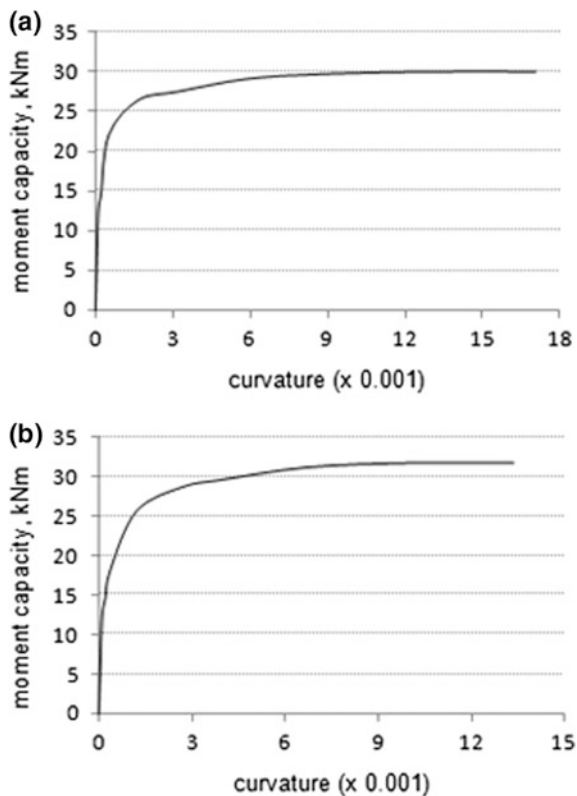
Beam parameters	Beam-		
	1	2	3
Size of SFRC beam (mm)	152 × 254	152 × 254	152 × 254
Span of the beam (mm)	2200	2200	2200
Fibre volume fraction, $V_f$ (%)	0.5	1.0	0.5
Fibre Aspect ratio, $l/d$	60	60	60
Conventional tensile rebars detail	2–16 mm diameter	2–16 mm diameter	2–16 mm diameter
Cracking strain value, $\epsilon_{cr}$	0.0001	0.0001	0.0001
Concrete modulus of elasticity, E (MPa)	25300	25300	25300
Cracking tensile strength of the concrete, $\sigma_{cr} = \epsilon_{cr} E$ (MPa)	2.53	2.53	2.53
Concrete compressive strength, $f_{ck}$	27.2	27.2	27.2
Yield strength of tensile rebars, $f_y$ (MPa)	450	450	450
Residual tensile strength of the SFRC, $\sigma_t$ (MPa)	0.938	1.878	0.9387
$\beta$ -value = $\frac{\sigma_c}{f_{ck}}$	0.0345	0.069	0.0345
$\omega$ -value = $p_t \frac{f_y}{f_{ck}}$	0.1894	0.1894	0.3788
Depth ratio = $\frac{d'}{D}$	0.0906	0.0906	0.0906
Analytical Moment Capacity, $M_{th}$ (kN m) (Eq. 3.10)	34.47	36.11	46.25
Reported experimental Moment Capacity, $M_{ex}$ (kN m)	36.00	38.00	45.00
$(M_{th}/M_{ex})$ -ratio	0.96	0.95	1.03
Failure observed	Yielding of rebars	Yielding of rebars	Concrete crushing

addition to the concrete mix at the time of the concrete production. The beam specimens reported in the experimental investigations by Lini et al. (1998) was considered in the case study to check and compare the moment-curvature response of the SFRC beams with those obtained from the analytical model (Eq. 3.10).

Figure 3.13 presents a typical set of the moment-curvature responses exhibited by the SFRC beams (Fig. 3.13a for the beam-1 and Fig. 3.13b for the beam-2). These moment-curvature response curves have been plotted using the constitutive models and corresponding flexural model, given in the Sect. 3.3. A similar trend has been reported by Lini et al. (1998) for the various test specimens considered in the experimental study.

Figure 3.13 indicate that the beam-2 (designed with  $\beta = 0.069$ ) exhibits a slightly higher flexural capacity (+5.38 %) than the beam-1 which has been proportioned using the fiber index  $\beta = 0.0345$ . The corresponding value of the beam curvature for the beam-2 reduces by 27.75 % in comparison to the beam-1, determined corresponding the strain value of 0.004. However, the toughness of beams, measured by the area under the moment-curvature curves, remains almost the same in both cases. This happens because of the increase in the value of the fiber-index ( $\beta$ ) caused by a relatively higher fiber content (1 %) in the beam-2 than

**Fig. 3.13** Typical moment-curvature response of SFRC member—The charts in the figure depicts a typical moment-curvature response exhibited by the beam-1 (a) and the beam-2 (b). These diagrams indicate that the toughness of the beams (measured by the area under the curve) increases significantly by considering a higher value of the fiber-index in the design of an SFRC flexural member. This index is linearly related to the fiber aspect ratio or its quantity expressed by means of volume fraction irrespective of the compressive strength of the concrete at the low values, generally used in practice



in the beam-1, which has a fiber content of 0.5 %; the value of the reinforcement-index ( $\omega$ ) was kept same in both of the cases. The increase in the fiber content enhances the residual tensile strength of the SFRC and, accordingly, there is a slight increase in the section flexural capacity. Nevertheless, the increase in the fiber content bridges the cracks more effectively and it consequently delays the straining of the longitudinal reinforcement present on the tensile face of the beams.

This delay in the rebar straining indirectly effects the mobilization of the tensile stresses in the longitudinal rebars provided in the beam sections; thereby, it becomes responsible for the insignificant increase in the flexural capacity of the beam and the lowering of the ultimate curvature value. This prediction is in close agreement with the experimental results reported in Lini et al. (1998). It is therefore suggested to use minimum possible quantity of the conventional reinforcement in SFRC beams just to meet the difference between the moment-demand and flexural capacity contributed by the steel fibers alone in the concrete. In terms of energy absorption, the SFRC beams, with or without conventional reinforcing rebars, failing in flexure is capable to absorb significantly more energy than a plain concrete or a RC beam. This makes the use of SFRC beams an attractive alternative for the structures located in earthquake prone zones or that need a blast protection.

### 3.10 Design Method Assisted by Experimental Investigations

It was described in the previous section that any SFRC beam section must carry, safely, the applied load both at the identified service load as well as its ultimate state. The residual-tensile strength of the SFRC, unlike the conventionally reinforced concrete sections, is influenced by the crack-width appearing in the beam section. It is therefore advisable to go for actual experimental studies of SFRC beam specimens cast using a casting and placement technique similar to that one going to be used at the site. The purpose is to obtain a fiber orientation in the test specimens similar/identical to that would develop or form during the actual construction and therefore would be a representative of the fiber orientation in the structural application. Based on the testing results, an average and a characteristic response of the SFRC should be identified to establish the safe design stress values. The design in the serviceability limit state should be based on assumed or measured characteristic values, while it should be based on the characteristic values modified by suitable safety factors for a design in the ultimate limit state. Nevertheless, the crack-width ( $w$ ) plays a vital role in controlling the safe stress value for a SFRC section both at the serviceability and the ultimate states. The safety factors can be used similar to a set of factors prescribed for the conventional RC sections by different design guidelines, such as FIB (2010), ACI (2002, 2008), CNR-DT (2006).



Methods for the direct determination of a stress-strain response of SFRC are typically based on the standard uniaxial tension test. Some recent research studies, however, have found merit in using the standard bending testing for this purpose and recommended inverse analysis technique in this regards. The test data is obtained from the standard bending tests (see, Chap. 2 for details) to derive the upper and the lower characteristic value of the design strength of the SFRC [RELIM (2001, 2002, 2003)]. The more critical value out of these two should be adopted to determine the key-parameters of the prescribed tensile stress blocks by different guidelines and subsequently, to check the adequacy of the SFRC beam section with respect to the ultimate limit state and the serviceability states. Generally, the lower characteristic value obtained from the test data gives the critical value of the design stress. This can be obtained from Eq. 3.18.

$$f_{t1} = f_{ml} - k_x s \quad (3.18)$$

The design value of the stress at the limit of proportionality (LOP) for SFRC should be taken as a maximum of the strength value ( $f_{t1}$ ) determined from Eq. 3.18 and the strength value ( $f_{t2}$ ). The stress ( $f_{t2}$ ) represents the modulus of rupture of the plain concrete ( $=0.7\sqrt{f_{ck}}$ ). This is mainly because of the fact that the steel fibers in the concrete activates only after the initiation of cracking in the section and subsequently, the fibers start transferring the tensile force across the crack opening.

In Eq. 3.18,  $f_{ml}$  is a mean value of LOP (in MPa) taken from the (n) number of the test specimens. The parameter (s) is the standard deviation (in MPa) of the experimental test data. It can be determined from Eq. 3.19 depending upon the sample size (n).

$$s = \sqrt{\frac{\sum (f_{ml} - f_i)^2}{n - 1}} \quad (3.19)$$

The parameter  $k_x$  in Eq. 3.18 also depends upon the sample size (n). This value can be taken from the Table 3.7 depending upon the size of the test sample with a known coefficient of variation.

It is worth to note that the strength ( $f_{t1}$ ), determined from the experimental test results, using Eq. 3.18, is influenced by the fiber parameters used in the production of SFRC and the testing method used in the investigations. It takes into account the effect of the fiber orientation and their distribution in the concrete; effect of the mould boundaries; loading type, etc. whereas, the strength ( $f_{t2}$ ) is the first cracking strength of concrete, which is a function of the concrete grade only; the fiber parameters have a little influence over this value of the strength.

**Table 3.7** Value of the factor ( $k_x$ ) for different sample sizes

Sample size	1	2	3	4	5	6	8	10	20	30	$\infty$
$k_x$	2.31	2.01	1.89	1.83	1.80	1.77	1.74	1.72	1.68	1.67	1.64

The design strength values obtained using the procedure, described above, are used to classify SFRC for the specification purposes in the contract documents (also see, Chap. 6). Two parameters are needed for this purpose: the residual flexural strengths  $f_{R1}$  and  $f_{R4}$ . The first strength parameter ( $f_{R1}$ ) is a value of the residual tensile strength of the SFRC, reduced to the nearest multiple of 0.5 MPa, at 0.5 mm CMOD value (or at the deflection of 0.46 mm); whereas, the second parameter ( $f_{R4}$ ) represents the material strength corresponding to a CMOD value of 3.5 mm (or at the deflection of 3.0 mm), again rounded off to the nearest multiple of 0.5 MPa. These two strength parameters denote the minimum guaranteed characteristic residual strengths at the CMOD values of 0.5 and 3.5 mm, respectively, e.g., an SFRC with a characteristic compressive strength of 30 MPa, and having a  $f_{R1} = 2.2$  MPa and  $f_{R4} = 1.5$  MPa (experimental test data) would be rounded off as  $FL_{0.5} = 2.0$  MPa and  $FL_{3.5} = 1.5$  MPa. It is then classified and specified in the design specifications and related documents as M30 FL 2.0/1.5. Alternatively, it can be denoted in terms of the fiber-index ( $\beta$ ) at a specified value of the crack-width, e.g.  $\beta$ -3.3/1.85 representing a fiber-index value of 3.3 % ( $=0.45f_{R1} k_h/30$ ) and 1.85 % ( $=0.37f_{R4} k_h/30$ ) at a specified crack-width ( $w$ ) of 0.5 mm and 3.5 mm, respectively. The parameter  $k_h$  is beam-depth factor (see, Chap. 2 for the detail). In the design, these values of the fiber-index are used to compute the ultimate flexural strength of SFRC member and to check their adequacy at the service loads.

#### Example 3.4

*M35 grade SFRC with a fiber volume fraction of 1 % was used to cast 6 numbers of standard prisms  $150 \times 150 \times 750$  mm. The aspect ratio of the hooked-end steel fibers taken in the investigations was 60. The specimens were tested under the standard 3-point loading conditions, with an effective span of 500 mm. Table 3.8 gives the test results at various prescribed values of the CMOD. The results from the standard 150 mm concrete cubes indicate that the SFRC possesses a 28 days compressive strength of 42.58 MPa. Classify the SFRC and determine the safe value the residual tensile strength.*

#### Solution

The test data given in Table 3.8 and Eq. 3.18 can be used to calculate the value of the parameter  $f_{t1}$ . It is given below:

$$f_{t1} = 7.51 - 1.77 \times 0.763 = 6.15 \text{ MPa}$$

And, the value of the parameter  $f_{t2}$  is obtained as 4.15 MPa for the M35 grade concrete. The greater of these two values ( $f_{t1}$  and  $f_{t2}$ ) represents the design value of the characteristics LOP of the SFRC. This value is obtained as 6.15 MPa for the present case.

Similarly, the characteristics values of other residual tensile strength of the SFRC ( $f_{R1}$ ) at the CMOD of 0.5 mm and  $f_{R4}$  at the CMOD of 3.5 mm is obtained as 8.502 MPa and 2.213 MPa, respectively from the test data (Table 3.8) and Eq. 3.18. Using these two strength values, the SFRC can be classified as M35 FL 8.5/2.2.

**Table 3.8** Test results of a 3-point bending test

Specimen	The stress values (MPa) corresponding to the CMOD of			
	0.05 mm	0.5 mm	2.5 mm	3.5 mm
	$f_L$	$f_{R1}$	$f_{R3}$	$f_{R4}$
1	9.14	13.53	9.60	3.09
2	7.20	10.03	6.72	2.98
3	7.09	10.60	6.17	2.67
4	7.55	11.79	6.40	2.71
5	7.49	10.11	6.56	2.88
6	6.76	9.48	6.08	2.15
Average value, $f_{ml}$ (MPa)	7.51	10.92	6.92	2.75
SD (s) (MPa)	0.763	1.366	1.217	0.303

The test data can also be used to get the design tension stress block of the SFRC. The material model and other design guidelines given in Chap. 2 can be used for this purpose.

- **The RELIM model** (Eqs. 2.12–2.16)

The value of the shape factor,  $k_h = 1 - 0.6 \frac{D \text{ (in cm)} - 12.5}{47.5} = 0.9684$

$$\sigma_1 = 0.7 \times 0.75 \sqrt{35} (1.6 - 0.15) = 4.504 \text{ MPa}$$

at the strain  $\varepsilon_1 = \frac{\sigma_1}{5000 \sqrt{f_{ck}}} = 0.000152$

$$\sigma_2 = 0.45 f_{R1} k_h = 0.45 \times 8.502 \times 0.9684 = 3.705 \text{ MPa}$$

at the strain  $\varepsilon_2 = \varepsilon_1 + 0.0001 = 0.000252$

$$\sigma_3 = 0.37 f_{R4} k_h = 0.37 \times 2.213 \times 0.9684 = 0.793 \text{ MPa}$$

at the strain  $\varepsilon_3 = 0.025$

- **Analytical Model** (Eq. 2.8)

$\sigma_u = 2 \times 0.3 \times V_f \times \frac{1}{d} \sqrt{f_{ck}} = 2.13 \text{ MPa}$  at a design strain,  $\varepsilon_u = 0.015$

- **CNR-DT 204 (2006)** (Eqs. 2.17 and 2.18)

$$f_{eq1} = \frac{6.150 + 8.502}{2} = 7.326 \text{ MPa for } w_{i1} = \frac{0.05 + 0.5}{2} = 0.275 \text{ mm}$$

$$f_{eq2} = \frac{8.502 + 2.213}{2} = 5.357 \text{ MPa for } w_{i2} = \frac{0.5 + 3.5}{2} = 2.0 \text{ mm}$$

The corresponding values of the tensile stress block of the SFRC can be derived using Eqs. 2.17 and 2.18.

$$\sigma_1 = 0.45f_{eq1} = 0.45 \times 7.326 = 3.29 \text{ MPa, at strain } \varepsilon_1 \text{ of } 0.00015.$$

$$\sigma_2 = k \left[ \sigma_1 - \left( \frac{w_u}{w_{f2}} \right) (\sigma_1 - 0.5f_{eq2} + 0.2f_{eq1}) \right] = 0.17 \text{ MPa } (\geq 0), \text{ at the strain } \varepsilon_2 = 0.020.$$

The magnitude of  $\sigma_1$  and  $\sigma_2$  indicate that the SFRC exhibits a strain-softening behavior in its post-cracking range. The material is termed as a strain-softening if the value of the residual stress in its post-cracking stage reduces with an increase of strain value in the material post-cracking stage. For such a material, the maximum value of the strain on the extreme beam face should be limited to the least of 0.020 and  $3/l_{cs}$ . The parameter  $l_{cs}$  is the characteristic length for the beam specimen. It can be taken as a least of the average crack spacing and the position of the section neutral-axis ( $h_2$ ). The values of these two parameters should be observed carefully during the conduct of the bending tests. For the present case, the permitted ultimate value of the strain is obtained as 0.020.

It is worth to check especially for the strain-softening material, the characteristic value of the residual-tensile strength of the SFRC should be at least 20 % of the strength exhibited by the material at the service load in order to consider it fit for any structural application.

In the present case, the characteristics LOP (=6.15 MPa) of the SFRC can be considered as the material strength at the service load. Hence, its minimum value of the post-cracking tensile strength should be 1.23 MPa (=0.2  $\times$  6.15) in order to use this concrete for any structural application. This can be achieved by controlling the strain on the tensile face of the SFRC member by taking a suitable value of the fiber-index ( $\beta$ ) in the design. This will help to reduce the crack-width at the ultimate state and achieve the minimum strength requirements. The fiber parameters needed in this regards can be selected using Eqs. 2.8–2.10.

### Example 3.5

*M20 grade SFRC with a fiber volume fraction of 1 % was used to cast 6 numbers of standard prisms 100  $\times$  100  $\times$  500 mm. The hooked-end steel fibers 60/35 were used in the concrete mix. The specimens were tested under the standard 3-point loading conditions, with an effective span of 500 mm. Figure 3.14 shows the load-deflection response (average values) exhibited by the specimens. Formulate the design stress-block of SFRC.*

### Solution

The specified steel fiber in the example is designated as 60/35. It indicates that the fiber has an aspect ratio of 60 and is 35 mm long. The experimental data shown in Fig. 3.14 can be used to derive the residual tensile strength value of the SFRC. The strength value  $f_{R1} = 2.21$  MPa can be taken corresponding to the midspan deflection value of 0.46 mm and the strength  $f_{R4} = 3.62$  MPa will be a value taken corresponding to the deflection of 3 mm.

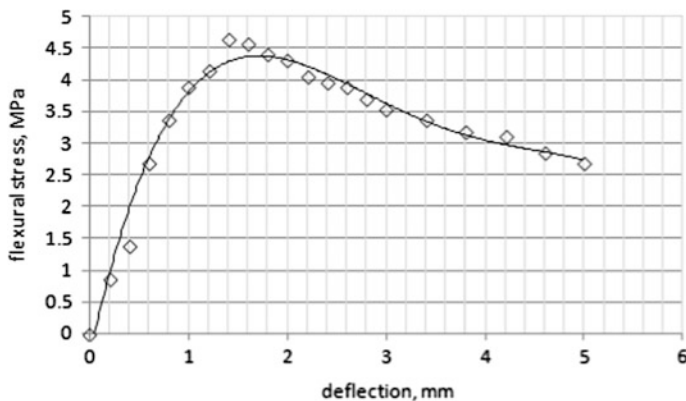


**Fig. 3.14** Load-deflection response of SFRC member—The chart indicates the variation of an average value of the flexural stress at different deflection values

With this test data, the RELIM model (Eqs. 2.12–2.16) gives various key-parameters required to obtain the tension constitutive model of the SFRC. These are given below:

The beam-shape factor,  $k_h = 1$  for  $100 \times 100 \times 500$  mm prisms.

$$\sigma_1 = 0.7 \times 0.75\sqrt{20} (1.6 - 0.10) = 3.52 \text{ MPa}$$

at a strain value  $\varepsilon_1 = \frac{\sigma_1}{5000\sqrt{f_{ck}}} = 0.000158$

$$\sigma_2 = 0.45f_{R1}k_h = 0.45 \times 2.21 \times 1 = 0.994 \text{ MPa}$$

$$\text{and } \varepsilon_2 = \varepsilon_1 + 0.0001 = 0.000258$$

$$\sigma_3 = 0.37f_{R4}k_h = 0.37 \times 3.62 \times 1 = 1.34 \text{ MPa}$$

at the strain  $\varepsilon_3 = 0.025$

The stress values  $\sigma_i$  indicate that the SFRC exhibits a strain-hardening behavior in its post-cracking range as the magnitude of the stress increased to 1.34 MPa from a strength value of 0.99 MPa exhibited by the SFRC earlier. The stress block, subsequently, can be used to derive the theoretical flexural capacity of the SFRC member (see, Sect. 3.3).

### 3.11 Design of SFRC Doubly-Reinforced Members

Two distinct zones exist in all flexural members, namely the compression zone normally above the neutral-axis of the beam and the tension zone below it in case of the beams subjected to the gravity loads; otherwise, their position will be reversed

with a tension zone moving to the top face of the beam and the compression zone shifting to its bottom face. The plane separating these two zones in the member is termed as its neutral-axis. Because SFRC possesses a sustainable value of the residual-tensile strength over a large spectrum of strains, the tensile zone in the members cast using SFRC contribute significantly towards its flexural capacity, unlike the members cast using the plain concrete which fails abruptly on reaching its limiting tensile straining capacity and the RC members, wherein the rebars in its tensile zone maintain the tensile capacity of the member that otherwise gets lost once the strain on the extreme tension face of the member reaches the limiting concrete tensile-straining capacity. The inclusion of steel fibers in the concrete mix, generally, leads to the transformation of otherwise under-reinforced section to an over-reinforced section. In such cases, either the combination of the steel fiber dosage and the percentage of the conventional longitudinal rebars should be such that the final section must behave as an under-reinforced one; or alternatively, additional longitudinal rebars in the beam compression zone could help to prevent the change of the section status from a desirable one (under-reinforced) to a section (over-reinforced) that must be avoided in all practical designs due to reduction in ductility and ensuing brittle nature of the failure at the ultimate load (provided that the beam section possess adequate shear strength to avoid the premature shear failure that may proceed the flexural failure in the absence of adequate transverse reinforcement). The beam sections reinforced using both the compression as well as the tensile reinforcing bars is termed as doubly reinforced section. It is important to note that the steel area of less than 0.2 % (of the beam cross-sectional area) in the compression zone did not produce a doubly-reinforced section as the magnitude of the compressive force so induced in the rebars, placed in the beam compression zone, are not enough to contribute anything significant to the section flexural capacity. If the area of the compression steel is more than 0.2 % of the beam cross-section area, then the effect of these rebars should be considered towards the section flexural capacity.

The distribution of stresses and strains in a doubly reinforced section are exactly similar to that of a section having rebars only in its tensile zone except that in this case, the stresses will also mobilize in the compression steel. The summation of compression force in all rebars placed in the compression zone of the beam will constitute a force ( $C_1$ ) in addition to the force ( $C$ ) induced in the concrete upon loading. The value of  $C$  is  $0.416\xi f_{ck}Bh_1$  when the beam is subjected to a ultimate crushing strain of 0.004. The factor ( $\xi$ ) denotes the effect of the fiber addition on the concrete compressive strength which tries to improve the crushing strain of the plain concrete (0.0035) to a generally accepted strain value of 0.004 for a SFRC section. The value of the factor ( $\xi$ ) should be taken as unity for the SFRC; otherwise, it is 0.86 for the normal concrete. The magnitude of the force ( $C_1$ ) depends upon the strain value prevailing at the level of the compression steel rebars. The value can be easily determined, similar to a strain value calculation for the tensile steel, using the strain-compatibility conditions. The similarity of the strain-triangles created by the condition that the plane sections normal to the beam-axis remain

plane after bending can be used for this purpose. The position of the compression rebars having area ( $A_{sc}$ ) is taken at a distance of ‘d’ taken from the beam top face. Figure 3.15 show a typical distribution of the strain and stresses in the doubly reinforced SFRC beam section at the ultimate state along with a typical material constitutive relationship of SFRC and the conventional reinforcing bars, both in the compression and the tension.

Similar to the singly-reinforced beams, the position of the neutral-axis in the section can be determined by considering the force equilibrium along the member-axis i.e.  $C + C_1 = T_1 + T_2 + T_3$ ; where, C and  $C_1$  are the compressive force mobilized in the concrete and the compression reinforcing bars (with an area of  $A_{sc}$ ) above the neutral-axis of the member, respectively depending upon the value of the strain prevailing at the rebar level (for the force,  $C_1$ ) and the value of the concrete crushing strain (for the force, C) adopted in the design.

It is important to note that the rebars, in most of the cases, will attain the design yield stress of  $0.87f_y$  in the case of Fe 250 grade steel but it will rarely do so, if the Fe415 or Fe500 grade rebars have been used as a compression steel in the section. The Fe415 or Fe500 grade rebars have a high strain value at the yield which is very difficult to achieve, as these bars are normally placed close to the compression face of the beam where the strain value is limited to the design strain of 0.0035

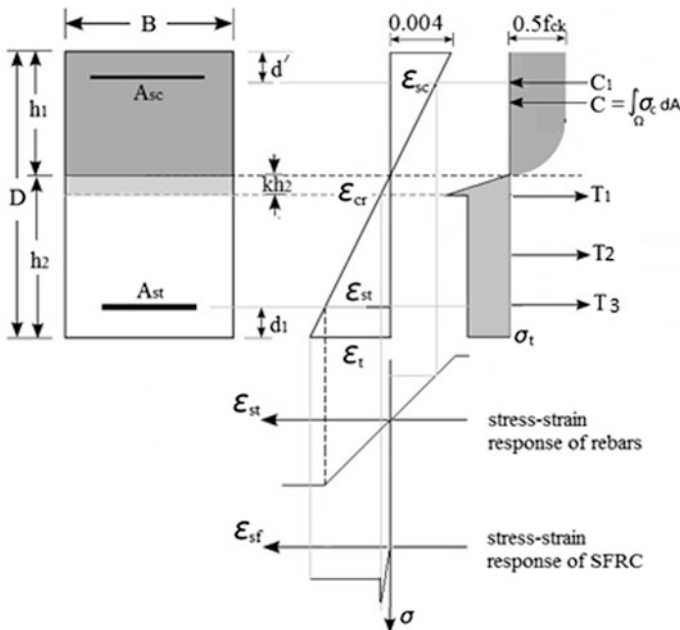


**Fig. 3.15** Stress-profile model—A schematic representation of a SFRC-beam section reinforced with the conventional reinforcing bars on its compression and the tensile zone. It also shows a strain and stress distribution along with the tension-constitutive relationships of conventional rebars and SFRC



(for RC sections) and 0.0040 (for SFRC sections) and in most of the cases, it will remain less than these two values. In other words, the strain in the compression rebars will rarely touch the yield strain value ( $=0.0038$  for Fe415 grade steel) if provided in the SFRC section and will never do so in case of a conventional RC section.

The value of the stress mobilized in the compression rebars can be determined using the data given in the Table 3.1 depending upon the prevailing strain value ( $\epsilon_{sc}$ ) at the rebar level. Equation 3.20 has been developed using the similarity of the strain triangles above and below the section neutral-axis. It can be used to find the strain value ( $\epsilon_{sc}$ ) at the level of the compression steel in the section. Using the constitutive relationship of the steel rebars, the corresponding value of the design stress can be determined for use at a later stage in the analysis.

$$\epsilon_{sc} = 0.004\xi \left( 1 - \frac{d' D}{D h_1} \right) \quad (3.20)$$

The magnitude of the force (C) can be determined by integrating the area of the concrete stress-block lying in the compression zone. The area occupied by the compression rebars in the zone can be ignored in the calculation for sake of simplicity. The value of force ( $C_1$ ) can be obtained by multiplying the area of the compression steel ( $A_{sc}$ ) with the stress value ( $\sigma_{sc}$ ) taken corresponding to the prevailing value of the strain ( $\epsilon_{sc}$ ) in the rebar. The value of the strain ( $\epsilon_{sc}$ ) can be determined using Eq. 3.20 for an assumed value of the neutral-axis. The values of  $T_1$ ,  $T_2$  and  $T_3$  are the tensile forces in the uncracked concrete below the neutral-axis, the residual tensile strength of SFRC and the tensile steel rebars, respectively. Again for the sake of simplicity, the force  $T_1$  is ignored in the analysis because of their negligible contribution towards the section flexural capacity, especially for a case; wherein, the accidental overloading has produced the tensile cracks deep enough to extend this right up to the position of the neutral-axis at the ultimate state.

$$\begin{aligned} C + C_1 &= T_1 + T_2 + T_3 \rightarrow 0.4167\xi f_{ck} h_1 B + \sigma_{sc} A_{sc} = 0 + \sigma_t h_2 B + \sigma_{st} A_{st} \\ \Rightarrow \frac{h_1}{h_2} &= \frac{\sigma_t + \sigma_{st} p_t \left( \frac{D}{h_2} \right) - \sigma_{sc} p_c \left( \frac{D}{h_2} \right)}{0.4167\xi f_{ck}} = \frac{2.4}{\xi} \beta + \frac{2.4 D}{\xi h_2} (\omega_t \gamma_t - \omega_c \gamma_c) \end{aligned} \quad (3.21)$$

In Eq. 3.21, the parameters  $p_t (=A_{st}/BD)$  and  $p_c (=A_{sc}/BD)$  denotes the percentage steel area of the reinforcing bars provided in the tensile zone and the compression zone of the beam, respectively. These two parameters have been converted to the respective reinforcement-indexes, namely  $w_t$  and  $w_c$ , respectively for the sake of simplicity.  $\beta$  is a value of the fiber-index adopted in the design. The above expression can be further simplified to Eq. 3.22, which defines the position of the neutral-axis in the beam section from its top face ( $h_1/D$ ) and the bottom face ( $h_2/D$ ), respectively (see Fig. 3.15). It is pertinent to note that the position of the



neutral-axis depends entirely on the material properties of the SFRC and the extent to which the stress in the conventional rebars, both in the tension zone expressed by the parameter ( $\omega_t$ ) and in the compression zone by the parameter ( $\omega_c$ ), are mobilized under a given load.

$$\frac{h_2}{D} = \left[ \frac{1 - 2.4(\omega_t \gamma_t - \omega_c \gamma_c)}{\xi (1 + 2.4\beta)} \right] \text{ and } \frac{h_1}{D} = \left( 1 - \frac{h_2}{D} \right) \quad (3.22)$$

The Eq. 3.22 provides a closed-form solution of the neutral-axis coefficients ( $h_1/D$  and  $h_2/D$ ) only in the cases where both the tensile steel as well as the compression steel have reached their yield strain; otherwise, the strain-compatibility approach should be used to arrive at the exact values of  $h_1/D$  and  $h_2/D$ . In the equation, the parameter ( $\beta$ ) is a fiber-index adopted in the design of SFRC; and  $\omega_t$  and  $\omega_c$  represents the reinforcement-index of the tensile and compression rebars, respectively. The parameters  $\gamma_t$  and  $\gamma_c$  denotes the extent to which the stress in the tensile and the compression reinforcement bars is mobilized, respectively under the prevailing strain condition in the beam section. The value of the stress-mobilisation factors ( $\gamma_t$  and  $\gamma_c$ ) for reinforcing bars at different strain values is given in Table 3.1. The moment capacity ( $M_u$ ) of the SFRC beam section can be determined using the equation of statics. This is given in Eq. 3.23. The insignificant contribution ( $T_1$ ) towards the section flexural capacity from the uncracked concrete portion existing below the neutral-axis is ignored in the expression.

$$M_u = C (0.5833h_1) + C_1(h_1 - d') + T_2 \left[ \frac{h_2}{2} \right] + T_3(h_2 - d_1) \quad (3.23)$$

Equation 3.23 can be simplified to a non-dimensional form as given in Eq. 3.24. In this equation, a factor ( $\xi$ ) has been introduced to take care of the cases when the normal concrete is used in the beam section instead of SFRC. This replacement of the SFRC in the beam section to the plain concrete reduces the design crushing strain of the material from 0.004 (for SFRC) to 0.0035 (for the plain concrete) thereby leading to the reduction of the force ( $C$ ) expressed by the parameter ( $\xi$ ).

$$\frac{M_u}{f_{ck}BD^2} = 0.24\xi \left( \frac{h_1}{D} \right)^2 + \left\{ 0.5\beta + \gamma_t \omega_t \left( \frac{D}{h_2} \right) \left( 1 - \frac{d_1 D}{D h_2} \right) \right\} \left( \frac{h_2}{D} \right)^2 + \gamma_c \omega_c \left( 1 - \frac{d'}{D} \right) \quad (3.24)$$

The value of the neutral-axis coefficients ( $h_1/D$ ,  $h_2/D$ ) can be determined using a set of expressions given in Eq. 3.22. The strain-compatibility method has to be used in case the strain at the rebar level (both for the tensile and compression steel) is not enough to cause their yielding. The value of stress-mobilization factors ( $\gamma_t$  and  $\gamma_c$ ) can be taken from Table 3.1 depending upon the value of the strain at the rebar level in the beam section.

**Example 3.6**

A reinforced concrete beam of rectangular section has the -cross sectional dimensions of 300 mm × 600 mm. The beam is reinforced with 4No.—25 mm diameter rebars in its tensile zone at an effective depth of 550 mm. 3No.—20 mm diameter rebars are also provided in the compression face at a distance of 50 mm from the beam top face. Assuming M20 concrete and Fe 415 grade steel, compute the ultimate capacity of the beam.

**Solution**

- Given: B = 300 mm, D = 600 mm, d = 550 mm, d' = 50 mm, A<sub>st</sub> = 1963 mm<sup>2</sup>, A<sub>sc</sub> = 942 mm<sup>2</sup>, f<sub>y</sub> = 415 MPa, f<sub>ck</sub> = 20 MPa
- The value of the reinforcement-index ( $\omega_t$ ) =  $\frac{1963 \times 415}{300 \times 600 \times 20} = 0.2263$
- The value of the reinforcement-index ( $\omega_c$ ) =  $\frac{942 \times 415}{300 \times 600 \times 20} = 0.1086$
- $\frac{d'}{D} = \frac{50}{600} = 0.0833$
- $\frac{d_t}{d} = \frac{50}{550} = 0.0910$
- $\frac{d_t}{D} = \frac{50}{600} = 0.0833$
- $\frac{d}{D} = \frac{550}{600} = 0.917$
- For Fe 415 steel, the limiting value of the neutral-axis ( $h_1/D$ ) = 0.479 ( $d/D$ ) = 0.479 × 0.917 = 0.439
- Assuming a strain value in the compression and the tensile steel is more than their yielding strain; thereby giving  $\gamma_c$  and  $\gamma_t = 0.87$ . In the following equations, the effect of the force in the concrete area displaced by the steel compression bars Stressed to a level of the stress in concrete (= 0.5 f<sub>ck</sub>) is ignored.

$$\frac{h_1}{D} = \frac{2.4}{\xi} (\omega_t \gamma_t - \omega_c \gamma_c) = 0.2857 < 0.439$$

The section is under-reinforced thereby indicating that the strain at the level of the tensile and the compression steel is more than the yield strain.

$$\begin{aligned} \epsilon_{st} &= 0.0035 \left( \frac{D}{h_1} \frac{d}{D} - 1 \right) = 0.00773 > 0.0038 \\ \epsilon_{sc} &= 0.0035 \left( 1 - \frac{d'}{D} \frac{D}{h_1} \right) = 0.00248 < 0.0038 \end{aligned} \quad (\text{OK})$$

(It therefore needs correction in the  $\gamma_c$  value)

The value of the rebar stress-mobilization factor ( $\gamma_c$ ) at this strain value can be obtained from the Table 3.1 as 0.8506. Using this value, new value of the  $h_1/D$  can be determined again and this process will continue till the difference between the new and the last value leads to a insignificant value.

2nd cycle:

$$\frac{h_1}{D} = \frac{2.4}{\xi} (\omega_t \gamma_t - \omega_c \gamma_c) = 0.2916 < 0.439$$

$$\Rightarrow \varepsilon_{sc} = 0.00250 \Rightarrow \Upsilon = 0.8509$$

3rd cycle:

$$\frac{h_1}{D} = \frac{2.4}{\xi} (\omega_t \gamma_t - \omega_c \gamma_c) = 0.29156 < 0.439$$

$$\Rightarrow \varepsilon_{sc} = 0.00250 \Rightarrow \Upsilon = 0.8509$$

The difference of the values of the neutral-axis as obtained from the 2nd and the 3rd cycle becomes approximately zero; therefore, the value determined at the 3rd cycle can be adopted as its true value. The value of the  $h_2/D$  can be determined as 0.7084 (= 1 - 0.2916)

The section flexural capacity can be determined using Eq. 3.24 by substituting these values in the expression reproduced below:

$$\frac{M_u}{f_{ck} B D^2} = 0.24 \zeta \left( \frac{h_1}{D} \right)^2 + \left\{ \gamma_t \omega_t \left( \frac{D}{h_2} \right) \left( 1 - \frac{d_1}{D} \frac{D}{h_2} \right) \right\} \left( \frac{h_2}{D} \right)^2 + \gamma_c \omega_c \left( 1 - \frac{d'}{D} \right)$$

$$\frac{M_u}{f_{ck} B D^2} = 0.1872 \Rightarrow M_u = 404.47 \text{ kN m}$$

### Example 3.7

Repeat the problem in Example 3.6, considering  $A_{st}$  as 3054 mm<sup>2</sup> and  $A_{sc}$  as 982 mm<sup>2</sup>

### Solution

- Given: B = 300 mm, D = 600 mm, d = 550 mm, d' = 50 mm,  $A_{st} = 3054 \text{ mm}^2$ ,  $A_{sc} = 982 \text{ mm}^2$ ,  $f_y = 415 \text{ MPa}$ ,  $f_{ck} = 20 \text{ MPa}$
- The value of the reinforcement-index ( $\omega_t$ ) =  $\frac{3054 \times 415}{300 \times 600 \times 20} = 0.3521$
- The value of the reinforcement-index ( $\omega_c$ ) =  $\frac{982 \times 415}{300 \times 600 \times 20} = 0.1132$
- $\frac{d'}{D} = \frac{50}{600} = 0.0833$
- $\frac{d_1}{d} = \frac{50}{550} = 0.091$
- $\frac{d_1}{D} = \frac{50}{600} = 0.0833$
- $\frac{d}{D} = \frac{550}{600} = 0.917$
- For Fe 415 steel, the limiting value of the neutral-axis ( $h_1/D$ ) = 0.479 ( $d/D$ ) = 0.439

1st cycle:

Assuming a strain value in the compression and the tensile steel is more than their yielding strain; thereby giving  $\Upsilon_c$  and  $\Upsilon_t = 0.87$

$$\frac{h_1}{D} = \frac{2.4}{\xi} (\omega_t \gamma_t - \omega_c \gamma_c) = 0.5802 > 0.439$$

The section is over-reinforced thereby requiring that the actual value of the strain at the level of the tensile and compression steel should be determined by the strain-compatibility conditions.

$$\epsilon_{st} = 0.0035 \left( \frac{D}{h_1} \frac{d}{D} - 1 \right) = 0.00203 < 0.0038$$

(Needs correction in  $\gamma_t$  value)

$$\epsilon_{sc} = 0.0035 \left( 1 - \frac{d' D}{D h_1} \right) = 0.00299 < 0.0038$$

(Needs correction in  $\gamma_c$  value)

The value of the rebar stress-mobilization factors  $\gamma_t$  and  $\gamma_c$  at these two values of the strains ( $\epsilon_{sc}$  and  $\epsilon_{st}$ ) can be obtained from the Table 3.1 as 0.8162 and 0.8582, respectively. Using these values, new value of the  $h_1/D$  can be determined again and this process will continue till the difference between the new and the last value becomes insignificant.

2nd cycle:

$$\frac{h_1}{D} = \frac{2.4}{\xi} (\omega_t \gamma_t - \omega_c \gamma_c) = 0.5309 > 0.439$$

$$\Rightarrow \epsilon_{sc} = 0.00295 \Rightarrow \gamma_c = 0.8575 \text{ and } \epsilon_{st} = 0.00254 \Rightarrow \gamma_t = 0.8515$$

3rd cycle:

$$\frac{h_1}{D} = \frac{2.4}{\xi} (\omega_t \gamma_t - \omega_c \gamma_c) = 0.5658 > 0.439$$

$$\Rightarrow \epsilon_{sc} = 0.00298 \Rightarrow \gamma_c = 0.8580 \text{ and } \epsilon_{st} = 0.00217 \Rightarrow \gamma_t = 0.832$$

4th cycle:

$$\frac{h_1}{D} = \frac{2.4}{\xi} (\omega_t \gamma_t - \omega_c \gamma_c) = 0.5465 > 0.439$$

$$\Rightarrow \epsilon_{sc} = 0.00297 \Rightarrow \gamma_c = 0.8577 \text{ and } \epsilon_{st} = 0.00237 \Rightarrow \gamma_t = 0.8455$$

5th cycle:

$$\frac{h_1}{D} = \frac{2.4}{\xi} (\omega_t \gamma_t - \omega_c \gamma_c) = 0.5598 > 0.439$$

$$\Rightarrow \epsilon_{sc} = 0.00298 \Rightarrow \gamma_c = 0.8579 \text{ and } \epsilon_{st} = 0.00223 \Rightarrow \gamma_t = 0.8362$$

6th cycle:

$$\frac{h_1}{D} = \frac{2.4}{\xi} (\omega_t \gamma_t - \omega_c \gamma_c) = 0.5506 > 0.439$$

$$\Rightarrow \varepsilon_{sc} = 0.00297 \Rightarrow \Upsilon_c = 0.8577 \text{ and } \varepsilon_{st} = 0.00232 \Rightarrow \Upsilon_t = 0.8425$$

7th cycle:

$$\frac{h_1}{D} = \frac{2.4}{\xi} (\omega_t \gamma_t - \omega_c \gamma_c) = 0.5518 > 0.439$$

$$\Rightarrow \varepsilon_{sc} = 0.002976 \Rightarrow \Upsilon_c = 0.8578 \text{ and } \varepsilon_{st} = 0.00226 \Rightarrow \Upsilon_t = 0.8382$$

The difference between values of the neutral-axis as obtained from the 5th and the 6th cycle becomes approximately zero; therefore, the value determined at the 5th cycle can be adopted as its true value. The value of the  $h_2/D$  can be determined as 0.4381 ( $= 1 - 0.5518$ ). The flexural capacity can be determined using Eq. 3.24.

$$\frac{M_u}{f_{ck} B D^2} = 0.24 \xi \left( \frac{h_1}{D} \right)^2 + \left\{ \gamma_t \omega_t \left( \frac{D}{h_2} \right) \left( 1 - \frac{d_1}{D} \frac{D}{h_2} \right) \right\} \left( \frac{h_2}{D} \right)^2 + \gamma_c \omega_c \left( 1 - \frac{d'}{D} \right)$$

$$\frac{M_u}{f_{ck} B D^2} = 0.216 \Rightarrow M_u = 466.39 \text{ kN m}$$

## References

- ACI: Standard 318 (2008) Building code requirements for reinforced concrete. American Concrete Institute (ACI), Farmington Hills
- ACI Committee 544 (2002) Design considerations for steel fiber reinforced concrete, ACI 544.1R-96. American Concrete Institute (ACI), Farmington Hills
- Bureau of Indian Standards (BIS) (2000) Plain and reinforced concrete—code of practice. IS 456 (4th rev.), New Delhi, India
- CNR-DT 204 (2006) Guidelines for design, construction and production control of fiber reinforced concrete structures. National Research Council of Italy, Rome
- de Renaud M, Bruno M, Jean-Philippe C (2012) Design of SFRC structural elements: flexural behaviour prediction. *Mater Struct* 45:623–636
- FIB (2010) Model code 2010—first complete draft. International Federation for Structural Concrete, Lausanne
- Giuseppe C, Maria LM (2008) Fibrous reinforced concrete beams in flexure: experimental investigation, analytical modelling and design considerations. *Eng Struct* 30:2970–2980
- Lini T-Y, Paramasivam P, Lee S-L (1998) Behavior of reinforced steel-fiber-concrete beams in flexure. *J Struct Eng* 113(12):2439–2458. doi:10.1061/(ASCE)0733-9445(1987)113:12(2439)
- RILEM (2001) RILEM TC 162-TDF—tests and design methods for steel fibre reinforced concrete: uniaxial tension test for steel fibre reinforced concrete. *Mater Struct* 34:3–6

- RILEM (2002) RILEM TC 162-TDF—tests and design methods for steel fibre reinforced concrete: design of steel fibre reinforced concrete using the  $\sigma$ - $w$  method: principles and applications. Mater Struct 35:262–278
- RILEM (2003) RILEM TC 162-TDF—tests and design methods for steel fibre reinforced concrete:  $\sigma$ - $\epsilon$  design method—final recommendation. Mater Struct 36:560–567
- Singh H (2014) Flexural modeling of steel fiber-reinforced concrete members: analytical investigations. Pract Periodical Struct Des Constr 20(4):1–10, 04014046
- Singh H (2015) Flexural modelling of steel-fibre-reinforced concrete member with conventional tensile rebars. Build Struct 169(SB1):44–56

# Chapter 4

## Design of SFRC Members for Shear

### 4.1 Introduction

Unlike a plain concrete, the SFRC in its hardened state possesses improved mechanical properties with an enhanced post-cracking tensile resistance and the toughness because of the steel fibers which are randomly distributed and orientated in the concrete mix. These fibers transfer the tensile stresses across the cracks formed in the structural member once the strain caused by external loading exceeds the limiting cracking strain of the material. The fibers significantly delay the widening of the cracks and their subsequent propagation in the member. The enhanced post-cracking tensile strength of the concrete also leads to the improvement in the shear capacity of SFRC member. Because of this, the use of SFRC helps to meet the minimum shear reinforcement requirements in structural concrete members and this also helps to reduce the consumption of the conventional tension steel rebars required in the form of stirrups, provided in the members to resist the shear stresses higher than the concrete shear capacity (Swamy et al. 1974; Sharma 1986; Ashour et al. 1992; Khuntia et al. 1999; Ahmed et al. 2015). Nevertheless, this improvement depends largely on the pouring methods and the procedure employed in the SFRC placement and its compaction in the moulds.

The failure of a concrete member under shear is generally brittle in nature. However, unlike the flexural failure, the failure of a member under the shear, particularly in the flexural-shear mode may not lead to an immediate collapse by itself, but it generally reduces the flexural strength of the member as well as the ductility exhibited by it [Lim et al. (1987)]. The state of impending shear failure, because of this characteristic, is generally treated as a separate ultimate limit state for the design purpose in most of the design code and guidelines. It must be independently satisfied by the flexural member in addition to the other limit states [IS 456 (2000)]. The present chapter discusses different design concepts and procedures recommended by various guidelines and codes for the design of SFRC members in shear.

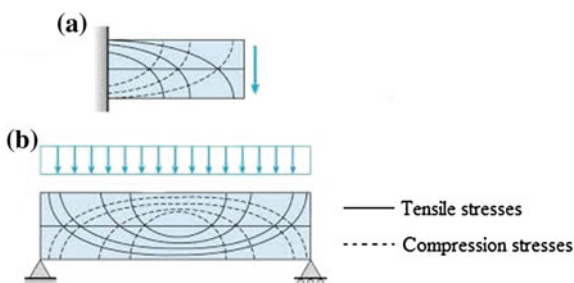
## 4.2 Shear Behavior of Beams

The concrete beams (cast either using conventional longitudinal rebars or the steel fibers as their tensile reinforcement) prior to their cracking behave similar to the beams made up of steel or any other similar structural material. These are carrying the flexural stresses as well as shear stresses induced in the section because of the external loading. The magnitude of these stresses varies from point-to-point along the span depending upon the type of the loading and the support conditions. This variation of the stresses along the span can be transformed into an equivalent set of the principal stresses. Figure 4.1 shows typical trajectories of the principal stresses (both, the compressive and the tensile) in a flexural member. Each point over these stress trajectories in the beam indicates two types of the principal stress: namely, the tensile stress and the compression stress, acting orthogonal to each other.

At the beam top and the bottom face, where the shear stress is zero, one of the principal stresses act in the direction parallel to the surface, and the other acts perpendicular to it. Therefore, the non-zero stress acting parallel to the top face is always a compressive in nature; whereas it is tensile in nature at the bottom face of the beam under the gravity loading conditions. The change in the direction of the loading reverses the nature of the stresses at the beam top and the bottom face. Therefore, in a material which is weak, especially in tension, e.g. Plain concrete, the tension cracks form in the direction perpendicular to the axis of the principal tensile stress trajectories once the magnitude of the stress caused by the load exceeds the cracking tensile strength of the concrete. As the principal compressive stress in a beam acts normal to its counterpart tensile stress, the trajectories showing the variation of the compressive stress indicate the potential direction of the tensile cracks that would develop at that point laying over the tensile stress trajectory. At the beam mid-span, therefore the tensile cracks originate from to its bottom face (usually carrying a highest possible value of the tensile strain) and extend towards the section neutral-axis; whereas, near the end zone of the beam, it appears at some angle to the beam-axis (see, Fig. 4.1).

At the neutral-axis where the beam section is subjected to a state of pure shear presents a different picture in contrast to its top and the bottom faces. The principal stresses here act at an angle of  $45^\circ$  to the beam neutral-axis, thereby leading to the

**Fig. 4.1** *Stress-trajectories in a flexural member—A typical plot of the stress trajectories formed in a) a cantilever beam carrying a concentrated load at its free end; b) a simple beam under a uniformly distributed load over its entire span*





formation of cracks in the web of the beam. These cracks form along the axis of the principal compressive stresses and are termed as web-shear cracks or diagonal tension cracks. These tensile cracks are often termed as diagonal-tension cracks because of their inclination to the beam axis; generally along the diagonals at an angle of  $45^\circ$  to the beam-axis. This usually happens in the regions of a high shear and smaller flexural stresses in the beam. In such locations, high magnitude of the principal tensile stress causes inclined cracking in the mid-depth region of the beam before flexural cracking occurs on the beam extreme fibers (for instance, the bottom beam face for a gravity loading conditions). Generally, this type of cracking occurs on the beams with a relatively thin web, e.g. I or T-shaped sections. In the regions of the flexural members, where both the moment and shear force are relatively large or of comparable magnitude, flexural cracks first develop normal to the beam (bottom) face at the point of maximum moment (under the gravity load conditions). These cracks become inclined as they extend deeper into the beam section, towards its neutral-axis. The presence of relatively large shear stress near the neutral-axis changes the direction of the crack propagation. These inclined cracks are called flexure-shear cracks. It is important to note that the behavior of the concrete beams did not remain the same as predicted by assuming an elastic distribution of the stresses after the onset of the cracking. Once that happened, a number of additional factors come into the picture that influences and controls the shear capacity of concrete members, depending upon the extent of the cracking and the crack-width, the presence of the tensile reinforcing bars (both the transverse as well as the longitudinal rebars), etc. Figure 4.2 depicts typical shear cracks that would develop in a flexural member depending upon different factors that controls their formation.

Addition of the longitudinal reinforcing bars in the tensile zone of a plain concrete beam changes its flexural response. The flexural strength of the beam increases significantly depending upon the percentage of the steel area provided in the tension zone. It exhibits more flexural cracks than the concrete beam without or inadequate tensile reinforcing bars. The ability of the reinforcing bars to bridge cracks and transfer the tensile stress to the concrete through various bond mechanisms plays a great role in improving the shear capacity. The RC beam can fail in flexure or shear. If the beam is slender ( $a/d > 5$ ), it is likely to fail in the flexure. The yielding of the longitudinal reinforcing bars in the beam depends on the percentage steel area ( $p_t$ ). If the reinforcing bars yield extensively, the beam exhibits a ductile behavior and gives ample warning before the failure occurs.

A heavily reinforced slender beam or a short beam, however, fails abruptly with the formation of the diagonal cracks. These cracks generally form at the mid-depth of the beam and extend towards its top face or the bottom face depending upon the shear-span depth ratio ( $a/d$ ) and the percentage tensile steel area ( $p_t$ ) provided in the section; thereby, leading to either a shear-compression failure (Fig. 4.2b) or the shear-tension failure (Fig. 4.2c), respectively. The beam collapses immediately at the low value of the percentage tensile steel area ( $p_t$ ), caused by a widely-opened

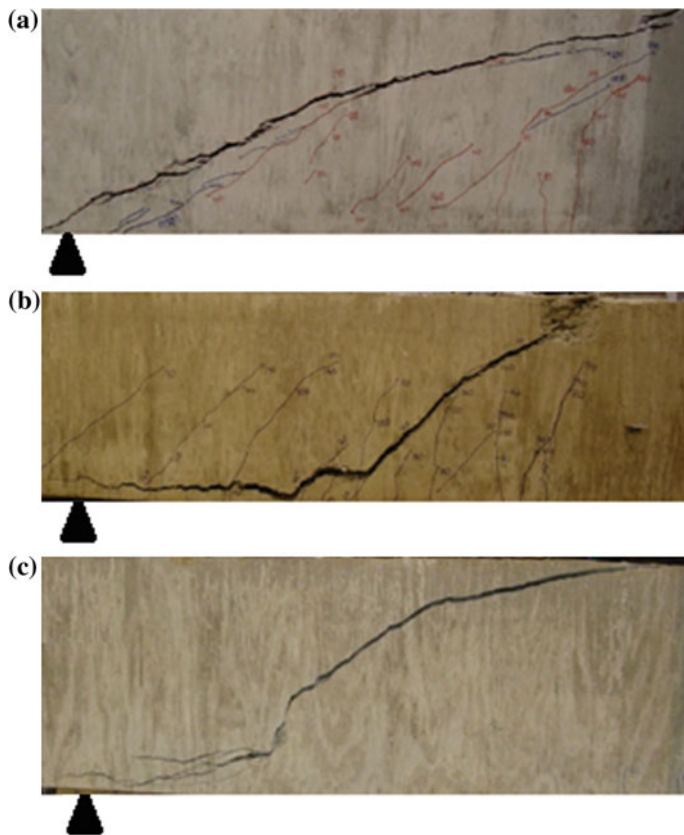


**Fig. 4.2** *Typical shear cracks*—The photographs depict a set of typical shear cracks formed in reinforced concrete beams depending upon the different factors that influence it. **a)** Shows a diagonal shear crack; **b)** represents a typical shear-compression failure and **c)** depicts shear-tension failure

diagonal crack (Fig. 4.2a); otherwise, it sustains additional loads before a failure occurs. Nevertheless, it always happened with initiation of either shear-compression failure or shear-tension failure depending upon a number of parameters that control it: these are described in the following section.

### 4.3 Shear-Transfer Mechanism

Cracks develop in an RC beam once the tensile stress in the member exceeds the concrete tensile strength. It can happen anywhere in the beam along its span. Generally, the flexural cracks form near the mid-span of the beam, in case it is inadequately reinforced. And when the effect of the shear force dominates over the

flexural effects, the diagonal-tension stresses and the diagonal-compression stresses induce simultaneously in a beam section, thereby leading to the formation of diagonal cracks on the beam web (see Fig. 4.2). This normally takes place when the magnitude of the diagonal-tension equals the limiting tensile strength of the concrete. However, in case, the beam is adequately reinforced using stirrups, the section fails by crushing of the concrete when the value of the diagonal-compression stress reaches the concrete crushing strength (see Fig. 4.2b). This type of failure is brittle in nature and occurs abruptly. Because of this fact, most of the design guidelines have put an upper limit to the shear stress caused by the loading and an attempt should be made to keep the magnitude of the shear stress less than the allowable maximum concrete shear strength [IS 456 (2000)]. It can be managed in the design, either by increasing the cross-sectional size of the member or by increasing the value of the maximum permissible shear stress. This can be done by selecting higher concrete grade, e.g. from M20 to M25, and so on, or by increasing the percentage of tensile steel in the section, till the value of the nominal shear stress becomes less than the permitted value of shear capacity.

The diagonally-cracked beam continues to carry the shear force through a number of shear-transfer mechanisms. Considerable stress redistribution takes place in the beam during this process. At present, five types of the shear-transfer mechanisms are identified that are believed to be responsible for the shear strength exhibited by a reinforced concrete section. These are identified as: (1) uncracked concrete existing in the flexural-compression zone of the beam; (2) interfacial shear transfer arising because of aggregate interlock; (3) dowel action of the longitudinal reinforcing bars; (4) arch action; and (5) residual-tensile stresses transmitted directly across the cracks. The question of what mechanisms of shear-transfer will contribute most to the resistance of a particular beam section is difficult to answer as a number of factors contribute towards mobilization of the shear-transfer mechanism; the most significance among them is the crack-width that forms in the member at failure. Most of the other shear-transfer mechanisms depend heavily on the crack-width that finally forms in the section. These factors are described in the following sections.

### ***4.3.1 Uncracked Concrete in the Flexural Compression Zone***

In the uncracked portion of the beam, especially in the shear zone lying above the neutral-axis, the shear force is transferred by a resistance offered by the concrete to the principal tensile and compressive stresses. Figure 4.1 depicts a typical pattern of the principal stress-trajectories, both the compression as well as tension, in a flexural member upon its loading. The integration of these stresses over the depth of the compression zone, lying above the section neutral-axis, gives a shear force component. Nevertheless, the contribution from the concrete compression zone will

be small and sometimes insignificant in case the beam is under-reinforced due to their smaller depth of the neutral-axis and it will be quite significant if the beam section is over-reinforced. The enhanced post-cracking response of the SFRC provides a significant concrete contribution in the flexural compression zone of the beam, especially when it is provided with conventional longitudinal rebars in the tension zone in comparison to the conventionally reinforced concrete sections. The enhanced strength of the tension zone because of the conventional longitudinal rebars and the steel fibers in the concrete causes a downward movement of the neutral-axis in the beam section; thereby leading to the improved contribution from the flexural compression zone.

### ***4.3.2 Interface-Shear Transfer***

The interface-shear transfer mechanism activates once the cracks develop in the beam section and it contributes most, if the crack-width is small; ranging from 0.1 to 0.5 mm. The coarse aggregates protruding from the crack surface provide resistance against the slip caused by the shear stresses. The concrete grade, surface conditions of the failure surface and types of the coarse aggregates greatly influence the shear transfer through this mechanism. As the lightweight concrete uses relatively porous aggregates to reduce the concrete density, cracks easily go through these aggregate and subsequently, the contribution towards the shear capacity would be insignificant. A similar phenomenon happens in case of a high strength concrete wherein the high strength of the hydrated cement paste in the concrete causes the cracks to penetrate through the relatively weak coarse aggregates. But, in case of the SFRC, the bridging action of the steel fibers considerably reduces the crack-width both in case of the lightweight concrete as well as the high strength concrete that leads to the enhanced shear capacity of the section.

### ***4.3.3 The Dowel Action of Longitudinal Reinforcement***

The presence of the longitudinal tensile steel bars in the tension zone of flexural beams (both, the RC as well as the SFRC sections) also contributes towards the shear capacity as these bars provide a resistance against the slip occurring along the failure surface in the beam. This mechanism is termed as dowel-action. It is reported that the share of this mechanism is higher in the members having large amounts of the longitudinal reinforcement, particularly when this reinforcement is distributed in more than one layer and the section has an adequate transverse reinforcement too to confine the concrete and the longitudinal rebars. The transverse steel significantly increases the dowel-action in the beam section by confining the concrete. The addition of the fibers also leads to a relatively higher tensile strength of the concrete cover in the SFRC section than the plain concrete in the

case of RC beams. This enhanced strength of the concrete cover in the section indirectly increases the dowel-action being activated in the section as the collapsing segments of the beam slips along the relatively longer failure surface formed in the SFRC beam section.

#### **4.3.4 Arch Action**

This type of shear-transfer mechanism activates in the members which are deep enough to form an arch action in the beam. This action generally develops in the members who have a shear span-to-depth ratio of 2.5 or less. Because, it is easier for the shear to be transmitted directly to the support through a compression strut that would develop between the two adjacent web-shear cracks formed in a member, if it is deep.

#### **4.3.5 Residual-Tensile Stresses Across Cracks**

After the formation of a shear crack in the section, a clean/smooth break never occurs along the failure plains. It is always accompanied by a rough surface caused by the protruding coarse aggregates and the uneven concrete surface. The random orientation and the presence of the steel fibers in the SFRC bridges the crack surfaces and aids in the tensile stress transfer across the crack. As a result, the cracked surface continues to transfer the tensile forces across the crack. These stresses if integrated over the cracked surface in the beam constitute a shear force component. This phenomenon is most effective at the smaller crack widths formed in the range of 0.05–0.15 mm. The SFRC possess residual tensile strength that is good enough to keep the crack-width in the section sufficiently small to ensure an effective and efficient transfer of the shear stresses through this mode. The residual-tensile stresses provide a significant portion of the concrete shear capacity in case of shallow members having depths less than about 100 mm, or so, e.g. The slabs and the SFRC members where the flexural and the diagonal cracks extends over a larger area.

### **4.4 Factors Influencing Shear Capacity**

The steel fibers play a multiple role in enhancing the shear capacity of longitudinally reinforced SFRC beams. The steel fibers delay the opening and propagation of the diagonal cracks in beams. They subsequently carry the redistributed tensile stress across the crack and prevent the premature concrete splitting that generally occurs otherwise along the tensile reinforcement in the beam section (Fig. 4.2b, c).

The fibers are even more effective in the beams constructed using a strain-hardening SFRC. Broadly; they (1) transfer the tension stresses across the diagonal cracks; (2) allow the additional transfer of interfacial shear through an enhanced aggregate interlock caused by the reduced crack-opening of the diagonal cracks; and (3) increases the dowel action due to enhanced tensile strength. However, the relative contribution to the shear capacity of a flexural member from the diagonal tension resisted by the fibers and from the aggregate interlock changes as the beam is loaded. Immediately after the diagonal cracking, both the fibers and the aggregate interlock contribute towards the shear capacity, but with increasing load, as the diagonal (or flexural-shear) cracks widen, the shear resisted by the aggregate interlock decays at a much faster rate than the contribution from the steel fibers. In such cases, the fibers play the role of the transverse steel in beams and control the amount of shear resisted by the web prior to the shear failure. The important factors influencing the shear capacity of reinforced concrete beams are described below.

#### **4.4.1 Depth of Member ( $D$ )**

The beam depth has a significant effect on the shear capacity, especially for the members without transverse reinforcement. A higher beam depth results in the formation of longer diagonal shear cracks at failure. The formation of relatively longer cracks are one of the reasons for a higher shear resistance exhibited by the deeper RC beams as these significantly reduces the magnitude of the effective stresses to be transferred across the crack widths. Consequently, a relatively higher force is needed to cause the failure of a deep beam than the beams having a smaller inclined crack length.

#### **4.4.2 Shear Span-to-Depth Ratio ( $a/d$ )**

This parameter controls the magnitude of the flexural stresses and the shear stresses being induced in beams upon loading. It is an accepted index to measure the relative magnitudes of the flexural and the shear stress that would act at some section in a flexural member [Naik and Kute (2013)]. As the development and growth of the inclined shear cracks in the RC beam depends upon the relative magnitude of the moment and shear force, this parameter plays a vital role in controlling the shear capacity and the mode of the failure that the member would exhibit at the failure. At a smaller value of  $a/d$  ( $<2.5$ ), the beam acts more as a deep beam and exhibits a higher shear capacity than the cases having a higher value ( $>2.5$ ). This happens because of the fact that, as beam becomes deeper; it is easier for the shear to be transmitted directly to the support by means of a compression strut that would form between the two adjacent inclined shear cracks in the member. At a smaller value of  $a/d$  ( $<2.5$ ), the beam generally fails by initiation of the inclined cracks. The final

failure would take place either by crushing of the reduced concrete section above the crack tip (termed as shear-compression failure, see Fig. 4.2b) or by formation of the cracks along the longitudinal tension steel when the inclined crack extends downside and joins along the longitudinal tension steel rebars near the beam tensile face (termed as shear-tension failure, see Fig. 4.2c). The beam having a large ( $a/d$ )-value ( $>5.0$ ) always fails in flexure with the formation of vertical flexural cracks in the region of maximum moments. These cracks can extend to form inclined flexural-shear cracks in the web, particularly if they are thin as in case of the I-shaped sections, for the beams having a shear-span to depth ratio ( $a/d$ ) in the range 2.5–5.0.

#### 4.4.3 Longitudinal Reinforcement ( $p_t$ )

The RC beams having a smaller percentage of the tensile steel area generally exhibit a very low shear capacity. This happens because of the formation of wider crack widths in the member that leads to the lower interface-shear transfer across the cracks. This process is simultaneously accompanied by a reduction in the depth of the flexural-compression zone in the beam and the lesser dowel action. For this reason, most of the design guidelines/codes have prescribed a minimum percentage of the tensile steel to ensure a bare minimum value of the beam shear capacity. And a beam provided with a relatively higher amount of the longitudinal steel exhibits a higher shear capacity and attains a constant value where the effect of the rebar addition did not influence the crack-width, or the position of the neutral-axis, or it leads to a premature failure through concrete crushing at the beam compression face.

#### 4.4.4 Axial Force ( $A$ )

It is an established fact that the presence of axial-tension in the section reduces the shear capacity of a beam section, whereas, the axial compression has an opposite effect to increase the shear resistance. The axial forces influence the crack-width; all other related mechanisms of the shear-transfer are directly related to the crack-width. If axial force is tensile in nature, it results in increased crack-width, thereby leading to a reduction in the shear capacity. On the contrary, the effect of the compressive force is to delay the formation of both flexural as well as inclined shear cracks in the section, thereby leads to enhanced shear capacity of the beam section. It also reduces the angle of inclination of web cracks with reference to the longitudinal steel that results in relatively high shear capacity exhibited by section.

## 4.5 Design Shear Strength of SFRC Beams

The design guidelines CNR-DT (204) and MC2010 prescribe the use of experimental test data to determine the safe shear stress ( $\tau_f$ ) of SFRC beam section. The safe value of the shear stress is a direct function of the material characteristic tensile strength ( $\sigma_{tuk}$ ). When the steel fibers are used alone in the section to provide the flexural capacity, the design guidelines stipulate that the crack-width ( $w_u$ ) in the section should be restricted to 1.5 mm. In no case, the principal tensile stress  $\sigma_1$  should be allowed to exceed the design tensile strength of SFRC determined by applying a partial safety factor to the characteristic tensile strength ( $\sigma_{tuk}$ ). If SFRC undergoes strain-softening in its post-cracking range, the beam section must be adequately reinforced using both the longitudinal steel on its tension zone as well as the transverse (stirrups) reinforcing bars.

There is no need to use conventional transverse reinforcement in the form of stirrups if the characteristic tensile strength ( $\sigma_{tuk}$ ) of the SFRC is reported to be more than  $0.05\sqrt{f_{ck}}$ ; otherwise, the section must be provided with some minimum amount of the transverse reinforcement to ensure that the shear capacity of the section is greater than its first cracking strength,  $\tau_{cr}(=0.67f_{ctk})$ . And in case, the nominal shear stress in the section exceeds the safe shear stress ( $\tau_f$ ), it should be provided with the transverse reinforcement, in the form of stirrups, for a force determined by taking a difference of the safe shear strength ( $\tau_f$ ) and design shear force ( $\tau_v$ ). The procedure for determining the stirrup spacing is exactly similar to that used in the shear design of a conventionally reinforced concrete flexural member. The members can be designed as per the procedure prescribed by the design codes, such as IS 456 (2000), etc. However, the spacing between the two adjacent stirrups along the beam length shall not exceed the value 0.8D, where D is the depth of the member.

In case of the SFRC beams reinforced with conventional longitudinal rebars in its tensile zone, at an effective depth ( $d$ ), the safe value of the shear stress ( $\tau_f$ ) can be determined from Eq. 4.1.

$$\tau_f = \frac{1}{\gamma} \left\{ 0.18k \left[ 0.8p_t f_{ck} \left( 1 + 7.5 \frac{f_{tuk}}{f_{ctk}} \right) \right]^{\frac{1}{3}} \right\} \quad (4.1)$$

In the above equation,  $\gamma$  is the partial safety factor ( $=1.5$ ) for the concrete;

- $k$  is a beam size factor  $= 1 + \sqrt{\frac{200}{d}} \leq 2$ ; (the depth  $d$  in 'mm')
- $p_t$  is a percentage tensile steel area ( $\leq 2\%$ ), the longitudinal rebars representing the percentage steel area ( $p_t$ ) in the beam section must be extended for a distance of ( $d +$  anchorage) beyond the section considered in the analysis. This is suggested to consider the tension-offset in the design.
- $f_{tuk}$  is the characteristic value of the residual tensile strength for the SFRC computed at the crack-width ( $w_u$ ) of 1.5 mm;
- $f_{ctk}$  is the characteristic value of the tensile strength of the concrete, generally taken as  $0.7\sqrt{f_{ck}}$ ;
- $f_{ck}$  is the characteristic cube compressive strength in MPa.



The design guidelines RELIM also prescribed an expression similar to that given in Eq. 4.1 for determining the value of the safe shear stress ( $\tau_f$ ) of SFRC sections. It contains two parts, reflecting the contribution from the concrete section alone (Eq. 4.2) and that's coming from the addition of the steel fibers in the concrete (Eq. 4.3). The shear capacity of a rectangular SFRC beam can be obtained by adding Eqs. 4.2 and 4.3. The size-effect factor ( $k$ ) can be taken from the expression given in Eq. 4.1. The parameter  $f_{R4}$  represents a value of the residual-stress corresponding to the ultimate state and it is generally taken corresponding to the CMOD of 3.5 mm or a deflection value of 3.00 mm observed in the specimens during the conduct of the standard bending tests (see, Chap. 2 for details).

$$\tau_c = 0.12k[0.8p_f f_{ck}]^{\frac{1}{3}} + 0.15\sigma_{cp} \quad (4.2)$$

$$\tau_f = 0.7k[0.12f_{R4}] \quad (4.3)$$

The shear capacity computed using Eqs. 4.2 and 4.3 already includes the partial safety factor ( $\gamma$ ) of 1.5 for the concrete without fibers.  $\sigma_{cp} = N/A_c < 0.2f_{ck}/\gamma$  is the average axial stress acting on the concrete cross section,  $A_c$  due to an axial force  $N$ . These expressions are applicable for the rectangular beam sections.

In absence of the experimental data (during preliminary studies), the value of the  $f_{R4}$  can be taken from the expression given in Chap. 2 and reproduced below for the SFRC made using plain steel fibers. Nevertheless, it must be multiplied by the fiber shape factor to get residual tensile strength of the SFRC in case of the fibers having shape other than the plain one; it is two for the hooked-end steel fibers and three for the wavy shaped fibers.

$$f_{R4} = \sigma_u = 0.3V_f \frac{1}{d} \sqrt{f_{ck}}$$

#### Example 4.1

*M35 grade was used to cast an SFRC beam of size 300 × 450 mm. It contains hooked-end steel fibers having an aspect ratio of 60 and volume fraction of 1 %. Six numbers of standard prisms 150 × 150 × 750 mm were cast and tested under the standard 3-point loading conditions, with an effective span of 500 mm. Table 4.1 gives the test results at various prescribed values of the CMOD. The results from the standard 150 mm concrete cubes indicate that the SFRC possesses a 28 day compressive strength of 42.58 MPa. Determine the safe shear strength of SFRC.*

#### Solution

The characteristic value of the residual-tensile strength of the SFRC can be determined using Eq. 3.18 and Table 3.7.

$f_{R4} = 2.75 - 1.77 \times 0.303 = 2.213$  MPa, computed corresponding to the CMOD of 3.5 mm. The safe shear stress of the SFRC can be determined using Eqs. 4.3, with a beam size factor,  $k = 1 + \sqrt{\frac{200}{d}} = 1.66 \leq 2$ ;

**Table 4.1** Test results of a 3-point bending test

Specimen	The stress values (MPa) obtained corresponding to a CMOD of			
	0.05 mm	0.5 mm	2.5 mm	3.5 mm
	$f_L$	$f_{R1}$	$f_{R3}$	$f_{R4}$
1	9.14	13.53	9.60	3.09
2	7.20	10.03	6.72	2.98
3	7.09	10.60	6.17	2.67
4	7.55	11.79	6.40	2.71
5	7.49	10.11	6.56	2.88
6	6.76	9.48	6.08	2.15
Average value, $f_{m1}$ (MPa)	7.51	10.92	6.92	2.75
SD (s) (MPa)	0.763	1.366	1.217	0.303

The safe value of shear stress =  $\tau_f = 0.7k[0.12f_{R4}] = 0.308$  MPa

Therefore, the shear capacity of the SFRC beam section =  $0.308 \times 300 \times 450 = 41580$  N (=41.58 kN).

Alternatively, a reasonably good representative value of the stress ( $f_{R4}$ ) can be obtained using the analytical expression as given below:

$$\sigma_{R4} = \sigma_u = 2 \times 0.3 \times V_f \times \frac{1}{d} \sqrt{f_{ck}} = 2.13 \text{ MPa}$$

And, the corresponding value of the safe shear stress =  $\tau_f = 0.7k[0.12f_{R4}] = 0.297$  MPa; thereby giving a shear capacity of the SFRC beam section =  $0.297 \times 300 \times 450 = 40096$  N (=40.10 kN).

### Example 4.2

The SFRC beam in the Example 4.1 is provided with 4 no.—20 mm diameter bars in its tensile zone. What would be the shear capacity of the section considering the contribution from the tensile rebars?

### Solution

In the absence of the longitudinal reinforcing bars, the SFRC rectangular section provides a shear capacity of 0.308 MPa (see Example 4.1). The additional resistance from the longitudinal bars can be determined using Eq. 4.2.

$$\text{The beam size factor, } k = 1 + \sqrt{\frac{200}{d}} = 1.66 \leq 2;$$

$$pt = 4 \times 314 \times 100/300 \times 425 = 0.985 \%$$

$$\begin{aligned} \tau_c &= 0.12k[0.8p_t f_{ck}]^{\frac{1}{3}} \\ &= 0.12 \times 1.66 \times [0.8 \times 0.985 \times 35]^{1/3} = 0.6 \text{ MPa} \end{aligned}$$

Therefore, the total shear resistance of the SFRC section reinforced longitudinally by means of conventional rebars can be obtained by totalling the contribution from the steel fibers (see Example 4.1) and the longitudinal rebars. It is given below:

$$\text{Safe shear stress} = 0.308 + 0.60 = 0.908 \text{ MPa}$$

$$\text{Shear capacity} = 0.908 \times 300 \times 450 = 122580 \text{ N}(= 122.58 \text{ kN})$$

### Example 4.3

Six numbers of standard prisms  $150 \times 150 \times 750 \text{ mm}$  were cast and tested under the standard 3-point loading conditions, with an effective span of 500 mm. The hooked-end steel fibers having an aspect ratio of 60 and the volume fraction of 1 % were used in the production of the SFRC. Table 4.2 gives the test results at various prescribed values of the CMOD. The results from the standard 150 mm concrete cubes indicate that the SFRC possesses a 28 day compressive strength of 42.58 MPa. Determine the safe shear strength of SFRC using CNR-DT CNR-DT guidelines.

### Solution

The characteristic tensile strength ( $f_{\text{tik}}$ ) of the SFRC corresponding to CMOD of 1.5 mm can be determined using Eq. 3.18 and Table 3.7. As the values corresponding to the CMOD of 1.5 mm are not reported, an average value is taken for the calculations.

$f_{\text{tik}} = 8.92 - 1.77 \times 1.29 = 6.63 \text{ MPa}$ , computed corresponding to the CMOD of 1.5 mm.

The safe shear stress of the SFRC can be determined using Eq. 4.1, with a beam size factor,  $k = 1 + \sqrt{\frac{200}{d}} = 1.66 \leq 2$ ;

The percentage longitudinal steel ( $p_t$ ) = 0;

**Table 4.2** Test results of a 3-point bending test

Specimen	The stress values (MPa) obtained corresponding to a CMOD of			
	0.05 mm	0.5 mm	2.5 mm	3.5 mm
	$f_L$	$f_{R1}$	$f_{R3}$	$f_{R4}$
1	9.14	13.53	9.60	3.09
2	7.20	10.03	6.72	2.98
3	7.09	10.60	6.17	2.67
4	7.55	11.79	6.40	2.71
5	7.49	10.11	6.56	2.88
6	6.76	9.48	6.08	2.15
Average value, $f_{\text{ml}}$ (MPa)	7.51	10.92	6.92	2.75
SD (s) (MPa)	0.763	1.366	1.217	0.303

$$\begin{aligned}
 f_{ctk} &= 0.7\sqrt{42.58} = 4.56 \text{ MPa} \\
 \tau_f &= \frac{1}{\gamma} \left\{ 0.18k \left[ \left( 7.5 \frac{f_{tuk}}{f_{ctk}} \right) \right]^{\frac{1}{3}} \right\} \\
 &= \frac{1}{1.5} \left\{ 0.18 \times 1.66 \left[ \left( 7.5 \frac{6.63}{4.56} \right) \right]^{\frac{1}{3}} \right\} = 0.44 \text{ MPa}
 \end{aligned}$$

A comparison of the results computed in Examples 4.1 and 4.3 indicates that the SFRC section exhibits higher shear strength if it is found for a CMOD of 1.5 mm (in Example 4.3) in comparison to those given in Example 4.1; wherein the CMOD adopted as per the provisions of RELIM is 3.5 mm. It is caused by an effective transfer of the interfacial stresses at a smaller value of the crack-width (see, Sect. 4.3).

## References

- Ahmed E, Legeron F, Ouahla M (2015) Steel fiber as replacement of minimum shear reinforcement for one-way thick bridge slab. *Constr Build Mater* 78:303–314
- Ashour SA, Hassanain GS, Wafa FF (1992) Shear behavior of high strength fibre reinforced concrete beams. *ACI Struct J* 89(2):176–184
- Bureau of Indian Standards (BIS) (2000) Plain and reinforced concrete-code of practice. IS 456 (4th rev.), New Delhi, India
- Khuntia M, Stojadinovic B, Goel SC (1999) Shear strength of normal and high-strength fibre-reinforced-concrete beams without stirrups. *ACI Struct J* 96(2):282–289
- Lim TY, Paramsivam P, Lee SL (1987) Shear and moment capacity of reinforced steel-fiber concrete beams. *Mag Concr Res* 39:148–160
- Naik and Kute (2013) Span-to-depth ratio effect on shear strength of steel fiber-reinforced high-strength concrete deep beams using ANN model. *Int J Adv Struct Eng* 5:29
- Sharma AK (1986) Shear strength of steel-fibre-reinforced-concrete beams. *ACI J* 83(4):624–628
- Swamy RN, Mangat PS, Rao CVSK (1974) The mechanics of fibre reinforcement of cement-matrices. *Fibre-Reinf-Concr ACISP-44*:1–28

# Chapter 5

## Analysis and Design of SFRC Slabs

### 5.1 General

The main aim of the structural engineer is to suggest a safe and economical structural system. Safety not only implies resistance to the external actions, but it also concentrates on the ductility and robustness of the system. The design should aim to proportion the structural member in a manner that its collapse should be preceded by perceivable deformations and in case of the failure; the damage should not extend to the whole structure. As described in the Chap. 3, a limit state is a state of impending failure, beyond which the structure ceases to perform its intended function satisfactorily, both in term of its safety as well as serviceability. Accordingly, two types of the limits: namely, the limit state of collapse and the limit state of serviceability are proposed by most of the design codes that any structural system must fulfil for the satisfactory performance. The former limit deals with the strength of a structural member, its buckling and the sliding/overturning, etc., whereas the later limit state deals with the discomfort to occupancy and/or malfunction caused by the excessive deflection, the cracking, and the vibration, or the loss of durability, etc. The procedure for the analysis and design of SFRC members is presented in the Chaps. 3 and 4. It can be used to proportion SFRC members with and without conventional reinforcing bars in the section. This chapter presents the applications of the design concept and procedure given in the earlier chapters to the steel fibers reinforced slab-system (SFRC slab-system); the use of steel fibers is found to be more effective in the thin members, such as slabs because of their smaller thickness that acquires a preferential orientation of the fibers along the tensile face of the section. This chapter starts with the fundamentals of the limit analysis and later, its use was extended to predict the ultimate load carrying capacity of SFRC slab-system.

## 5.2 Limit Analysis

Limit Analysis is a powerful tool for modelling the structural behavior of any system or its constituent members at the ultimate state and gaining an understanding of their safety. It tries to establish the load factor for a structural system by exploring the inherent reserve strength laying in the system beyond the elastic range by assuming the section sufficiently ductile to enable it to behave in the rigid perfectly plastic range. In this approach, the materials with a sufficient ductility are considered or are made to behave in a ductile fashion by means of adequate detailing of the reinforcements in a structural member such that the stress redistribution required by the plastic theory could occur. Although the plain concrete is not a particularly ductile material, but it can be made to behave as a sufficiently ductile material by carefully selecting material properties and reinforcing it either using the conventional reinforcing steel bars, or by mixing short steel fibers randomly in the concrete at the time of the production, or a combination of the conventional rebars and the steel fibers can also be tried to meet the strength demand and the ductility requirements of the system.

The theorems of the derive from the application of the principle of virtual work to a rigid-perfectly plastic system. A rigid-perfectly plastic material absorbs no energy during the deformations that it undergoes upon loading. This means that the work done by the external forces is completely dissipated in the plastic deformations occurring along the plastic hinge(s) and/or the yield line pattern developed in the structural element (e.g. the beams and the slab, respectively). This unique behavior of the structural system at collapse ensures that the total work done by the internal forces and the external forces must disappear for any admissible virtual displacement given to the system. In other words, it can be stated that a set of real forces acting on a rigid body is always in equilibrium if the work done by these external forces as they move through a set of the compatible virtual displacement is equal to zero. In this statement, the line ‘the compatible virtual displacements’ means that all the displacements that the rigid-body undergoes upon loading should be consistent with the rigid-body motion; thereby indicating that all displacements in the system at the collapse are linked together through some geometric relations. During these deformations, there is generally no change in the shape of different segments of the body formed after the collapse as the stress levels there are usually small in comparison to those existing at the position of the yield lines/plastic hinge. Nevertheless, the bending moment distribution in a structural system at the collapse must satisfy the following three conditions in order to support a given set of an external load.

### 5.2.1 Mechanism Conditions

This condition requires that the moment field caused by the external load must approach the flexural capacity of the structural system and/or its members at sufficient number of sections and/or points for the structure, or part of it, to develop plastic hinge(s) (in case of the beams) and/or the yield line pattern (in case of the slabs) in a manner to convert the system into a mechanism.

### 5.2.2 Equilibrium Conditions

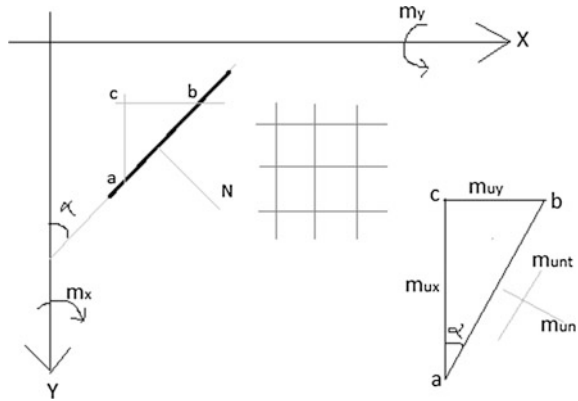
The moment field induced in the structural system by the external load must represent the state of equilibrium between the system and the load acting over it.

### 5.2.3 Yield Conditions

The yield condition defines the strength of the structural member subjected to a general moment field. This condition distinguishes the safe state of stress from those for which a given set of reinforcement in the structural member is not sufficient to support the external load. In other words, it requires that the moment field in the structural system should nowhere be allowed to exceed the flexural capacity of the section. One such criterion was proposed by Johansen (1967) for the analysis of reinforced concrete slabs. It is known as 'normal-moment yield criterion' and it requires that at any point in the slab, the normal moment per unit width ( $m_u$ ) due to the design moment field ( $m_x$ ,  $m_y$  and  $m_{xy}$ ) should not exceed the ultimate normal resisting moment ( $m_{un}$ ) of the slab section in that direction. The validity and accuracy of this criterion was established experimentally by a number of researchers in the subsequent years and it was found to work reasonably good within the domain of following assumptions (Kemp 1965; Moley 1965; Lenschow and Sozen 1967; Jain and Kennedy 1973).

- The actual yield lines formed in the slab can be replaced by a series of steps both along its x-axis and the y-axis; these steps represent the moments ( $m_x$  and  $m_y$ ), respectively. The yield lines in the slab are subjected to the moments ( $m_x$  and  $m_y$ ) only and it carries no torsional moment ( $m_{xy}$ ).
- Kinking of the reinforcing bars across the yield lines and the biaxial-stress conditions in the concrete compression zone of the slab does not influence the strength of the slab section.
- The tensile reinforcing bar crossing the yield line both along the x-axis and y-axis of the slab has reached its yield strength.
- In-plane membrane forces in the slab section are assumed to be negligible.

**Fig. 5.1** Moments acting on a triangular element of RC slab-rebars spacing and free-body diagram



Based upon these assumptions, an expression defining the yield criterion for a RC slab section can be easily derived using the principles of statics. Consider a triangular slab element **abc** subjected to a general moment field. It is assumed to act along the yield line in the direction (**t**) at an angle ( $\alpha$ ) to the y-axis. The actual yield line can be replaced by a series of small steps along its length for the sake of simplification; each representing the components of the ultimate resisting moments along the x-axis ( $m_{ux}$ ) and the moment ( $m_{uy}$ ) along the y-axis of the slab. The ultimate normal resisting moment acting in the n-direction along the yield line can be found from the consideration of equilibrium of the triangular element **abc** by taking moments of the components of the moment of resistance ( $m_{ux}$ ) and the ( $m_{uy}$ ) about **ab**, as shown in Fig. 5.1.

$$m_{un}ab = m_{ux}ac \cos\alpha + m_{uy}bc \sin\alpha$$

Or

$$m_{un} = m_{ux}\cos^2\alpha + m_{uy}\sin^2\alpha \quad (5.1)$$

And,

$$m_{unt}ab = m_{ux}ac \sin\alpha + m_{uy}bc \cos\alpha$$

Or

$$m_{unt} = (m_{ux} - m_{uy}) \sin\alpha \cos\alpha \quad (5.2)$$

The moments per unit width ( $m_n$  and  $m_t$ ) and the associated torsional moment ( $m_{nt}$ ) due to the given moment field in the slab element can be obtained by summing the components of  $m_x$ ,  $m_y$  and  $m_{xy}$  in the **n**- and **t**-directions using the right hand screw rule. The angle ( $\alpha$ ) between the x- and n-axis is measured clockwise



from the x-axis. The equilibrium of the moments acting on the element in the n-direction requires that

$$m_n ab = m_x ac \cos\alpha + m_y bc \sin\alpha + 2 m_{xy} bc \cos\alpha$$

Or

$$m_n = m_x \cos^2\alpha + m_y \sin^2\alpha + m_{xy} \sin 2\alpha \quad (5.3)$$

Similarly,

$$m_t = m_x \sin^2\alpha + m_y \cos^2\alpha - m_{xy} \sin 2\alpha \quad (5.4)$$

And,

$$m_{nt} = (m_x - m_y) \sin\alpha \cos\alpha - m_{xy} \cos 2\alpha \quad (5.5)$$

This yield criterion assumes that the reinforced concrete slab element reaches its when the normal moment ( $m_n$ ) due to the given moment field becomes equal to the ultimate normal resisting moment ( $m_{un}$ ), i.e.  $m_{un} \geq m_n$ . Therefore, using Eqs. 5.1 and 5.3, following expression can be formulated defining the yield criterion for the RC slab element subjected to a normal moment field ( $m_x$ ,  $m_y$  and  $m_{xy}$ ).

$$(m_{ux} \cos^2\alpha + m_{uy} \sin^2\alpha) \geq (m_x \cos^2\alpha + m_y \sin^2\alpha + m_{xy} \sin 2\alpha) \quad (5.6)$$

Equation 5.6, applicable for all values of the variable  $\alpha$ , can be simplified to an easily usable form; it is given in Eq. 5.7.

Dividing through by  $\cos^2\alpha$

$$(m_{ux} + m_{uy} \tan^2\alpha - m_x - m_y \tan^2\alpha - 2 m_{xy} \tan\alpha) \geq 0 \quad (5.7)$$

Left-hand side of above equation is function of  $(\tan\alpha)$  and it represents the excess of the moment ( $m_{un}$ ) over the moment ( $m_n$ ) and for this excess to be a minimum:

$$\frac{\partial f(\tan\alpha)}{\partial \alpha} = \frac{\partial f(\tan\alpha) d \tan\alpha}{\partial \tan\alpha d\alpha} = \frac{\partial f(\tan\alpha) \sec^2\alpha}{\partial \tan\alpha} = 0$$

Since  $\sec^2\alpha \neq 0$ ,

$$\Rightarrow (2 m_{uy} \tan\alpha - 2 m_y \tan\alpha - 2 m_{xy}) = 0$$

$$m_{uy} = m_y + \frac{m_{xy}}{\tan\alpha} \quad (5.8)$$

And, if  $f(\tan\alpha)$  is to represent the minimum excess moment, then

$$\frac{\partial^2 f(\tan\alpha)}{\partial(\tan\alpha)^2} = 2m_{uy} - 2m_u \geq 0$$

$$\text{or } m_{uy} \geq m_u \quad (5.9)$$

Combining Eqs. 5.8 and 5.9, we have  $\frac{m_{xy}}{\tan\alpha} \geq 0$

Therefore, if  $m_{xy}$  is positive,  $\tan\alpha$  must be taken as positive, and the vice versa. Substituting Eq. 5.8 into Eq. 5.7 gives

$$m_{ux} \geq m_x + m_{xy}\tan\alpha \quad (5.10)$$

The resisting moments ( $m_{uy}$  or  $m_{ux}$ ), therefore, can be selected from Eqs. 5.8 and 5.10 for any given moment field ( $m_x$ ,  $m_y$ , and  $m_{xy}$ ) and the predefined arrangement of the reinforcing bars.

### 5.3 Solution Using Energy Principle

The magnitude of the load that satisfies, simultaneously, the three conditions of the collapse: namely, the collapse mechanism, the equilibrium and the yield criterion represents the true collapse load of the structural system; there exists a unique load factor at the collapse that meets all the three conditions simultaneously. The value of the load factor can be determined without the necessity of calculating deformations, either at the collapse or at any other stage of loading, using the minimum and maximum principles. According to these principles, the collapse load factor for any structural system is a minimum load factor that has been obtained by fulfilling the equilibrium condition for all possible collapse-mechanisms of the system, and it will be the maximum load factor if it has been calculated by considering all those moment fields that satisfy the equilibrium and the applicable yield conditions. Therefore, these two conditions help the analyst to predict the lower and the upper bound to the true value of the load factor. Nevertheless, the true value of the load factor is obtainable if the analyst is able to successfully determine the load factor that simultaneously satisfies the three fundamental conditions.

It is worth to note that the value of this load factor increases or at least remains the same with the addition of any restraint, whether internal or external, in the structural system and it would reduce with the removal of the restraint. This condition can be used very conveniently to predict the collapse load of a slab restrained on all its four sides by reducing it into a slab that rests over the simple supports on its outer boundaries. It can then be suitably reinforced on its top face, near the outer continuous edges, to resist at least cracking moment without lowering the load factor. It is always advisable rather mandatory to check the crack-width as the

arbitrary selection of the moment there could lead to excessive crack-opening displacements caused by the redistribution of the moments, as the slab deflects under the applied load.

In the analysis, a set of yield line patterns compatible with Yield line the boundary conditions of the slab-system are assumed and it then proceeds by evaluating the ultimate load of each presumed yield line pattern. All the yield line patterns considered in the analysis must be kinematically admissible. While ascertaining whether a yield line pattern is kinematically admissible or not, the following kinematic conditions should be checked and an attempt must be made to satisfy these conditions in the analysis:

- (1) Every yield line or its extension must pass through the intersection point of the axes of rotation of the two deflecting slab segments, which intersect to form the yield line.
- (2) For a slab segment associated with a supported edge, its axis of rotation is the supported edge; while for a slab segment associated with a supported corner, its axis of rotation must pass through the supported corner.
- (3) Every yield line is a straight line ending either at a nodal point where the other yield lines meet, or at the free edge (an unsupported edge). The yield lines are not allowed to intersect each other, but their ends may meet at common nodal points.

It is important to note that a kinematically admissible displacement field controls the deformation of various rigid-segments of the collapsing slab. These segments are regarded as rigid bodies because the deformations in the collapsing slab-system are concentrated only along the yield lines under the increasing load. At ultimate state, the segments of the slab under the influence of external loading are in the state of equilibrium with the internal forces, for instance, the bending moments and the shear forces, acting along the yield lines in the slab. Needless to repeat, the torsional forces are zero along the yield line developed in the slab at the ultimate state. The equilibrium of the slab can be ensured by equating the work done by the external force (e.g. surface load) with that produced by the internal system of forces in moving through a small virtual compatible displacement field.

The reactions at the outer edges/supports of the slab-system will not contribute towards the external work, as they do not undergo any displacement. The work done by the internal forces at the yield lines will be due to the bending moments only, because the work done by the torsional moments and the shear forces, when summed over the entire slab, is zero. Moreover, the zero relative movement between the sides of the yield line corresponding to the torsional moment and the shear forces makes their contribution zero. Accordingly, the bending moments in the slab alone should be considered while calculating the internal work. They do so because of the relative rotation that occurs about the yield line between the two adjacent sides of the collapsed slab. The work done by the ultimate resisting moment per unit width of the slab ( $m_{un}$ ) at a yield line of length ( $l_n$ ), where the relative rotation about the yield line of the two segments is  $\theta_n$ , can be obtained from

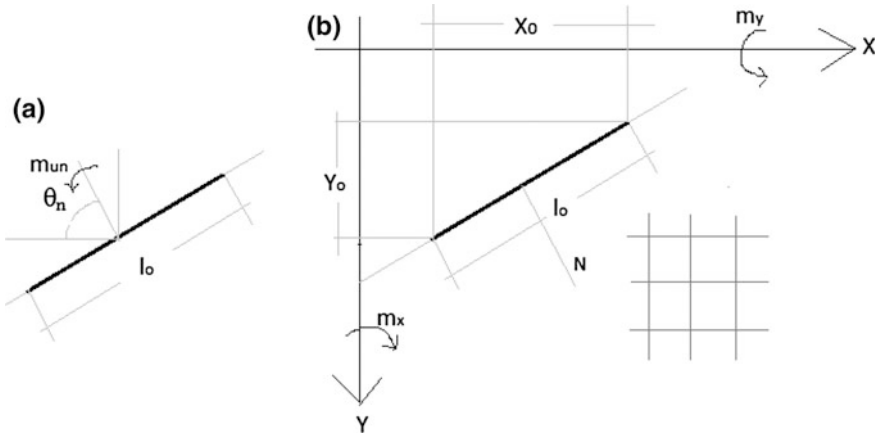


**Fig. 5.2** A typical yield line (shown by a *thick line*) inclined to the direction of orthogonal reinforcing bars in the RC slab

the work equation:  $-m_{un} \theta_n l_o$ . This is shown in Fig. 5.2. The work done by the bending moment is taken as negative because the direction of the rotation of the slab-segment, if it is displaced in the direction of the loading, will be opposite to the direction of the bending moment. The total work done by the resisting moments acting along the complete yield line pattern in the slab will be  $-\sum m_{un} \theta_n l_o$ . And, for the equilibrium of the slab-system, the summation of the total work performed by the internal forces in the section and the external force acting over the surface of the slab, ( $=\sum P_u \delta$ ) must vanish. The work equation of the slab-system at collapse is given in Eq. 5.11.

$$\sum P_u \delta - \sum m_{un} \theta_n l_o = 0$$

$$\text{or } \sum P_u \delta = \sum m_{un} \theta_n l_o \tag{5.11}$$

However, it is a common practice to provide the reinforcing steel in the slab(s) along the two orthogonal directions, x- and y-axis. But as the yield line is free to form in any direction (albeit along the lines representing maximum curvature in the slab) under the external load; therefore, these develop mostly inclined to the reinforcing bars (see, Fig. 5.2b). It is therefore always better and easier to deal separately with the x-axis and y-axis components of the internal work performed by the ultimate resisting moments ( $m_{ux}$  and  $m_{uy}$ ). For a yield line inclined at an angle ( $\alpha$ ) to the y-axis, Eq. 5.1 can be used to compute the components of the ultimate resisting moment ( $m_{ux}$  along the x-axis, and  $m_{uy}$  along the y-axis). The expanded form of a work equation is written below:



$$\begin{aligned}
\sum m_{un}\theta_n l_o &= \sum (m_{ux}\cos^2\alpha + m_{uy}\sin^2\alpha)\theta_n l_o \\
&= \sum m_{ux}\cos^2\alpha \theta_n l_o + \sum m_{uy}\sin^2\alpha \theta_n l_o \\
&= \sum m_{ux}\theta_x l_y + \sum m_{uy}\theta_y l_x
\end{aligned} \tag{5.12}$$

In Eq. 5.12,  $\theta_x$  and  $\theta_y$  are the rotations that the rigid segments of the collapsing slab undergo about its x-axis and y-axis, respectively. The parameters  $l_x$  and  $l_y$  are the projections of the yield line of length ( $l_o$ ) over the x-axis and the y-axis of the slab-system, respectively. At the ultimate state, Eqs. 5.11 and 5.12 can be equated to satisfy the equilibrium conditions of the slab-system. Equation 5.13 gives a complete work equation of the slab-system.

$$\sum P_u\delta = \sum m_{ux}\theta_x l_y + \sum m_{uy}\theta_y l_x \tag{5.13}$$

Equation 5.13 will ensure that the collapsed-interconnected segments of the reinforced concrete slab are in equilibrium with the external loading at the ultimate state. This condition along with the applicable yield criterion and a correct collapse mechanism predicts the true collapse load of the slab-system.

## 5.4 Flexural Modeling of Reinforced Concrete Rectangular Slabs

A reinforced concrete slab progressively loaded to failure develops a band of flexural cracks along the lines of maximum curvature on its tensile face. The distribution of the bending moments and the displacement field in the slab exactly follow the elastic plate theory at the low load levels when the tensile stresses in the section are well below the cracking flexural strength of the concrete. The slab section undergoes cracking once the magnitude of the tensile stresses under the increasing load exceeds the concrete flexural strength. Once that happens, the distribution of the moment field undergoes significant changes after development of cracks in the slab. This happens due to a reduction in the flexural stiffness of the slab section. With further increase in the loading, a large redistribution of the moment field takes place in the slab-system; thereby leading to the formation of lines of intense cracking in sufficient numbers on its tensile face. This process results in the division of the slab into a number of interconnected segments and it leads to the formation of the collapse mechanism as the external load magnitude approaches the ultimate load value. At this stage, the yielding of the tensile steel in the slab eventually occurs along the lines of maximum moments and the slab section undergoes a large change in the curvature along these lines of the yielding, with the moment there remaining practically constant at the ultimate moment of resistance of the slab section. After the formation of a collapse mechanism, the slab fails to support any further increase in the load. The number and the shape of

various segments into which the slab divides at the collapse depend upon its geometry, the boundary conditions, orthotropy and type of the load.

The band of this intense cracking across which the tensile steel in the slab has been yielded is represented by a single line at the center of the band; all plastic rotations of the slab segments are assumed to occur along this straight line. This straight line is termed as yield line and it represents the line of discontinuity of the displacement field, caused by the infinite value of the curvature existing along its length. The plastic deformations occurring along the yield lines are much greater than the elastic deformations that the slab segments undergoes in-between the yield lines, and therefore, it is reasonably good to assume the segments of the collapsing slab in an elastic state of the load-deformation response that undergo a rigid body movements under the increasing load.

After the formation of a complete yield line pattern, the slab-system starts behaving as a rigid-perfectly plastic material that absorbs no energy during the deformations that it undergoes under increasing loads. The work done by a set of the external forces over the slab surface is completely dissipated in the plastic deformations occurring along the yield lines. At ultimate state, therefore, the total work done by the internal forces in the slab section and the external load acting over it must disappear for an arbitrarily applied kinematically admissible virtual displacement to the mechanism. This condition will ensure the equilibrium of the assumed collapse mechanism of the slab-system at ultimate state. The collapse load predicted by using this condition would be on the higher side or at the most equal to the true value.

## 5.5 Assumptions

It is assumed that the load-deformation response of a reinforced concrete can be idealized as a rigid-perfectly plastic at and/or near the collapse, which requires a sufficiently ductile slab response either attained by using the conventional reinforcing bars, properly anchored and uniformly distributed, on its tensile face; or through the use of the steel fibers in the concrete section. In addition to this major requirement, following assumptions are taken in the analysis.

1. The slab and the supporting beams have been Beams cast monolithic and in case of a composite construction, the slab and the beam sections have been properly anchored together to prevent the separation of two sections at the ultimate load.
2. The slab-system is subjected to an out-of-plane uniform area load applied over its entire top face.
3. The slab-system has been divided into a number of panels of equal length using a set of internal beams provided parallel to its short span (see, Fig. 5.3).
4. Orthotropic reinforcement is provided in the Reinforcementtensile face of the slab with reinforcing steel bars placed parallel to the edges of the slab. In case of the steel fiber reinforced concrete, the steel fibers are assumed to be present

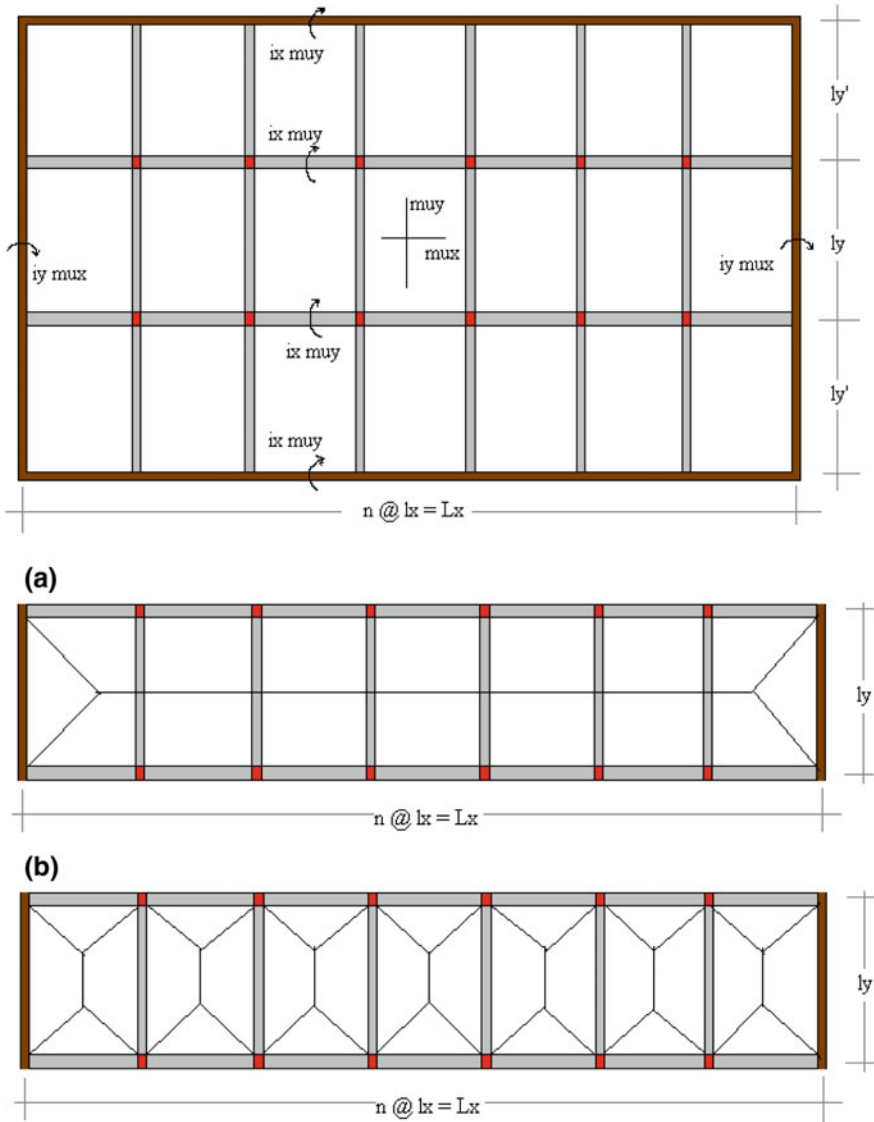


**Fig. 5.3** Schematic Diagram of the model of the slab-system, **a** *Global Failure of a typical Middle Panel of the Slab*—The yield line in the slab develops along the line of maximum curvature and it cross through the internal beams at the point of their plastic hinge to form the collapse mechanism in the slab-system. **b** *Local Failure* *Local Failure of a typical Middle Panel of the Slab*—SlabThe yield line pattern develops locally and simultaneously in all panels of the slab-system; the stiff and/or strong internal beams do not allow the yield lines to cross into the adjacent panels

everywhere in the section; thereby giving an identical moment of resistance throughout the slab-system.

5. Membrane forces in the slab section are ignored.
6. There is a no opening in the slab. The slab section has been assumed to possess an adequate punching and the shear strength to prevent its premature failure.
7. The effect of kinking of the reinforcing bars across the crack/yield line and the biaxial stress conditions in the concrete compression zone of the slab section has been ignored.

## 5.6 Development of the Model

Consider a rectangular slab of length,  $L_x$  and width,  $l_y$  divided into  $n$ -number of panels with length,  $l_x$  each. It is assumed that the rectangular slab is resting over the non-yielding supports at its outer boundary. Orthotropic reinforcement has been provided in the slab-system with the ultimate resisting moment,  $m_{ux}$  along the long span ( $L_x$ ) and  $m_{uy}$  along the short span ( $l_y$ ) of the slab, with an orthotropy ( $\mu$ ). The orthotropy is defined as the ratio of the ultimate resisting moment-capacity of the slab along the width,  $l_y$  to that along its length,  $L_x$  ( $=m_{uy}/m_{ux}$ ). The schematic diagram of the proposed model of the slab-system has been shown in Fig. 5.3, along with a set of the possible mode of failures in Fig. 5.3a, b.

The slab-system consists of a number of equally spaced panels along the long span ( $L_x$ ). It has been cast monolithic along with  $(n - 1)$  number of equally spaced internal shallow beams having moment-capacity,  $m_b$  ( $=\alpha_b m_{ux} l_x$ ) each. These beams are provided along the short span ( $l_y$ ) of the slab. The shallow beam is a flexural member that deflects along with the supported-slab and thus, is incapable of providing a non-yielding edge to the supported slab when subjected to some external load. The depth of the beam must be kept less than  $span/10$ ; otherwise, it would act as a non-shallow beam and starts producing negative yield line along its axis at the top face of the slab [Singh et al. (2010)]. The span ( $l_y$ ) of the beams should be considered in the calculation. Nevertheless, the beam maintains compatibility conditions with respect to the displacement-field along its interface with the monolithically cast slab. At collapse, the beam allows the yield line developed in the slab to pass through it at the point of the plastic hinge.

The supporting beams along the long span ( $L_x$ ) of the slab-system are assumed to be adequately stiff to provide a non-yielding edge to the slab. These supporting beams are necessary to provide an adequate strength against the possible punching shear failure of the slab near the column face. The slab would behave as a single panel slab of size ( $L_x \times l_y$ ) if the strength of the beams provided along the short span ( $l_y$ ) of the slab were taken as zero and/or is not adequate to initiate the composite action between the slab and the supporting beams as shown in Fig. 5.3a. In case of the adequately stiff and/or strong internal beams (provided along the span  $l_y$ ), the slab system would be transformed into a slab-system consisting of a number



of smaller rectangular slabs of size ( $l_y \times l_x$ ) resting over the internal beams as shown in Fig. 5.3b.

In the model shown in Fig. 5.3, the ultimate negative resisting moments per unit length of the slab are defined in terms of the ultimate positive resisting moments per unit length in those directions of the slab. The ultimate negative resisting moments in the slab-system at its edges along the long length ( $L_x$ ) are taken as  $i_x m_{uy}$ ; whereas these moments along the width ( $l_y$ ) are taken as  $i_y m_{ux}$ . The case of simple supports can be obtained by putting these  $i$ -values in the expression as zero.

### 5.6.1 Collapse Mechanism

A reinforced concrete slab develops a unique pattern of yield lines at the collapse load. The shape of the yield line pattern of a reinforced concrete slab depends upon the loading, its boundary conditions and the slab-constants. The development of a complete yield line pattern at ultimate state leads to the formation of a collapse mechanism and afterwards, the slab fails to support any further increase in the loading. The load applied to the slab-system at this stage represents its collapse load.

Any rectangular slab supported over the non-yielding edges on its outer boundary, and cast monolithic with the equally spaced internal shallow beams has equal probability to fail either with the formation of the plastic hinge in the supporting beams, simultaneously, along with the development of a yield line pattern in the slab. In this failure mode, all the supporting beams will allow the yield line in the slab to pass through it as shown in Fig. 5.4a, or alternatively, the internal supporting beams will not allow the yield line in the slab-system to pass through it; the yield line pattern in this case develops, locally and simultaneously, in all panels of the slab-system as shown in Fig. 5.4b. This will happen only if the supporting beams are strong or stiff enough that does not allow the yield lines in the slab to cross through into the adjacent panels of the slab-system, thus leading to the formation of a yield line pattern locally in all panels of the slab-system. This type of failure mechanism is called as local-collapse mechanism (see, Fig. 5.4a). Otherwise, it is called as global-collapse mechanism (see, Fig. 5.4b).

The shape of the collapse mechanism in the present analytical modeling was selected following the contours of the maximum slab deflection under the uniform load. Alternatively, the shape of the yield line pattern in a rectangular slab-system failing either in the global-collapse mechanism or in the local-collapse mechanism can be derived by considering the laws of mechanics of rigid bodies. The theorems postulated by Johansen (1967), Jennings (1996), Quintas (2003) also help in assuming a suitable valid collapse mechanism.

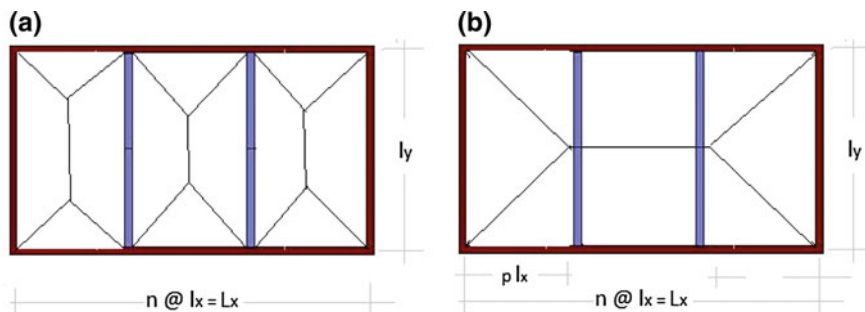


**Fig. 5.4** Schematic representation of a typical Collapse Mechanism in the RC slabs: **a** Local mechanism, **b** Global mechanism

### 5.6.2 Equilibrium and Yield Criterion

After the formation of a complete yield line pattern, the slab-system starts behaving as a rigid-perfectly plastic material that absorbs no energy during the deformations caused by the external load; the work done by these forces is completely dissipated in the plastic deformations occurring along the yield lines. At the collapse, therefore, the total work done by the external load and the internal forces, acting over the rigid bodies in equilibrium with the external load, must disappear for an arbitrarily selected value of the kinematically admissible virtual displacement field. This condition ensures equilibrium of the assumed collapse mechanism at the ultimate state. The collapse load predicted by using this condition will come out either on the higher side or at the most equal to its true value. The true value of the collapse load of the slab-system can, however, be achieved either by satisfying the yield criterion at all points in the slab or by selecting a yield line pattern that corresponds to the lines of the maximum curvature under applied loading. But it is always simpler and mathematically easier to examine all possible collapse mechanisms rather than to check the yield criterion at all the points in the slab, and the collapse mechanism giving the lowest value of the load will postulate a true value of the collapse load.

### 5.6.3 Solution

The slab-system has been assumed to fail in the global-collapse mechanism at the ultimate state. Figure 5.5 depicts the corresponding yield line pattern of the slab subjected to uniform area load ( $w$ ) over its entire top face. This figure also shows the numbering scheme used to identify different segments of the collapse mechanism. This numbering scheme is used for computing the external work done by various segments of the slab-system as they move in the direction of the load.

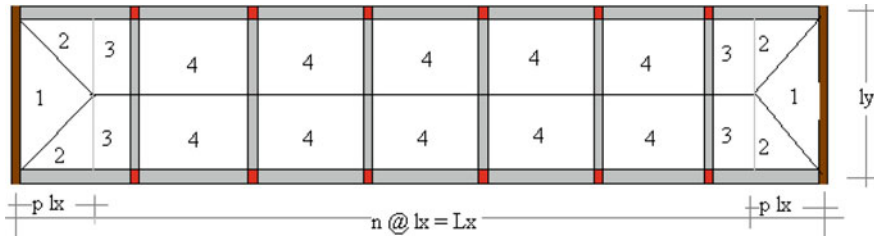


**Fig. 5.5** Yield line pattern of the slab-system failing in the Global-Collapse Mechanism. It also depicts the numbering scheme used to identify the different segments of the slab

The work done by the external uniform area load of intensity ( $w$ ) can be determined by multiplying the total load acting at the centre of gravity of each segmental area of the collapse mechanism by a distance moved in the direction of the load due to a kinematically admissible arbitrary displacement ( $\delta$ ) given to the yield line pattern.

The work done by the different segments of the collapse mechanism as they move through a kinematically admissible displacement ( $\delta$ ) under the influence of the external load ( $w$ ) is given below:

$$\text{Slab segment-1} = \frac{\delta w p r_p l_x^2}{6}$$

$$\text{Slab segment-2} = \frac{\delta w p r_p l_x^2}{12}$$

$$\text{Slab segment-3} = \frac{\delta w(1-p) r_p l_x^2}{4}$$

$$\text{Slab segment-4} = \frac{\delta w r_p l_x^2}{4}$$

The sum total of the work contributed by different segments of the collapsing slab gives the total work by the external load (EWD). It is given in Eq. 5.14.

$$\text{EWD} = 2 \left[ \frac{\delta w p r_p l_x^2}{6} \right] + 4 \left[ \frac{\delta w p r_p l_x^2}{12} \right] + 4 \left[ \frac{\delta w(1-p) r_p l_x^2}{4} \right] + 2(n-2) \left[ \frac{\delta w r_p l_x^2}{4} \right]$$

$$\text{or EWD} = \frac{\delta w r_p l_x^2}{6} (3n - 2p) \tag{5.14}$$

The work by the internal forces in the slab-system can be computed using Eq. 5.12. The moments ( $m_{ux}$  and  $m_{uy}$ ) acting along the different edges of the segments in the collapse mechanism dissipates the energy as they rotate about their



respective axis. The segment wise contribution of the work in the slab-system is given below:

$$\text{At edge of the segment-1} = m_{ux} \theta_x l_y = m_{ux} l_y \frac{\delta}{p l_x} = \frac{m_{ux} \delta r_p}{p}$$

$$\begin{aligned} \text{At edge of the segment-2} &= m_{uy} \theta_y p l_x = \mu m_{ux} p l_x \frac{\delta}{l_y/2} \\ &= \frac{2\mu p \delta m_{ux}}{r_p} \end{aligned}$$

$$\begin{aligned} \text{At edge of the segment-3} &= m_{uy} \theta_y (1-p) l_x \\ &= \mu m_{ux} (1-p) l_x \frac{\delta}{l_y/2} = \frac{2\mu (1-p) \delta m_{ux}}{r_p} \end{aligned}$$

$$\text{At edge of the segment-4} = m_{uy} \theta_y l_x = \mu m_{ux} l_x \frac{\delta}{l_y/2} = \frac{2\mu \delta m_{ux}}{r_p}$$

$$\text{At the plastic hinge of the beam} = m_b \theta_y = m_b \frac{\delta}{l_y/2} = \frac{2 m_b \delta}{l_y} = \frac{2 m_b \delta}{r_p l_x}$$

Equation 5.15 gives the work by the positive moments ( $m_{ux}$  and  $m_{uy}$ ) in the slab-system and that contributed by the beams at the point of the plastic hinge in them. It has been obtained by totally the individual contributions of different segments and the internal beams of the slab-system; Eq. 5.15 gives the final expression of the internal work done (IWD).

$$\begin{aligned} \text{IWD} &= 2 \left[ \frac{m_{ux} \delta r}{r_p} \right] + 4 \left[ \frac{2\mu p m_{ux} \delta}{r_p} \right] + 4 \left[ \frac{2\mu m_{ux} (1-p) \delta}{r_p} \right] \\ &\quad + 2(n-2) \left[ \frac{2\mu m_{ux} \delta}{r_p} \right] + 2(n-2) \left[ \frac{2m_b \delta}{r_p l_x} \right] \\ \text{or IWD} &= 2 m_{ux} \delta r \left[ \frac{1}{p} + \frac{2\mu n}{r_p^2} + \frac{2(n-1) \alpha_b}{r_p^2} \right] \end{aligned} \quad (5.15)$$

In Eq. 5.15,  $\alpha_b \left( = \frac{m_b}{m_{ux} l_x} \right)$  is the beam-strength parameter of the slab-system and  $r_p \left( = l_y/l_x \right)$  denotes its panel aspect ratio.

Similarly, the contribution from the negative moments acting along the different rigid edges of the slab-system can be evaluated, as given below:

Along x-axis of the slab =  $(2 i_x m_{ux}) n l_x \theta_y$

Along y-axis of the slab =  $(2 i_y m_{ux}) l_y \theta_x$

and at negative plastic hinge of the beam =  $2(n-1)k m_b \theta_y$   
 $= 2(n-1)k \alpha_b m_{ux} l_x \theta_y$

The total internal work by the negative moments acting at the outer rigid edges of the slab-system can be determined by summing up their individual contribution; it is given in Eq. 5.16.

$$\begin{aligned}
 &= (2 i_x \mu m_{ux}) n l_x \frac{\delta}{l_y/2} + (2 i_y m_{ux}) l_y \frac{\delta}{p l_x} + 2(n-1)k \alpha_b m_{ux} l_x \frac{\delta}{l_y/2} \\
 &= \left[ \mu m_{ux} (2 i_x) \frac{2\delta n}{r_p} \right] + \left[ m_{ux} (2 i_y) \frac{\delta r_p}{p} \right] + \left[ 2(n-1)k \alpha_b m_{ux} \frac{2\delta}{r_p} \right] \\
 &= 2m_{ux} \delta r_p \left[ (2 i_x) \frac{\mu n}{r_p^2} + (2 i_y) \frac{1}{2p} + 2(n-1) \frac{k \alpha_b}{r_p^2} \right] \quad (5.16)
 \end{aligned}$$

Finally, the total work done by the internal forces (IWD), such as the ultimate resisting moments in the slab and that contributed by the supporting beams at the position of the plastic hinge can be obtained by adding Eqs. 5.15 and 5.16. It is given in Eq. 5.17.

$$\begin{aligned}
 &= 2m_{ux} \delta r_p \left[ \frac{1}{p} + \frac{2\mu n}{r_p^2} + (2 i_x) \frac{\mu n}{r_p^2} + \frac{2(n-1)\alpha_b}{r_p^2} \right. \\
 &\quad \left. + \frac{2(n-1)k\alpha_b}{r_p^2} + (2 i_y) \frac{1}{2p} \right] \\
 &= 2m_{ux} \delta r_p \left[ (2+2 i_x) \frac{1}{2p} + (2+2 i_y) \frac{\mu n}{r_p^2} + 2(n-1)(k+1)\alpha_b \frac{1}{r_p^2} \right] \\
 &\text{or IWD} = 2m_{ux} \delta r_p \left[ \frac{d}{2p} + \frac{\mu n e}{r_p^2} + \frac{2f}{r_p^2} \right] \quad (5.17)
 \end{aligned}$$

In Eq. 5.17, the parameters (d, e, f) represents the continuity-constants of the slab-system. The continuity conditions at the outer boundaries and the beam-strength parameter ( $\alpha_b$ ) of the slab-system defines the values of these constants. These can be evaluated using the expressions given below:

$$d = 2(1 + i_x); \quad e = 2(1 + i_y); \quad \text{And, } f = \alpha_b(n - 1)(k + 1)$$

The equilibrium of the slab-system can be ensured by equating the work done by the external load ( $w$ ) with that produced by a set of the internal forces, such as  $m_{ux}$  and  $m_{uy}$  and  $m_b$  in the slab-system when it moves by a small virtual kinematically admissible displacement field ( $\delta$ ). The final expression of the slab moment ( $m_{ux}$ ) is given in Eq. 5.18. It has been obtained by equating the Eq. 5.14 with Eq. 5.17.

$$\Rightarrow \frac{\delta w r_p l_x^2}{6} (3n - 2p) = 2m_{ux} \delta r_p \left[ \frac{d}{2p} + \frac{\mu n e}{r_p^2} + \frac{2f}{r_p^2} \right]$$

$$\text{or } m_{ux} = \frac{(3n - 2p)}{\left( \frac{d}{2p} + \frac{\mu n e}{r_p^2} + \frac{2f}{r_p^2} \right)} \frac{w l_x^2}{12} \quad (5.18)$$

Equation 5.18 can be simplified to a readily usable form, given in Eq. 5.19.

$$m_{ux} = \frac{(3n - 2p)}{\left[ \frac{1}{2p} + \left( \frac{\mu n e + 2f}{d r_p^2} \right) \right]} \frac{w l_x^2}{12 d}$$

$$\text{or } m_{ux} = \frac{(3n - 2p)}{\left( \frac{1}{p} + 2\beta \right)} \frac{w l_x^2}{6d} \quad (5.19)$$

In Eq. 5.19,  $\beta \left( = \frac{\mu n e + 2f}{d r_p^2} \right)$  is a *slab-constant* that depends upon the aspect ratio ( $r_p$ ) of the slab-panel, the orthotropy ( $\mu$ ) and the number of panels ( $n$ ) into which the slab has been divided. The Eq. 5.19 gives the maximum value of the positive resisting moment ( $m_{ux}$ ) in the slab only, if  $\frac{\partial m_{ux}}{\partial p} = 0$  along with a negative value of the second derivative of the moment field ( $m_{ux}$ ). This condition can be used to find the value of the parameter ( $p$ ) that if substituted back into Eq. 5.19 gives the value of the maximum moment ( $m_{ux}$ ) in the slab; the value of parameter ( $p$ ) is given in Eq. 5.21.

$$\frac{\frac{\partial}{\partial p} (3n - 2p)}{\frac{\partial}{\partial p} \left( \frac{d}{2p} + \frac{\mu n e}{r_p^2} + \frac{2f}{r_p^2} \right)} = \frac{(3n - 2p)}{\left( \frac{d}{2p} + \frac{\mu n e}{r_p^2} + \frac{2f}{r_p^2} \right)}$$

$$\text{or } 3n - 2p = \frac{4p^2}{d} \left( \frac{d}{2p} + \frac{\mu n e}{r_p^2} + \frac{2f}{r_p^2} \right)$$

$$\text{or } \left( \frac{4\mu n e}{d r_p^2} + \frac{8 f}{d r_p^2} \right) p^2 + 4p - 3n = 0$$

$$\text{or } 4\beta p^2 + 4p - 3n = 0 \quad (5.20)$$

The p-value defining the position of the branching point of the yield line pattern formed in the slab-system [see, Fig. 5.5] at collapse can be calculated by solving the quadratic equation, given in the Eq. 5.20. The solution of this quadratic equation is given below:

$$\Rightarrow p = \frac{-4 \pm \sqrt{4^2 + 4 \times 4\beta \times 3n}}{2 \times 4\beta}$$

$$\text{or } p = \frac{\sqrt{1 + 3n\beta} - 1}{2\beta}$$

The above equation can be expressed in terms of a single parameter known as slab-parameter,  $A = (\sqrt{1 + 3n\beta})$  by combining the slab-constant ( $\beta$ ) and the number of panels ( $n$ ) in the slab-system; it is given in Eq. 5.21.

$$p = \frac{3n}{2} \left( \frac{A - 1}{A^2 - 1} \right) = \frac{3n}{2(A + 1)} \quad (5.21)$$

The Eq. 5.21 defines the exact shape of the yield line pattern for a reinforced concrete slab failing in the global-collapse mechanism. In this failure mode, the supporting beams allow the yield line in the slab to pass through it at the point of the plastic hinge, developing at the point of the maximum moment in the beams, simultaneously along with the formation of the yield line pattern in the slab. However, it must be ensured that the p-value must be kept less than unity for the slab to fail in the global-collapse mechanism; otherwise, it may violate the yield criterion. This can be controlled by selecting the value of the slab-parameter ( $A$ ) from Eq. 5.22. This equation has been obtained by modifying the Eq. 5.21 to a more workable form given in Eq. 5.22.

$$A \geq \frac{3n - 2}{2} \quad (5.22)$$

The maximum value of the positive ultimate slab moment ( $m_{ux}$ ) for the slab-system can be obtained by substituting the p-value from Eqs. 5.21 into 5.19. The final expression for the maximum value of the slab moment ( $m_{ux}$ ) is given in Eq. 5.23.

$$m_{ux} = \left( \frac{3}{A+1} \right)^2 \frac{w L_x^2}{12d} \quad (5.23)$$

The value of the slab parameter ( $A$ ) for a single panel slab having an aspect ratio of unity becomes two, thereby giving the slab moment ( $m_{ux}$ ) that compare favourably well with the results available in the literature (Hillerborg 1975; Johansen 1967; Sukla 1973; Park and Gable 2000).

The Eq. 5.23 can be used for the analysis of a slab-system that is continuous over the non-yielding edges over its boundary, and is cast monolithic with the internal equally spaced shallow beams. The slab and the internal beams of the slab-system [having a number ( $n$ ) of internal panels] can be designed for any value of beam-strength parameter ( $\alpha_b$ ) and orthotropy ( $\mu$ ), subjected to a uniform load ( $w$ ) over its entire top face. The value of the beam-strength parameter ( $\alpha_b$ ) of the slab-system should be selected in a manner that the slab-beam system must operate in the global-collapse mechanism at collapse. This mode is more desirable than the local-collapse mode as it did not require any negative steel, especially over the internal beams, because of a negligibly small magnitude of the negative moment field that would induce there due to the shallow beam depth of the internal beams in the slab-system. This helps to simplify the reinforcement detailing and save a considerable construction time that would otherwise go into the cutting and fixation of the negative steel and supporting chairs, etc.

This condition can be checked by calculating the ultimate resisting moment of the slab-system failing in the local-collapse mechanism. In the local-collapse mechanism, the slab fails with a formation of the yield line pattern, locally and simultaneously, in all panels of the slab-system [see, Fig. 5.4(a)] and then, comparing this value of the moment with that obtained from the Eq. 5.23. The slab-system would fail in the global-collapse mechanism only if the value of the slab moment ( $m_{ux}$ ) in this failure mode is more than that obtained from the failure of the slab-system in the local-collapse mechanism.

The slab-system will be converted into a number of smaller slabs, separated by the internal shallow-beams after the formation of the local-collapse mechanism. Thus, the slab-beam system will consist of a number ( $n$ ) of smaller isolated rectangular slabs with an aspect ratio ( $R$ ) at the collapse. The ultimate moment ( $m_{ux}$ ) of these smaller rectangular slabs can be obtained by modifying the Eq. 5.23. For a single panel discontinuous rectangular slab:

$$\begin{aligned} n &= 1 \\ e &= d = 2; \end{aligned}$$

And  $f = 0$  for a single panel ( $n = 1$ ) rectangular slab.

$$\Rightarrow \beta = \frac{2\mu(1) + 0}{2R^2} = \frac{\mu}{R^2} \quad (5.24)$$



The slab-parameter for the single panel slab,

$$A_1 = \sqrt{1 + 3\beta} \quad (5.25)$$

Equation 5.24 can be modified to gives

$$m_{ux} = \left( \frac{3}{A_1 + 1} \right)^2 \frac{w l_x^2}{24} \quad (5.26)$$

In Eq. 5.26, the long span ( $l_x^1$ ) and the short span ( $l_y^1$ ) of the smaller rectangular slabs formed in the slab-system at ultimate load should be replaced by its short span ( $l_y$ ) and the panel length ( $l_x$ ), respectively, while calculating its aspect ratio. In other words, the aspect ratio ( $R$ ) of the smaller rectangular slabs formed in different panels of the slab-system can be expressed in the term of its aspect ratio,  $r (=l_y/L_x)$ . This is given in Eq. 5.27.

$$R = \frac{l_y^1}{l_x^1} = \frac{l_x}{l_y} = \frac{l_x}{r L_x} = \frac{1}{n r} \quad (5.27)$$

By combining Eqs. 5.24 and 5.27, the value of the slab-constant ( $\beta$ ) for the single-panel rectangular slab having an aspect ratio ( $R$ ) that forms in the slab-system can be further simplified. This is given in Eq. 5.28.

$$\beta = \frac{\mu}{R^2} = \mu n^2 r^2 \quad (5.28)$$

Equation 5.26 can be made more users friendly by replacing the long span ( $l_x^1$ ) of the smaller rectangular slabs with the  $l_y (=r L_x)$  of the slab-system. Therefore, the moment capacity ( $m_{ux}$ ) for the single panel rectangular slab can be determined from Eq. 5.29; the value of the slab-parameter ( $A$ ) for this slab can be taken from Eqs. 5.24 and 5.25.

$$m_{ux^1} = \left( \frac{3 r}{A_1 + 1} \right)^2 \frac{w L_x^2}{24} \quad (5.29)$$

The relative magnitude of the moment field given by Eqs. 5.23 and 5.29 determines the failure mode of the slab-system. The slab would fail in the global-collapse mechanism only if the moment capacity of the slab given by Eq. 5.23 is more than that predicted by Eq. 5.29. Otherwise, the same slab would fail following the local-collapse mechanism.

Figure 5.6 depicts the variation of the slab moment-coefficient ( $m_{ux}/wL_x^2$ ) with the slab-parameter ( $A$ ) adopted in the design. It indicates that the moment-demand for the slab drops rapidly with increasing value of the slab-parameter ( $A$ ) and it changes the failure mode of the slab-system, from the global collapse mechanism to the local collapse mechanism, depending upon the relative magnitude of the slab moment ( $m_{ux}$ ) in comparison to the moment determined using Eq. 5.29.

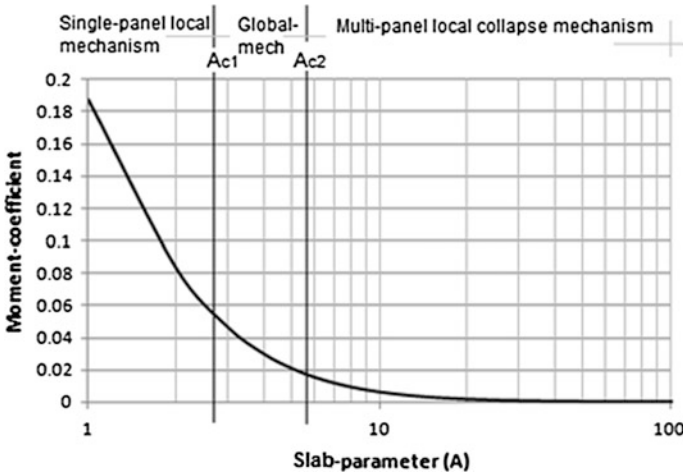


**Fig. 5.6** Design chart for a slab moment ( $m_{ux}$ ): The slab moments ( $m_{ux}$  and  $m_{uy}$ ) reduces with an increase of the slab-parameter ( $A$ ). Nevertheless, it results in the corresponding increase in the beam moment. In such cases, the slab-system requires stronger beam section to support the imposed load. This process results in the transformation of the collapse mechanism from the global to local one in the slab-system.

## 5.7 Strength Requirement of the Supporting-Beams

The strength requirement of the internal beams provided along the length ( $l_y$ ) of the slab-system depends upon the beam-strength parameter,  $\alpha_b$  ( $=m_b/m_{ux} l_x$ ) for any given value of the slab moment capacity ( $m_{ux}$ ) and the panel length ( $l_x$ ). Therefore, the strength requirement of these beams can be calculated by substituting the expression of the slab moment ( $m_{ux}$ ) from the Eq. 5.23. This has been worked out below and the final expression of the beam moment ( $m_b$ ) is given in Eq. 5.30.

$$m_b = \alpha_b m_{ux} l_x$$

$$m_b = \left\{ \left( \frac{n}{n-1} \right) \left[ \frac{(A^2 - 1)r^2}{3} - \mu \right] \right\} \times \left[ \left( \frac{3}{A+1} \right)^2 \frac{w L_x^2}{12d} \right] \frac{L_x}{n}$$

$$m_b = \left[ \left( \frac{A-1}{A+1} \right) r^2 - \frac{3\mu}{(A+1)^2} \right] \frac{w L_x^3}{4(n-1)d} \quad (5.30)$$

Therefore, the design moment field ( $m_{ux}$ ,  $m_{uy} = \mu m_{ux}$ , and  $m_b$ ) in the laterally loaded slab-system can be obtained from Eqs. 5.23 and 5.30 for any valid value of the slab-parameter ( $A$ ). The minimum value of the slab-parameter ( $A$ ) can be calculated from the Eq. 5.31 so that the slab-system must have a positive-non-zero beam moment capacity ( $m_b > 0$ ). Otherwise, the slab-system would start behaving

as an ordinary single panel rectangular slab. It is important to note that the moment field for this type of the slab-system (with  $m_b = 0$ ) compares favourably well with the results obtained from the well-established formulae of the slab analysis. The value of the slab-parameter ( $A$ ) required for this condition can be obtained by equating expression in the Eq. 5.30 to zero. The final expression for the minimum value of the slab-parameter ( $A$ ) is given in Eq. 5.31, which depends only upon the aspect ratio ( $r$ ) of the slab-system and its orthotropy ( $\mu$ ).

$$A_{\min} = \sqrt{\frac{3\mu}{r^2} + 1} \quad (5.31)$$

Therefore, the lower limit of the slab-parameter,  $A_{c1}$  of the slab-system can be determined by adopting the higher value of the slab-parameter ( $A$ ) from Eqs. 5.22 and 5.31. The value of the slab-parameter ( $A$ ) taken at its lower limit ensures that the slab-system possesses supporting-beams of adequate strength that does not allow the branching point of the yield line pattern in the slab to cross through their axis at the collapse. The final expression of the lower limit of the slab-parameter ( $A_{c1}$ ) is given in Eq. 5.32.

$$A_{c1} = \left\{ \begin{array}{l} \frac{3n-2}{2} \\ \sqrt{\frac{3\mu}{r^2} + 1} \end{array} \right\}_{\text{higher}} \quad (5.32)$$

The expression for the capacity of the beams given in the Eq. 5.30 can be further simplified to a more workable form by combining Eqs. 5.32 and 5.30. This is given in Eq. 5.33.

$$m_b = \left\{ \frac{r^2(A^2 - A_{c1}^2)}{(A+1)^2(n-1)} \right\} \frac{wL_x^3}{4d} \quad (5.33)$$

Equation 5.33 can be used to plot the variation of beam moment ( $m_b$ ) with the slab parameter ( $A$ ). It is given in Fig. 5.7 that indicates that the strength requirement for the internal beams of the slab-system increases proportional to the slab-parameter  $A$ . Higher the value of the slab-parameter ( $A$ ), stronger the beam section must be to support the load. When the strength of the beams approaches its upper limit  $A_{c2}$  (see, Sect. 5.8), it will repel the branching point of the yield line pattern to an extent that it leads to the failure of the slab-system in the local-collapse mechanism irrespective of the beam stiffness, expressed in terms of the depth of the beams. At this value of the slab-parameter, the beam section would require a large depth or a larger rebar area to provide a requisite flexural capacity. Consequently, the stiffness of the internal beams becomes large enough to cause a change in the curvature of the slab across its member-axis; thereby leading to the formation of the negative yield lines in the slab. Nevertheless, the slab designed for this value of the slab-parameter requires special

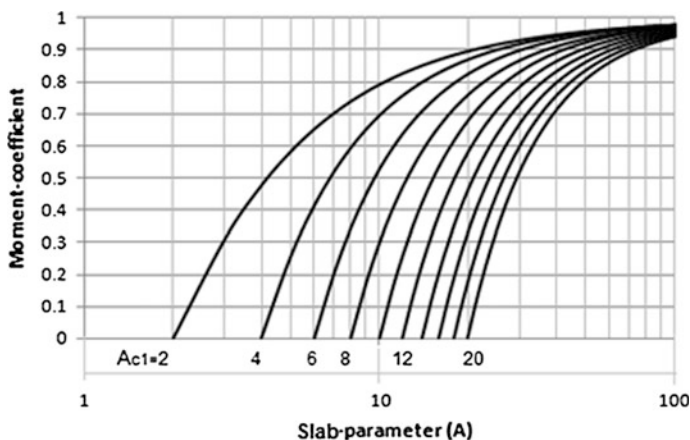


Fig. 5.7 Design chart for a beam-moment ( $m_b$ )

attention while detailing to provide enough steel at the tensile face of the slab for the negative moments being inducted into the slab-system.

The very purpose of using the internal beams in the slab-system, therefore, remains only to stiffen the laterally loaded slab to enable it to satisfy the serviceability requirement of applicable design codes; the strength requirement for these internal beams can be worked out from the valid values of the slab-parameter ( $A$ ).

This would enable the designer to use reinforced concrete slab, more judiciously with a minimum possible thickness, stiffened by a set of equally spaced internal beams having an adequate matching flexural strength required for supporting the load in the global-collapse mechanism mode, and vice versa. The depth of these internal beams should be selected in a manner that it must satisfy the serviceability conditions of the applicable design code and the depth criterion required for the initiation of a global collapse mechanism in the slab-system. The charts shown in Figs. 5.6 and 5.7 supplements the available design guidelines, such as IS 456 (2000), Shukla (1973), Park and Gamble (2000), etc. by providing a generalized approach that could be used both for a single-panel as well as a multi-panel rectangular slab-system.

## 5.8 Critical Beam-Strength Parameter

The moment field ( $m_{ux}$ ,  $m_{uy}$  and  $m_b$ ) induced in a rectangular slab-system under the external load depends only on the slab-constant ( $\beta$ ) irrespective of the failure mode (see, Eqs. 5.23 and 5.29). The value of the slab-constant in turn depends mainly upon the beam-strength parameter ( $\alpha_b$ ) for a given set of the slab geometrical parameters, viz. aspect ratio, and number of panels and orthotropy of the slab-system. Therefore, the beam-strength parameter ( $\alpha_b$ ) is the only parameter that dictates the failure mode of the slab-system at collapse. The value of the Beam

strength parameter ( $\alpha_b$ ) at which the failure mode of the slab-system changes from the global-collapse mechanism to the local-collapse mechanism is called as critical beam-strength parameter ( $\alpha_{bc}$ ). This parameter defines the minimum strength of the supporting beams that leads to the formation of the global and the local-collapse mechanism, simultaneously, in a laterally loaded slab-system at collapse. The slab-system would fail in the local-collapse mechanism if it has been designed with the value of beam-strength parameter ( $\alpha_b$ ) more than the critical value of the beam-strength parameter ( $\alpha_{bc}$ ).

It is convenient to express the beam strength parameter ( $\alpha_b$ ) in the form of a slab parameter (A). The value of the slab-parameter (A) which leads to the formation of a local collapse mechanism from the global collapse mechanism in the slab-system can be determined following a procedure similar to that used for the critical beam-strength parameter ( $\alpha_{bc}$ ); it can be done by equating the Eqs. 5.23 and 5.29. It will define the upper limit of the slab-parameter ( $A_{c2}$ ). The expression for this limiting value of the parameter is given in Eq. 5.34.

$$\left(\frac{3}{A_{c2} + 1}\right)^2 \frac{w L_x^2}{12d} = \left(\frac{3r}{A_1 + 1}\right)^2 \frac{w L_x^2}{24}$$

$$\text{or } A_{c2} = \sqrt{\frac{2}{d}} \left(\frac{A_1 + 1}{r}\right) - 1 \quad (5.34)$$

The final expression of the upper limit of the slab-parameter ( $A_{c2}$ ) at which the supporting-beams allow the slab to fail by the formation of the global-collapse and the local-collapse mechanism simultaneously in the slab-system can be obtained by substituting the value of the slab-parameter ( $A_1$ ) in Eq. 5.34; it is given in Eq. 5.35. The upper limit of the slab-parameter ( $A_{c2}$ ) ensures that the slab-beam system would sustain the lateral load (w) in the global-collapse mechanism mode if it has been designed with the slab-parameter,  $A < A_{c2}$ ; otherwise, it leads to the collapse in a local-collapse mechanism.

$$A_{c2} = \sqrt{\frac{2}{d}} \left[ \frac{1 + \sqrt{1 + 3\mu(nr)^2}}{r} \right] - 1 \quad (5.35)$$

The corresponding value of the critical beam-strength parameter ( $\alpha_{bc}$ ) can be determined by solving Eq. 5.35, when the value of the slab-parameter (A) in the equation,  $A = \sqrt{1 + 3n\beta}$  approaches its upper limit ( $A_{c2}$ ). At this stage, the value of the slab-constant ( $\beta$ ) would approach its limiting value ( $\beta_c$ ); the final expression of  $\alpha_{bc}$  is given in Eq. 5.36.

$$A_{c2} = \sqrt{1 + 3n\beta_c}$$

$$\text{or } \beta_c = \frac{A_{c2}^2 - 1}{3n} = \frac{\mu n + (n-1)\alpha_{bc}}{n^2 r^2}$$

$$\text{or } \alpha_{bc} = \left(\frac{n}{n-1}\right) \left\{ \frac{(A_{c2}^2 - 1)r^2}{3} - \mu \right\} \quad (5.36)$$

Equation 5.36 can be further simplified to a more workable form by combining it with Eq. 5.32; it is given in Eq. 5.37.

$$\alpha_{bc} = \frac{r^2}{3} \left(\frac{n}{n-1}\right) [A_{c2}^2 - A_{c1}^2] \quad (5.37)$$

Nevertheless, Eq. 5.37 can also be used to calculate the value of the beam-strength parameter ( $\alpha_b$ ) of a slab-system by substituting a suitable value of the slab-parameter (A) in place of  $A_{c2}$  from its valid range; it is given in Eq. 5.38.

$$\alpha_b = \frac{r^2}{3} \left(\frac{n}{n-1}\right) [A^2 - A_{c1}^2] \quad (5.38)$$

Equation 5.35 is simplified for different boundary conditions of the slab-system. Table 5.1 gives the value of  $A_{c2}$  for some of commonly used boundary conditions in practice.

It is worth mentioning that the lower and the upper limit of the slab-parameter (A) is a fundamental property of any slab-system. These two limits depend upon the aspect ratio (r), number of panels (n), orthotropy ( $\mu$ ) and the continuity conditions at boundary of the slab-system. The first two parameters viz: aspect ratio (r) and number of panels (n) of the slab-system are independent variables and are, normally, fixed by the architectural constrains in the routine design practice; whereas, the third parameter namely the orthotropy ( $\mu$ ) of a slab-system is a dependent variable. Its value is influenced by the aspect ratio and the number of panels of the slab-system in addition to the stiffness of the internal beam(s). It should therefore be very carefully chosen for the design purpose. A large deviation of value of the orthotropy from that required for an elastic distribution of the moment field causes a significant cracking at the service load on tensile face of the in the slab.

Figures 5.8 and 5.9 depict the effect of the beam-stiffness, expresses in terms of the beam *span/depth ratio* (L/d), the aspect ratio (r) of the slab-system and the number of panels (n) on the value of the orthotropy required to ensure a moment distribution in the slab-system similar to that would cause an elastic distribution of moments. These charts have been developed from a parametric study conducted using a finite element based software on a large number of slab-system by taking aspect ratio, number of panels, and depth of the beam as variables [Singh (2011a, b), Singh (2014)]. The value of the orthotropy ( $\mu$ ) can be taken from the chart shown in Fig. 5.8 for a slab-system with  $nr < 2$  and for a slab-system with  $nr \geq 2$ , it can be taken from Fig. 5.9.

**Table 5.1** Slab-parameter ( $A_{c2}$ ) for various boundary conditions

S. No	Boundary condition at edges of a panel
1	Discontinuous edges at outer boundary of the slab-system and without any negative reinforcement over the internal beams. $i_1 = i_2 = i_3 = i_4 = 0$ $A_{c2} = n\sqrt{3\mu\left(\frac{A_1+1}{A_1-1}\right)} - 1$ $\beta_1 = \frac{(nr)^2}{\mu}$ for calculating $A_1$ parameter
2	The slab-system with no negative reinforcement over the internal beams and the outer boundaries along its short span ( $l_y$ ). $i_2 = 0; i_4 = i_y$ and $i_1 = i_3 = i_x$ $A_{c2} = n\sqrt{\frac{6\mu}{d}\left(\frac{A_1+1}{A_1-1}\right)} - 1$ $\beta_1 = \frac{2(nr)^2}{\mu d}$ for calculating $A_1$ parameter.
3	The slab-system with no negative reinforcement over the internal beams and some negative reinforcement over the outer boundaries, defined by $i_x$ and $i_y$ . $i_2 = i_4 = i_y$ and $i_1 = i_3 = i_x$ $A_{c2} = n\sqrt{\frac{3\mu}{4}\left(\frac{e}{d}\right)\left(\frac{A_1+1}{A_1-1}\right)} - 1$ $\beta_1 = \frac{(nr)^2}{4\mu}\left(\frac{e}{d}\right)$ for calculating $A_1$ parameter

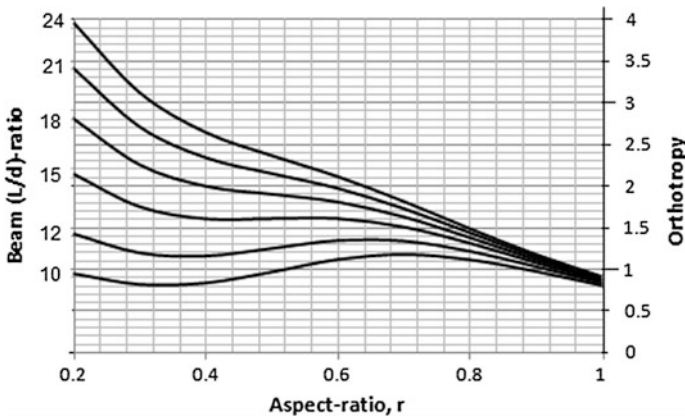


**Fig. 5.8** Orthotropy for a slab-system with  $nr < 2$



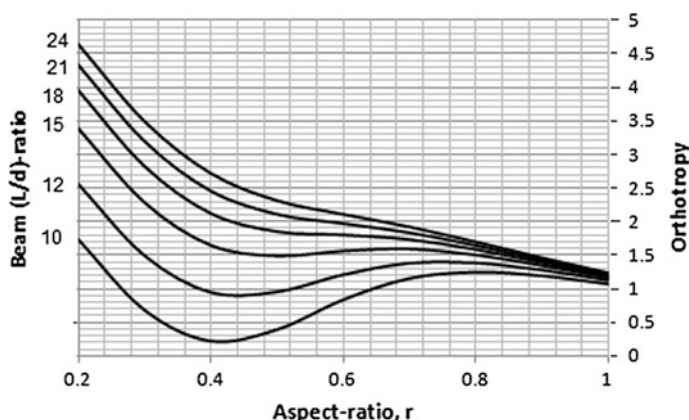


Fig. 5.9 Orthotropy for a slab-system with  $nr \geq 2$

## 5.9 Some Important Observations

A slab-system designed with  $A < A_{c1}$  leads to the formation of a single-panel local collapse mechanism forming in the panel area of size  $L_x \times l_y$ ; the beams did not have any relevance in this particular case. On the other hand, if the slab-system has been designed with a very large value of the slab-parameter ( $A > A_{c2}$ ), it will lead to the formation of a number of smaller rectangular slab of size  $l_x \times l_y$  resting over the internal beams of the slab-system at collapse. This is called as a multi-panel local collapse mechanism (see, Fig. 5.3b). In this case, the behavior of the internal beams of the slab-system would be quite analogous to the behavior of the internal panels for any two-way slab-beam system having non-yielding edges at the outer boundary of the slab panels. The strength requirement of the beams, at this value of the slab-parameter ( $A = A_{c2}$ ), matches favorably well with the values obtained from the design procedure recommended by the design code IS 456 (2000). This fact has been shown in Fig. 5.7, which indicates that the beam-moment ( $m_b$ ) approaches, asymptotically, its maximum value at a very large value of the slab-parameter ( $A$ ). At this value of the slab-parameter ( $A > A_{c2}$ ), the slab must be designed as a continuous slab resting over the internal beam(s) of the slab-system. Therefore, the internal beams of the slab-system can be made to behave similar to a non-yielding supporting beams and/or walls by the suitable selection of the slab-parameter ( $A \geq A_{c2}$ ). However, detailing of the rebars in a reinforced concrete rectangular slab-system should be done to take care of both the positive as well as the negative moment field that would induce in the slab-system when designed for a slab-parameter ( $A > A_{c2}$ ).

This unique characteristics of the slab-system helps to utilize the strength of the slab materials (the reinforcement and the concrete) to its full allowable capacity by selecting an appropriate value of the slab-parameter ( $A$ ). Because all design codes restricts the maximum and the minimum spacing of the reinforcing bars in the slab



section; thereby, providing some inherent minimum slab flexural-capacity, corresponding to the maximum allowable bar spacing. The designer can choose an appropriate value of the slab-parameter ( $A$ ) from the valid range of the slab-parameter  $A_{c1} < A < A_{c2}$  for the design purpose, corresponding to the minimum available flexural capacity of the slab-system; thereby, utilizing the strength of all reinforcement bars to its full allowable capacity, and simultaneously satisfying the detailing-clauses of the design codes.

## 5.10 Slab-System with Discontinuous Edges at Outer Boundary

The ultimate positive resisting moment of a reinforced concrete rectangular slab resting over the simple and the non-yielding edges at its outer boundaries and cast monolithic along with the equally spaced ( $n - 1$ ) number of the supporting beams (see, Fig. 5.3) can be derived by slight modification of Eq. 5.23. The value of the parameter ( $i$ ) in the expression will be zero for the simple edge conditions. If the internal supporting in the slab-system provided along its short span ( $l_y$ ) are also discontinuous at edges, the parameter ( $k$ ) will also be zero.

$$\Rightarrow e = d = 2;$$

$$\text{And } f = (n - 1)\alpha_b$$

The value of the slab-constant,  $\beta$  for this case simplifies to Eq. 5.39.

$$\beta = \frac{\mu n + (n - 1)\alpha_b}{r_p^2} \quad (5.39)$$

The slab moment ( $m_{ux}$ ) can be determined from Eq. 5.23 by substituting the value of the slab-parameter ( $A$ ) computed for the slab-constant given in Eq. 5.39. The final expression for the slab moment ( $m_{ux}$ ) is given in Eq. 5.40.

$$m_{ux} = \left( \frac{3}{A + 1} \right)^2 \frac{w L_x^2}{24} \quad (5.40)$$

The moment capacity required for the supporting beams of the slab-system can be obtained by modifying Eq. 5.23; it is given in Eq. 5.41.

$$m_b = \left\{ \frac{r^2 (A^2 - A_{c1}^2)}{(A + 1)^2 (n - 1)} \right\} \frac{w L_x^3}{8} \quad (5.41)$$

Equations 5.40 and 5.41 completely define the moment field for a slab-system having discontinuous edges on its outer boundary. The moment field can be

determined for any arbitrarily chosen valid value of the slab-parameter (A) from its range:  $A_{c1} < A < A_{c2}$ .

### Example 5.1

A typical rectangular slab consists of three panels in the two orthogonal directions. The spacing of beams along these two directions is 6 m and 7.5 m c/c each. Based upon the preliminary estimates, the columns are of size 400 mm × 400 mm and the beams are of size 400 mm × 550 mm. The floor to floor height is 3.5 m. assume a live load of 5 kN/m<sup>2</sup> and a finish load of 1 kN/m<sup>2</sup>. Determine the design moments for the interior panel of the slab-system.

### Solution

Number of panels in each direction of the slab-system = 3.

Assuming the slab thickness as 180 mm. This satisfies the deflection criterion of the design code. Therefore, total factored design load =  $1.5(5 + 1 + 0.18 \times 25) = 15.75$  kN/m<sup>2</sup>.

- Long span of the slab,  $L_x = 18$  m and its short span,  $l_y = 7.5$  m.
- Therefore, aspect ratio of the slab-system,  $r = 7.5/18.0 = 0.4167$ .
- The value of the continuity constants viz:  $i_b$ ,  $i_x$  and  $i_y$  are taken as 1.25, 1.333 and 0.0 respectively.
- Orthotropy,  $\mu = 1.40$ .
- The lower limit of the slab-parameter,  $A_{c1} = 5.022$
- The upper limit of the slab-parameter,  $A_{c2} = 6.915$

The moment field induced in the slab can be calculated at different values of slab-parameter (A). A comparison of the moment field is given in Table 5.2 against the results obtained from the Direct Design Method and the output of a finite element based software.

It is indicated in Table 5.2 that the average value of the moment field in the slab-system compare favourably well with the results obtained from the finite element analysis and the direct design method prescribed by the design code. The

**Table 5.2** Comparison of the moment-field at different slab-parameters (A)

S. No.	Slab-parameter (A)	Moment field (kN m/m and kNm)				
		$m_{ux}$	$m_{uy}$	$-m_{ux}$	$-m_{uy}$	$m_b$
1	$A_{c1} = 5.022$	22.60	31.67	–	42.12	0.0
2	5.453	19.68	27.58	24.59	36.68	46.28
3	5.893	17.69	24.45	21.81	32.59	106.37
4	6.227	15.69	21.99	19.61	29.24	110.78
5	6.580	14.26	19.90	17.83	26.58	134.28
6	$A_{c2} = 6.915$	13.08	18.33	16.35	24.44	153.99
Average moment field		17.15	23.98	21.44	31.94	110.34
Moment field (FEM)		16.47	19.46	24.83	26.57	111.44
Moment field (Direct design method)		16.13	19.18	22.02	25.57	128.00

magnitude of the slab moments reduces with an increase of the slab-parameter ( $A$ ) and the slab-system needs, simultaneously, stronger beams to carry the design load. Unlike the finite element or design code based solutions, this design procedure gives more flexibility to the designer in choosing the moment field for the design by selecting an appropriate value of the slab-parameter ( $A$ ) that fulfils the serviceability as well as the strength criterion. This enables the designer to use the slab, more judiciously with a minimum possible thickness, stiffened by a set of equally spaced internal beams with a matching strength required for supporting the load in the global-collapse mechanism mode, and vice versa. Nevertheless, the depth of these internal beams should be selected in a manner that it must satisfy the serviceability conditions of the applicable design code and the depth criterion required for the initiation of a global collapse mechanism in the slab-system. It is important to note that the moment field induced in the slab-system at the lower limit ( $A_{c1}$ ), and at the upper limit ( $A_{c2}$ ) matches exactly with the values recommended by design code for a rectangular slab with discontinuous edges at the outer boundary.

## 5.11 Design of SFRC Slabs

It is experimentally verified fact that the load carrying capacity of the SFRC slabs is more alike to that of an equivalently designed slab-system using the conventional reinforcing rebars on its tensile face [Michels et al. (2012), Singh (2015), Singh (2016)]. This mainly happens because of the smaller slab thickness (in comparison to the beams, etc.) that acquires a preferential fiber orientation along its length and breadth and consequentially leads to a favorable alignment of the fibers along the principle directions of the moment trajectories. Importantly, the flexural resistance of the SFRC slab-system did not change even if the conventional reinforcement in the slab section was totally dispensed with and it was replaced with a suitably designed dose of the steel fibers in the concrete mix. The SFRC section can be proportioned using the procedure described in Chap. 3. However, it is important to note that in case of SFRC slab-system, the expressions derived in the previous section for the analysis of a conventional reinforced concrete slab-system need slight modification as the characteristics of an SFRC slab are entirely different from a conventionally reinforced concrete slab; although both the slab-systems, whether constructed using the steel fibers (e.g. SFRC) or using conventional reinforcing bars in the concrete section always fail following an identical failure mechanism at the collapse load. This permits the extension of the expressions derived in the previous section to use for the analysis of SFRC slab sections; albeit with a slight modification.

The RC slabs are usually designed as an isotropically reinforced or orthotropically reinforced member, depending upon its aspect ratio, etc.; whereas, the slabs constructed using SFRC behave more as an isotropically reinforced member ( $\mu = 1$ ) than the conventionally reinforced slabs owing to the random distribution and the uniform presence of the steel fibers in the concrete mass. This allows the simplification of Eqs. 5.40 and 5.41 along with the value of  $A_{c2}$  (given in

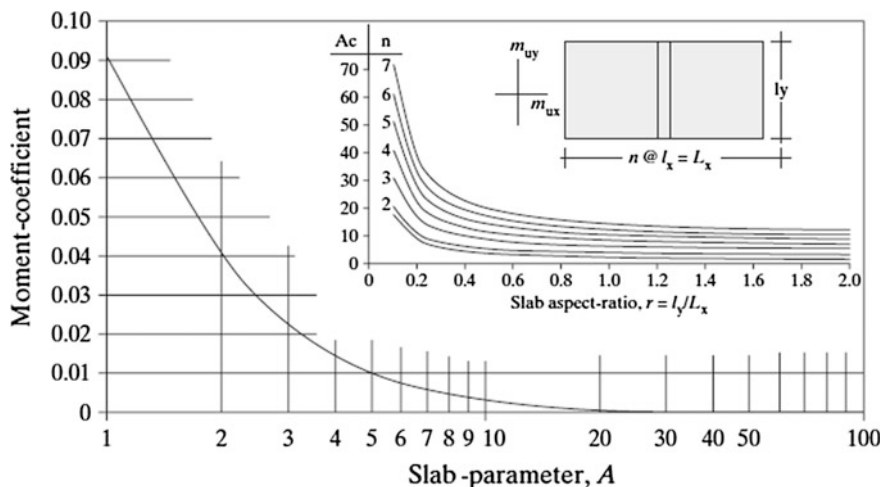


Fig. 5.10 Design chart for an SFRC slab-system [Singh 2016]

Table 5.1) for the SFRC-slabs. The modified expression has been used to plot the design charts that could be of help in deciding the lower and the upper limits of the slab-parameters ( $A_{c1}$  and  $A_{c2}$ ) for the slab-system. The sub-chart in the Fig. 5.10 defines the range of applicable values of the critical value of the parameter  $A_c$  for an SFRC-slab depending upon its aspect ratio ( $r$ ) and the number of internal panels ( $n$ ). The value of slab-parameter ( $A$ ) less than the upper limit  $A_c$  ensures that the slab-system behaves in the global collapse mode at the service load—a desirable feature of the slab-system that did not cause negative moments along the beam-axis in the slab. The chart shown in the Fig. 5.10 also gives the value of the design moment,  $m_{ux}$  (=coefficient  $w L_x^2$ ) for a rectangular SFRC slab-system subjected to a uniform load ( $w$ ) over its entire top surface. The moment field in the slab ( $m_{ux} = m_{uy}$ ) can be determined for any arbitrarily selected value of the slab-parameter ( $A$ ), albeit having value less than the  $A_c$ .

It is worth to note that the magnitude of the slab moment ( $m_{ux}$ ) changes with the variation of the slab-parameter ( $A$ ). Thus, it can be used as a control-switch to decide the fiber parameters (the fiber volume fraction, the aspect ratio and the concrete compressive strength) as per the moment-demand raised by the slab-system for an arbitrary value of the slab parameter ( $A$ ) selected from the range given by its lower limit,  $A_{c1}$  and the upper limit,  $A_{c2}$ .

Nevertheless, it is really improbable that the yield criterion would be violated anywhere in the slab-system because of the uniform and the random presence of the steel fibers throughout the concrete mass and their horizontal alignment, especially parallel to the tensile face of the slab caused by the boundary effects. Therefore, it enables the analytical model developed in the previous sections to satisfy the basic requirements of the equilibrium, true mechanism and yield criterion. Various design code, such as ACI 318 (2008), IS 456 (2000) permits the exercise of any such method for the analysis of a structural system that meets these necessities.

**Example 5.2**

A rectangular slab of size  $3950 \text{ mm} \times 2280 \text{ mm}$  (c/c) is taken for the illustration purpose. One internal beam ( $350 \text{ mm} \times 150 \text{ mm}$ ) was provided in the middle of the  $75 \text{ mm}$  thick slab that divides the slab into two equal panels. This beam is primarily used to control the magnitude of the moment field in the slab system and set it to the limiting flexural capacity of the SFRC section. The slab-system is to be designed using the hooked-end steel fibers, randomly mixed, in M20 grade concrete to obtain the SFRC. The yield strength of the steel fibers is taken as  $1050 \text{ MPa}$  and the yield strength of rebars is  $500 \text{ MPa}$ . The 28 days cube compressive strength of the concrete obtained from the standard tests is  $26 \text{ MPa}$ .

**Solution**

- The slab is assumed discontinuous at its outer boundary.
- Number of panels in the slab-system,  $n = 2$
- Long span of the slab,  $L_x = 3.95 \text{ m}$  and its short span,  $l_y = 2.28 \text{ m}$ .
- Therefore, aspect ratio of the slab-system,  $r = 2.28/3.95 = 0.577$
- Taking the value of the orthotropy,  $\mu = 1$  for the SFRC slab due to the inherent uniform strength in each direction of the slab-system.
- The lower limit of the slab-parameter,  $A_{c1} = 3.164$
- The value of the constant,  $A_1 = 2.235$
- And, the upper limit of the slab-parameter,  $A_{c2} = 5.606$

The moment field induced in the slab-system is calculated using the chart given in Fig. 5.10, for a value of the slab parameter,  $A = 4.25$  (say). This selected value of the parameter ( $A$ ) must lie within the limit given by  $A_{c1}$  and  $A_{c2}$  to ensure the global collapse mechanism of the slab-system at a beam span-depth ratio of 15.2 ( $=2.28/0.15$ ) at the ultimate state. It should be kept more than 10, as the value of the span-depth ratio lesser than this value leads to the failure of the slab-system in the local collapse mode; the slab requires tensile steel on its top face to resist the tensile forces caused at the top face of the slab, normal to the axis of the internal beam.

Figure 5.10 gives the value of the moment coefficient for the slab-system (for  $A = 4.25$ ) as 0.0136. Alternatively, it can be obtained from Eq. 5.40.

An overall slab depth of  $75$  is adopted in the design to ensure that the alignment of the steel fibers remains parallel to the tensile face of the slab.

- Self weight of the slab  $= 0.075 \times 25 = 1.88 \text{ kN/m}^2$
- Assuming floor finish  $= 1.45 \text{ kN/m}^2$
- External load (say)  $= 10.00 \text{ kN/m}^2$

$\Rightarrow$  The factored load  $= 1.5 (1.88 + 1.45 + 10.00) = 20 \text{ kN/m}^2$

And, the factored slab bending moment,  $M_{ux} = 0.0136 \times 20 \times 3.95^2 = 6.375 \text{ kN m/m}$  and, the corresponding moment coefficient,  $M_u/(f_{ck} BD^2) = 0.0567$

The value of the fiber-index ( $\beta$ ) needed to provide the requisite flexural strength can be computed using the design chart given in Fig. 3.4; it is obtained as 0.1185, which is more than its critical value ( $\beta_c = 0.1123$ ). This mandatory requirement is to limit the tensile strain on the extreme face of the slab to a permitted value of 0.015.

The value of the fiber parameters ( $l/d$  and  $V_f$ ) required to attain the desired value of the fiber-index ( $\beta$ ) can be computed using Eq. 3.13; a fiber shape factor of 2 for the hooked-end fibers has been used in the calculation.

$$\begin{aligned}\beta &= (0.3V_f(l/d))/\sqrt{f_{ck}} \\ &= (0.3 \times 2 \times V_f(l/d))/(\sqrt{26}) = 0.1177 V_f(l/d)\end{aligned}$$

By equating the fiber-index adopted for the design ( $=0.1185$ ) with an expression simplified above, a suitable combination of the fiber volume fraction ( $V_f$ ) and the fiber aspect ratio ( $l/d$ ) can be obtained to meet the requisite flexural strength of the SFRC slab. The final design combination of the fiber parameters ( $V_f$  and  $l/d$ ) obtained for the present case is given below:

$$V_f(l/d) = 1.0$$

It is important to note that the longer fibers and/or high volume fraction of the steel fibers in the concrete generally leads to poor the concrete workability. Therefore, it is equally important in the design is to select a suitable fiber aspect-ratio for the SFRC mix that meets the workability requirements as well as the strength demand of the structural member. It should not exceed the critical fiber-aspect ratio to ensure a ductile response of the SFRC slab in the material post cracking range. The critical fiber-aspect ratio ( $l/d$ )<sub>c</sub> for the present example is found to be 60  $[=(0.58 \times 1050)/(2 \times \sqrt{26})]$ . The maximum fiber-aspect ratio should, therefore, be limited to less than 60 if it gives a workable concrete mix; otherwise the fiber aspect ratio for the mix should be reduced with a corresponding increase of the fiber volume fraction ( $V_f$ ) to ensure a ductile post-cracking and to avoid the brittle form of the section failure that would occur otherwise. A fiber shape factor of 2 for the hooked-end fibers has been used in the calculation. Therefore, using hooked-end steel fibers with an aspect ratio of 60 with a corresponding value of volume fraction of 1.67 % will achieve the desired moment requirement in the slab. The fiber aspect ratio of more than 100 requires special mixing equipments and operational procedure in the production of SFRC. It is therefore always desirable to keep the fiber aspect ratio in the mix less than 100, preferably in the range 50–80.

It is important to note that the SFRC in this example would exhibit a strain-softening response in its post-cracking range as the value of the fiber fraction ( $V_f$ ) is kept less than the value required to ensure the strain hardening response (see, Eq. 2.10), which is obtained as 1.94 % for the present case.

The values of the section neutral-axis coefficients corresponding to  $\beta = 0.1185$  can be calculated using Eq. 3.17. These values are given below:

$$h_1/D = 0.2197 \text{ and } h_2/D = 0.7803$$

The corresponding value of the ultimate moment capacity ( $M_u$ ) of the SFRC slab section can be determined from Eq. 3.16. It is given below:

$$M_u / (f_{ck} B D^2) = \left[ 0.24(0.2197)^2 + 0.5 \times 0.1183(0.7803)^2 \right] = 0.0475$$

$$\text{or } M_u = 0.0475 \times 26 \times 1000 \times 752 = 6,946,875 \text{ N m} (=6.94 \text{ kN m})$$

Therefore, the factored moment of resistance of the slab,  $m_u = 6.94 \text{ kN m} > 6.375 \text{ kN m}$  indicates that the selected dose ( $V_f = 1.67 \%$ ) of the steel fibers with an aspect ratio of 60 meets the strength requirements imposed by the slab-system.

The internal beam in the slab-system can be designed as per the procedure given in Chap. 3 (see, Figs. 3.4–3.6) for a moment ( $m_b$ ) of  $= 0.0121 \times 20 \times 3.95^3 = 15 \text{ kN m}$ ; the beam moment has been determined using Eq. 5.41 corresponding to the value of the slab-parameter ( $A$ ) = 4.25. Therefore, by providing 3 No.-10 mm diameter rebars at the bottom tensile face and 2 No.-8 mm diameter rebars at the compression face of the SFRC beam (350 mm wide and 150 mm deep) can achieve the moment demand of 15 kN m.

## References

- ACI: Standard 318 (2008) Building code requirements for reinforced concrete. American Concrete Institute (ACI), Farmington Hills
- Bureau of Indian Standards (BIS) (2000) Plain and reinforced concrete-code of practice. IS 456 (4th rev.), New Delhi, India
- Hillerborg A (1975) Strip method of design. Viewpoint, London
- Jain SC, Kennedy (1973) Yield criterion for reinforced concrete slabs. J Struct Div ASCE 100 (ST3):631–644
- Jenning A (1996) On the identification of yield-line collapse mechanism. Eng Struct 18(4):332–337
- Johansen KW (1967) Yield line theory. Cement and Concrete Association, London
- Michels J, Waldmann D, Maas S, Zürbes A (2012) Steel fibers as only reinforcement for flat slab construction—experimental investigation and design. Constr Build Mater 26:145–155
- Kemp KO (1965) The yield criterion for orthotropically reinforced concrete slabs. Int J Mech Sci 7 (11):737–746
- Moley CT (1965) On the yield criterion of an orthogonally reinforced concrete slab element. J. Mech Phys Solids 14:33–47
- Park R, Gamble WL (2000) Reinforced concrete slabs. Wiley, New York
- Lenschow R, Sozen MA (1967) A yield criterion for reinforced concrete slabs. Proc ACI 64:266–273
- Shukla SN (1973) Handbook for design of slabs by yield-line and strip methods. Structural Engineering Research Centre Roorkee, India
- Singh H (2011a) Laterally loaded reinforced concrete stiffened plates: analytical investigations. Pract Periodical Struct Des Constr 17(1):21–29
- Singh H (2011b) Prediction of collapse load of three-side supported reinforced concrete rectangular slabs: a simplified approach. Indian Concr J 85(7):21–28
- Singh H (2014) Analytical investigations and design charts for rectangular reinforced concrete stiffened-plates. Eng Mech 21(4):239–256
- Singh H (2015) Steel fibers as the only reinforcement in concrete slabs: flexural response and design chart. Struct Eng Int 25(4):432–441

- Singh H (2016) Strength and performance of steel fibre-reinforced concrete stiffened plates. *Mag Concr Res* 68(5):250–259
- Singh H, Kumar M, Kwatra N (2010) Behavior of shallow beam supported reinforced concrete rectangular slabs: analytical and experimental investigations. *Adv Struct Eng* 13(6):1183–1198
- Quintas V (2003) Two main methods for yield line analysis of slabs. *J Eng Mech* 129(2):223–231



# Chapter 6

## Construction Practice

### 6.1 Introduction

Fibers are added to the concrete to modify its structural properties and/or to achieve some other design objectives—for instance, to reduce the risk of plastic shrinkage, or to improve the behavior of concrete in fire, etc. When fibers are designed to contribute to the load-bearing capacity of a concrete element, these are classified as structural fibers. In such cases, the residual-tensile strength of SFRC is an accepted key performance parameter and it is generally expressed by means of fiber index ( $\beta$ ) [see Chaps. 2 and 3 for details]. Its value depends largely on the amount and type of steel fibers added to the concrete, as well as the properties of the concrete matrix itself. Now-a-days, numerous types of fibers are available in the market to achieve the desired design objectives, e.g. residual-tensile strength, toughness, etc. in the strength limit state and the crack-width, effective moment of inertia of the section at the service load during the serviceability limit state checks.

The steel fibers are generally available in bundles consisting of a number of fibers glued together using a water soluble glue, or wrapped as “pucks” or supplied in a belt to facilitate easy dosing and mixing. This processing of the steel fibers also helps to achieve consistency during the mixing operations. The anchorage of the steel fibers into the adjoining concrete mass in a structural member is a sole source of the improved mechanical properties exhibited by the SFRC, therefore, it is always better to try different values of the fiber parameters (e.g. fiber aspect ratio and its volume fraction), fiber shape/profiles while designing a SFRC structural member to get the desired post-cracking performance of the SFRC structural members. Nevertheless, the mixing of the steel fibers in the concrete and the concrete placement operations at site greatly influence the strength properties exhibited by the SFRC [Al-Mattarneh (2014)]. Every attempt, therefore, should be made to ensure consistency in the mixing and during the concrete placement operations. This chapter describes the effects of the steel fiber addition to be expected on the fresh and the hardened concrete properties and various ins-and-outs

to ensure a design value of the key strength parameters of SFRC during and after the construction.

## 6.2 Effect of the Fiber Addition on Concrete Properties

Addition of the fibers into the concrete affects its fresh properties. Consistency, air content, bleeding and pumpability, for example, could be affected as a result of the fiber addition in the concrete. In this respect, it is important to understand the likely effects of the fiber addition on the concrete properties and measures to ensure an adequately workable concrete mix in its fresh state along with the attainment of desired design strength in the hardened state.

### 6.2.1 Consistency

The consistency describes the ease of flow with which the concrete moves without losing its stability. It is used as a simple index to indicate the flowability of a fresh concrete. The efforts required to compact a concrete are governed by its flow characteristics. Generally a standard slump cone or Vebe apparatus is used to indicate the consistency of the concrete. The addition of the fibers to the concrete increases its cohesiveness thereby leading to the reduction in the slump value and consequentially, its workability and placability. Like a normal concrete, the addition of water alone to the concrete mix will not serve any purpose in this regards as it generally leads to a poor quality concrete. This should therefore be compensated for by either using plasticisers or by adjusting the concrete mix proportions. Laboratory study/trials could help to arrive at an appropriate dosage of the plasticisers, cement-content and/or relative content of the coarse and the fine aggregates in the concrete mix. Use of additional supplementary cementitious materials, such as natural pozzolana, fly ash, silicafume, etc. can also be tried because their use as additives helps to increase the concrete viscosity and workability [Sahmaran and Yaman (2007)]. The smaller size of these particles provides ball bearing effects and it reduces internal friction in the fresh concrete; thereby leading to increase in the flowability. This has an add-on advantage of evenly dispersion of the fibers during the mixing operations. The smaller sizes also help to fill the voids in the matrix gaps, resulting in an increased fiber–matrix adhesion. The smaller specific gravity of the fly ash is also reported to be one of the reasons for an increase of the workability of the concrete. The weight to weight replacement of the fly ash with the cement in the concrete mix always results in an increase in the paste volume, which indirectly controls the concrete workability.

The slump flow is a common key parameter used to evaluate the deformability of a fresh concrete in the absence of obstructions. It is measured as an ability of the fresh concrete to flow freely on a horizontal plan surface. The test method is very

similar to the testing procedure employed for determining the slump of a concrete. The difference is that instead of measuring the loss in height of collapsing concrete under its own weight, the diameter of the concrete-spread is observed and measured in the two perpendicular directions. The average value is recorded as a slump-flow. This parameter is a measure of the viscosity of the concrete and indicates its stability. A high value of the slump flow indicates concrete's ability to fill the formworks/moulds on its own. During the slump-flow test, the time required for the concrete to reach a diameter of 500 mm is also measured and it is recorded as  $t_{500}$ . A lower value of the time  $t_{500}$  points to a greater fluidity or smaller workability loss, and vice versa.

A J-ring test is used to determine the passing ability of the concrete through obstructions, unlike the slump-flow test which is a measure of the deformability of the fresh concrete in absence of obstructions. It is just an extension of the slump-flow test, in which a ring is used to create obstructions to the flowing concrete. The retention of the concrete inside the ring ( $h_1$ ) and the height of the concrete after passing through the J-ring on its outer side ( $h_2$ ) is measured. The difference of the height ( $h_2$ ) and the height ( $h_1$ ) gives an indication of the passing ability and restricted deformability of the concrete.

The V-funnel test is used to determine the fluidity or viscosity of concrete. It evaluates the ability of the concrete to achieve smooth flow through restricted spacing without blockage. The V-funnel is filled with concrete and the time it takes for the concrete to flow through the apparatus is measured in seconds. Good flowable and stable concrete would take a short time to flow out from the apparatus. The addition of the steel fiber reduces the concrete fluidity that is a measure of the ability of fresh concrete to flow and fill the mould. Laboratory trials should be conducted in order to determine the amount of the paste in the mix to ensure a uniform and easy dispersion of the fibers. Increasing the cement content, reduction in the ratio of the fine aggregate content to coarse aggregates content and/or using pozzolanic and chemical admixtures are other options to achieve a desired level of the concrete fluidity. An attempt should be made to satisfy the bare minimum requirements established by the EFNARC (1996, 2002) and other applicable design guidelines, such as IS 10262 (2009), etc. in this regards.

### 6.2.2 Pumpability

The pumpability indicates effort needed to ensure an easy delivery of the concrete at the point of the pouring. It involves good lubrication of the pumping unit and selection of adequate pipe diameter, and controlling the pressure of the pump. However, as with the normal concrete, it is much more a matter of the concrete mix proportions than these factors, as a small change in the aggregates ratio, cement-content in the mix has a significant effect on the pumpability. Working experience of the plant operator plays a crucial role in delivering a consistent batch of concrete at the job site. In the case of long or complicated pump

lines, pumping difficulties may be experienced despite proper adjustments of the mix design. In such cases, concrete producers should conduct pumping trials before the work starts and must take contractual steps to clarify responsibility.

The cohesiveness describes the stability/lack of the bleeding and segregation characteristics of the concrete. The addition of the steel fibers makes concrete relatively more cohesive than the normal concrete; thereby leading to a reduced pumpability. Therefore, it needs relatively more pumping efforts to deliver the SFRC at the point of the pouring in comparison to the normal concrete. It is generally observed that the concrete containing shorter steel fibers do not cause many problems in this regards. However, a high fiber dosage (typically, more than  $25 \text{ kg/m}^3$ ) and longer steel fibers (with an aspect ratio of more than 100) may require special attention in the mix design as these two parameters greatly affect the fresh properties of the concrete. The shape and profile of steel fibers also affects the pumpability of concrete [Mehta (1986)]. It is recommended that the diameter of the pump pipeline should not be less than one and a half times the fiber length to ensure easy movement of SFRC through the pipe.

### 6.3 Mix Proportioning of SFRC

The right selection of the concrete ingredients and their optimized proportions is essential for obtaining a satisfactory SFRC, which can provide high flowability, pumpability, resistance to segregation and bleeding. Similar to the normal concrete, the particle packing concept can be used to get an optimized mix proportions that results in improved fresh and hardened properties. Packing density of aggregates can be arrived by using slump cone and the powder content needed for this purpose can be obtained by conducting Puntke test. A Marsh cone study gives an optimized dosage of plastisers to get desired flow characteristics of the concrete. Steel fibers were added to enhance the mechanical properties. The dosage and aspect ratio of the fibers can be obtained from the analytical model and the design procedures, given in the previous chapters for a given moment demand. However, it is highly desirable that before finalizing the fiber parameters for the design, the flow studies should be carried out to optimize their values regarding the flowability, etc.

### 6.4 Specifications

The term 'specification' indicates how the steel fibers are specified in the drawing and/or in a contract document. These are generally specified by means of either, (1) fiber type and content; expressed in terms of fiber-aspect ratio ( $l/d$ ) and volume fraction ( $V_f$ ); or (2) by performance of the SFRC, expressed either in terms of the residual-tensile strength/fiber-index ( $\beta$ ) or the permitted crack-width ( $w$ ).

### 6.4.1 *Specification by Type and Fiber Content*

The simplest and most common method for a designer is to define the fiber type and the fiber content per  $m^3$  (specified as a minimum quantity) that should be included in the concrete to attain requisite strength properties. In this case, the responsibility of a concrete producer is limited only to adding as per the mix proportions (see, Sect. 6.3) and mixing the right type and quantity of fibers in the concrete mix and ensuring that the fibers are homogeneously mixed and other specified requirements with regards to the consistency and the target compressive strength are achieved. The contractor/designer take responsibility for the desired concrete performance resulting from the addition of the steel fibers in a concrete mix, e.g. workability, pumpability, postcracking flexural tensile strength, etc.

### 6.4.2 *Specification by SFRC Performance*

In this type, SFRC is specified in the drawing/contract document by means of the performance expected from a SFRC member, such as characteristics concrete compressive strength, post-crack behaviour at the ultimate and the serviceability limit states, flexural-tensile strength, early-age shrinkage, and consistency, etc. The concrete producer is solely responsible for the design and performance of the concrete, including decisions on the fiber type and content as per the terms of agreement and the mix proportions required for a desirable level of the concrete mix consistency, pumpability, etc. Nevertheless, if SFRC is specified in this way, the test method and conformity procedures must be agreed with the concrete producer and it must be clearly mentioned in the contract documents to avoid problem at a later stage.

## 6.5 Storage of Fibers

After the procurement of the steel fibers a standard procedure should be adopted for their storage during the construction. The steel fibers are normally supplied by the manufacturer in the form of pre-packed bags of 25 kg. These bags should be stored in a manner that prevents their degradation over a storage period. Sometimes, steel fibers, especially having an aspect ratio greater than 50, are supplied in water-soluble storage bags. In such cases, the instructions given by the manufacturer regarding packaging should be followed. If these are supplied in double bags, wherein the outer bag protects an inner water-soluble bag, the outer protective cover should be removed before pouring the fibers on to the conveyor belt or into the concrete mixer. The storage place should be kept dry and an attempt should be made to keep the relative humidity in the storage area around 30–50 % to avoid the fiber rusting, etc.

## 6.6 Addition of Steel Fibers to Concrete

Adding and mixing steel fibers directly at the plant mixer is the best way to ensure an uniform and homogeneous mixing of fibers in the concrete as these are added in a controlled way under the regular and direct supervision of the plant operator. Fibers can also be added directly into the truck mixer and these go on mixing into the concrete during its transit to the job-site. Mixing fibers with water only leads to the balling. The fibers, therefore, should be added first to the mixer along with the aggregates or cement and the mixing should be continued for a minimum time of 5 min (or at a rate of 1 min per  $m^3$ ) at the maximum speed of the drum to ensure good fiber distribution in the dry mix. The fibers should be added slowly and uniformly into the mixer to reduce the chances of balling. Generally, the steel fibers with an aspect ratio of more than 50 require special procedures to ensure their uniform distribution in the concrete mix. In such cases, it is recommended to use either bundled fibers wherein these are glued together with a water soluble gum or should be packed in the water soluble bags. Device and other equipment, such as pneumatic blast machines, etc. can also be used to blow the fibers evenly into the truck mixer. However, it must be ensured while dosing that, (1) the correct type and quantity of fibers are added to the mix; (2) the fibers are evenly distributed throughout the concrete and there is no balling; and (3) the addition of fibers should not compromise other aspects of the concrete specifications, such as workability, pumpability, etc. After ensuring a uniform dispersion of the steel fibers in the dry mix, the water and other constituent materials of the concrete as per the mix proportions decided to achieve the desirable material performance in its fresh and hardened state should be added. The mix procedure to be adopted for ensuring the consistency of the mix is given in the next section.

## 6.7 Mixing and Placement Operations

An effective mixing procedure and sequence is a prerequisite to get a homogeneous concrete mix. The uniform mixing of the fibers in concrete must be ensured and every attempt should be made to avoid the ball formation. In case, it formed during the mixing operations, then the bundle of the fibers in the form of ball should be removed and equivalent weight of the steel fibers may be added manually to the concrete mix to make up the loss of the volume fraction caused by the ball formation. The procedures for mixing the SFRC generally involved the following. First, the coarse and fine aggregates are dry mixed for about 1 min in a concrete mixer. In case, two or more sizes of coarse aggregates are used in the mix, these should be mixed first for about 30–45 s to get a homogeneous mixture of the aggregates. Second, the cement and the steel fiber are spread into the mixer and dry mixed for about 1 min. The steel fibers should be introduced slowly and

continuously into the dry mix. Uniform distribution of the fibers must be ensured without balling. Third, the mixing water (about 80–90 %) is added and mixed for approximately 2 min. Fourth, the plasticizer and the remaining mixing water is added and mixed for about 3–5 min. Finally, the freshly mixed SFRC was cast into specimen moulds and vibrated simultaneously to remove any air remained entrapped in the concrete. Compaction shall be carried out only by means of external tapping and external vibrations. The use of an internal (needle/poker) vibrator should be avoided. Internal tamping is not recommended for the compaction purpose as it generally results in a non-uniform distribution of the steel fiber; thereby giving a high variability in the material behavior. The use of a high frequency vibrating table is advised for the compaction purpose. Care should be taken not to allow the steel fibers to segregate (by sinking and/or floating up to the surface) by too long duration of the vibration. Care shall also be taken to avoid realignment and/or preferential orientations of the fibers during the compactions. After casting, each of the specimens was allowed to stand for about 24 h in laboratory before their demolding. The demolded specimens then should be stored in water at a temperature of  $23 \pm 2$  °C until the date of the testing.

## References

- Al-Mattarneh H (2014) Electromagnetic quality control of steel fiber concrete. *Constr Build Mater* 73:350–356
- Bureau of Indian Standards (BIS) (2009) Recommended guidelines for concrete mix design. IS 10262, New Delhi, India
- EFNARC (1996) European specification for sprayed concrete, European Federation of producers and contractors of special products for structures
- EFNARC (2002) Specification and guidelines for self-compacting concrete, English (ed). European Federation for Specialist Construction Chemicals and Concrete Systems, Norfolk, UK
- Mehta PK (1986) Concrete, structure, properties and materials. Prentice-Hall, Englewood Cliffs
- Sahmaran M, Yaman IO (2007) Hybrid fiber reinforced self-compacting concrete with a high volume coarse fly ash. *Constr Build Mater* 21:150–156

# Index

## A

ACI, 7, 8, 17, 19, 23, 29, 31, 60, 94, 154  
Aggregates, 4, 9, 10, 12, 13–15, 19, 21, 30, 33, 47, 114, 115, 161, 162, 164  
Allowable capacity, 150, 151  
Analysis, 7, 29, 30, 37, 38, 40, 42, 60, 64, 66, 67, 71, 72, 74, 102, 118, 123–125, 129, 132, 142, 145, 152–154  
Analytical model, 39, 46, 93, 97, 135, 154, 162  
Aqueduct, 2  
Arch action, 113, 115  
Aspdin, Joseph, 6  
Aspect ratio, 30, 31, 36, 38, 43, 49, 59, 66–68, 73, 78, 80–82, 84, 85, 87, 89–92, 96, 98, 119, 121, 140, 142, 143, 147, 148, 152–157, 159, 162–164  
Axial force, 117, 119

## B

Balanced-state, 26, 27, 69, 72, 75, 79, 80, 82, 88  
Balling, 164, 165  
Batches, 49  
Beam, 24–27, 30, 34, 35, 40, 46, 47, 49, 50, 54, 60, 62–80, 82–95, 98–104, 110–121, 124, 125, 132–135, 139, 141, 142, 144–149, 151–155, 157  
Beam-depth factor, 49, 96  
Beam moment, 144–146, 150, 157  
Beam strength, 138, 139, 142, 144, 146–148  
Bending test, 35, 46–48, 50, 51, 54, 95, 97, 98, 119–121  
Bilinear relationship, 38  
BIS, 17, 23, 60  
Bleeding, 11, 15, 160, 162  
Bond, 12, 22, 24, 26, 33, 36, 40, 42, 43, 63, 111  
Bond mechanisms, 25, 36, 63, 111

Bond strength, 42

Bond stress, 25, 42, 43  
Boundary conditions, 129, 132, 135, 148, 149  
Branching point, 141, 145  
Bridge, 14, 22, 30, 33, 35, 59, 63, 94, 111, 115  
Brittle, 16, 20, 26, 27, 29, 33, 70, 73, 87, 100, 109, 113, 156

## C

Calcium hydroxide, 11–13, 15  
Casting method, 35, 46  
Casting procedures, 34, 38  
Cement, 1, 4–14, 17, 30, 31, 33, 35, 64, 160, 161, 164  
Cementitious material, 1, 3, 4, 6, 34  
Centre of gravity, 5, 137  
Characteristics, 7, 8, 13, 20, 21, 23, 29, 31, 38, 39, 61, 67, 68, 81, 84, 87, 96, 98, 150, 153, 160, 162, 163  
Characteristics compressive strength, 19, 32  
Characteristics tensile strength, 24, 73, 96, 121  
Cistern, 2, 3  
Clay, 5, 6  
Clinker, 5, 6, 12, 13  
CNR-DT, 50, 52, 94, 118  
Coarse aggregates, 9, 10, 12–15, 19, 21, 22, 24, 30–33, 114, 115, 161, 164  
Collapse, 27, 42, 50, 60, 65, 109, 111, 123, 124, 128, 130–132, 134–137, 141–147, 150, 153–155  
Compaction, 34, 42, 47, 59, 81, 109, 165  
Compression, 7, 9, 12, 16, 17, 19, 21, 23, 24, 26, 27, 29–32, 60, 65, 67, 69, 73, 75, 77, 80, 92, 99, 100, 101–106, 110–117, 125, 157  
Compression face, 26, 27, 65, 73, 101, 104, 117  
Compression failure, 27, 112, 117



- Compressive strength, 8, 9, 15, 17, 19, 20, 22, 29, 31, 32, 49, 54, 63, 65, 70, 72, 85, 91, 93, 96, 100, 118, 119, 121, 154, 155, 163
- Compressive zone, 63, 75
- Concrete, 1–17, 19–27, 30–43, 46, 47, 50, 54, 59, 63–71, 73, 75–96, 98, 100–104, 107, 109–119, 121, 127, 131, 132, 135, 141, 146, 150, 151, 153–156, 159–161, 163–165
- Concrete compressive strength, 8, 16, 17, 19, 23, 29, 31, 32, 39, 49, 63, 92, 154, 163
- Concrete flowability, 160, 162
- Concrete grade, 16, 29, 79, 90, 91, 95, 113, 114
- Concrete grades, 85
- Concrete placement, 90, 159
- Concrete pumpability, 160–164
- Concrete tensile strength, 112
- Concrete workability, 156, 160
- Consistency, 159, 160, 163, 164
- Constituent materials, 9, 10, 164
- Constitutive law, 23, 61
- Constitutive model, 30, 40, 43, 52, 54, 67, 92, 93
- Constitutive relationship, 15, 35, 38, 46, 53, 61, 70, 91, 101, 102
- Control methods, 23
- Corrosion, 23, 59, 60
- Corrosion potential, 23
- Cost-benefit ratio, 87
- Cracked-transformation section, 64
- Cracking tensile strength, 33, 92, 98, 109, 110
- Crack-mouth-opening-displacement (CMOD), 35, 47–49, 51, 54, 66, 72, 96, 97, 119–122
- Crack propagation, 17, 111
- Crack-release energy, 17, 19, 25
- Crack-width, 25, 33, 35–38, 40, 43, 49–54, 59, 60, 63, 64, 66, 67, 71, 72, 75, 78, 79, 81, 82, 84, 88–90, 94, 96, 98, 111, 113–115, 117, 118, 122, 128, 159, 162
- Critical aspect ratio, 43
- Critical beam strength parameter, 146, 147
- Critical fiber index, 73, 80, 84
- Critical stress, 17
- Cross section, 42, 54, 67, 76, 82, 104, 113, 119
- Crushing, 17, 26, 27, 59, 65, 73, 75, 87, 88, 92, 113, 117
- Crushing strain, 19, 22, 26, 29, 70, 79, 92, 100, 101, 103
- Crystalline compounds, 11
- CTOD, 50, 51
- Curvature, 17, 27, 46, 63, 66, 68, 89, 91, 93, 94, 130–133, 136, 146
- D**
- Deep beam, 116
- Deeper cracks, 89
- Deflection, 27, 46–49, 52, 60, 62–67, 96, 98, 99, 119, 123, 135, 152
- Density, 15, 114, 162
- Depth-ratio, 72–75, 85
- Design chart, 73, 78, 82, 144, 146, 154, 155
- Design code, 23, 59, 60, 87, 109, 118, 123, 146, 150–154
- Design guidelines, 9, 23, 50, 61, 78, 94, 97, 113, 117–119, 146, 161
- Design Method, 20, 94, 152
- Design shear strength, 118
- Design value, 25, 32, 38, 95, 96, 160
- Diagonal-tension, 111, 113
- Dimensions, 4, 17, 42, 47, 60, 71, 76, 82, 103, 104
- Discontinuity, 10, 11, 19, 132
- Distress-signal, 27
- Domes, 4, 5, 7
- Doubly reinforced concrete, 99–101
- Dowel action, 114–117
- Drop, 32, 35, 37, 51, 64, 65, 143
- Drop-constant relationship, 37, 39
- Drop-down, 36
- Ductile, 24–26, 36, 38, 72, 74, 80, 85, 87–89, 111, 124, 156
- Durability, 59–61, 123
- E**
- Eddystone Lighthouse, 5, 6
- Effective span, 47, 49, 54, 96
- Elastic modulus, 13, 16, 22, 36
- Elongation, 43
- Energy, 12, 14, 17, 19, 25, 31, 52, 88, 91, 94, 124, 132, 136, 137
- Energy principle, 128
- Equilibrium, 25, 27, 40, 67, 101, 124–130, 132, 136, 140, 154
- Equilibrium conditions, 51, 67, 128, 131
- Ettringite, 11–13
- Experimental, 118
- Experimental investigations, 13, 23, 30, 84, 91, 93, 94
- Experimental test data, 95, 96
- F**
- Face, 59, 75
- Fatigue strength, 23

- Fiber, 19–24, 31–37, 40–43, 51, 54, 59, 63–65, 70, 73, 78–81, 84–92, 94–96, 98, 100, 132, 156, 159–164
- Fiber anchorage, 20–22, 33, 49, 51, 64, 78, 159
- Fiber aspect ratio, 22, 25, 31, 36, 39, 40, 43, 93
- Fiber content, 72, 85–87, 89–91, 93, 94, 163
- Fiber diameter, 42
- Fiber dosage, 74, 75, 91, 162
- Fiber elongation, 22, 33
- Fiber fracture, 36, 59, 73, 80, 87
- Fiber fracture strength, 43
- Fiber index, 65, 66, 70, 72–76, 78–82, 84–86, 88–91, 93, 96, 98, 102, 103, 155, 156, 159, 162
- Fiber length, 42, 84, 162
- Fiber mixing, 21, 29, 40, 59, 91, 124, 159, 160, 163, 164
- Fiber orientation, 33, 42, 43, 67, 94, 95, 153
- Fiber orientation factor, 53
- Fiber parameters, 25, 29–31, 33, 38, 49, 53, 65, 68, 79, 80, 81, 84, 85, 90–92, 95, 98, 154, 156, 159, 162
- Fiber pull-out behavior, 37, 41, 42, 80
- Fiber reinforcement, 54, 70, 76, 85–89, 94, 102, 103, 110, 124, 134, 142, 149–151, 153
- Fiber reinforcement concrete, 88, 125
- Fiber shape, 30, 33, 41, 119, 156, 159
- Fiber shape factor, 42, 80, 84
- Fiber slip, 22, 33
- Fiber specifications, 23
- Fiber storage, 163
- Fib model, 53, 55
- Fictitious crack approach, 33
- Fine aggregates, 8, 10, 161, 164
- First crack strength, 22
- Flexural capacity, 40, 55, 67, 71, 75, 76, 78, 82–86, 87, 89, 92–94, 99, 100, 102, 103, 105, 107, 118, 125, 145, 151
- Flexural model, 75, 78, 93
- Flexural strength, 8, 9, 22, 23, 59, 81, 96, 131, 146, 155, 156
- Force, 24, 25, 27, 33, 34, 37, 40–42, 52, 59, 65, 67, 71, 86, 95, 100, 129, 130
- Four-point testing, 46, 50, 51
- Free-body diagram, 126
- G**
- Global failure, 133
- Gravity loading, 24, 25, 110, 111
- H**
- Higgins, Bry, 5
- Hooked fiber, 42, 54, 80, 82, 84, 96, 98, 119, 121, 155, 156
- Hooks law, 36, 63
- Hydrated cement paste, 9, 10, 13, 14, 21, 29, 41, 114
- Hydraulic concrete, 2, 3
- Hydroxyl ions, 12
- I**
- Impact strength, 23
- Inelastic behavior, 14, 61
- Institution of Civil Engineers (ICE), 7
- Interfacial shear stress, 41
- Interfacial transition zone, 9–15, 17, 19–22, 27, 29–33
- Inverse analysis, 46, 95
- Isaac Johnson, 6
- Isotropically reinforced, 153
- J**
- Jordan, 2
- K**
- Key-parameters, 47, 48, 52, 79, 95, 99
- Kinematically admissible displacement field, 129, 137, 140
- L**
- Layer, 9, 19, 114
- Le Chatelier, Henri, 7, 13
- Lever arm, 27
- Lime, 1–7, 20
- Limestone, 1, 2, 5, 6
- Limit analysis, 123, 124
- Limiting strain, 27, 37, 64, 75, 77, 80
- Limiting tensile strength, 67, 69, 90, 113
- Limit of proportionality (LOP), 48, 63, 95, 96, 98
- Linear-elastic, 14, 16, 17, 19, 31, 36, 37, 44, 48, 50–53, 62–64
- Linear-elastic model, 50, 51, 53
- Load factor, 124
- Loading-setup, 46
- Local failure, 133
- Longitudinal axis, 47
- Longitudinal steel, 26, 67, 85, 117, 118, 121
- Long span, 134, 143, 152, 155
- Lower limit, 145, 152–155
- M**
- Material, 1–5, 7–10, 14–16, 19, 20, 22–24, 27, 29, 30, 34, 36, 38–40, 43, 46, 48, 50, 52, 53, 59–61, 63, 64, 66, 67, 70, 75, 79–81, 91, 96–98, 102, 103, 109, 110, 124, 132, 136, 150, 156, 164, 165
- Material model, 30, 50, 53, 97

- Mechanism, 20, 22, 24, 25, 33, 36, 63, 92, 111, 113, 114, 125, 128, 131–133, 135–137, 141–143, 145–147, 150, 153–155
- Membrane forces, 125
- Microcracking, 11, 15, 19–22, 27, 29–33
- Microstructure, 8, 9, 13, 15, 16, 29, 31
- Mid-span deflection, 47, 48
- Mix proportioning, 50, 160–164
- Model, 19, 23, 27, 29, 30, 37–40, 43
- Modelling, 9, 124
- Mode of failure, 26, 73, 134
- Modulus of rupture, 95
- Moment, 23, 24, 26, 40, 47, 61–63, 78, 80, 82, 87, 91, 92, 94, 111, 116, 117, 124–131, 134, 138–143, 148, 150–155, 157, 159, 162
- Moment capacity, 27, 52, 69, 71, 103, 134, 143, 144, 151, 156
- Moment coefficient, 74, 75, 79, 80, 82, 87, 143
- Moment-curvature responses, 91, 93
- Mortar mix, 21, 37
- Moxon, Joseph, 5
- Mould, 1, 33, 34, 47, 81, 161
- Multilinear relationship, 37
- N**
- Nabataea, 2
- Neutral-axis, 25, 53, 63
- Non-yielding edge, 134, 135, 142, 150, 151
- Notch, 47
- O**
- Oil shale, 1
- Orthotropic reinforcement, 132
- Orthotropy, 134, 140, 142, 145, 147–149, 152
- Over-reinforced, 26, 27, 76, 77, 87, 88, 100, 106, 114
- P**
- Panel aspect ratio, 138, 140, 142, 143, 147, 148, 154
- Parker, James, 5
- Partial safety factor, 32, 43, 60, 61, 118, 119
- Percentage steel area, 102, 111, 118
- Performance, 8, 9, 20, 23, 29, 40, 51, 60, 84, 90, 91, 123, 159, 162–164
- Performance level, 51
- pH, 12
- Physical properties, 10, 71
- Plain concrete, 32, 33, 46, 59, 63, 70, 75, 83, 94, 95, 103, 109–111, 114, 124
- Plain fiber, 45
- Plastic rigid model, 50, 53
- Portland cement, 6, 8, 12
- Post-cracking behavior, 22, 32, 48, 80
- Post-cracking strength, 46, 50, 52
- Pozzolanic, 4, 161
- Principal stress, 22, 59, 110, 113
- Pull-out tensile strength, 41
- Pure shear, 110
- Q**
- Quasi-brittle, 20, 21, 29
- Quicklime, 1, 2, 4
- R**
- Radius of curvature, 68
- Randomness, 21, 39, 60
- Random orientation, 20, 37, 115
- RC, 24, 26, 27, 54, 59, 61, 62, 75–77, 83, 85, 86, 88, 92, 94, 100–102, 111, 112, 114–117, 136, 153
- RC section, 26, 76, 83, 88, 92, 102
- RC slab, 126, 127, 130
- Rebar, 19, 24–27, 54, 59, 65, 67–77, 83–86, 88–92, 94, 100–102, 104, 106, 109–111, 114, 117, 118, 121, 124, 126, 145, 150, 153, 155, 157
- Rebar strain, 88, 89, 94
- Rebar stress, 77, 86, 104, 106
- Reinforcement, 19, 24, 26, 54, 72–76, 83, 85–89, 94, 100, 102–105, 109, 114–116, 118, 132, 142, 150, 151, 153
- Reinforcement index, 70, 72, 74, 76, 83, 85, 86, 88, 89, 94, 102–105
- Residual flexural strength, 96
- Residual tensile strength, 21, 23, 25, 29, 30, 33, 37–40, 42, 43, 48, 50, 51, 53, 64–66, 68, 70–73, 85, 90, 92, 94, 96, 98, 100, 102, 115, 118, 119, 159, 162
- RILEM, 30, 33, 35, 46, 47, 51, 52, 59
- Roman Empire, 4
- Roman Pantheon, 4, 5
- Rotation, 129–132
- S**
- Sample size, 54, 95
- Sand, 1, 8–10, 20
- Servicability state, 50, 51, 53, 64, 95, 123, 159, 163
- Serviceability, 66, 78, 94
- Serviceability state, 54
- SFRC, 20, 23, 24, 29–43, 46–55, 59, 61–73, 75, 78–87, 89–103, 109, 114, 115, 118–123, 153, 154, 156, 157, 159, 160, 162–165
- SFRC section, 25, 30, 52, 63, 64, 66, 67, 75, 78, 80, 82, 83, 85, 86, 88, 89, 91, 94, 100–102, 114, 119, 121, 153, 155

- SFRC slab, 82, 153–156  
 Shallow beam, 134, 135, 142  
 Shear behavior, 110  
 Shear capacity, 34, 109, 111, 113–121  
 Shear crack, 111, 112, 115–117  
 Shear strength, 23, 100, 113, 118, 119, 121, 122  
 Shear stress, 41, 110, 111, 113, 115, 116, 118–121  
 Shear-span depth ratio, 111  
 Shear-transfer mechanism, 112, 113, 115  
 Short span, 132, 134, 143, 149, 151, 152, 155  
 Singh, 29, 30, 59, 79, 85, 134, 148, 153, 154  
 Size-effect, 49, 119  
 Slab, 80–82, 115, 123–157  
 Slab aspect ratio, 80–82, 138, 140, 142, 143, 145, 147, 148, 152, 154–157  
 Slab-parameter, 141, 143, 144, 146–155, 157  
 Slab-system, 123, 129–133, 134–147, 149–155, 157  
 Slender, 111  
 Slender beam, 111  
 Smeaton, John, 5, 6  
 Span, 2, 24, 47, 49, 54, 67, 68, 80, 92, 96, 98, 110–112, 115, 117, 119, 121, 134, 143, 149, 151, 152, 155  
 Span/depth ratio, 148, 155  
 Specimen, 11, 16, 17, 23, 30–32, 34–40, 42, 46–49, 51–53, 87, 93–119, 120, 165  
 Standard cube, 32  
 Standard deviation, 95  
 Stiffened slab, 146, 153  
 Stiffness, 13, 14, 25, 131, 145, 148  
 Strain, 14–17, 19–22, 25–27, 29–33, 36–40, 43, 46–50, 52–54, 59, 63–65, 67, 68, 70, 71, 74–77, 79–81, 83, 84, 88–93, 97–106, 109, 110, 116, 118, 155, 156  
 Strain-compatibility conditions, 53, 77, 79–81, 83, 99, 100, 106  
 Strain-hardening, 52, 54, 156  
 Straining, 21  
 Strain rate, 32  
 Strain softening, 16, 19, 20, 29, 50, 52, 53, 79, 98, 100  
 Strength, 5–11, 13, 15–17, 19–22, 24, 27, 29–33, 35–43, 46, 48–54, 60, 63–69, 73, 79–82, 85, 89, 90, 92–96, 98–100, 102, 109, 111, 113–116, 118, 119, 123–125, 127, 131, 134, 142, 144–148, 150, 151, 153, 155–157, 159, 160, 163  
 Stress, 5, 7, 15–17, 19, 20, 22, 26, 27, 29–38, 42, 43, 46, 49–52, 59–67, 69–72, 75, 76, 86, 94, 95, 97–104, 106, 109–113, 115, 116, 118–122, 124, 125, 131  
 Stress-crack opening, 33, 37, 38, 43  
 Stress-crack opening displacement, 48  
 Stress-crack opening relationship, 37, 38, 43  
 Stress-crack width, 35, 52  
 Stress-mobilization factor, 70, 76, 77, 103, 104, 106  
 Stress-profile model, 67, 68, 101  
 Stress-strain response, 16, 17, 29, 31, 32, 36–39, 46, 48, 55, 95  
 Stress trajectory, 34, 110, 113  
 Structural design, 60, 61  
 Supported edge, 129  
 Supporting beams, 132, 134, 135, 139, 141, 145, 147, 150, 151  
 Syria, 2
- T**  
 Tensile failure, 14, 59  
 Tensile strength, 9, 14, 16, 19, 20, 22, 23, 29, 32, 33, 36–43, 46, 48, 50, 51, 53–55, 63–72, 85, 89, 90, 92, 94, 96, 98, 100, 102, 110, 112, 113, 115, 118, 119, 121, 163  
 Tension, 6, 7, 16, 22–27, 29–33, 35–37, 43, 46, 51, 54, 59, 60, 63–69, 71, 75, 80–82, 85, 86, 88–90, 92, 95, 97, 99, 100, 103, 109–114, 116–118  
 Tension face, 59, 63–65, 81, 89, 100  
 Tension zone, 25, 26, 63, 64, 66, 71, 82, 85, 86, 90, 92, 99, 102, 111, 114, 118  
 Three-point testing, 46, 47, 53  
 Tiryns, 2, 3  
 Toughness, 52, 59, 79, 89, 91–93, 109, 159  
 Transverse reinforcement, 114  
 Transverse steel, 114, 116  
 Truss-action, 24, 25  
 Truss mechanism, 24
- U**  
 Ultimate limit state, 49–51, 64, 71, 78, 94, 95, 109  
 Ultimate limit state, 66  
 Ultimate load, 46, 53, 66, 81, 100, 123, 129, 131, 132, 143  
 Ultimate resisting moment, 126, 129, 130, 134, 139, 142  
 Ultimate state, 38, 49, 51, 52, 65–67, 80, 84, 87, 94, 98, 102, 119, 124, 129, 131, 132, 135, 136, 155  
 Ultimate strength, 8, 16, 19, 27, 60, 79  
 Uncracked phase, 62, 63  
 Uncracked section, 40, 69  
 Under-reinforced, 26, 27, 83, 88, 100, 104, 114  
 Uniaxial, 15, 16, 19, 32, 35, 46, 50, 95, 155  
 Uniaxial test, 45

Upper limit, 53, 78, 113, 145, 147, 148, 152–154

## V

van-der Waals forces, 13, 15

Vibration, 35, 47, 60, 123, 165

Voids, 2, 8, 9, 11, 14, 15, 30, 160

Volume fraction, 25, 30, 31, 36, 38–40, 49, 54, 67, 68, 73, 81, 84, 85, 90–93, 96, 98, 119, 121, 154, 156, 159, 162, 164

Volumetric dilation, 15

## W

Wall-effect, 34

Water, 1–3, 5–15, 23, 32, 159, 160, 163–165

Water-cement ratio, 11–15, 23

Wavy fiber, 42

Weakness, 11

Web-like, 21, 22, 31

Work, 7, 124, 125, 129–132, 136–140, 162

Workability, 8, 81, 87, 90, 156, 160, 161, 163, 164

## Y

Yield conditions, 125, 128

Yielding, 26, 42, 43, 72, 86, 89, 92, 103–105, 111, 131

Yield line, 126, 129–133, 135–137, 141, 142, 145, 146

Yield line pattern, 124, 125, 129, 130, 132, 133, 135–137, 141, 142, 145

Yield strength, 42, 43, 70, 80, 82, 92, 125, 155